Molecular pathogenesis of serrated carcinoma of the colon

Winnie Collet Fernando
Master of Molecular Biology
Bachelor of Technology in Industrial Biotechnology

Griffith School of Biomolecular and Physical Sciences
Science, Environment, Engineering and Technology Group
Griffith University

Submitted in fulfilment of the requirements of the degree of
Doctor of Philosophy

February 2014

Abstract

Colorectal cancer (CRC) progresses from precursor lesions or polyps via two main pathways – the traditional and serrated pathway. The traditional pathway is the conventional type, while the serrated neoplastic pathway has been recently identified and is not well characterised. The aim of this study was to evaluate molecular factors associated with the serrated pathway and study its progression from a serrated polyp to colorectal cancer using patient samples and mouse models. The first part of the study was to evaluate CIMP status of all the serrated polyp subtypes and its association with functionally important genes such as *MLH1, p16* and *IGFBP7* in patient samples. The mouse models were then utilized to assess the contribution of *BRAF* V600E mutation along with the cell cycle regulators and tumour suppressor genes, *p16Ink4a* and *p19Arf* in the initiation and progression of CRC.

The CIMP study was a prospective study in which the real-time based MethyLight assay was employed to evaluate CIMP and methylation status of *p16*, *IGFBP7* and *MLH1* in 154 serrated polyps and 63 adenomas. Samples were subjected to bisulfite modification and methylation levels were assessed using the Weisenberger *et al* panel of methylation markers (*IGF2*, *SOCS1*, *NEUROG1*, *RUNX3* and *CACNA1G*) with *ALU* as the reference gene.

In the mouse study, a *Braf* V600E mouse ($BRaf^{CA}$) was used to assess the role of *BRAF* oncogene in the development of CRC. This was crossed with a mouse carrying the Cre recombinase gene (*A33CreERT2*). The mice were treated with tamoxifen to convert the inactive form of the allele ($BRaf^{CA}$) into its active form ($BRaf^{VE}$). Initial assays were performed to evaluate the conversion rate of $BRaf^{CA}$ into $BRaf^{VE}$ in different regions of the small intestine and colon of tamoxifen and olive oil treated (control) mice. The hyperplasia analysis involved measuring crypt and villus lengths in the colon and small intestine of tamoxifen treated and control (six weeks post treatment) mice. Methylation analysis of the duodenum region was performed using Methyl PCR arrays specific for colon cancer. A panel of 94 genes was assessed for changes in methylation levels of tamoxifen treated mice. Longitudinal studies were also carried out and mice were monitored for development of lesions or tumours in the small intestine and colon.

In order to investigate the effect of *p16Ink4a* and *p19Arf* along with oncogenic *Braf* V600E mutation, mice with ubiquitous loss of *p16Ink4a* and *p19Arf* genes (homozygous and heterozygous) were crossed with $BRaf^{CA}$ mice. Mice were treated

with tamoxifen to induce *Braf* V600E mutation and observed for hyperplastic changes such as lengthening of the crypt and villus in the colon and small intestine.

Results from the CIMP study showed that CIMP-high serrated polyps were strongly associated with *BRAF* mutation and proximal colon. CIMP-high was uncommon in conventional adenomas (1.59%), occurred in 8.25% of hyperplastic polyps (HPs) and became common in sessile serrated adenomas (SSAs) (51.43%). *MLH1* methylation was mainly observed in the proximal colon and was significantly associated with *BRAF* mutation and CIMP-high. The number of samples methylated for *p16* and *IGFBP7* was highest in SSAs.

The observed level of A33-mediated conversion of the $BRaf^{CA}$ allele to $BRaf^{VE}$ was the highest in the duodenum region of the small intestine, followed by the jejunum and ileum and a lower level in the colon. Hyperplasia analysis demonstrated crypt and villus lengthening in the colon and small intestine of the tamoxifen treated mice compared to the controls. However, methylation changes were observed only in few genes such as *Bhlhb9*, *Uchl1* and *Wif1*.

An increase in cellular proliferation and development of TSAs and adenocarcinomas were observed in the longitudinal studies. The lesions were mainly prevalent in the duodenum and jejunum regions of tamoxifen treated mice older than 85 weeks, while no lesions were detected in the controls. The mice also developed extracolonic tumours in the lungs and liver and survived up to 97 weeks (tamoxifen treated), while the controls survived between 112 and 116 weeks. The activation of Mapk and Wnt pathways was observed in the tamoxifen treated mice based on increased expression of total Erk and phospho Erk (Mapk) and nuclear accumulation of β-catenin (Wnt).

The cell cycle regulators and tumour suppressor genes, *p16Ink4a* and *p19Arf* have been known to play an important role in the development of CRC. Similar to the $BRaf^{VE}$ mice, hyperplasia followed by development of TSAs and adenocarcinomas in the tamoxifen treated mice were observed. Due to the absence of these tumour suppressor genes, mice develop more extracolonic tumours at an earlier age compared to the $BRaf^{CA}$ mice. This reduced the survival rate of tamoxifen treated mice to about 82 weeks in the $BRaf^{VE}$/*p16Ink4a* group, while the $BRaf^{VE}$/*p19Arf* null and $BRaf^{VE}$/*p19Arf* het mice survived up to 67.71 and 82 weeks respectively. The loss of these genes also increased the incidence of polyps and tumours in the tamoxifen treated mice compared to mice with only *Braf* mutation.

The methylation panel that was used to detect CIMP is highly specific for CIMP-high cancers. With this panel, we demonstrate that CIMP-high is much more common in SSAs than HPs. This suggests that CIMP-high correlates with increased risk of malignant transformation which was also observed in methylation of functionally important genes. The study involving human colorectal polyps showed that *BRAF* mutation and CIMP along with *p16* are key players in the serrated pathway. The interaction of *Braf* V600E mutation with loss of *p16Ink4a* and *p19Arf* gene expression resulted in the rapid development of small intestinal TSAs and adenocarcinomas compared to the effect of only *Braf* V600E mutation. The $BRaf^{VE}$ mouse model was effective in studying the gradual transformation of normal mucosa into hyperplasia, followed by the development of more advanced lesions eventually leading to the formation of adenocarcinomas. These results provide an insight into the oncogenic activity of *BRAF* V600E mutation and help gain a better understanding of the key factors involved in colorectal tumorigenesis via the serrated pathway.

Statement of Originality

This work has not previously been submitted for a degree or diploma in any university. To the best of my knowledge and belief, the thesis contains no material previously published or written by another person except where due reference is made in the thesis itself.

_____

Winnie Fernando

Table of Contents

List of Figures

List of Tables

List of Abbreviations

- ACF - aberrant crypt foci
- AFAP - attenuated familial adenomatous polyposis
- AOM - azoxymethane
- APC - adenomatous polyposis coli
- BER - base excision repair
- BSA - bovine serum albumin
- CAD - conventional adenoma
- CDK – cyclin-dependent kinase
- CID - chemical inducers of dimerization
- CIM - CpG island methylation
- CIMP - CpG island methylator phenotype
- CIN – chromosomal instability
- CP - central phenyl ring
- CRC - colorectal cancer
- CRD - cysteine-rich domain
- DAB - 3,3'-Diaminobenzidine
- DP - distal pyridyl ring
- DMEM - Dulbecco's Modified Eagle Medium
- ECF - ectopic crypt formation
- ERK - extracellular-signal-regulated kinase
- FAP - familial adenomatous polyposis
- FBS - Fetal Bovine Serum
- FHIT - fragile histidine triad
- GCHP - goblet cell hyperplastic polyp
- H&E - hematoxylin and eosin
- HGD - high-grade dysplasia
- HIC1 - hypermethylated in cancer 1
- HIER - heat-induced epitope retrieval
- hMLH1 - mutL homolog 1
- hMSH2 - mutS homolog 2
- HNPCC - hereditary nonpolyposis colorectal cancer
- HP - hyperplastic polyp
- HPP - hyperplastic polyposis
- HRAS - Harvey murine sarcoma virus
- HRM - high resolution melt
- IGFBP7 – insulin growth factor binding protein 7
- IPTG - isopropyl beta-D-thiogalactoside
- JNK - c-Jun N-terminal
- KRAS - Kirsten murine sarcoma virus
- LGD - low-grade dysplasia
- LOH - loss of heterozygosity

- loxP - locus of X-over of P1
- MAP - MUTYH-mutated polyposis
- MAPK - mitogen activated protein kinase
- MDM2 – mouse double minute 2
- MEF - mouse embryonic fibroblasts
- MEM - Minimum Essential Medium
- MGMT - O-6-methylguanine-DNA methyltransferase
- MHAP - hyperplastic adenomatous polyp
- MINT - Methylated In Tumour
- MM - muscularis mucosa
- MMR - mismatch repair
- MP - mixed polyp
- MPHP - mucin poor hyperplastic polyp
- MSH6 - mutS homolog 6
- MSI - microsatellite instability
- MSI-H - microsatellite instability high
- MSP – methylation specific PCR
- MSS - microsatellite stable
- mtDNA - mitochondrial DNA
- MUTYH - mutY homolog
- MVHP - microvesicular hyperplastic polyp
- NM - normal mucosa
- NRAS - SK-N-SH neuroblastoma transforming gene
- OIS – oncogene-induced senescence
- PBS – phosphate buffered saline
- PFA - paraformaldehyde
- PFF – primary foreskin fibroblast
- PKC - protein kinase C
- PMR - percentage of methylated reference
- PMS2 - postmeiotic segregation increased 2
- pRB - retinoblastoma protein
- PRLBD - progesterone receptor ligand binding domain
- RASSF2 - Ras association (RalGDS/AF-6) domain family member 2
- RBD - RAS-binding domain
- RBWH - Royal Brisbane and Women's Hospital
- rtTA - reverse tetracycline-controlled transactivator
- SAHF - senescence-associated heterochromatin foci
- SAM - S-adenosylmethionine
- SAPK - stress-activated protein kinase
- SCFA - short-chain fatty acid
- SA-β-gal - senescence-associated-β-galactosidase
- shRNA – small hairpin RNA

- SLC5A8 - solute carrier family 5 (sodium/monocarboxylate cotransporter), member 8
- SP - serrated polyp
- SSA - sessile serrated adenoma
- TA - tubular adenoma
- TBS - tris-buffered saline
- TE - Tris-EDTA
- Tet - tetracycline
- TIMP3 - TIMP metallopeptidase inhibitor 3
- TP - trifluoromethyl phenyl ring
- TSA - traditional serrated adenoma
- TVA - tubulovillous adenoma
- UDG - uracil DNA glycosylase
- VA - villous adenoma

Acknowledgements

I would like to thank my supervisors in a very special way for all their help, support and guidance throughout the entire duration of my PhD – **Assoc Prof Kevin Spring, Prof Barbara Leggett and Assoc Prof Dianne Watters**. I sincerely appreciate all the help I received with experimental work, project planning, my reviews, submission of my first research paper and the never-ending corrections for my PhD thesis.

I would like to thank in a special way all the past and present members of the **Conjoint Gastroenterology Laboratory** especially **Diane, Ron, Troy, Mark, Cath and Vicki**. You were/are a wonderful group of people to work with, always encouraging me when I had my share of bad days at work with the love and all the food.

I would like to extend my heartfelt thanks to the number of people who have made this thesis possible – members of the Animal House facility and the Histology facility at QIMR Berghofer; for answering my numerous, sometimes silly questions patiently.

I would also like to thank **Griffith University** for their generous funding towards my scholarships, without which this research would not have been possible.

Finally I acknowledge my family and all my friends who have stood by me throughout my joyous and difficult times; especially my wonderful house mates **Ram** and **Ramanathan** who always believed in me and encouraged me and never complaining inspite of all my tantrums. A special word of thanks to my best friend **John** for encouraging and believing in me. I dedicate this work to my family who have sacrificed a lot over the years to put me where I am right now. Thank you for always supporting and encouraging me and for having complete faith in my work.

Statement of Contribution by others to the thesis as a whole:

- **Mariska Miranda** evaluated *IGFBP7* and *p16* methylation in colorectal tumours and polyps. The experimental work involved optimizing the MethyLight assay for *IGFBP7*, bisulfite modification of the colorectal tumours and *IGFBP7* and *p16* MethyLight assays. Preliminary data analysis was also carried out correlating the methylation status of *IGFBP7* and *p16* with CIMP status, *BRAF* and *KRAS* mutations in colorectal polyps and tumours.
- **Mark Bettington and Paul Waring** assessed the mouse H&E stained slides and classified all the samples based on standard pathology criteria as explained in the thesis.
- **Sonia Greco and Ingunn Ramses** evaluated CIMP status in the colorectal tumours. This involved bisulfite modification of the tumour samples, MethyLight assays for the following CIMP markers – *IGF2*, *SOCS1*, *NEUROG1*, *RUNX3* and *CACNA1G* and *ALU* as the reference gene.
- **Sally Pearson** performed the IHC staining for Ki-67 on the mouse samples using standard IHC procedure as explained in the thesis.
- **Animal House facility at QIMR Berghofer Medical Research Institute** was involved in the general maintenance of the mice which included providing food and water for the animals, recording birth of new litters, mice weanings and regular changes of the mice cages.
- **Histology facility at QIMR Berghofer Medical Research Institute** processed all the mouse samples (paraffin blocks), cut sections for H&E staining and other IHC stains.

Publications and Presentations

Publications during candiature

Winnie C. Fernando, Mariska S. Miranda, Daniel L. Worthley, Kazutomo Togashi, Dianne J. Watters, Barbara A. Leggett, and Kevin J. Spring . *The CIMP phenotype in BRAF mutant serrated polyps from a prospective colonoscopy patient cohort*. **Gastroenterology Research and Practice.** 2014. Published online April 10, 2014. **(Appendix)**

Presentations

Oral Presentations

1. QIMR Berghofer Medical Research Institute's Student Symposium (Nov 2012)
2. 21st Annual Royal Brisbane and Women's Hospital Health Care Symposium (2012)

Poster Presentations

1. 24th Lorne Cancer Conference (2012)
2. ASMR Postgraduate Student Conference (2012)

A note on nomenclature:

Within this thesis, genes and proteins are named according to standard nomenclature. Human gene symbols are all in uppercase and italicised (*BRAF*, *KRAS*, *ERK*), and human proteins are all uppercase, without italicisation (BRAF, KRAS, ERK, MAPK). Mouse gene symbols are all italicised, with only the first letter in uppercase (*Braf*, *Kras*, *Pten*, *Erk*) and mouse proteins are non-italicised, with only the first letter in uppercase (Braf, Kras, Pten, Erk).

CHAPTER 1

LITERATURE REVIEW

1. LITERATURE REVIEW

1.1 THE COLON AND CANCER

The human colon is responsible for the absorption of water and salts. It contains approximately 99.9% of the gastrointestinal microorganisms which aid in the fermentation of carbohydrates into short-chain fatty acids (SCFAs) (Moran & Jackson, 1992). The human colon is divided into two major regions: a) the proximal colon which consists of the caecum, appendix, ascending colon, hepatic flexure, transverse colon and the splenic flexure and b) the distal colon which includes the descending and sigmoid colon (Figure 1.1). The normal mucosal architecture of the colon is composed of a single layer of columnar epithelial cells which forms the colonic crypt lining. Beneath this layer are the lamina propria and a thin layer of smooth muscle fibres called the muscularis mucosae. The epithelium is supported by the lamina propria and consists of absorptive and goblet cells. The base of the colonic crypts contains numerous stem cells, which are responsible for the continuous renewal of the epithelial layer. The proliferative zone is restricted to the bottom of the crypt, while the rates of cellular differentiation and apoptosis are higher in the middle and uppermost regions of the colonic crypt respectively (Figure 1.2) (Levine & Haggitt, 1989).

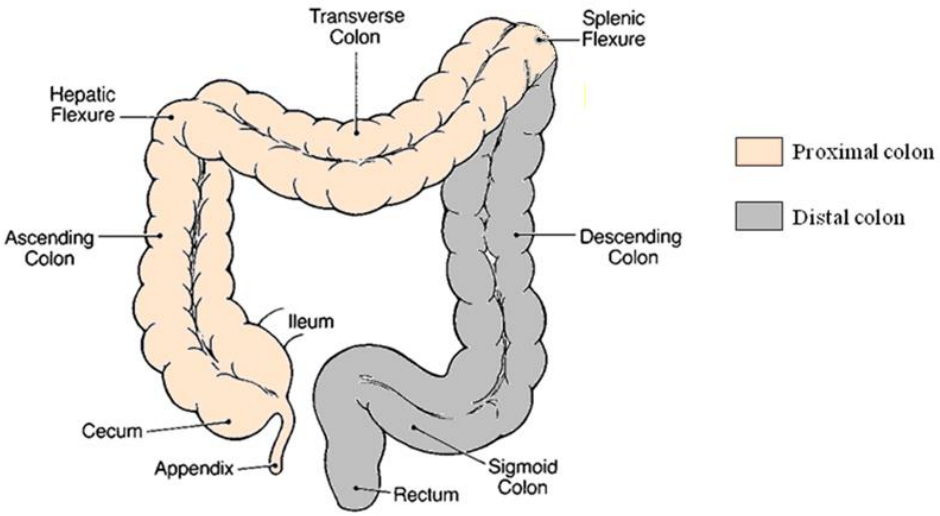

Figure 1.1 - Anatomy of the human colon. *The colon is primarily divided into two main regions - proximal or right colon and distal or left colon. The proximal colon begins at the caecum and ends with the splenic flexure, while the distal colon begins with the descending colon and terminates in the rectum [Adapted from (Levine & Haggitt, 1989)].*

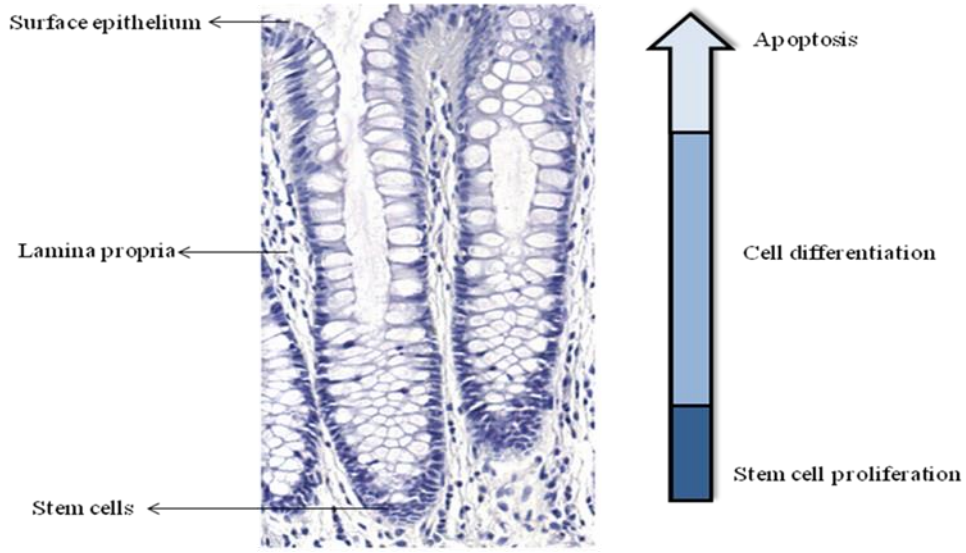

Figure 1.2 - Organization of the colonic crypt. *The crypt is the basic functional unit of the epithelial lining of the colon, which has a rapid cell turnover rate. The base of the crypt contains numerous stem cells and these are responsible for the generation of new cells which migrate from the base to the surface epithelium as they differentiate (Humphries & Wright, 2008).*

Colorectal cancer (CRC) also known as bowel cancer is the second most common cancer in Australia with 15,840 cases reported in 2012 (Figure 1.3A). It has the second highest mortality rate in Australia after lung cancer (Figure 1.3B). The risk of being diagnosed by the age of 85 is 1 in 10 for men and 1 in 14 for women (AIHW & AACR, 2012). Lifestyle factors such as smoking, high alcohol intake and red meat consumption increases the risk of CRC (Moskal *et al*, 2007; Wakai *et al*, 2006; Wogan *et al*, 2004).

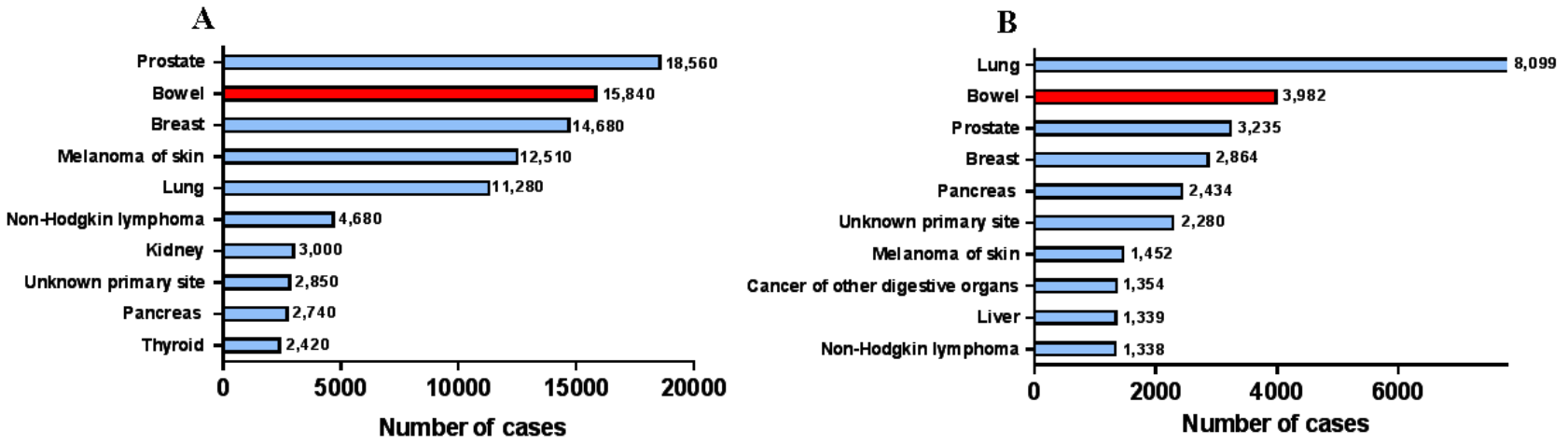

Figure 1.3 - Cancer incidence and mortality in Australia. *Bowel cancer is the second most common cancer in Australia after prostate cancer with an average incidence of 15,840 cases in 2012 (A). Bowel cancer is also the second highest cause of cancer-related deaths in Australia with 3,982 cases after lung cancer (B) [Data adapted from (AIHW & AACR, 2012)].*

Colorectal cancer can develop sporadically (no family history) or can be inherited; it can arise due to the activation of oncogenes (*BRAF* V600E, *KRAS*) or the inactivation of tumour suppressor genes by mutation (*p53)* or DNA hypermethylation (*p16INK4a, p14ARF)* and the resulting tumours can possess varying degrees of genetic instability, such as microsatellite or chromosomal instability. These factors help characterise the different types of CRC and the precursor lesions from which they originate (Bond *et al*, 2012; Chan *et al*, 2003; Kominami *et al*, 2009; Lee *et al*, 2006). In the subsequent sections, the various genes and pathways associated with CRC (Sections 1.2 and 1.6); familial (Section 1.3) and sporadic CRC; the traditional and serrated pathways (Section 1.4) that give rise to CRC and the colorectal precursor lesions or polyps (Section 1.5) will be discussed.

1.2 GENES AND PATHWAYS

1.2.1 MAPK pathway – RAF and RAS protein families

The RAF protein kinase family comprising ARAF (v-raf murine sarcoma 3611 viral oncogene homolog), BRAF (v-raf murine sarcoma viral oncogene homolog) and CRAF (v-raf-1 murine leukaemia viral oncogene homolog 1; also known as RAF-1) regulates various cellular processes including proliferation, differentiation and apoptosis via the mitogen activated protein kinase (MAPK) pathway (Figure 1.4) (Daum *et al*, 1994; Ikawa *et al*, 1988). MAPK, a 42 kDa protein can be activated by cellular responses such as mitogenesis, ligand signalling via G-protein coupled receptors or tyrosine kinase receptors and activators of protein kinase C (PKC). MAPK consists of three major subfamilies - extracellular-signal-regulated kinases (ERK), c-Jun N-terminal (JNK) or stress-activated protein kinases (SAPK) and MAPK14 (Fang & Richardson, 2005; Leevers & Marshall, 1992).

Kirsten murine sarcoma virus (*KRAS*) is a member of the RAS protein family which also comprises *Harvey murine sarcoma virus* (*HRAS*) and *SK-N-SH neuroblastoma transforming gene* (*NRAS*) (Shimizu *et al*, 1983). The activation of the RAS protein family GTPases results in the transmission of signals from the cytoplasmic membrane receptors to the interior of the cell. This occurs by the conversion of guanosine diphosphate (GDP) (inactive form) into guanosine triphosphate (GTP) (active form), catalysed by G-protein coupled receptors. This results in the dissociation of α-

GTP from β and γ dimers (Crespo *et al*, 1994; Fang & Richardson, 2005). Activated RAS induces heterodimer formation of BRAF and CRAF with the help of 14-3-3 proteins which bind at carboxy-terminal of serine 621 in CRAF (Weber *et al*, 2001). The C-terminal catalytic domain of the activated RAF complex interacts with MEK1 and MEK2 and activates them by phosphorylation and this bond is much weaker than the RAS-RAF association. In the next step, ERK is activated by interaction of MEK1 and MEK2 and in turn triggers a large number of transcription factors which mediates cellular proliferation, differentiation, apoptosis, angiogeneis and metastasis (Fang & Richardson, 2005; Van Aelst *et al*, 1993).

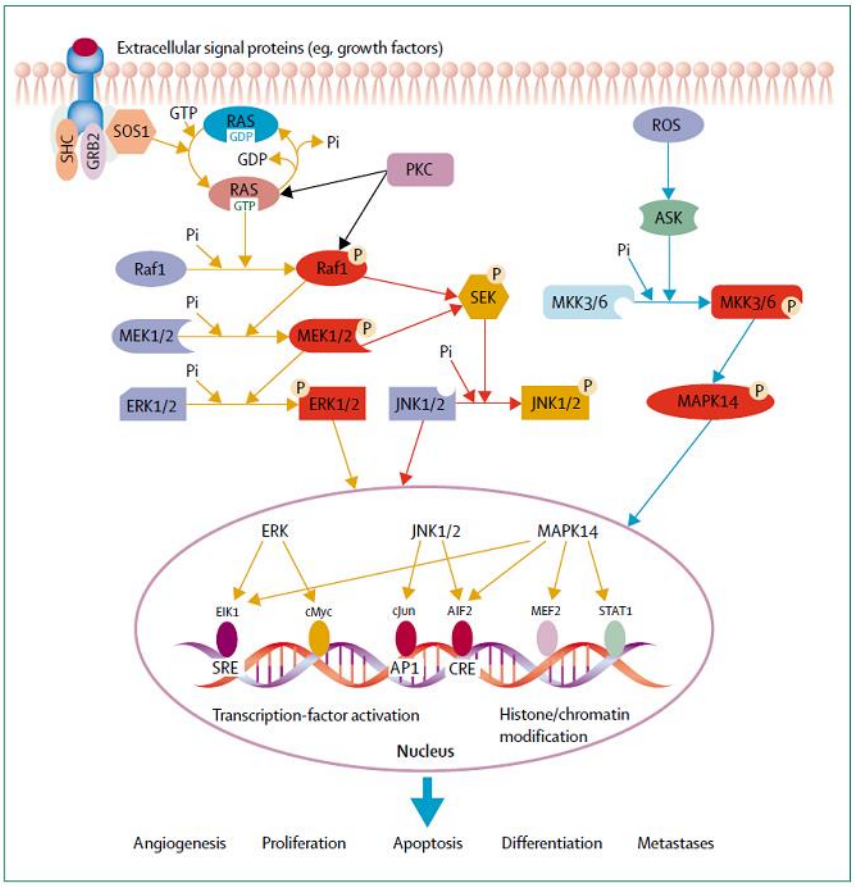

Figure 1.4 - The RAS-RAF-MEK-ERK-MAP Kinase Pathway. *The oncogenes – BRAF and KRAS are activated via the mitogen activated protein kinase (MAPK) pathway. The RAF kinase family serves as an immediate downstream effector of RAS. RAF kinase is a prototypical MEK Kinase that directly phosphorylates and activates MEK. This is one of the most important pathways for cell proliferation, growth and differentiation [Adapted from (Fang & Richardson, 2005)].*

1.2.1.2 Structure and activation of BRAF

The RAF protein structure consists of three conserved regulatory regions - 1) CR1 contains the RAS-binding domain (RBD) and the cysteine-rich domain (CRD) 2) CR2 which is rich in serine and threonine residues also contains some regulatory phosphorylation sites and 3) CR3 which comprises the activation segments and the negatively charged regulatory region (N-region) (Figure 1.5) (Daum *et al*, 1994; Michaloglou *et al*, 2008). The amino acid sequence of the kinase domains of the RAF isomers showed about 75% homology. It was initially proposed that a deletion of this sequence could result in the activation of the *RAF* oncogenes (Ikawa *et al*, 1988).

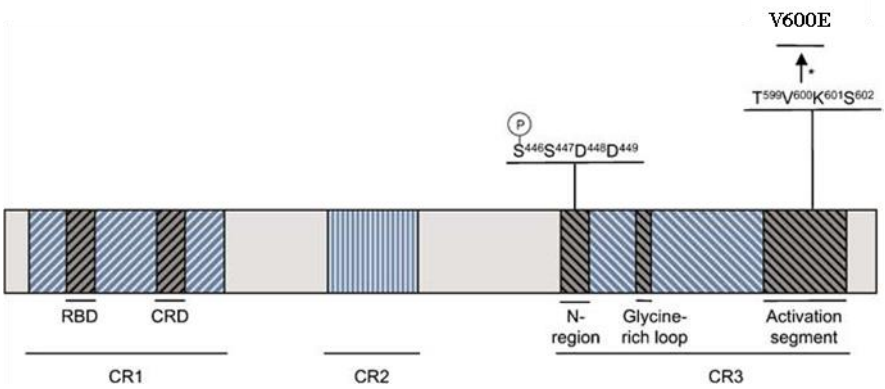

Figure 1.5 - Schematic representation of primary structure of BRAF. *The structure of the BRAF protein denotes the three conserved regions (highlighted in blue). CR1 and CR2 are regulatory domains and CR3 represents the catalytic domain. The RAS-binding domain (RBD) and cysteine-rich domain (CRD) are located in CR1. The N-region, Glycine-rich loop (G loop) and activation segment are located in CR3. S^{446} in the SSDD motif is responsible for the negative charge of the negatively charged regulatory-region (N-region) in BRAF. Phosphorylation of residues T^{599} and S^{602} result in BRAF activation. The position of the mutational hotspot V600E is also indicated [Adapted from (Michaloglou et al, 2008)].*

The kinase domain of BRAF is bilobed, a characteristic feature of the protein kinase family (Figure 1.6). The inhibitor molecule BAY43-9006 is located between the N and C lobes and consists of a distal pyridyl ring (DP), a central phenyl ring (CP) and a lipophilic trifluoromethyl phenyl ring (TP). The DP ring is located in the ATP adenine binding pocket and interacts with three aromatic residues - Trp530, Phe582 and Phe594. The TP ring lies between the αC and αE helices and N-terminal regions of the catalytic loop and DFG motif. BRAF contains five phosphorylation sites - Thr598, Ser601,

Ser604, Ser606 and Ser613, of which Ser615 is highly conserved and Ser604 and Ser606 are the PKC phosphorylation sites (Wan *et al*, 2004; Zhang & Guan, 2000).

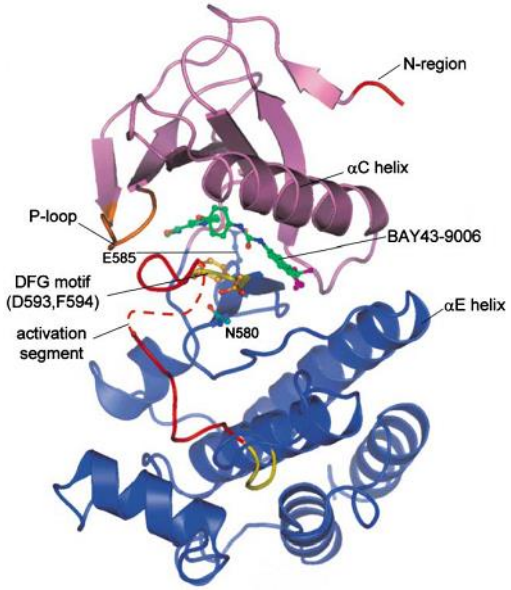

Figure 1.6 - Structure of wt-BRAF kinase domain. *A change in the position of the DFG motif (yellow) or the activation segment results in the activation of BRAF. The P loop (orange) or activation segment is the region in which 89% of the BRAF mutations are observed. Residues 600-611 of the activation loop are represented by dashed lines [Adapted from (Wan et al, 2004)].*

BRAF activation requires just a change in the position of the DFG motif or the activation segment which lies adjacent to it and results in the formation of a β sheet interaction with the β6 strand. About 89% of BRAF mutations are found in either the P loop or the activation segment (a region of 10 to 30 amino acids) or adjacent to the DFG motif and the levels of kinase activity depend on the amino acid substitution. Based on the ability of mutant BRAF to stimulate *in vitro* kinase activity, they have been classified into high, intermediate or impaired activity groups. In the high and intermediate activity groups, the amino acids (like Val600) are substituted at the non-conserved positions or replaced with amino acids normally found in kinases (like Glu or Asp). However, in the impaired activity group, substitutions occur in the highly conserved residues. A constant feature in all BRAF mutants is the destabilisation of the DFG motif-activation segment due to the disruption of the hydrophobic cluster between the P loop and DFG motif. This feature along with the interaction of Val600 with Lys506 of αC helix helps trigger the activation of BRAF. Results showed that Glu (95%

mutations due to single base substitution) and Asp substitutions at position 599 were 2- to 4-fold higher than the Arg and Lys amino acids (Davies *et al*, 2002; Wan *et al*, 2004).

1.2.2 The INK4a locus

p16INK4a, a tumour suppressor is a member of the cyclin-dependent kinase family of inhibitors (CDK4 and CDK6) which includes p15INK4b, p18INK4c and p19INK4d and is involved in the regulation of retinoblastoma protein (pRB) (Hirai *et al*, 1995; Roussel, 1999; Serrano *et al*, 1993). The INK4 family binds to CDK4/6 and inhibits the kinase activity of cyclin D-CDK4/6 complex (Thullberg *et al*, 2000). The activation of *p16INK4a* in human diploid fibroblasts was found to be dependent on JMJD3 - a histone lysine demethylase, which is involved in demethylation of histone H3 Lys 27 trimethylation (H3K27me3) (Agger *et al*, 2009). Inhibition of CDK4/6 by p16INK4a prevents phosphorylation of pRB which results in cell cycle arrest at the G1 phase (Figure 1.7) (Roussel, 1999). Ectopic expression of JMJD3 in the presence of oncogenic *RAS* results in elevated ARF and INK4a levels, which cause senescence and is mediated by the RAS-RAF-MEK pathway. In this case, up regulation in Ink4a/Arf locus is only seen in mice and not in humans (Barradas *et al*, 2009).

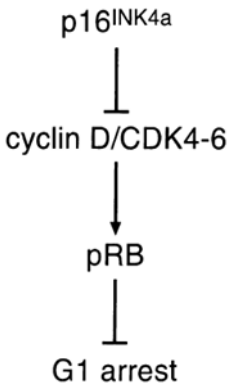

Figure 1.7 - The INK4a locus and cell cycle arrest. *p16INK4a inhibits cyclin-dependent kinases 4 and 6 (CDK4/6) which prevents the phosphorylation of retinoblastoma protein (pRB). This causes a cell cycle arrest at the G1 phase [Adapted from (Roussel, 1999)].*

1.2.3 p19/p53 pathway

p53 is a key tumour suppressor gene and is located on chromosome 17. In the p19/p53 pathway, p14ARF (known as p19Arf in mice) binds to the C-terminal domain

of mouse double minute 2 (MDM2). MDM2 binds to p53 through the N-terminal domain and a ternary complex is formed with ARF-MDM2-p53 (Figure 1.8). The expression of exon 1β-encoded domain is responsible for activating ARF to induce a G1 cell cycle arrest and cells undergo senescence. The introduction of ARF into cells expressing high levels of p53 and MDM2 restores senescence along with normal p53 expression and increased levels of p21 (Zhang *et al*, 1998).

Figure 1.8 - p53-mediated cell cycle arrest. *p19ARF binds to the C-terminal domain of MDM2 and this in turn interacts with p53 at its N-terminal domain. An increase in p53 and MDM2 expression results in a cell cycle arrest at G1 and G2 phases and the cells undergo senescence [Adapted from (Roussel, 1999)].*

1.2.4 IGFBP7

A genome-wide small hairpin RNA (shRNA) screening was carried out to identify potential genes required for the inhibition of cellular proliferation along with BRAF V600E in human primary foreskin fibroblasts (PFF). Insulin growth factor binding protein 7 (IGFBP7), a secreted protein identified in this screening was found to induce senescence and apoptosis. Loss of IGFBP7 expression could be attributed to promoter hypermethylation and this was mainly seen in *BRAF* V600E-positive melanomas, but was not present in nevi harbouring *BRAF* mutations (Wajapeyee *et al*, 2008). IGFBP7 expression was silenced in CRC cell lines - HCT116, HT29, RKO and SW48 and was down regulated in Colo320 and DLD1. This showed an inverse correlation with the *IGFBP7* promoter methylation status of these cell lines (Suzuki *et al*, 2010).

1.3 FAMILIAL CRC

Familial or hereditary CRC accounts for about 26% of all CRC cases and some of the well known inherited forms are familial adenomatous polyposis (FAP) and Lynch syndrome [formerly known as hereditary nonpolyposis colorectal cancer (HNPCC)], hyperplastic polyposis (HPP) and MUTYH-mutated polyposis (MAP) (Aaltonen *et al*, 1993; Jasperson *et al*, 2010).

1.3.1 Familial Adenomatous Polyposis (FAP)

FAP, an autosomal dominant disorder represents about 1% of familial CRC and is characterised by the presence of numerous colonic adenomas (>100) mainly in the distal colon which arise at an early age. It is highly penetrant and the average age of onset is approximately 39 years (Half *et al*, 2009; Rustgi, 2007). FAP is also associated with extracolonic tumours arising in various parts of the body like the central nervous system (Turcot's syndrome), pancreas, adrenal and thyroid glands (Parks *et al*, 1970). Attenuated FAP (AFAP) is a distinct variant of FAP which is characterized by a smaller number of adenomas (1-50) occurring primarily in the proximal colon and the average age for the onset of CRC is 55 years (Lynch & de la Chapelle, 2003; Lynch *et al*, 1995). The development of FAP is linked to mutations in the tumour suppressor gene, *adenomatous polyposis coli* (*APC*). This gene is located on chromosome 5 at q21-22 and *APC* inactivation has been correlated to numerous mutations (Bodmer *et al*, 1987; Groden *et al*, 1991). Frequent loss of heterozygosity (LOH) on chromosome 5q near the location of *APC* was also found to increase the incidence of CRC (Miyaki *et al*, 1990).

1.3.2 Lynch syndrome

Lynch syndrome comprises about 5% of CRC cases with an average age of CRC onset of 44 years (Lynch *et al*, 1991). It is predominantly proximal in nature, shows severe microsatellite instability (MSI) with no physical manifestations and accelerated colorectal carcinogenesis (Aaltonen *et al*, 1993; de la Chapelle, 2004; Jasperson *et al*, 2010). As indicated, a large proportion of Lynch patients have tumours which exhibit MSI which is caused by germline mutations in one of the DNA mismatch repair (MMR) genes. This MMR system helps repair mutations that occur during DNA replication and recombination and comprises four main genes – *mutS homolog 2* (*hMSH2*), *mutL homolog 1* (*hMLH1*), *mutS homolog 6* (*MSH6*) and *postmeiotic segregation increased 2*

(*PMS2*) (Aaltonen *et al*, 1994; Vogelstein & Kinzler, 2002). Studies show that mutations in *hMLH1* and *hMSH2* result in adenomas with high levels of microsatellite instability (MSI-H), which can drive the development of CRC in Lynch patients (Aaltonen *et al*, 1994; Fishel *et al*, 1993; Thibodeau *et al*, 1996).

1.3.3 Hyperplastic polyposis (HPP) syndrome

Hyperplastic polyposis (HPP) syndrome originates from large, abundant, proximally located hyperplastic polyps (HP) with dysplastic epithelium and few cases also exhibit MSI. A minor group of the polyps also involved in HPP were serrated adenomas and mixed polyps with areas of HP and adenoma (Hyman *et al*, 2004; Jass *et al*, 2000; Leggett *et al*, 2001). The diagnosis of HPP depends on the following criteria: a) At least five proximal HPs, of which two should be greater than 10 mm in diameter or b) an individual with a first degree relative diagnosed with HPP and with numerous proximal HPs or c) more than 30 HPs distributed throughout the colon (Kleihues & Sobin, 2000).

1.3.4 MUTYH-mutated polyposis (MAP)

MUTYH-mutated polyposis (MAP) is caused by biallelic mutations in the *mutY homolog* (*MUTYH*) gene, which encodes for the DNA glycosylase enzyme involved in the base excision repair (BER) pathway. In 2002, Al-Tassan and colleagues observed multiple colorectal adenomas and carcinomas in three siblings belonging to a family under study (family N). The absences of *APC* gene inactivation and mutations in MMR genes ruled them out as the primary inherited defects, which gave rise to the lesions and carcinomas. There was a significant increase in the number of G:C → T:A transversions and this led to the analysis of the enzymes involved in the BER pathway and two mutations in the MUTYH gene were identified (Al-Tassan *et al*, 2002).

Patients with MAP are more similar to AFAP patients and on an average MAP is identified in symptomatic patients at 45 years of age (Nielsen *et al*, 2009b; Woods *et al*, 2010). A majority of the MAP cancers positively stain for functional p53 (57%); are microsatellite stable (MSS), mucinous, less metastatic than sporadic CRCs; display accelerated carcinogenesis and 64% of the cancers have *KRAS* mutations. Proximal MAP tumours are mainly located in the caecum and ascending colon. The risk of CRC

in MAP patients is not associated with the number of adenomas as in AFAP (Nielsen *et al*, 2009a; Nieuwenhuis *et al*, 2012).

1.4 SPORADIC CRC

A vast majority of CRC cases are sporadic (74%) and arise from two main pathways: the traditional pathway and the serrated neoplastic pathway (de la Chapelle, 2004). Sporadic CRC are associated with characteristic features such as genomic instability - microsatellite instability (MSI) and chromosomal instability (CIN); mutations in *BRAF*, *KRAS*, *p53*, *APC*; methylation of genes such as *MLHI*, *p16INK4a*, *O-6-methylguanine-DNA methyltransferase* (*MGMT*) and CpG island methylator phenotype (CIMP) depending on the precursor lesion (adenomas or serrated polyps) and the pathway by which they progress into CRC (Deng *et al*, 2004; Dong *et al*, 2005; Goel *et al*, 2003; Smith *et al*, 2002; Toyota *et al*, 1999).

1.4.1 Traditional pathway

Fearon and Vogelstein proposed a genetic model, which showed the development of CRC from a hyperproliferative epithelium through three stages of adenoma. The main feature of this model was that an accumulation of numerous genetic alterations could result in CRC, irrespective of the order in which these genetic changes occur. This formed the basis of the "traditional" pathway or the "adenoma-carcinoma sequence". These genetic changes include oncogenic mutation, multiple allelic losses on chromosomes 5q, 17p and 18q, inactivation of tumour suppressor genes such as *p53* and epigenetic DNA hypomethylation (Figure 1.9) (Fearon & Vogelstein, 1990; Hill *et al*, 1978).

Ostwald and colleagues classified 130 CRCs into seven groups based on molecular data such as expression of β-catenin, MLH1, MSH2; MSI analysis; mutations in *BRAF*, *KRAS*, *p53* and *APC* and methylation analysis. Standard type sporadic CRC were distal, mucinous, CIMP negative, microsatellite stable (MSS) and CIN positive similar to the tumours arising via the traditional pathway (Ostwald *et al*, 2009). The results were similar to a recent study by Marisa and colleagues. A consensus unsupervised analysis of 443 colorectal tumour samples showed six clusters - C1 to C6. A majority of the tumours in clusters C1 and C5 was CIN positive, CIMP positive, *p53* mutant and found in the distal colon. These tumours were considered to be the

'conventional type' arising via the traditional pathway. The tumours in the other clusters - C2, C3, C4 and C6 were characteristic of the serrated pathway which will be discussed in Section 1.4.2 (Marisa *et al*, 2013).

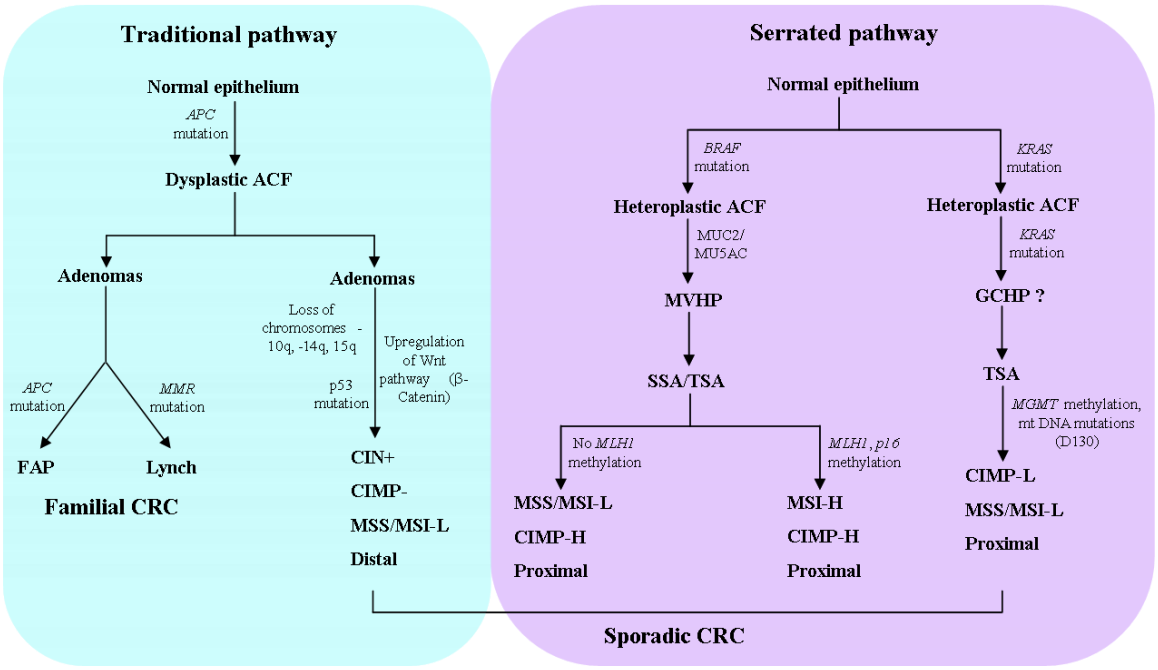

Figure 1.9 - Pathways to the development of CRC. *The traditional pathway to the development of CRC is the adenoma-adenocarcinoma sequence. This pathway is initiated by mutations and/or deletions in APC, Wnt pathway (β-catenin) and p53 and is also characterized by CIN. Both FAP and Lynch syndrome also arise from adenomas and are characterised by mutations in APC and MMR genes respectively. The recently described serrated pathway is characterized by methylation (CIMP), BRAF and KRAS mutations and methylation of key genes such as p16, MLH1 and MGMT. These cancers originate in serrated polyps.*

1.4.2 Serrated neoplastic pathway

The recently identified serrated neoplastic pathway underlies the development of colorectal carcinoma from serrated polyps (Section 1.5.3). These serrated polyps differ from adenomas (Section 1.5.2) in many ways including frequent *BRAF* mutation and increased methylation, MSI and low levels of *KRAS* mutation. The revised serrated neoplastic pathway has been proposed to give rise to MSI-H/CIMP-H carcinoma which is initiated by *BRAF* mutation and increased methylation from dysplastic SSAs (Snover, 2011). Jass had earlier classified CRC originating from serrated polyps into three types.

Type 1 is associated with CIMP-H, methylation of *MLH1*, *BRAF* mutation and MSI-H; type 2 includes CIMP-H, *BRAF* mutation, partial methylation of *MLH1* and MSS/MSI-L; while type 3 cancers are characterised by CIMP-L, *MGMT* methylation, *KRAS* mutation, MSS/MSI-L and CIN which also originate from adenomas (Jass, 2007).

Initially, studies were carried out to evaluate the MSI status of serrated polyps and it was found that the majority of HPs and SAs were MSI-L. About 10% of sporadic MSI-L cancers were assumed to develop from these MSI-L lesions and suggested an alternate to the traditional pathway (Figure 1.9) (Iino *et al*, 1999). Jass and colleagues suggested that CRC could evolve via three pathways - suppressor pathway which involves CIN; mutator pathway which results in MSI and a novel pathway which combines the features of these two pathways (Jass *et al*, 1999). The development of MSI-H cancers in HPP patients without the involvement of an adenoma supported the existence of this novel pathway (Jass *et al*, 2000). Another characteristic feature was included in this mechanism in the form of CpG island methylator phenotype (CIMP) (Section 1.5.2.3) (Toyota *et al*, 1999). These results showed that CRC developing from a serrated polyp is driven by a whole new set of genetic alterations not significantly associated with the traditional pathway.

1.5 PRECURSOR LESIONS OF CRC

1.5.1 Aberrant Crypt Foci (ACF)

ACF are considered to be the earliest preneoplastic precursors to adenomas and CRC and are more prevalent in the distal colon and rectum (Takayama *et al*, 1998). They were first identified in methylene blue stained colon sections from mice injected with azoxymethane (AOM) (Bird, 1987). ACF are individual large crypts (diameter is 3 times larger than normal), which are elongated and have thicker epithelial linings. They are also characterised by distorted luminal orientation, large, hyperchromatic nuclei and a zone of increased cellular proliferation (McLellan & Bird, 1988; Pretlow *et al*, 1991; Roncucci *et al*, 1991). ACF are classified into two types: dysplastic and heteroplastic. Sporadic ACF are mainly heteroplastic, while a majority of the ACF from familial adenomatous polyposis (FAP) patients are dysplastic. CpG island methylation (CIM) and *KRAS* mutations are more prevalent in sporadic ACF (dysplastic) compared to ACF from FAP patients (Chan *et al*, 2002; Nucci *et al*, 1997).

1.5.2 Adenoma

Adenomas are the precursor lesions associated with the traditional pathway (Section 1.4.1) and may be sessile (attached to the base without a stalk), semisessile (attached to the base by a very short stalk) or pedunculated (attached by a very long stalk) (Figure 1.10) (Fenoglio-Preiser & Hutter, 1985; Fenoglio & Lane, 1974; Morson, 1974). Based on the arrangement of the dysplastic epithelium, adenomas are classified as tubular adenomas or TAs (≥80% tubular), villous adenomas or VAs (≥80% finger-like pattern or straight villous fronds) and tubulovillous adenomas or TVAs with an intermediate structure (15%) (Konishi & Morson, 1982; Rubio, 2002). Adenomas can be graded based on the levels of epithelial dysplasia: mild, moderate and severe (carcinoma *in situ*) which eventually will lead to invasive carcinoma (Konishi & Morson, 1982). TAs comprise 75% of the total adenoma population and generally display mild to moderate dysplasia while the less common VA (10%) shows severe dysplasia and has high malignant potential (Morson, 1974).

The main feature of an adenoma is the cerebriform, which is created by a pattern of ridges and grooves that resembles the surface of the brain. Deep, continuous grooves give rise to lobules and the number of lobules correlates with the degree of villosity. Based on the lobule number, adenomas can be classified into: TAs (≤3 lobules), TVAs (3 to 10 lobules) and VAs (>10 lobules) (Thompson & Enterline, 1981). A major proportion of the adenomas are present in the sigmoid colon followed by the descending colon and the highest incidences of dysplasia, carcinoma *in situ* and invasive carcinoma are also present in the sigmoid region (Shinya & Wolff, 1979). Studies show that a positive correlation could be established between severity of dysplasia, increasing adenoma size (>5mm) and villous growth pattern (Griffioen *et al*, 1989; Kellokumpu & Husa, 1987).

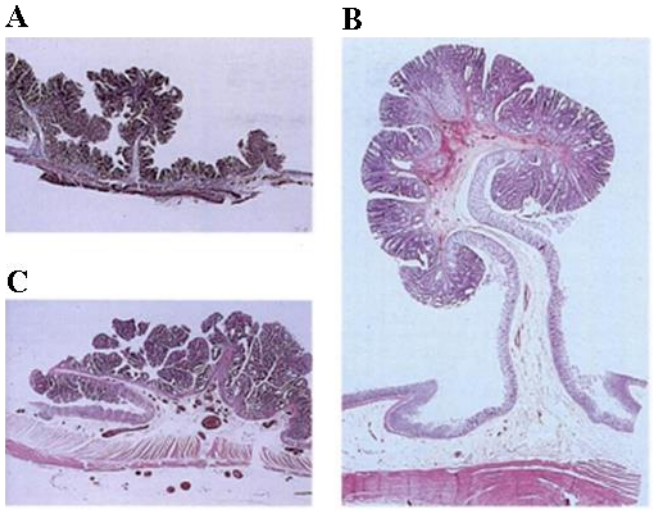

Figure 1.10 Structural classification of adenomas. *Sessile adenoma (attached to the base- no stalk)* ***(A)****. Pedunculated adenoma (attached by a very long stalk)* ***(B)****. Semisessile adenoma (attached to the base by a very short stalk)* ***(C)*** *[Adapted from (Fenoglio-Preiser & Hutter, 1985)]*.

Mutation in the *KRAS* gene (mainly codons 12 and 13) is present in about 7.3% in sporadic adenomas and is strongly associated with large adenomas (size >0.5 cm), a high degree of villosity (TVAs and VAs) and is mainly found in rectal adenomas (Barry *et al*, 2006; Smith *et al*, 2002; Takayama *et al*, 2001). Adenomas are generally not associated with *BRAF* mutations, *MLH1* methylation and CpG island methylator phenotype (CIMP) (Burnett-Hartman *et al*, 2013). Early events in colorectal tumorigenesis such as methylation of *MGMT*, *Ras association (RalGDS/AF-6) domain family member 2* (*RASSF2*) and *p16INK4a* were more prevalent in TVAs and VAs. The methylation levels were found to increase from TAs to TVAs and VAs and this could be attributed to the villous nature of the polyp. Large, proximally located adenomas showed higher levels of methylation (Kakar *et al*, 2008; Psofaki *et al*, 2010). A recent study by Ishii and colleagues showed that a TA with less than 20% villosity was more closely related to a TVA than a TA with no villosity based on molecular features such as *KRAS*, *BRAF* and *p53* mutations (Ishii *et al*, 2011). This could possibly cause a shift in the classification of adenomas and place villosity as a very important feature to determine the progression of CRC via the traditional pathway.

1.5.3 Serrated polyp (SP)

Serrated polyps were initially considered as non-malignant lesions and were not well classified (Frazin *et al*, 1984). In 2003, Torlakovic and colleagues performed a histopathologic review of serrated polyps and reclassified them into six subtypes - hyperplastic polyps (HP) comprising microvesicular HP (MVHP), goblet cell HP (GCHP) and mucin poor HP (MPHP); traditional serrated adenoma (TSA) and sessile serrated adenoma (SSA) (Torlakovic *et al*, 2003). This classification has been further refined over recent years and was revised by Snover in 2011. The subtypes of HPs remained the same as the previous classification. However, TSAs were divided into - with conventional dysplasia and without conventional dysplasia and SSAs were divided into - with cytological dysplasia and without cytological dysplasia (Snover, 2011). These serrated polyps will be discussed in detail in the following section.

1.5.3.1 Hyperplastic polyp (HP)

Hyperplastic polyps (HP) are mainly small (<5mm in diameter) lesions that comprise about 29% of the total number of polyps and are mainly present in the distal colon and rectum (Fenoglio-Preiser & Hutter, 1985; Spring *et al*, 2006). A typical HP has elongated crypts and a serrated or saw-toothed appearance of the upper and middle levels of the epithelial crypt due to infolding of the epithelium in a semicircular fashion (Figure 1.11). They are mainly sessile, display no dysplasia and have a large number of goblet cells mainly in the upper parts of the crypt (Aust & Baretton, 2010; Estrada & Spjut, 1980; Spjut & Appel, 1979). The nuclei are small, round and basally located and mitosis normally occurs in the basal region of the crypt (Longacre & Fenoglio-Preiser, 1990). Some characteristic differences can be identified between the HPs present in the proximal and distal colon. Patients with proximal HPs were found to be 10 years younger and had a higher serration index than those with distal hyperplastic lesions (Baker *et al*, 2004). HPs in the proximal colon were larger, had increased abnormal proliferation and distorted architecture (Torlakovic *et al*, 2003).

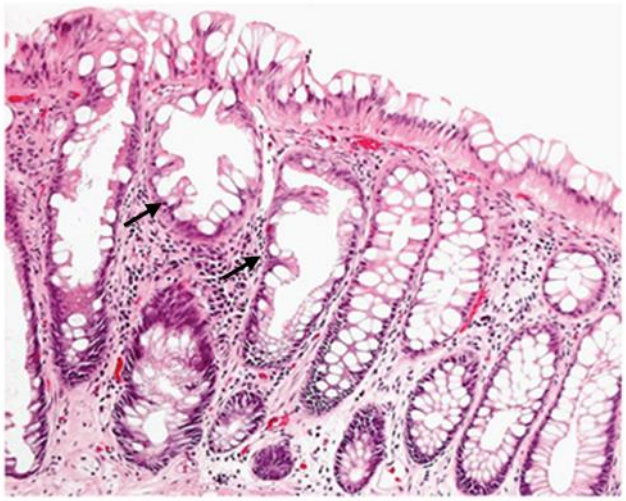

Figure 1.11 - Hyperplastic polyp (HP). *A characteristic feature of HP is the infolding of the epithelial crypt as seen on the left (arrows) giving rise to a serrated appearance. The crypts on the right are normal, straight and not serrated [Adapted from (Cunningham & Riddell, 2006)]*.

HPs are classified based on the mucin and goblet cell content, polyp architecture, crypt serration and type of proliferation into three subtypes: microvesicular HP (MVHP), goblet cell HP (GCHP) and mucin poor HP (MPHP) (Figure 1.12). MVHPs, considered as the typical HP are the most common subtype with an average size of 3.2 mm and are mainly located in the distal region of the colon. They are serrated, sessile, have numerous vesicular cells, a large basal proliferative compartment and very minimal crypt dilation. GCHPs are also mainly found in the distal colon, are smaller in size (mean size 2.4 mm) and fewer in number than MVHPs. These polyps are sessile with minimum serration at the crypt surface and have a large number of goblet cells. MPHPs, as the name suggests lack mucin, have hyperchromatic nuclei, a minute percentage of goblet cells and are quite rare (Torlakovic *et al*, 2003).

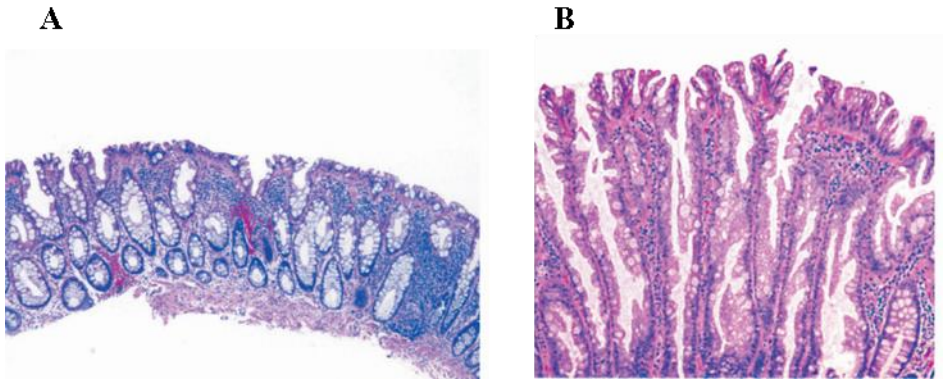

Figure 1.12 - Classification of HPs. *Goblet cell HP (GCHP) - this polyp was located in the rectum with KRAS mutation in codon 12 and is CIMP-negative. An increased number of goblet cells can be observed when compared to normal mucosa and it has a thickened basement membrane* ***(A)****. Microvesicular HP (MVHP) - this was located in the transverse colon and displays a high level of CIMP (CIMP-H) (Section 1.5.2.3) and is KRAS wild type. Serration can be observed in a typical MVHP and this extends into the lower part of the crypt. Microvesicular cells and slight thickening of the basement membrane can also be observed* ***(B)*** *[Adapted from (O'Brien et al, 2004)].*

In 1997, Otori and colleagues identified possibly the first genetic alteration in HPs - *KRAS* mutations with a mutational frequency similar to that observed in adenomas (Otori *et al*, 1997). Another study revealed that the *KRAS* mutations mainly identified in codon 12 were found only in 39 out of 61 HPs and there was a strong association between *KRAS* mutations and the distal colon. GCHPs had the highest frequency of *KRAS* mutations (50%), followed by MVHPs (11%). Conversely, there is a positive correlation between HPs, *BRAF* V600E mutation and proximal location (Spring *et al*, 2006). HPs showed a significant correlation with CIMP, with about 50.6% classified as CIMP-H based on the Methylated In Tumour (MINT) panel of methylation markers. GCHPs and MVHPs showed similar levels of methylation and were mainly associated with proximal location of the colon (O'Brien *et al*, 2004). CIMP-H was found to be directly proportional to size of the hyperplastic lesion which ranged from 5-15 mm (Wynter *et al*, 2004). *BRAF* also exhibited a positive correlation with CIMP in a majority of the hyperplastic lesions (Kambara *et al*, 2004).

1.5.3.2 Traditional serrated adenoma (TSA)

Snover recently classified traditional serrated adenomas (TSAs) into TSAs with conventional dysplasia and those without conventional dysplaia (Snover, 2011). Longacre and Fenoglio proposed the term "serrated adenoma" to describe lesions which included dysplasia and serration and could not be classified as a HP or an AD (Cooper *et al*, 1979; Frazin *et al*, 1984; Longacre & Fenoglio-Preiser, 1990). TSAs constitute a minor portion of colonic polyps (0.7%) with an average size of 5.8 mm, are mainly located in the rectosigmoid region of males and are usually pedunculated (attached by a stalk) (Bariol *et al*, 2003; Spring *et al*, 2006; Torlakovic *et al*, 2003). The relationship between the colonic crypts and the muscularis mucosa (MM) is another criterion for distinguishing between the serrated lesions. The base of the crypt is anchored to the MM in normal mucosa (NM). In TSAs, a disruption of this anchorage gives rise to ectopic crypt formation (ECF). Other important features prevalent only in TSAs include formation of mucosal bridges and mucosal tennis-racquet-like protrusions which are contributions of ECF (Figures 1.13 and 1.14) (Torlakovic *et al*, 2008).

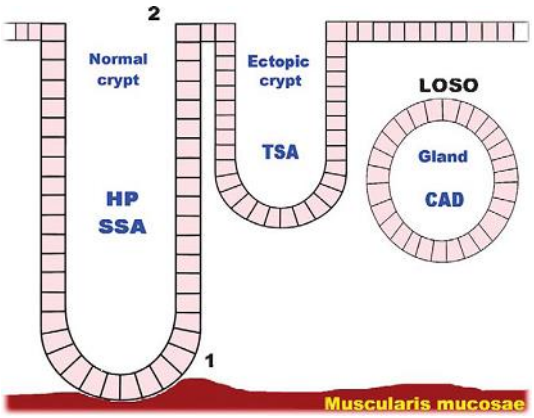

Figure 1.13 - Structural alterations in crypt architecture in polyps. *In HPs and SSAs, the base of the crypt is attached at point 1 to the muscularis mucosae and oriented maturation towards the surface epithelium indicated by point 2. In TSAs, there is a disruption of point 1 leading to ectopic crypts which are no longer anchored to the muscularis mucosae and point 2 is intact. However, when both points 1 and 2 are disrupted, they give rise to conventional adenomas (CAD) [Adapted from (Torlakovic et al, 2008)].*

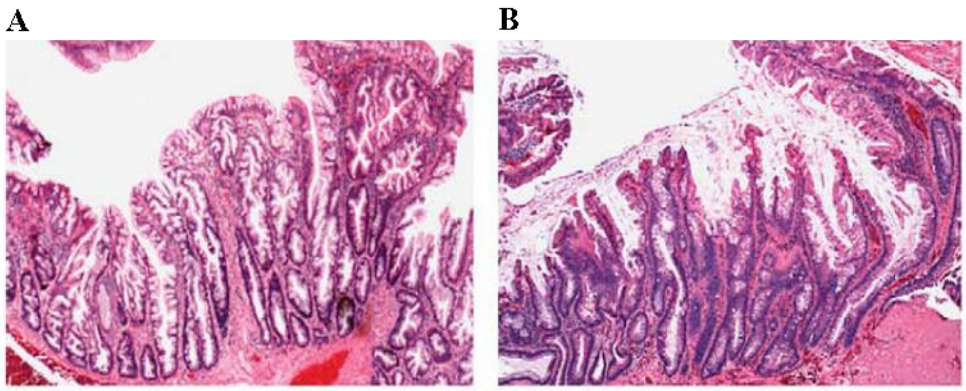

Figure 1.14 - Structure of TSA. *TSAs are mainly flat which make them appear as SSAs and are characterized by mucosal bridges* ***(A)****. Flat TSAs with a large amount of eosinophilia* ***(B)*** *[Adapted from (Torlakovic et al, 2008)]*.

Conventional epithelial dysplasia was observed in TSA and the dysplastic changes included hyperchromatic chromatin, high nuclear/cytoplasmic ratio, higher mitotic rate and extensive pseudostratification. Dysplastic TSAs are larger in size and characterised by abnormal nuclear expression of p53 (Fu *et al*, 2012). Genetic alterations such as mutations in *APC*, *p53*, *p16INK4a* and *KRAS* were identified in TSAs (Fogt *et al*, 2002). *KRAS* and *p53* mutations were present only in the distal colon and rectum and none in the proximal colon (Konishi *et al*, 2004). Somatic mitochondrial DNA (mtDNA) mutations were significantly more prevalent in TSAs than in HPs, SSAs and colorectal carcinomas. These mutations are in the D310 mononucleotide repeat of mtDNA and can be used as a molecular feature to distinguish between TSAs and SSAs (Shimomura *et al*, 2011).

The transition from TSA to serrated carcinoma is associated with *BRAF* or *KRAS* mutations (two variants of TSA), nuclear accumulation of p53 mainly in *BRAF* mutant TSAs and low levels of microsatellite instability (MSI-L) (Fu *et al*, 2012; Han & Zhou, 2011; Konishi *et al*, 2004). There was a significant difference between the number of MSI-H TSAs (21%) and MSI-H conventional adenomas (CADs) (5%), with the TSAs being associated with high-grade dysplasia (HGD) (Konishi *et al*, 2004). A group of colorectal carcinomas was associated with an immediately adjacent SA and most of these were MSI tumours. This indicated that the carcinomas could have possibly originated from a TSA as they exhibited serrated patterns in their epithelium (Makinen *et al*, 2001).

Polyps from patients with HPP were found to be more similar to TSAs than HPs. Seven criteria were listed which would help distinguish a HP-like TSA from a HP - (1) crypt dilation at the base (2) horizontally oriented crypts (3) lack of endocrine cells in large areas (4) nuclear atypia - enlarged, hyperchromatic nuclei with prominent nucleoli (5) overproduction of focal mucus (6) zone of proliferation in the upper and middle portions of the crypt and numerous goblet cells at the crypt base and (7) high frequency of eosinophilia of the cytoplasm. Based on these observations, it was suggested that serrated adenomatous polyposis should be used instead of HPP (Torlakovic & Snover, 1996).

1.5.3.3 Sessile serrated adenoma (SSA)

SSAs are currently classified into SSAs without cytological dysplasia and those with cytological dysplasia. They were initially defined as a subtype of large, sessile, serrated lesions with an abnormal zone of proliferation, dilation of distorted crypts mainly at the base, nuclear atypia and a decrease or absence of cell maturation along the crypt length. In a study by Goldstein and colleagues, this variant form of HPs (HP-like lesions) was identified as a precursor to MSI CRC. These lesions were wrongly diagnosed as HPs and they were termed sessile serrated adenomas (Goldstein *et al*, 2003; Jass *et al*, 2006; Torlakovic *et al*, 2003; Torlakovic & Snover, 1996). SSAs form a small, but significant portion of serrated polyps (7-22%) and represent only 2-9% of the total colonic polyps and are more common in females (65%) (Lash *et al*, 2010; Spring *et al*, 2006). They are more prevalent in the proximal colon unlike the HPs which are mainly found in the distal colon and rectum. Crypt branching, dilation and horizontal crypts are more prevalent in SSAs than in TSAs, while serration is a prominent feature in TSA (Lee *et al*, 2008b).

The crypts of SSAs have a large proportion of goblet cells and the undifferentiated cells are very few or absent and unlike TSAs, ECF is not prevalent in the colonic crypts of SSAs (Sandmeier *et al*, 2007; Torlakovic *et al*, 2008). SSAs are >5mm in diameter, have T- and L-shaped crypts and pseudoinvasion (inverted crypts found below the muscularis mucosa) (Figure 1.15) (Aust & Baretton, 2010). They have increased mitotic activity in the middle regions of the crypt with round to oval shaped nuclei and prominent nucleoli (Farris *et al*, 2008). 33% of SSAs showed a higher proliferative index than HPs (8%) mainly at the crypt base with the proliferation marker,

Ki-67 (Chung *et al*, 2008; Higuchi *et al*, 2005). A large number of SSAs also show a strong staining pattern (>76%) with MUC2 (intestinal mucin) and MUC5AC (gastric mucin). The MUC2 staining was found to be higher than normal in non-mucinous cytoplasm of columnar and goblet cells of SSAs, while the MUC5AC expression was found to be the highest among HPs, TSAs and ADs (Higuchi *et al*, 2005).

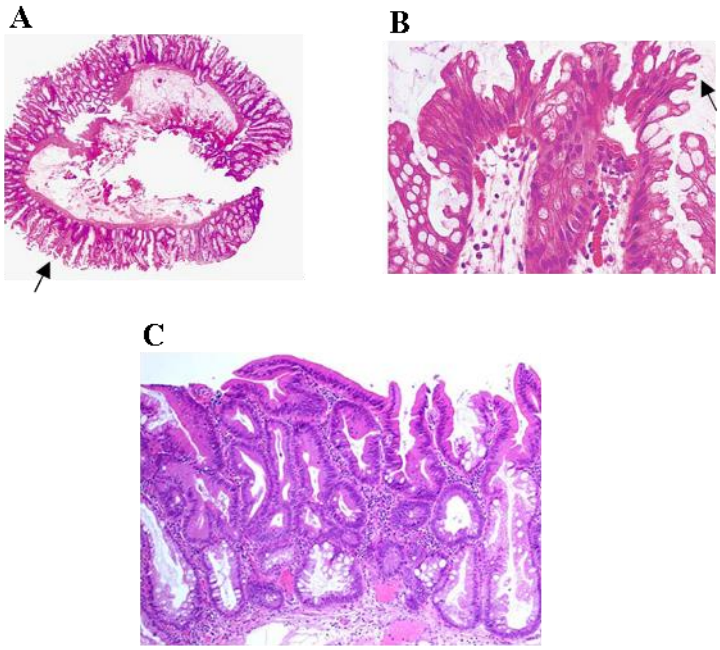

Figure 1.15 - Structure of SSA. *Serration can be observed (arrow) along the entire length of the crypts along with crypt branching* ***(A)****. The upper surface of the SSA appears to be tufted (arrow) and could possibly consist of eosinophilic cells with pseudostratified nuclei* ***(B)****. SSA with dysplastic foci* ***(C)*** *[Adapted from (Sandmeier et al, 2007)]*.

SSAs have a strong association with *BRAF* mutations (78-81%) compared to SAs, but a very low percentage of *KRAS* mutations (3%) (Jass *et al*, 2006; Spring *et al*, 2006). CIMP is also mainly observed in proximal SSAs harbouring *BRAF* mutations. The presence of *BRAF* mutations and similar methylation profiles in SSAs and MSI-H CRCs suggests that SSAs could be the potential precursors of microsatellite unstable colorectal carcinomas (Gaiser *et al*, 2013; Maeda *et al*, 2011). Methylation of genes such as *p16INK4a*, *MGMT, hypermethylated in cancer 1* (*HIC1*), *MINT1*, *RASSF2* and *MLH1* were mainly observed in proximal SSAs. A positive correlation could also be established between MGMT loss and size of SSA (>10 mm) (Higuchi *et al*, 2005; Kim *et al*, 2008). β-catenin immunolabeling revealed abnormal nuclear accumulation in 67%

of SSAs and this percentage varied with the levels of dysplasia. 29% of SSAs without dysplasia displayed abnormal β-catenin expression, while this was present in all the SSAs with dysplasia (Yachida *et al*, 2009). SSAs increase the risk of developing CRC and more synchronous colorectal carcinomas are observed in patients with only serrated lesions compared to those with both SPs and ADs (Vu *et al*, 2011).

A case presented by Oono and colleagues discussed the malignant transformation of a SSA into a carcinoma. The initial lesion identified was a large, proximal HP and after eight months, the resected lesion was diagnosed as an early invasive cancer with TA and SSA components (Oono *et al*, 2009). About 12% of patients with SSAs were diagnosed with low-grade dysplasia (LGD) and this proportion decreased as the SSAs progressed to adenocarcinoma (1%) (Lash *et al*, 2010). The adenocarcinoma arising from a SSA did not necessarily retain the serrated structure and instead developed with tubular adenomatous components. However, this adenocarcinoma did not show any deviation from molecular characteristics associated with a typical SSA such as *BRAF* mutation and increased extracellular production of mucin. HGD and invasive carcinoma areas of SSAs showed aberrant p53 expression and absence of *PIK3CA* mutations. This showed that *BRAF* mutations could possibly play a key role in the malignant transformation of a SSA to CRC (Fujita *et al*, 2011).

1.5.3.4 Mixed polyps (MPs)

The World Health Organization characterised a MP as a combination of an adenoma (like TA, TVA or VA) with varying degrees of dysplasia and a serrated polyp. Based on their components, MPs can be categorised into: SSA and TSA, SSA and CAD, TSA and CAD, HP and CAD (rare) (Figures 1.16 and 1.17) (Aust & Baretton, 2010). Some polyps studied in the 1980's displayed both hyperplastic and adenomatous characteristics and were called mixed hyperplastic adenomatous polyps (MHAP) by Urbanski and colleagues. Major parts of the polyps were serrated, characteristic of a HP with certain areas exhibiting severe dysplasia and the adenomatous part with carcinoma *in situ* (Teoh *et al*, 1989; Urbanski *et al*, 1984).

MHAPs were mainly located in the rectosigmoid region of the colon. About 37% of MHAPs contained dysplastic areas, while 10% had intramucosal carcinoma. MHAPs could possibly trigger CRC in a manner similar to the traditional pathway (Section 1.4.1), but little was known about its malignant potential. Some features in

MHAPs such as elongated and irregular nuclei, surface mitoses and nuclear to cytoplasmic ratio would help distinguish between HPs and MHAPs (Longacre & Fenoglio-Preiser, 1990). MPs are present in very small numbers (0.8-1.7%) (Higuchi *et al*, 2005; Spring *et al*, 2006). The proliferation index of a MP varied depending on the component - if its non-dysplastic, it is similar to a HP or SSA (crypt base), while the dysplastic portion lies between a TSA (base to upper zones of the crypt) and AD (upper and middle zones of the crypt). Loss of MGMT expression was present in only two MPs, one was in the SSA region, while the other was in the dysplastic component (TSA) (Higuchi *et al*, 2005).

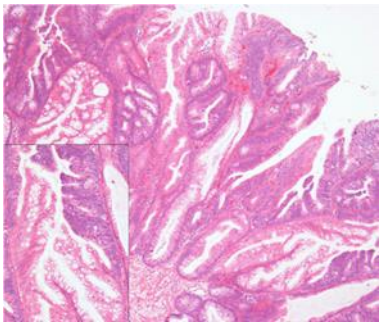

Figure 1.16 - Mixed polyp. *TA with high-grade intraepithelial neoplasia and SSA [Adapted from (Aust & Baretton, 2010)].*

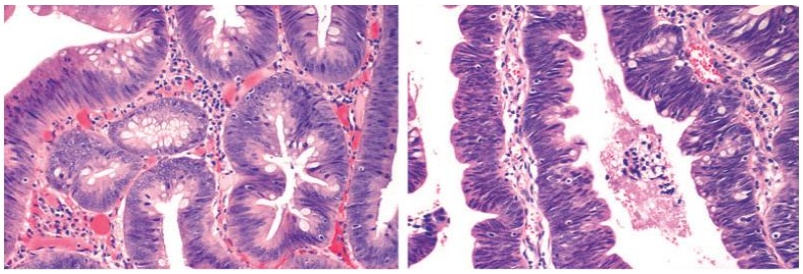

Figure 1.17 - Mixed polyps. *The mixed polyps contain TSA and TVA components and harbour KRAS mutations. The serrated epithelium consists of hyperchromatic nuclei and marked stratification which gives it an adenomatous appearance [Adapted from (Jass et al, 2006)].*

The lesions that comprise a MP have different genetic alterations and it was found that mutations in the *APC* gene were not present in MHAPs with an adenomatous component. Only one MHAP out of 12 had mutations in the *KRAS* gene, while *p53* mutations were present only in the cancerous part of MHAP and none was detected in the benign regions (Uchida *et al*, 1998). However, other studies showed that MPs harbour similar frequencies of *BRAF* (40-57%) and *KRAS* (43-50%) mutations (Jass *et*

al, 2006). The *BRAF* mutations are mainly present in proximal MPs, while a majority of the distal MPs are predisposed to *KRAS* mutations (Spring *et al*, 2006). A large proportion of the MPs had either low levels (MSI-L) or high levels of microsatellite instability (MSI-H) depending on their individual components. MHAPs were initially considered as the intermediate lesions in the development of adenomas from HPs (Fenoglio-Preiser & Hutter, 1985). But due to their rarity unlike HPs, MPs have been considered as a separate group of lesions under the category of serrated polyps and play a role in the serrated neoplastic pathway.

1.6 MOLECULAR FEATURES ASSOCIATED WITH THE SERRATED NEOPLASTIC PATHWAY

The molecular factors essential for the progression of CRC via the serrated athway include *BRAF* mutations, methylation of functional genes, CpG island methylator phenotype (CIMP) and microsatellite instability (MSI).

1.6.1 Prevalence of *BRAF* V600E mutations in CRC and colorectal polyps

Mutations in the *BRAF* gene have been detected in a wide range of cancers including melanoma (59%), CRC (11%), breast cancer (2%) and in ovarian carcinomas (4%). These mutations are somatic and are identified as single-base substitutions (T to A transversion at nucleotide 1796) in exon 15. This involves a substitution of valine with glutamic acid at position 600E (V600E). The V600E substitution results in the insertion of a negatively charged amino acid residue adjacent to a regulatory phosphorylation site. This leads to constitutive activation of BRAF by mimicking normal regulatory phosphorylation without the influence of KRAS. Other *BRAF* mutations like G468A, D586E, F594L and V599M are present in very few cancers (Chan *et al*, 2003; Davies *et al*, 2002).

In the case of cancers with V600E mutations, *BRAF* and *KRAS* mutations were found to be mutually exclusive events. In a study by Chan *et al*, *BRAF* mutations were mainly present in serrated polyps compared with adenomas. About 71% of *BRAF* mutations were present in polyps with mild dysplasia and none were present in lesions with severe dysplasia (Chan *et al*, 2003; Davies *et al*, 2002). Approximately 64% of serrated polyps harboured either *BRAF* or *KRAS* mutations, which suggested the activation of the MAPK pathway could possibly be an initiating event in the serrated

neoplastic pathway (Yang *et al*, 2004). The frequency of *BRAF* mutations was higher in hyperplastic serrated ACF (62.5%) when compared to non-serrated lesions (3%) and none in dysplastic ACF (Rosenberg *et al*, 2007).

Serrated polyps >5mm in size and proximally located (HPs, SAs and MPs) tend to harbour more *BRAF* mutations than serrated polyps present in the distal colon. 77% of CIMP-H cancers and 94% of CIMP-H, MSI-H CRC displayed *BRAF* mutations with 66% being methylated in the promoter region of *MLH1* (Kambara *et al*, 2004). *BRAF* mutations occur only in a minority of adenomas (2.7%) and are related to the villosity of adenomas. Hereditary CRC such as FAP have a very low frequency of *BRAF* mutations in adenomas and are absent in ACF (Beach *et al*, 2005; Yuen *et al*, 2002). However, there is an increased risk in first degree relatives harbouring *BRAF* mutations (12%) which predispose them to develop CRC via the serrated pathway (Wish *et al*, 2010). *BRAF* mutation is strongly associated with sporadic MSI-H CRC and its typical features are older age, proximal location, females, mucinous histology and high tumour grade. But, *BRAF* mutations are not present in MSI-H tumours with Lynch syndrome. The significant association between MSI-H, *BRAF* V600E mutations and CIMP-H in CRC and serrated polyps show that they are key features required for the development of MSI-H sporadic CRC via the serrated neoplastic pathway (Fransen *et al*, 2004; Kambara *et al*, 2004).

1.6.2 Methylation and CpG island methylator phenotype (CIMP)

1.6.2.1 DNA methylation

Methylation is an important epigenetic change that influences the progression of CRC in a significant manner. About 2 to 7% of the total cytosine in mammalian DNA is converted to 5-methylcytosine (m^5Cyt) by enzymatic methyl transfer from *S*-adenosylmethionine (SAM) to the fifth position in cytosine (Figure 1.18A). This methyl group is located in the major groove of the DNA helix and this in turn affects DNA-binding proteins like lac repressor, hormones and protein receptors. In eukaryotic DNA, about 90% of the m^5Cyt residues are found in CpG dinucleotides and also a high proportion in repetitive DNA. Different tissues have varying levels of DNA methylation and some sites may be frequently methylated or unmethylated. This shows that fully

methylated DNA in the sperm could be unmethylated in somatic cells (Drahovsky & Boehm, 1980; Razin & Riggs, 1980).

Aberrant DNA methylation can occur as a result of inactivation of DNA methyltransferases, absence of appropriate cofactors for methylation and chemical modification of DNA binding or methylation sites, which mainly modify guanine (G) residues (Drahovsky & Boehm, 1980; Razin & Riggs, 1980). Methylation sites can be present in three different states - unmethylated, hemi-methylated (methylation in one DNA strand) and fully methylated (symmetrical in both DNA strands). In human DNA, the methylated sites are fully methylated except during replication. A hemi-methylated site is created after replication which is restored to its fully methylated state by a maintenance DNA methyltransferase. In the absence of re-methylation, this hemi-methylated site can become unmethylated during the next replication in one daughter strand (Figure 1.18B) (Schulz, 2005).

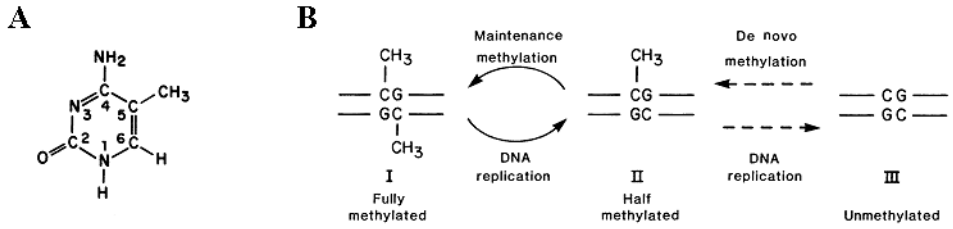

Figure 1.18 - Methylation states. *Structure of 5-methyl cytosine* ***(A)****. There are three DNA methylation states- fully methylated, half or hemi-methylated and unmethylated. Maintenance methylation normally occurs after DNA replication* ***(B)*** *[Adapted from (Razin & Riggs, 1980)]*.

1.6.2.2 DNA Methyltransferase

DNA methyltransferase catalyses two main functions - maintain identical methylation patterns following semi-conservative DNA replication and initiate methylation in umethylated regions (Drahovsky & Boehm, 1980). Methylated CGs are converted into hemimethylated states during DNA replication and they are rapidly converted into methylated CGs without the methylation of any unmethylated CG residues (Hermann *et al*, 2004). DNMT1 is responsible for maintaining the somatic methylation patterns in cells and is also implicated in a major portion of the global and gene-specific methylation observed in cancer cells and CpG islands. DNMT1 is mapped to chromosome 19 and is involved in maintaining hypermethylation in tumour cells

which results in the transcriptional silencing of key tumour suppressor genes (Robert *et al*, 2003; Yen *et al*, 1992). DNMT1 preferentially methylates hemimethylated DNA up to 1000 bp in a quick, accurate and processive manner, while it functions in a slow and distributive manner in unmethylated DNA (Hermann *et al*, 2004). The alternative splicing of *DNMT1* gives rise to DNMT1-a and DNMT1-b, with the latter exhibiting about 40-70% of expression levels of DNMT1 mRNA (Hsu *et al*, 1999).

The other methyltransferase enzymes responsible for different methylation-related functions are DNMT2, DNMT3a and DNMT3b (Kanai *et al*, 2001). The combined presence of DNMT1 and DNMT3a stimulates *de novo* methylation, which depends on the expression of these enzymes - high levels of DNMT3a increases *de novo* methylation, while an inverse relationship exists between *de novo* methylation and DNMT1 expression. Methyltransferases - DNMT1, DNMT3a and DNMT3b are required for efficient *de novo* and maintenance methylation in cells, while DNMT2 is not an essential component of *de novo* methyltranferase family. DNMT3a is a non-processive enzyme, which transfers some methyl groups to a target domain. These methyl groups are involved in the recruitment and activation of DNMT1 for *de novo* methylation and methylate the target sequence (Fatemi *et al*, 2002; Okano *et al*, 1998). A significant association exists between CIMP and over expression of maintenance methyltransferase DNMT1. In stomach and colon cancers, the levels of DNMT1 and DNMT3b were elevated, while the expression of DNMT2 was lower than normal mucosa and DNMT3a showed no change in mRNA levels (Kanai *et al*, 2001).

1.6.2.3 CpG island methylator phenotype (CIMP) in CRC

A prominent feature in CRC is the methylation of CpG islands at the 5' region which inhibits transcription and suppresses gene expression (Figure 1.19) (Bird, 1986). CpG islands (CGI) are 0.5 to 2 kb stretches of sequences which are rich in cytosine-guanine dinucleotides and are mainly present at the transcription start site in the basal promoter region (Schulz, 2005). Toyota and colleagues classified methylation patterns in CRC into two categories - type A or age-specific methylation and type C or cancer-specific methylation. In type A, about 75% of the tumours were methylated and low levels of methylation were also detected in normal mucosa, which increased with age. No methylation was detected in normal mucosa of type C and methylation was exclusively present in a small group of colorectal tumours (10 to 50%). CRC exhibited

high type C methylation levels in 3 or more loci and this novel feature was described as the CpG island methylator phenotype (CIMP). CIMP showed a significant association with proximal cancers (82%) and indicates the potential for silencing key tumour suppressor genes (Toyota *et al*, 1999).

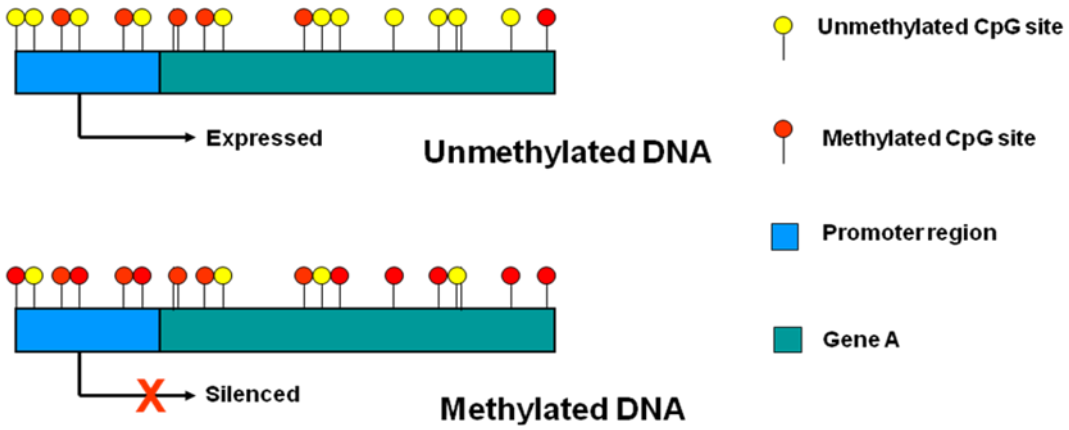

Figure 1.19 - Effect of CpG island methylation on gene expression. *CpG island methylation is mainly found in the promoter regions of genes. CpG islands display low methylation levels in normal, unmethylated DNA, which results in gene expression. Hypermethylation of the promoter region in methylated DNA results in gene silencing.*

The selection and design of a methylation assay plays an important role in the detection and evaluation of methylation levels. The initial methylation detection assay involved the digestion of DNA using a methylation sensitive restriction enzyme and analysis of the restriction digested products by Southern blotting or PCR (Razin & Riggs, 1980). This assay was not very sensitive in detecting methylation levels in small or mixed DNA samples and interpretation of sequencing gels generated some false positive results. In order to address these issues, another assay was developed based on deamination (removal of an amine group) reactivity patterns of cytosine and 5-methylcytosine. Single-stranded DNA was treated with sodium bisulphite, which causes deamination of cytosine resulting in thymine, while the 5-methylcytosine residues remain unchanged. This was followed by PCR and the amplified fragments were cloned into M13mp19 and the individual clones were sequenced by the chain-termination method (Frommer *et al*, 1992).

In 1996, a novel method called methylation specific PCR (MSP) was developed to rapidly detect CpG island methylation, which eliminated the need for cloning after PCR analysis. MSP is more rapid and sensitive than the other methylation assays and methylation levels in paraffin-embedded samples could also be analysed (Herman *et al*, 1996). A major breakthrough in methylation studies came in the form of MethyLight - a fluorescence-based, quantitative real time PCR assay. The bisulphite-treated DNA is amplified using locus-specific primers flanking an oligonucleotide probe, which contains a 5′ fluorescent reporter dye and a 3′ quencher dye. The sequence variations in the CpG dinucleotides can be identified based on methylated and unmethylated sites (Eads *et al*, 2000).

The choice of methylation markers can greatly influence the outcome of methylation status of samples. Initial methylation studies were carried out with methylation markers including *p16INK4A* (*CDKN2A*), *MLH1* and the *MINT* panel-*MINT1*, *MINT2* and *MINT31* which comprised the classic CIMP panel (Rashid *et al*, 2001; Toyota *et al*, 1999; Toyota *et al*, 2000). A new panel of methylation markers was identified by Weisenberger *et al* in 2006 from 2002 possible five-marker panels. They screened 195 MethyLight markers against five CIMP positive and five CIMP negative tumours and after the first screening, 92 cancer-specific methylation markers were identified which included the classic CIMP panel. The new five-marker CIMP panel, which is currently being used comprises *IGF2*, *SOCS1*, *RUNX3*, *CACNA1G* and *NEUROG1* and is more sensitive in identifying methylation patterns in *BRAF* and MSI-H sporadic CRC in comparison to the classic panel (Weisenberger *et al*, 2006).

Based on methylation status of the classic CIMP panel, Toyota *et al* classified CRC tumours into 1) CIMP positive tumours - MSI, *KRAS* and *TGFβRII* mutations and 2) CIMP negative tumours - mainly *p53* mutations along with few ‘classical’ genetic changes. CIMP, *p16INK4a* methylation and mutations in *p53* are considered to be early events in CRC progression due to their high frequency in preneoplastic adenomas. *p53* mutations were more prevalent in CIMP negative cancers and showed an inverse correlation with *p16INK4a* methylation (Toyota *et al*, 2000). A strong association exists between CIMP-H, *BRAF* V600E mutations, MSI-H and proximal location in CRC tumours (Weisenberger *et al*, 2006). Survival rates of patients reduced considerably in cases of MSS, CIMP-H tumours with *BRAF/KRAS* mutations compared to MSI-H tumours with the same criteria (Lee *et al*, 2008a). Methylation of *MLH1* is an important

factor in the development of MSI-H, CIMP-H tumours and is also responsible for the carcinomatous transformation of HPs (Chan *et al*, 2002).

In adenomas, the number of CIMP negative cases was higher than CIMP-H adenomas and this number varied with the extent of villosity and the polyp size. Incidences of methylation and CIMP status increased in the adenoma group based on villosity and size with large TVAs and VAs showing high levels of methylation. In adenomas, methylation showed no significant association with *KRAS* and *p53* mutations or loss of chromosome 18q and was inversely related with MSI status. Adenoma villosity and large size are two important factors that could predispose a lesion to transform into invasive carcinoma and along with methylation, this risk increases (Rashid *et al*, 2001).

HPs obtained from patients with hyperplastic polyposis showed equal frequencies of CIMP-H and CIMP negative, while sporadic HPs were classified as CIMP negative. All the proximally located HPs were methylated, while only 22% of distal HPs were methylated. None of the CIMP-H HPs had *KRAS* mutations or chromosomal loss in 1p. About 75% of TSAs were CIMP-H and a similar percentage of polyps were CIMP-L and CIMP negative (12%) (Chan *et al*, 2002). Methylation of *p14*, *TIMP metallopeptidase inhibitor 3* (*TIMP3*), *fragile histidine triad* (*FHIT*), *MGMT*, *solute carrier family 5 (sodium/monocarboxylate cotransporter), member 8* (*SLC5A8*) and *p16INK4a* increased significantly in proximal TSAs with low-grade atypism (21.05%) and hyperplastic areas to TSAs with carcinomas (37.72%) (Dong *et al*, 2005). There is a marked difference in the CIMP status in adenomas and serrated polyps and increasing levels of methylation followed by transcriptional silencing of important genes shows strong evidence of the role played by CIMP in the early stages of the serrated pathway.

1.6.3 Microsatellite instability (MSI)

Microsatellite instability (MSI) is a distinct feature and mainly occurs in cancers of the proximal region of the colon (Thibodeau *et al*, 1993). Microsatellites are repetitive sequences and any change in their repeating units due to insertions or deletions when compared to normal tissue leads to MSI (Boland *et al*, 1998; Schulz, 2005). MSI is identified by the presence of additional bands in PCR-amplified tumour DNA in comparison to the corresponding normal DNA. Depending on the number of

unstable loci, the tumours are classified as MSI (two or more unstable loci) and MSS (less than two unstable loci) (Bocker *et al*, 1997).

A panel of five markers *BAT25*, *BAT26* (mononucleotide repeating unit), *D5S346*, *D2S123* and *D17S250* (dinucleotide repeating unit) also known as the NCI (Bethesda) panel markers are used to classify tumours into microsatellite instability high (MSI-H) and microsatellite instability low/ microsatellite stable (MSI-L/MSS) (Boland *et al*, 1998; Dietmaier *et al*, 1997). MSI is a characteristic feature of Lynch syndrome and is also associated with a large number of HPs and TSAs (MSI-L) which give rise to about 10% of MSI-L CRC via the serrated pathway (de la Chapelle, 2004; Iino *et al*, 1999). MSI is significantly associated with tumours present in the proximal colon and in women; low stage and poor differentiation and these features result in a reduced five-year survival rate (Samowitz *et al*, 2001).

1.7 BIOLOGICALLY RELEVANT GENES ASSOCIATED WITH CRC

1.7.1 The INK4a locus

Mutations of *p16INK4a* in a majority of the tumours mainly target exon 2 and results in structural alterations of p16INK4a and p19ARF and causes *p16INK4a* gene silencing (Quelle *et al*, 1997). Absence of *p16Ink4a* in $Kras^{G12Dint}$/ *p16Ink4a*/$Arf^{-/-}$ mice resulted in cellular hyperproliferation in the colon, elongation of folds in the proximal colon and hyperplasia leading to the development of TSAs exclusively in the proximal colon in more than 50% of the mice. In about 76% of the mice, the TSAs developed into invasive adenocarcinoma and 62% of these cancers metastasized to the lung. In human colonic polyps and serrated adenocarcinomas, the level of p16INK4a increased with dysplasia and showed an inverse relation with the expression of the proliferation marker, Ki67. p16INK4a expression was detected by immunohistochemical staining in about 78% of colorectal tumours. Loss of p16INK4a expression was observed in one advanced adenocarcinoma with metastasis. Promoter hypermethylation of *CDKN2A* was the main cause behind this down regulation or loss of expression of p16INK4a (Bennecke *et al*, 2010; King-Yin Lam *et al*, 2006). *p16Ink4a* mutations in *Braf* V600E-induced mice caused widespread epithelial hyperplasia in the small intestine, while loss of p16Ink4a expression results in tumour formation in organs such as the lung, liver and

stomach. *Braf* V600E mutations were also found to induce CpG island methylation in exon 1 of *p16Ink4a* (Carragher *et al*, 2010).

1.7.2 p19/p53 pathway

p53 mutations are observed in 55-62% of CRC mainly between exons 5 and 8 which contain the functional domain required for DNA binding. The mutations are mainly G→A transitions and mutational rate increases with invasiveness of the cancer (Bond *et al*, 2012; Rubio & Rodensjo, 1995; Smith *et al*, 2002; Suehiro & Hinoda, 2008). p53 expression is higher in TSAs and dysplastic ACF in comparison with HPs, SSAs and hyperplastic ACF (Das *et al*, 2008; Ngo *et al*, 2010). Tumours with *p53* mutations are mainly MSS (*BRAF* mutant or wild-type) and distally located in the colon (Bond *et al*, 2012; Morikawa *et al*, 2012). An inverse relationship exists between *p53* and *KRAS* mutations and methylation of *p14ARF* (Kominami *et al*, 2009; Shen *et al*, 2003). *p14ARF* methylation could possibly be an early event in the progression of colorectal lesions and is also significantly linked to lower survival rates in CRC patients (Esteller *et al*, 2000; Nilsson *et al*, 2013). CIMP-H and MSI-H CRCs show a positive correlation with *p14ARF* methylation and an increase in frequency of *p14ARF* methylation is observed in *KRAS* mutant MSI-L CRC. Results show that methylation of *p14ARF* could be an important molecular entity for the development of MSI-L CRC via distinct pathways (Kominami *et al*, 2009; Shen *et al*, 2003).

1.7.3 Wnt pathway and β-catenin

Wnt pathway regulates cell proliferation, differentiation, apoptosis and epithelial-mesenchymal interactions (Behrens, 2005; Smalley & Dale, 1999). β-catenin is an important component of the Wnt pathway and has been implicated in colorectal tumorigenesis (Stanczak *et al*, 2011). In normal colonic cells and a majority of HPs, positively stained cells for β-catenin were observed only in the plasma membrane. The β-catenin staining pattern extended to the cytoplasm and nucleus in adenomas and adenocarcinomas (Iwamoto *et al*, 2000). Membranous β-catenin expression was significantly higher in TSAs compared to TAs; however, nuclear accumulation of β-catenin (activation of Wnt pathway) was more prevalent in TAs than in TSAS. In SSAs and HPs, nuclear β-catenin expression was predominant in proximally located polyps,

which suggests that Wnt activation could be an early event in the serrated pathway (Li *et al*, 2013).

1.7.4 IGFBP7

IGFBP7 methylation was analysed in colorectal tumours and adenomas and was correlated with various factors such as *BRAF*, *KRAS* and *p53* mutations; methylation of *p16INK4a* and *MLH1*; CIMP and MSI status. *IGFBP7* methylation in colorectal tumours showed a strong correlation with *BRAF* mutation, CIMP, MSI and *MLH1* and *p16INK4a* methylation. In adenomas, about 18% exhibited *IGFBP7* methylation and none of the adenomas showed *MLHI* methylation or MSI and this suggested that *IGFBP7* silencing is an early event in CRC progression (Suzuki *et al*, 2010). A study by Ruan and colleagues revealed that patients with IGFBP7 expression had a much better survival rate than those with silenced IGFBP7 gene expression. This epigenetic silencing of IGFBP7 is due to hypermethylation of exon 1 in colorectal tumours (Lin *et al*, 2007; Ruan *et al*, 2006). In IGFBP7 a p53-responsive element (p53-RE) was identified in intron 1 which indicated that IGFBP7 is directly targeted by p53. The region around the p53-RE is constantly methylated in normal tissues regardless of the gene expression and results showed that p53-dependent activation of IGFBP7 can be blocked due to hypermethylation (Suzuki *et al*, 2010).

Inducing BRAF V600E in melanocytes increased the level of IGFBP7 and this combination was introduced into naive melanocytes which resulted in a proliferation block mainly due to senescence. Low level of IGFBP7-regulated melanocyte proliferation and an increase in IGFBP7 expression triggered BRAF V600E-mediated senescence in melanocytes. *BRAF* mutated-melanoma cell lines do not express IGFBP7, while low levels of IGFBP7 are present in cell lines with *KRAS* mutations. Inducing IGFBP7 expression in these cells resulted in cellular growth inhibition and senescence in the presence of *BRAF* mutations, but showed no proliferation block in cell lines with wild-type BRAF (Wajapeyee *et al*, 2008).

The levels of IGFBP7 expression varied with normal human skin cells - low, but detectable levels; nevi - high levels with BRAF V600E; and melanocytes - no expression in BRAF V600E cells, but expressed in wt-BRAF melanomas. BRAF-MEK-ERK signalling pathway activates IGFBP7 which is present downstream of this pathway. BRAF V600E increases BRAF-MEK-ERK signalling and this generates a

signal that initiates proliferation. Inhibition of the BRAF-MEK-ERK signalling pathway resulted in a proliferation block in the presence of IGFBP7 and this helps activate the IGFBP7-mediated apoptosis pathway via autocrine/paracrine signalling (Figure 1.20) (Wajapeyee *et al*, 2008).

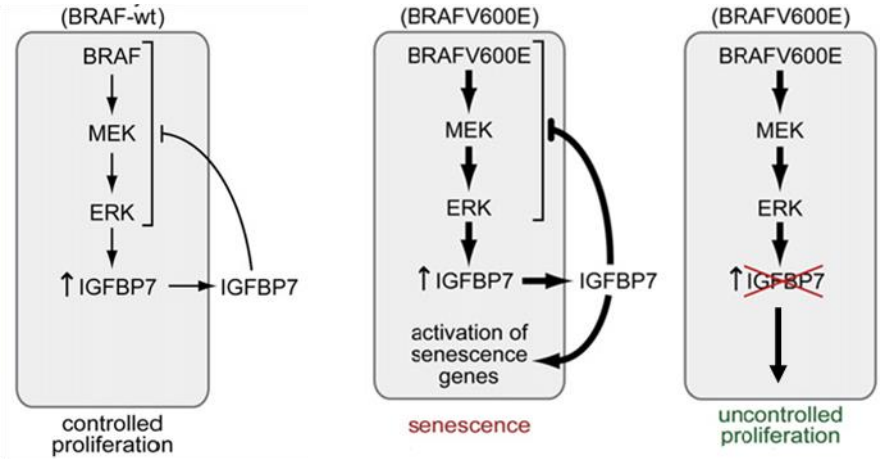

Figure 1.20 - Hypermethylation of IGFBP7 promoter in BRAF V600E: *The above figure is a schematic summary of BRAF V600E-mediated senescence and colorectal tumour progression. In the wild-type BRAF polyps, the proliferation is controlled, while in polyps harbouring BRAF mutations, the activation of the MAPK pathway increases expression of IGFBP7 and activates senescence. In certain BRAF V600E-positive polyps like the serrated ones, the IGFBP7 expression is lost and hence the cells escape senescence [Adapted from (Wajapeyee et al, 2008)].*

A study by Wajapeyee and colleagues showed that suppression of tumours in metatstatic melanoma mouse model and human CRC mouse xenografts could be achieved by the induction of IGFBP7 (Wajapeyee *et al*, 2009). The combination of *BRAF* V600E mutations and up regulation of IGFBP7 in triggering the senescence pathway is debatable. In a study by Scurr and colleagues, IGFBP7 expression was repressed by induction of *BRAF* V600E in fibroblasts and melanocytes and this occurred before *BRAF*-mediated senescence. This showed that *BRAF* V600E induces p16INK4a expression and mediates senescence irrespective of the level of IGFBP7 expression (Scurr *et al*, 2010).

Earlier reports identified a strong association between *BRAF* mutations and IGFBP7 expression in CRC cell lines, colorectal tumours and melanomas, but this was not observed in a series of melanoma cell lines and human benign nevi by Scurr and

colleagues. *BRAF* V600E mutations were found to down regulate IGFBP7 expression which contradicted the findings by Wajapeyee and colleagues. These results showed that IGFBP7 was not a key factor in the development of *BRAF* mutant melanomas and was not involved in activation of *BRAF*-induced senescence (Scurr *et al*, 2010). In response, Wajapeyee and colleagues confirmed their previous results stressing the role IGFBP7 plays in regulating BRAF-mediated senescence in melanomas. They pointed out that the cell populations being analysed for senescence were different in the study by Scurr and colleagued and this could be the reason behind their inability to detect IGFBP7-related proteins in *BRAF*-induced senescence. Results showed that loss of IGFBP7 expression could be observed in melanomas harbouring *BRAF* V600E mutations and IGFBP7 is an essential requirement in driving the senescence pathway along with *BRAF* V600E induction (Wajapeyee *et al*, 2010).

1.8 MOUSE MODELS AND TARGETING GENE EXPRESSION

1.8.1 Cre mediated recombination

In 1981, Sternberg and Hamilton characterized a highly efficient site-specific recombination system in bacteriophage P1. This site contained two essential components – *loxP* and a recombinase gene – Cre. The Cre recognizes the *loxP* (locus of X-over of P1) site which is a 34-bp region and causes the recombination of the sequences between the *loxP* sites. The orientation of the *loxP* sites determines if it will be a recombination (directly repeated *loxP* sites) or an inversion (*loxP* sited in inverted orientation) (Sauer, 1998; Sternberg & Hamilton, 1981). Different gene regulatory systems have been developed to establish inducible models to turn on gene expression only when required based on Cre-mediated recombination. Some of these regulatory systems include isopropyl beta-D-thiogalactoside (IPTG), tetracycline (tet), chemical inducers of dimerization (CID)-based, estrogen-based and mutated progesterone receptor ligand binding domain (PRLBD) (Burcin *et al*, 1998).

1.8.2 Braf mouse models

A number of mouse models have been developed to study the effect of *Braf* mutation in various diseases. The $BRaf^{CA}$ mouse which was developed by Dankort and colleagues was used in our study to evaluate the effect of *Braf* V600E mutations in

colorectal cancer. This conditional mouse was originally employed to study *Braf* mutations in the initiation, development and progression of lung tumours which was induced by Cre recombinase expressed by adenovirus (Ad-Cre) (Dankort *et al*, 2007). This *BRaf*^{CA} mouse was also used to analyse the effect of oncogenic *Braf* in melanocytes. The *BRaf*^{CA} mouse was crossed with a mouse carrying the *CreER*^{T2} gene under the control of the *Tyrosinase* promoter (Tyr::CreER transgene). The loss of *Pten* along with *Braf* mutation was also assessed in the promotion and invasion of metastatic melanoma (Dankort *et al*, 2009).

Another colon-based *Braf* mouse model was developed by Carragher and colleagues to study the effect of oncogenic *Braf* mutation in the gastrointestinal tract. A conditional *Lox-Stop-Lox-Braf*^{V600E} (*LSL-Braf*^{V600E}) mouse was employed to assess the progression of CRC via the serrated pathway. This mouse was crossed with the Ah*cre*ER^{T} mouse (Cre recombinase) to enable the induction of *Braf* mutation (Carragher *et al*, 2010). The *LSL-Braf*^{V600E} mouse strain was also employed to assess oncogenic *Braf* in embryonic development using a tyrosinase-drive Cre recombinase which directs the Cre expression to only melanocytes or the eye (retinal pigmented epithelium) with the help of tissue specific distal regulatory elements (Dhomen *et al*, 2010). Rad and colleagues recently reported another inducible *Braf* mouse model (*Braf*$^{LSL\text{-}V637E/+}$), which was crossed with *Villin-Cre* (*Vil-Cre*). This was then employed to assess the effect of oncogenic *Braf* in colorectal tumorigenesis via the serrated pathway (Rad *et al*, 2013).

1.8.3 p16Ink4a and p19Arf mouse models

The *p16Ink4a* and *p19Arf* mice utilized in this study were developed by Sharpless and colleagues. The *p16Ink4a* mouse was generated by a targeted germline deletion of exon-1α which included the translation start site and the first 35 codons of *p16Ink4a* and a Cre-mediated deletion of the neomycin-resistance cassette (*p16Ink4a*$^{+/-}$ mice crossed with Ella-Cre mice) (Sharpless *et al*, 2001). The *p19Arf* mouse model was similar to the *p16Ink4a* mouse in which a premature stop codon was generated in exon-1β (Sharpless *et al*, 2004).

The *p16Ink4a* and *p19Arf* mice were used in different types of cancer-based studies. These include the effect of *p16Ink4a* loss in pancreatic ductal adenocarcinoma,

analysis of different tumour suppressor mechanisms in the development and progression of lung cancer and assessing UV-induced melanomas (Bardeesy *et al*, 2006; Ji *et al*, 2007; Kannan *et al*, 2003). The tumour suppressors - *p16Ink4a* and *p19Arf* were also known to increase the risk of embryonal rhabdomyosarcoma (RMS) and UV-induced cutaneous malignant melanoma. *p16Ink4a* and *p19Arf* knockout mice were utilized to explore this aspect along with mice expressing the Met ligand hepatocyte growth factor/scatter factor (Ha *et al*, 2007). In my study, the *p16Ink4a* and *p19Arf* mice were employed to assess the effects of *p16Ink4a* or *p19Arf* loss along with *Braf* mutation in the initiation and progression of colorectal lesions and tumours.

1.9 SIGNIFICANCE OF THE STUDY

The serrated pathway has been recently identified and the molecular factors involved have not been fully characterised. Studies show an overlap of different pathways that lead to different subtypes of CRC and this will be investigated further. The aim of my doctoral studies is to investigate the mechanisms that underlie the serrated neoplastic pathway, which drives the progress of specific subsets of serrated polyps to carcinoma. The hypothesis that I will test is that oncogenic *BRAF* V600E mutation, combined with CIMP associated epigenetic silencing of *p16INK4a* and *IGFBP7* results in the initiation and progression of large proximally located serrated polyps.

BRAF V600E mutation has been closely linked to CRC and along with other molecular changes causes the development and progression of lesions via the serrated pathway. Methylation is also a key epigenetic factor which results in the silencing of important tumour suppressor genes. Studying the effect of *BRAF* mutation alone or in combination with loss of tumour suppressor genes such as *p16INK4a* and *p14ARF* (*p19Arf* in mice) would shed some light on the unknown aspects of the serrated pathway. In recent studies, the use of methylation and expression arrays has helped in the identification of numerous genes associated with the serrated pathway. This ever increasing gene list indicates the complexity of the serrated pathway and a complete understanding would be vital in reducing the incidence of CRC.

1.10 SPECIFIC AIMS OF RESEARCH PLAN

- Determine the *p16INK4a and IGFBP7* promoter hypermethylation and expression pattern in human colorectal cancers and serrated polyps stratified by *BRAF* mutation and CIMP.
- Conduct a detailed functional assessment of the tumour phenotype resulting from conditional oncogenic BRAF expression within the colon and small intestine of $BRaf^{VE}$ mice.
- Assess the interaction of *BRAF* V600E mutation with the cell cycle regulators, *p16Ink4a* and *p19Arf* using mouse models.

CHAPTER 2

MATERIALS AND METHODS

2. MATERIALS AND METHODS

2.1 CIMP AND METHYLATION OF *p16, IGFBP7* AND *MLH1*

2.1.1 Patient samples

A cohort of 154 serrated polyps and 63 adenomas were used in this study. All of these polyps were obtained from 112 patients derived from a larger consecutive unselected series of 189 patients who underwent colonoscopy at the Royal Brisbane and Women's Hospital (RBWH) in 2003 as previously described (Spring *et al*, 2006). All the patients gave written informed consent, and the Human Research Ethics Committee at the RBWH approved the study. Patients with familial adenomatous polyposis (FAP), hereditary non-polyposis CRC (HNPCC) and hyperplastic polyposis (HPP) were excluded from this study. Polyp location, histology, gender and polyp size were recorded at the time of collection. The 217 polyps included in this study consisted of 35 sessile serrated adenomas (SSAs), 3 traditional serrated adenomas (TSAs), 7 mixed polyps (MPs), 59 goblet cell (GC) hyperplastic polyps (HPs), 50 microvesicular (MV) hyperplastic polyps (HPs), 11 tubulovillous adenomas (TVAs) and 52 tubular adenomas (TAs). The 154 serrated polyps identified from the original series were from 75 patients, whilst the remaining patients (114) had adenomas only. Of the 154 serrated polyps in this study, a further seven GCHPs, four MVHPs and one SSA were excluded due to failure of these samples to amplify in the MethyLight assay. Fifty colorectal tumours were selected from the tumour bank of the Conjoint Gastroenterology Laboratory, QIMR Berghofer Medical Research Institute. The tumours were selected based on their *BRAF* and CIMP status - 26 *BRAF* mutant/CIMP-H cancers and 25 *BRAF* wt/ CIMP-negative cancers (controls).

2.1.2 DNA extraction from formalin-fixed, paraffin-embedded (FFPE) tissue

Two 15 μm sections were cut from paraffin blocks and transferred to an eppendorf tube which contained 200 μl 0.5% Tween-20 in 1X Tris-EDTA (TE) buffer (10 mM Tris, 1 mM EDTA, pH 8). The samples were vortexed and incubated at 90 °C for 10 min to melt the wax and then cooled to 55 °C. The samples were digested with 2 μl of 20 mg/ml Proteinase K (Sigma-Aldrich, St. Louis, USA) for 3 h at 55 °C with gentle mixing. The digested solution was then incubated at 99 °C for 10 min with 200 μl of freshly prepared 5% Chelex-100 (Bio-Rad Laboratories, Inc., Hercules, USA) in 1X

TE (pH 8). The samples were mixed and centrifuged at 10,600 rpm for 15 min and then placed on ice for 2 min. The hardened wax layer was lifted off using a pipette tip. The samples were heated at 45 °C and 200 µl of chloroform was added. The solution was mixed and centrifuged at 10,600 rpm for 15 min. The upper phase, which contained the DNA was removed and transferred to a new eppendorf tube.

2.1.3 *Sss*1 treatment of control DNA for MethyLight assay

The *Sss*1 treatment methylated all the cytosine residues within the double stranded dinucleotide recognition sequence (5′-CG-3′). The 20 µl reaction mix consisted of 1 µg DNA, 1X NEBuffer 2 (New England Biolabs, Ipswich, USA) (5 mM NaCl, 1 mM Tris-HCl, 1 mM $MgCl_2$ (Life Technologies Corporation, Carlsbad, USA), 0.1 mM dithiothreitol), 320 µM S-adenosylmethionine (New England Biolabs, Ipswich, USA) (SAM) and 2 U CpG Methyltransferase (M.*Sss*1) (New England Biolabs, Ipswich, USA). The samples were incubated for 2 h at 37 °C followed by heat-inactivating the enzyme at 65 °C for 20 min. One-tenth of the volume of 3 M sodium acetate was added to the tubes and mixed. The tubes were inverted with two volumes of cold 100% ethanol and placed at room temperature for 15 min to precipitate DNA. The samples were centrifuged at 13,200 rpm for 20 min at 4 °C and the supernatant was discarded. The samples were then mixed with 2.5 volumes of cold 70% ethanol and centrifuged at 13,200 rpm for 2 min at room temperature. This was followed by centrifugation at 13,200 rpm for 20 min at 4 °C. The supernatant was discarded and the DNA pellet was air dried and resuspended in 10 µl of PCR grade water.

2.1.4 Bisulfite modification of DNA

Bisulfite modification of DNA was carried out using EpiTect Bisulfite kit (Qiagen, Venlo, Netherlands) according to manufacturer's instructions. The bisulfite mix was dissolved in 800 µl of RNase-free water and vortexed until completely dissolved. A typical bisulfite reaction was a 140 µl reaction mix which included 500 ng DNA, 85 µl dissolved Bisulfite mix, 35 µl DNA Protect Buffer and PCR grade water. The sample tubes containing DNA were mixed and placed in a thermal cycler (Bio-Rad Laboratories, Inc., Hercules, USA). DNA was then bisulfite treated using the following cycling conditions: denaturation at 99 °C for 5 min, incubation at 60 °C for 25 min,

denaturation at 99 °C for 5 min, incubation at 60 °C for 85 min, denaturation at 99 °C for 5 min, incubation at 60 °C for 175 min and an indefinite hold at 20 °C.

After the bisulfite conversion, the samples were transferred to sterile tubes and 560 µl of loading buffer (Buffer BL) containing 10 µg/ml of carrier RNA was added. The tubes were mixed and the solution was transferred to EpiTect spin columns and centrifuged at 13,200 rpm for 1 min. The flow-through was discarded and 500 µl of wash buffer (Buffer BW) was added to the spin columns. The samples were centrifuged at 13,200 rpm for 1 min and the flow-through was discarded. The tubes were incubated at room temperature with 500 µl of desulfonation buffer (Buffer BD) for 15 min. The spin columns were centrifuged at 13,200 rpm for 1 min and washed with 500 µl of wash buffer (Buffer BW) twice. The final flow-through was discarded; the spin columns were placed into new collection tubes and were centrifuged at 13,200 rpm for 5 min. The spin columns were then placed into sterile 1.5 ml tubes and eluted with elution buffer (Buffer EB) in three elution steps (30 µl, 20 µl, 20 µl) and centrifuged at 13,200 rpm for 1 min.

2.1.5 Bisulfite modified DNA standards and samples for MethyLight assay

DNA was extracted from normal colonic mucosa obtained from patients and was subjected to *Sss*1 treatment (Section 2.1.3) and bisulfite modification (Section 2.1.4). A four-fold serial dilution series was prepared for generating standard curves - Standards 1 to 5 for MethyLight assay. The bisulfite modified DNA from polyps and tumours were diluted for the MethyLight assay (1 in 8 dilution).

2.1.6 MethyLight assay

The CIMP status in the bisulfite modified samples was assessed with the Weisenberger *et al* panel of CIMP markers - *IGF2*, *SOCS1*, *NEUROG1*, *RUNX3* and *CACNA1G* (Table 2.1) (Weisenberger *et al,* 2006). A 10 µl reaction mix consisted of 5 µl 1X Absolute QPCR Mix (Thermo Fisher Scientific, Waltham, USA), 0.4 µM forward primer (FP), 0.4 µM reverse primer (RP), 0.1 µM probe, 2 µl of bisulfite modified DNA (diluted). The methylation of *ALU* (housekeeping gene/standard), *MLH1*, *p16* and *IGFBP7* were also analysed using the MethyLight assay with the following cycling conditions - enzyme activation for 15 min at 95 °C for all runs; *ALU*, *IGFBP7*, *MLH1*, *NEUROG1* and *CACNA1G*: 15 sec at 95 °C and 60 sec at 60 °C, *IGF2*, *SOCS1* and *p16*:

10 sec at 95 °C and 30 sec at 60 °C and *RUNX3*: 15 sec at 95 °C and 60 sec at 62 °C. The samples were run on the Rotor-Gene 3000 (Qiagen, Venlo, Netherlands). The level of methylation was calculated based on the percentage of methylated reference (PMR) of each sample with *ALU* as the standard. Polyps and cancers were considered to be methylated if they had PMRs ≥7 and ≥10 respectively. They were designated as CIMP-H if three or more of the panel markers were methylated. The methylation and CIMP status of the polyps were correlated with *BRAF* V600E and *KRAS* mutations, polyp location, size, histology and patient gender.

2.1.7 Screening for *BRAF* V600E mutations

Allele-specific real-time PCR was carried out to detect *BRAF* V600E mutations in exon 15 which was considered as the hotspot for mutations. Two forward primers, each specific for the wild type (V) and the mutated variant (E) and one reverse primer (AS) were designed (Table 2.1). The bases in italics represented the polymorphic base and the bases in bold constituted the 17-bp GC clamp incorporated at the 5′ end of the mutant forward primer. A 3′ mismatch was also added to the mutant and wild type forward primers as represented by the lower case bases. The reaction mix (16 µl) consisted of 1X Platinum® SYBR® Green qPCR SuperMix-UDG (Platinum® *Taq* DNA Polymerase, SYBR® Green I dye, Tris-HCl, KCl, 3 mM $MgCl_2$, 200 µM dGTP, 200 µM dATP, 200 µM dCTP, 400 µM dUTP, uracil DNA glycosylase (UDG) and stabilizers) (Life Technologies Corporation, Carlsbad, USA), 3 µM forward primer (V), 9 µM mutant forward primer (E) and 3 µM reverse primer (AS) for amplifying 20 ng of genomic DNA. The PCR products were amplified followed by a melt curve analysis on the Rotor-Gene 3000 using the following cycling conditions: 50 °C for 2 min, 95 °C for 2 min followed by 40 cycles of 95 °C for 15 sec and 60 °C for 60 sec. During post amplification, samples were further subjected to a temperature ramp ranging from 72 °C to 95 °C, with a gradual increase in temperature by 1 °C/sec.

2.1.8 *KRAS* mutation analysis

Codons 12 and 13 of the *KRAS* gene were analysed for mutations using specifically designed and synthesized primers to generate 189 bp and 92 bp amplicons (Table 2.1). The 20 µl reaction mix consisted of 10 ng of genomic DNA, 1X PCR buffer (Life Technologies Corporation, Carlsbad, USA) (50 mM KCl, 15 mM Tris-HCl, pH 8),

2.5 mM $MgCl_2$, 200 nM of each primer, 200 µM dNTPs (Promega Corporation, Madison, USA), 5 µM intercalating dye, SYTO® 9 (Life Technologies Corporation, Carlsbad, USA) and 0.5 U of HotStarTaq polymerase (Qiagen, Venlo, Netherlands). The PCR cycling and high resolution melt (HRM) analysis was performed in duplicates on the Rotor-Gene 6000 (Qiagen, Venlo, Netherlands). The cycling conditions for the 189 bp amplicon were as follows: enzyme activation at 95 °C for 15 min followed by 40 cycles of 95 °C for 15 sec, 60.7 °C for 15 sec, 72 °C for 15 sec; 95 °C for 1 sec, 72 °C for 90 sec and a melt from 72 to 95 °C with an increase of 0.2 °C per sec. For the 92 bp amplicon, the cycling conditions were: one cycle of 95 °C for 15 min; 40 cycles of 95 °C for 15 sec, 67.5 °C for 15 sec, 72 °C for 15 sec; one cycle of 95 °C for 1 sec; and a melt from 72 to 95 °C with a temperature increase of 0.2 °C/sec.

Table 2.1 - Primers and probes for CIMP, methylation of MLH1, p16 and IGFBP7; BRAF and KRAS mutational analysis

Gene	Primers
ALU	**FP:** 5′-GGTTAGGTATAGTGGTTTATATTTGTAATTT-3′
	RP: 5′-ATTAACTAAACTAATCTTAAACTCCTAACCT-3′
	Probe: 5′-6FAM-CCTACCTTAACCTCCC-MGBNFQ-3′
IGF2	**FP:** 5′-GAGCGGTTTCGGTGTCGTTA-3′
	RP: 5′-CCAACTCGATTTAAACCGACG-3′
	Probe: 5′-6FAM-CCCTCTACCGTCGCGAACCCGA-BHQ-1-3′
SOCS1	**FP:** 5′-GCGTCGAGTTCGTGGGTATTT-3′
	RP: 5′-CCGAAACCATCTTCACGCTAA-3′
	Probe: 5′-6FAM-ACAATTCCGCTAACGACTATCGCGCA-BHQ-1-3′
NEUROG1	**FP:** 5′-CGTGTAGCGTTCGGGTATTTGTA-3′
	RP: 5′-CGATAATTACGAACACACTCCGAAT-3′
	Probe: 5′-6FAM-CGATAACGACCTCCCGCGAACATAAA-BHQ-1-3′
RUNX3	**FP:** 5′-CGTTCGATGGTGGACGTGT-3′v
	RP: 5′-GACGAACAACGTCTTATTACAACGC-3′
	Probe: 5′-6FAM-CGCACGAACTCGCCTACGTAATCCG-BHQ-1-3′
CACNA1G	**FP:** 5′-TTTTTTCGTTTCGCGTTTAGGT-3′
	RP: 5′-CTCGAAACGACTTCGCCG-3′
	Probe: 5′-6FAM-AAATAACGCCGAATCCGACAACCGA-BHQ-1-3′
MLH1	**FP:** 5′-AGGAAGAGCGGATAGCGATTT-3′
	RP: 5′-TCTTCGTCCCTCCCTAAAACG-3′
	Probe: 5′-6FAM-CCCGCTACCTAAAAAAATATACGCTTACGCG-BHQ-1-3′
p16	**FP:** 5′-TGGAGTTTTCGGTTGATTGGTT-3′
	RP: 5′-AACAACGCCCGCACCTCCT-3′
	Probe: 5′-6FAM-ACCCGACCCCGAACCGCG-BHQ-1-3′
IGFBP7	**FP:** 5′-GGTAAAGTCGGGGTAGTAGTCG-3′
	RP: 5′-ACAACCGCTCGAATAAATAATACCG-3′
	Probe: 5′-6FAM-CGCTACCGCACACCGAATAACGACTCTTA-BHQ-1-3′
BRAF	**V:** 5′-GTGATTTTGGTCTAGCTACt*G*T-3′
	E: 5′-**CGCGGCCGGCCGCGGCG**GTGATTTTGGTCTAGCTACc*G*A-3′
	AS: 5′-TAGCCTCAATTCTTACCATCCAC-3′
KRAS 189-bp	**FP:** 5′-TCATTATTTTTATTATAAGGCCTGCTGAA-3′
	RP: 5′-CAAAGACTGGTCCTGCACCAGTA-3′
KRAS 92-bp	**FP:** 5′-ttataagGCCTGCTGAAAATGACTGAA-3′
	RP: 5′-TGAATTAGCTGTATCGTCAAGGCACT-3′

All the oligonucleotides were purchased from Sigma-Aldrich Corporation, St. Louis, USA, except for the *ALU* probe which was purchased from Life Technologies Corporation, Carlsbad, USA.

2.1.9 Statistical analysis

GraphPad Prism6 V 6.02 software (GraphPad Software, Inc., San Diego, California) was used to perform the statistical analysis. Fisher's exact test and Chi-square test were used to calculate *P* values (two-tailed) depending on the data analysed.

2.2 BREEDING STRATEGIES

2.2.1 *BRaf^{VE}* mouse study

BRaf$^{CA/CA}$ mice (FVB/N strain) were developed by Dankort and colleagues at the San Francisco Comprehensive Cancer Center, USA and generously provided by Prof Martin McMahon (Dankort *et al*, 2007). These mice were crossed with *A33CreERT2$^{+/-}$ /Lacz$^{-/-}$* mice (C57/BL6/129sv strain) which were kindly provided by Assoc Prof Matthias Ernst, Walter and Eliza Hall Institute of Medical Research, Australia. All the pups were heterozygous for *BRaf^{CA}* and the genotypic ratio of *BRaf$^{CA/+}$/A33CreERT2$^{+/-}$ /Lacz$^{-/-}$* was 1:2. These mice were injected with tamoxifen (Sigma-Aldrich Corporation, St. Louis, USA) or olive oil (control) and were used for time point sacrifices and survival studies. For assessment of X-gal stain in mouse colon and intestines, *BRaf$^{CA/CA}$* mice were crossed with *A33CreERT2$^{+/-}$/Lacz$^{+/-}$*. All the pups were heterozygous for *BRaf^{CA}* and the genotypic ratio of *BRaf$^{CA/+}$/A33CreERT2$^{+/-}$/Lacz$^{+/-}$* was 1:4.

2.2.2 *BRaf^{VE}/p16Ink4a* mouse study

BRaf$^{CA/CA}$ mice were crossed with *p16Ink4a* null mice (FVB.129-*Cdkn2a^{tm1Rdp}* strain) which were obtained from the National Cancer Institute Mouse Repository, USA (Figure 2.1). All the pups which were heterozygous for *BRaf^{CA}* and *p16Ink4a* were intercrossed and the genotypic ratio of the required genotype, *BRaf$^{CA/CA}$/p16Ink4a$^{-/-}$* was 1:16. In a parallel breeding program, *p16Ink4a* null mice were crossed with *A33CreERT2$^{+/-}$/Lacz$^{-/-}$* and pups with the required genotype - *p16Ink4a$^{+/-}$ /A33CreERT2$^{+/-}$/Lacz$^{-/-}$* were in the ratio of 1:2. These mice were crossed with *BRaf$^{CA/CA}$/p16Ink4a$^{-/-}$* to get the endpoint mice with the following genotypes:

BRaf$^{CA/+}$*/p16Ink4a*$^{-/-}$*/A33CreERT2*$^{+/-}$*/Lacz*$^{-/-}$ and *BRaf*$^{CA/+}$*/p16Ink4a*$^{+/-}$*/A33CreERT2*$^{+/-}$*/Lacz*$^{-/-}$. The endpoint mice were treated with tamoxifen or olive oil (control) and were used for hyperplasia and survival studies.

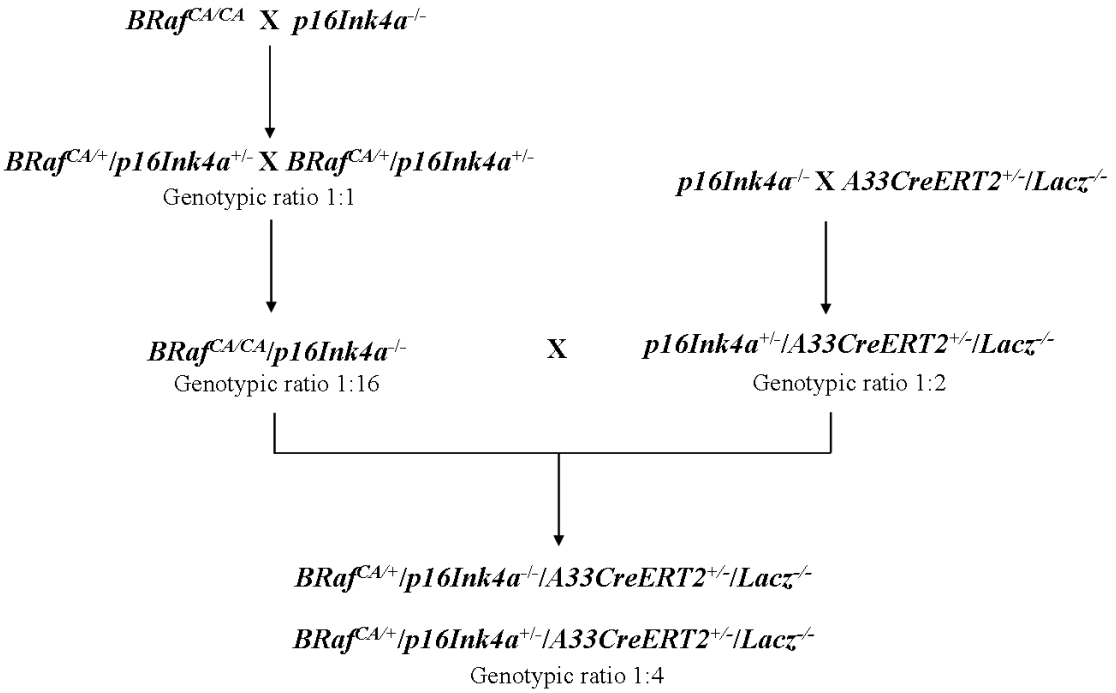

Figure 2.1 - Breeding strategy for BRaf^{VE}/p16Ink4a mice. *The endpoint mice which, were injected with tamoxifen or olive oil were divided into two groups: BRaf*$^{CA/+}$*/p16Ink4a*$^{-/-}$*/A33CreERT2*$^{+/-}$ *and BRaf*$^{CA/+}$*/p16Ink4a*$^{+/-}$*/A33CreERT2*$^{+/-}$*. There were 20-25 mice in each group/treatment (tamoxifen or olive oil).*

2.2.3 *BRaf^{VE}/p19Arf* mouse study

p19Arf mice (FVB.129-*Cdkn2a*^{tm1Nesh} strain) were kindly provided by Dr Graeme Walker, QIMR Berghofer Medical Research Institute, Australia and these were crossed with *BRaf*$^{CA/CA}$ and *A33CreERT2*$^{+/-}$*/Lacz*$^{-/-}$ in two parallel breeding plans (Figure 2.2). In the first breeding program, *BRaf*$^{CA/CA}$ mice were crossed with *p19Arf*$^{-/-}$ and all the pups were *BRaf*$^{CA/+}$*/p19Arf*$^{+/-}$. These mice were intercrossed and the mice with required genotype for the next breeding step - *BRaf*$^{CA/CA}$*/p19Arf*$^{-/-}$ had a ratio of 1:16. In the second breeding plan, *p19Arf*$^{-/-}$ mice were crossed with *A33CreERT2*$^{+/-}$*/Lacz*$^{-/-}$ and the genotypic ratio of the required genotype, *p19Arf*$^{+/-}$*/A33CreERT2*$^{+/-}$*/Lacz*$^{-/-}$ was 1:2. These mice were crossed with *BRaf*$^{CA/CA}$*/p19Arf*$^{-/-}$ for the endpoint mice which were treated with tamoxifen or olive oil (control) for hyperplasia and survival studies. The

genotypic ratio for these mice was 1:4 with the following genotypes – *BRaf*$^{CA/+}$/*p19Arf*$^{-/-}$/*A33CreERT2*$^{+/-}$/*Lacz*$^{-/-}$ and *BRaf*$^{CA/+}$/*p19Arf*$^{+/-}$/*A33CreERT2*$^{+/-}$/*Lacz*$^{-/-}$.

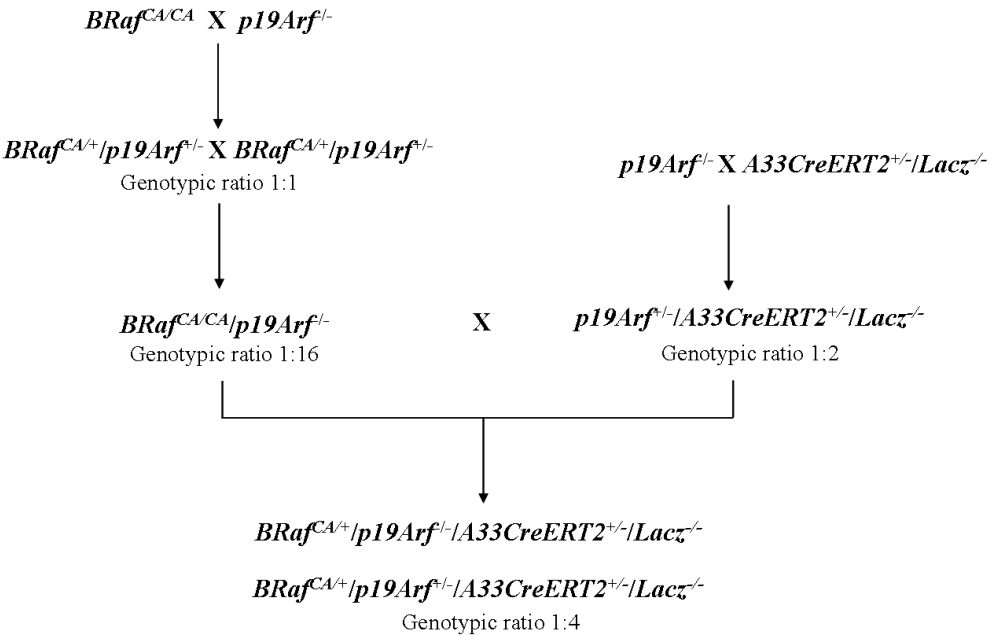

Figure 2.2 - Breeding strategy for BRaf^{VE}/p19Arf mice. *This breeding strategy was similar to the BRaf^{VE}/p16Ink4a study and the endpoint mice were injected with tamoxifen or olive oil. The endpoint genotypes were divided into two groups: BRaf^{VE}/p19Arf$^{-/-}$/A33CrERT2$^{+/-}$ and BRaf^{VE}/p19Arf$^{+/-}$/A33CrERT2$^{+/-}$. There were 20-25 mice in each group/treatment (tamoxifen or olive oil).*

2.3 GENERAL PROCEDURES FOR MOUSE STUDY

2.3.1 Animal ethics and housing

All animal work was approved by the Animal Ethics Committee of QIMR Berghofer Medical Research Institute Animal Ethics Committee and experimental procedures were carried out according to the prescribed guidelines. All the mice were housed in optiMICE cages (Animal Care Systems, Centennial, USA) on a 12 h light/dark cycle at 25 °C, within the QIMR Berghofer Medical Research Institute animal facility and all animal handling was performed in biohoods under sterile airflow conditions.

2.3.2 Tail tipping for genotyping

Pups were tail tipped and ear tagged using an ear punch at 12-14 days of age. The individual tail tips were transferred to sterile 1.5 ml tubes and DNA was extracted as described below (Section 2.3.3).

2.3.3 DNA extraction from tail tips

The DNA lysis buffer consisted of 50 mM Tris (pH 8), 20 mM EDTA (pH 8), 2% SDS. The tail tips were chopped and digested with 700 µl of DNA lysis buffer mixed with 0.5 mg/ml Proteinase K and incubated at 55 °C overnight. After complete digestion, the tubes were placed on ice for 10 min and 250 µl of saturated NaCl solution was added. The tubes were inverted and placed on ice for 5 min. The samples were centrifuged at 13,200 rpm for 5 min and the clear supernatant was transferred to sterile 1.5 ml tubes. The DNA was then precipitated by the addition of 700 µl of 100% isopropanol and the tubes were inverted gently. The samples were centrifuged at 13,200 rpm for 5 min and the supernatant was discarded. The DNA pellet was subsequently washed with 700 µl of 70% ethanol, 700 µl of 100% ethanol and 700 ul of diethyl ether. The tubes were centrifuged at 13,200 rpm for 5 min for all the washes and the supernatant was discarded after each centrifugation step. The pellet was air dried in a fume hood and resuspended in 50 µl of 1X TE buffer with 1 µl of 10 mg/ml Ribonuclease A (Roche, Basel, Switzerland).

2.3.4 Genotyping PCR

2.3.4.1 *BRaf*^{CA} and *BRaf*^{VE}

A 20 µl PCR reaction consisted of 300 ng genomic DNA, 1X PCR buffer (50 mM KCl, 15 mM Tris-HCl, pH 8), 2.5 mM $MgCl_2$, 250 µM dNTPs, 0.5 µM of each primer (Table 2), 3.75 U AmpliTaq Gold® DNA Polymerase (Life Technologies Corporation, Carlsbad, USA) and 0.75% Formamide Adjunct (Stratagene California, La Jolla, USA). The DNA samples were amplified using a thermal cycler under the following cycling conditions: 94 °C for 12 min followed by 34 cycles of 94 °C for 1 min, 55 °C for 30 sec and 73 °C for 40 sec; 72 °C for 2 min and an infinite hold at 4 °C. The PCR products were analysed for the following amplicon sizes: wild type - 185 bp and *BRaf*^{CA} - 308 bp on a 1.5% agarose gel stained with ethidium bromide and

visualized using a gel doc (Bio-Rad Laboratories, Inc., Hercules, USA). After Cre activation (Section 2.3.5), the *Braf*^{CA} genotyping PCR was carried out as explained in the above protocol with an increase in annealing temperature from 55 °C to 58 °C for 30 sec. The *BRaf*^{VE} mutant band at 335 bp was detected by visualising the PCR products on an 8% polyacrylamide gel (Bio-Rad Laboratories, Inc., Hercules, USA) stained with ethidium bromide.

2.3.4.2 *A33CreERT2*

The PCR reaction consisted of 300 ng genomic DNA, 1X PCR buffer (50 mM KCl, 15 mM Tris-HCl, pH 8), 2 mM $MgCl_2$, 200 µM dNTPs, 0.2 µM of each primer (Table 2.2), 2.5 U AmpliTaq Gold® DNA Polymerase in a total reaction volume of 20 µl. The PCR was carried out in a thermal cycler using the following cycling conditions: 95 °C for 10 min followed by 35 cycles of 95 °C for 30 sec, 63 °C for 30 sec and 72 °C for 30 sec; 72 °C for 10 min and an infinite hold at 4 °C. The amplicon size was 450 bp on a 1% agarose gel which was stained with ethidium bromide and visualized using a gel doc.

2.3.4.3 *Lacz*

The *Lacz* PCR generated a 600 bp amplicon and a 30 µl reaction consisted of 300 ng genomic DNA, 1X PCR buffer (50 mM KCl, 15 mM Tris-HCl, pH 8), 2.08 mM $MgCl_2$, 200 µM dNTPs, 0.27 µM of each primer (Table 2.2), 4.2 U AmpliTaq Gold® DNA Polymerase. The PCR cycling conditions on a thermal cycler were as follows: 94 °C for 10 min; 35 cycles of 94 °C for 30 sec, 64 °C for 30 sec and 72 °C for 30 sec; 72 °C for 10 min and an infinite hold at 4 °C. The PCR products were visualized using a gel doc on a 1% agarose gel stained with ethidium bromide.

2.3.4.4 *p16Ink4a*

A 20 µl PCR consisted of 300 ng genomic DNA, 1X PCR buffer (50 mM KCl, 15 mM Tris-HCl, pH 8), 2 mM $MgCl_2$, 200 µM dNTPs, 0.5 µM of each primer (Table 2.2), 0.75 U AmpliTaq Gold® DNA Polymerase. The samples were amplified in a thermal cycler with the following cycling conditions: enzyme activation at 94 °C for 3 min, which was followed by 35 cycles of 94 °C for 1 min, 65 °C for 2 min and 72 °C for 1 min; 72 °C for 3 min and an infinite hold at 4 °C. The wild type and knockout

amplicons were 189 bp and 243 bp respectively on a 1.5% agarose gel stained with ethidium bromide. The PCR products were visualized using a gel doc.

2.3.4.5 *p19Arf*

The *p19Arf* PCR was a 20 µl reaction which consisted of 300 ng genomic DNA, 1X PCR buffer (50 mM KCl, 15 mM Tris-HCl, pH 8), 2 mM $MgCl_2$, 200 µM dNTPs, 1% dimethyl sulfoxide, 0.5 µM of each primer (Table 2.2), 1.25 U AmpliTaq Gold® DNA Polymerase. The DNA samples were amplified using a thermal cycler under the following cycling conditions: 94 °C for 3 min, which was followed by 35 cycles of 94 °C for 1 min, 60 °C for 2 min and 72 °C for 1 min; 72 °C for 3 min and an infinite hold at 4 °C. The PCR products were analysed for the following amplicon sizes: wild type - 130 bp and null - 212 bp on a 1.5% agarose gel stained with ethidium bromide and visualized using a gel doc.

Table 2.2 - Primers for mouse genotyping PCR

Gene	Primers
BRaf^{CA}	AD FwdA1: 5′-TGAGTATTTTTGTGGCAACTGC-3′
	AD RevB1: 5′-CTCTGCTGGGAAAGCGGC-3′
A33CreERT2	A33geno-F: 5′-GGGCCTTTCATAGAGTAGGTGG-3′
	A33geno-R: 5′-GCTTGCAGGTACAGGAGGTAGT-3′
Lacz	pGKneo1: 5′-GTCTGCCGCGCTGTTCTCCTCTTC-3′
	pGKneo2: 5′-CTTCGCCCAATAGCAGCCAGTCC-3′
p16Ink4a	C015: 5′-GGCAAATAGCGCCACCTAT-3′
	C016: 5′-GACTCCATGCTGCTCCAGAT-3′
	C017: 5′-GCCGCTGGACCTAATAACTTC-3′
p19Arf	C029: 5′-ATGTTcAcGAAAGccAGAGc-3′
	C030: 5′-GTcGcAGGTTcTTGGTcAcT-3′

All the oligonucleotides were purchased from Sigma-Aldrich Corporation, St. Louis, USA.

2.3.5 Activation of Cre recombinase

The *A33CreERT2* gene, which encoded for the Cre recombinase enzyme was activated by tamoxifen. For a 1 ml solution (10 mg/ml), 10 mg of tamoxifen (Sigma-Aldrich Corporation, St. Louis, USA) was weighed and mixed with 100 µl of 100% ethanol and 900 µl of olive oil. The tamoxifen was dissolved by sonication using an ultrasonic bath (Branson Ultrasonics, Danbury, USA) set at 37 °C and this solution was also sonicated for 5 min at 37 °C before every injection. The mice aged between 6-8 weeks were injected with 100 µl of tamoxifen per injection intraperitoneally twice a day

for five days. The control mice were injected with 100 µl of 1:10 dilution of ethanol in olive oil.

2.4 *BRaf*^{VE} EXPRESSION IN CONDITIONAL BRAF MOUSE MODEL

2.4.1 Crypt isolation from colon and small intestine for *BRaf*^{VE} genotyping

Mice (*BRaf*$^{CA/+}$/*A33CreERT2*$^{+/-}$) were sacrificed six weeks after tamoxifen treatment – one control and one tamoxifen-treated mouse. The mice were dissected and the colons and small intestines were flushed with cold 1X phosphate buffered saline (PBS) and opened along their lengths and were washed three times in cold 1X PBS. The colon was divided into proximal and distal colon and the small intestine was divided into three regions – duodenum, jejunum and ileum. The colons and small intestines were incubated in 0.04% sodium hypochlorite for 15 min at room temperature and then washed twice in 1X PBS. The PBS was discarded and 12 ml of 3 mM EDTA/ 0.5 mM dithiothreitol in PBS was added to the tissues and incubated for 90 min at room temperature and then discarded. The tubes with the tissues were shaken vigorously for 15-20 sec with 20 ml of 1X PBS and then the tissues were discarded. The solution turned cloudy and the tubes were centrifuged at 800 rpm until the solution turned clear. The supernatant was discarded and DNA was extracted from the crypts according to Section 2.3.3. The samples were genotyped to evaluate the conversion of *BRaf*^{CA} into *BRaf*^{VE} in the tamoxifen-treated mice (Section 2.3.4.1).

2.4.2 X-gal staining in mouse colon and small intestine

Mice (*BRaf*$^{CA/+}$/*A33CreERT2*$^{+/-}$/*Lacz*$^{+/-}$) were sacrificed six weeks after treatment – one control and one tamoxifen-treated mouse. The mice were dissected and the colons and small intestines were flushed with 1X PBS and opened along their lengths. The colon was divided into proximal and distal colon and the small intestine was divided into three regions – duodenum, jejunum and ileum. The tissues were transferred to 30 ml tubes and washed with 1X PBS, placed in petri dishes and fixed with 4% paraformaldehyde (PFA) for 1 h at 4 °C. The tissues were washed thrice in 10 ml of wash buffer (20 mM $NaH_2PO_4.2H_2O$, 70 mM $Na_2HPO_4.7H_2O$, 2 mM $MgCl_2$, 0.02% Igepal® (Sigma-Aldrich Corporation, St. Louis, USA), 0.1% sodium deoxycholate (Sigma-Aldrich Corporation, St. Louis, USA), 0.2 g bovine serum

albumin (BSA)) on a rocker. The first wash was carried out at 4 °C for 30 min and the subsequent washes were at room temperature for 30 min per wash. The wash buffer was discarded and the tissues were incubated overnight with 10 ml of X-gal stain (0.082 g $K_3Fe(CN)_6$, 0.105 g $K_4Fe(CN)_6$, 0.24 M NaCl, 1 mg/ml X-gal, 49 ml wash buffer) at 37 °C in the dark with gentle rocking. The following day, the tissues were washed with 1X PBS twice and fixed with 2% PFA overnight at room temperature. After fixing, the tissues were made into swiss rolls and processed into paraffin blocks and the cut sections were counterstained with nuclear fast red stain.

2.4.3 Retro-cre activation of *BRaf*^{VE} in immortalized mouse embryonic fibroblasts

2.4.3.1 Isolation of mouse embryonic fibroblasts

Mice were set up for mating at 8 weeks of age (*BRaf*$^{CA/CA}$ x *A33CreERT2*$^{-/-}$/*Lacz*$^{-/-}$) and the females were checked for plugs the following morning. Pregnant females were sacrificed and dissected on day 14.5 of gestation under sterile conditions. Uterine horns were dissected and the embryos (8 in total) were transferred to a petri dish with 1X PBS. All the embryos were heterozygous for *BRaf*^{CA} and did not require any genotyping. The embryos were decapitated to remove neural cells and the soft organs and viscera were also discarded. Individual embryos were washed in 1X PBS in a 6-well tissue culture plate to remove residual red blood cells and debris. Each embryo was transferred to a well of a 24-well tissue culture plate with 300 µl of 0.25% Trypsin-EDTA (Life Technologies Corporation, Carlsbad, USA). The embryos were minced with a pair of sterile scissors and incubated at 37 °C in a 5% CO_2 incubator for 5 min. All the embryos were pooled and transferred to a 10 ml tube with 6 ml MEF media which consisted of Dulbecco's Modified Eagle Medium (DMEM) (Life Technologies Corporation, Carlsbad, USA) (4.5 g/L D-Glucose, L-Glutamine and 110 mg/L sodium pyruvate), 10% Fetal Bovine Serum (FBS) (Life Technologies Corporation, Carlsbad, USA), qualified, Australian origin (heat inactivated at 56 °C for 30 min) and 1% Penicillin Streptomycin (Life Technologies Corporation, Carlsbad, USA) (10,000 units/ml Penicillin, 10,000 µg/ml Streptomycin, 1X Minimum Essential Medium (MEM) Non-Essential Amino Acids (Life Technologies Corporation, Carlsbad, USA), 0.7% β-Mercaptoethanol in PBS. The tissue culture flasks were coated with 0.1% gelatin solution at least 1 h before the MEFs were plated. The cellular debris was

allowed to settle down and 2 ml was added to the gelatinised flasks containing MEF media, which was changed after 6 h and replaced with fresh MEF media.

2.4.3.2 Immortalization of mouse embryonic fibroblasts

Mouse embryonic fibroblasts were washed with 1X PBS twice and trypsinized with 0.25% Trypsin-EDTA. The cells were harvested and approximately 3.8 x 10^5 cells were plated with MEF media (Section 2.4.3.1) and incubated for 3 days at 37 °C with 5% CO_2. After incubation, the cells were harvested and this procedure was repeated for 20 to 25 passages until the proliferation rate of the cells increased.

2.4.3.3 Preparation of retro-cre virus

Phoenix Ecotropic packaging cells that were used for transfections were cultured in DMEM (4.5 g/L D-Glucose, L-Glutamine and 110 mg/L sodium pyruvate) with 10% FBS, qualified, Australian origin and 1% Penicillin Streptomycin (10,000 units/ml Penicillin, 10,000 µg/ml Streptomycin. On day 1, approximately 2-3 x 10^6 cells were plated in a T-75 tissue culture flask and incubated at 37 °C with 5% CO_2 overnight. On day 2, the media was removed and 10 ml of Opti-MEM® I Reduced Serum Medium (Life Technologies Corporation, Carlsbad, USA), Glutamax™ Supplement (Opti-MEM media) with 10% FBS, qualified, Australian origin was added followed by mixing Retro-cre maxiprep DNA (4.5 µg) with 2.25 ml of Opti-MEM media (diluted DNA). In a separate tube, a reaction mix of 54 µl of Lipofectamine 2000 (Life Technologies Corporation, Carlsbad, USA) and 2.25 ml of Opti-MEM media was incubated for 5 min at room temperature. This solution was added to the diluted DNA, mixed gently and incubated for 20 min at room temperature to form DNA-Lipofectamine 2000 complexes. These were added drop wise to the T-75 flasks containing the Phoenix-Ecotrophic packaging cells and incubated at 37 °C with 5% CO_2 overnight. On day 3, the media containing the DNA-Lipofectamine 2000 complexes was replaced with 10 ml of DMEM and incubated at 37 °C with 5% CO_2 overnight. Retro-cre virus was harvested 48 h post transfection (first harvest) by filtering the media containing the virus through a 0.45 µm filter. Fresh DMEM was added to the Phoenix-Ecotrophic cells and incubated at 37 °C with 5% CO_2 overnight and retro-cre virus was harvested 72 h post transfection (second harvest).

2.4.3.4 Infection of mouse embryonic fibroblasts with retro-cre virus

In a 6-well plate, approximately 2 x 10^5 mouse embryonic fibroblasts (MEFs) from *BRaf*^{CA} mice were plated per well on day 1 in MEF media (Section 2.4.3.1) to initially determine the viral titer. The virus was added to the cells the following day with two infections. The volume of the virus added to the cells (first harvest, Section 2.4.3.3) ranged from 0.5 ml to 2.5 ml in 0.5 increments, with the first well being the mock well (no virus). Polybrene was added at a final concentration of 4 μg/ml per well and incubated at 37 °C with 5% CO_2. The cells were infected for the second time (approximately 6 h after the first infection) and incubated at 37 °C with 5% CO_2 overnight. The media was replaced with fresh MEF media the following day and the cells were harvested 48 h post-infection (first infection). After the optimization of the viral titer, *BRaf*^{CA} MEFs were infected with the optimized amount of retro-cre virus. The retro-cre infected MEFs were harvested at different time points – 48 h, 72 h and 96 h post infection to assess the conversion of *BRaf*^{CA} into *BRaf*^{VE}.

2.4.3.5 *BRaf*^{VE} genotyping

DNA was extracted from the cells as described in Section 2.3.4 and the conversion of *BRaf*^{CA} into *BRaf*^{VE} was evaluated using genotyping assay as described in Section 2.3.4.1.

2.5 HYPERPLASIA AND SURVIVAL STUDIES

Hyperplasia and survival studies were carried out in all the mice groups - *BRaf*^{CA}, *BRaf*^{CA}/*p16Ink4a* and *BRaf*^{CA}/*p19Arf*. Mice were sacrificed at six weeks of age after tamoxifen/olive oil treatment for evaluating hyperplastic changes in all the mice groups. In the *BRaf*^{CA} mouse group, mice were sacrificed at 6 and 12 months after tamoxifen/olive oil treatment.

2.5.1 Specimen collection

Hyperplasia study involved the collection of samples for DNA extraction and paraffin blocks. Mice injected with tamoxifen or olive oil (control) were sacrificed six weeks after treatment - three mice/treatment. The colon and small intestines were removed after dissection and flushed with 1X cold PBS. Small intestine was divided

into three regions of approximately equal length – duodenum, jejunum and ileum. Fresh tissue samples were taken from the proximal end of the colon and small intestine for DNA extraction. Then the tissues were fixed with 10% phosphate buffered formalin, cut along their lengths and rolled into swiss rolls from the distal end. The samples were embedded in paraffin blocks and 4 μm sections were stained with hematoxylin and eosin (H&E) using standard protocols on a Leica ST5010 Autostainer XL (Leica Biosystems, Nussloch, Germany) (Figure 2.3). Mice treated with tamoxifen or olive oil were also set up for survival analysis and were observed for development of tumour phenotype. Mice that showed signs of sickness such as ruffled coat, rapid breathing and weight loss were sacrificed and checked for abnormalities in organs. Organs with lesions/tumours were collected, processed as described above, embedded into paraffin blocks and sections were stained with H&E for assessment.

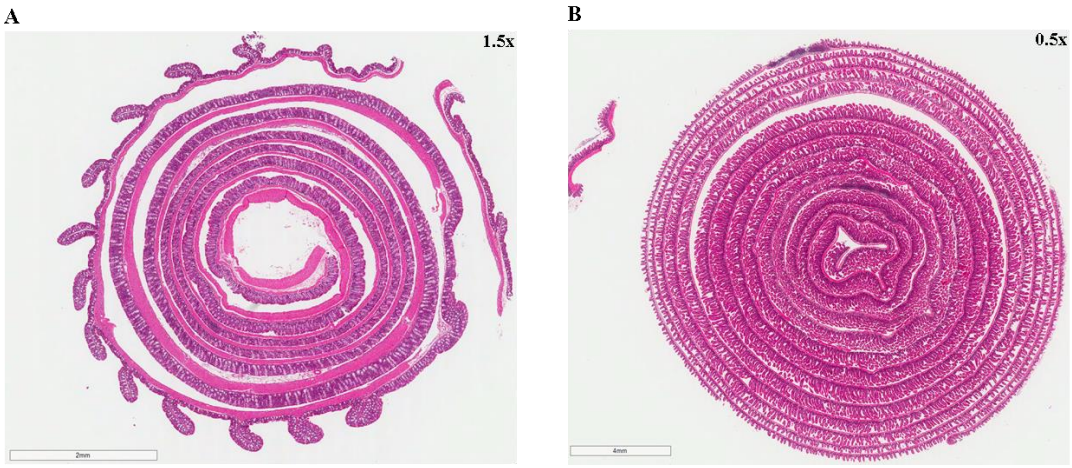

Figure 2.3 – Swiss rolls of mouse colon and small intestine. *Hematoxylin and eosin (H&E) stained sections of swiss rolls of mouse colon* ***(A)*** *and small intestine* ***(B)****. The orientation of the swiss roll is from the proximal end (outer) to the distal end (center) Scale bars represent 2 mm (A) and 4 mm (B); magnification 1.5x (A) and 0.5x (B).*

2.5.2 Measurement of intestinal villi and crypts

Hematoxylin and eosin (H&E) stained slides of mice sacrificed for hyperplasia study from all groups were scanned with Aperio XT (Aperio Technologies, Inc., Vista, USA). The length of fifty colonic crypts and fifty villi and crypts per region of the small intestine from the proximal end were measured using the ruler tool of ImageScope software (Aperio Technologies, Inc., Vista, USA).

2.5.3 Pathological assessment of mouse specimens

The H&E stained slides were assessed by Mark Bettington and Paul Waring. The small intestine and colon samples were classified according to standard pathology criteria. Hyperplasia was defined as an increase in the number of cells in a tissue or organ. In the small intestine, this was characterised by expansion of the proliferative zone in the crypt bases and elongation of the villous processes. The diagnosis of murine intestinal polyps was based predominantly on the features described in human colorectal polyps. In this study, the small intestine polyps were all traditional serrated adenomas. Features used to diagnose a traditional serrated adenoma include predominant villous growth pattern, presence of ectopic crypt foci and epithelial serrations (Bosman, 2010; Longacre & Fenoglio-Preiser, 1990; Torlakovic *et al*, 2003; Torlakovic *et al*, 2008).

Dysplasia was recognised by both architectural and cytological features. Architectural features include presence of cellular crowding, cribriform or back-to-back growth and decreased lamina propria. Cytological features include increased nuclear to cytoplasmic ratio, irregular nuclear outlines, vesicular nuclei, stratification of nuclei and prominent nucleoli (Bosman, 2010; Fu *et al*, 2012). Invasive malignancy was recognised by invasion through the muscularis mucosae.

2.5.4 Methylation analysis of hyperplasia samples

2.5.4.1 DNA extraction

Fresh tissue was collected from mice which were sacrificed six weeks after treatment - three tamoxifen and three olive oil (control) treated mice (Section 2.5.1). For methylation analysis, DNA was extracted only from the duodenum of the small intestine using DNeasy® Blood & Tissue kit (Qiagen, Venlo, Netherlands) according to manufacturer's instructions. Tissues were homogenized in tubes containing ceramic beads and 180 µl of lysis buffer (Buffer ATL) with Precellys 24 tissue homogenizer (Bertin Technologies, Montigny-le-Bretonneux, France). The tubes were spun at 6500 rpm for 30 sec at 4 °C and the homogenized tissue was transferred to sterile 1.5 ml tubes with 20 µl of Proteinase K (provided in the DNeasy® Blood & Tissue kit). The samples were mixed and incubated at 56 °C for 30 min. RNase A (2 mg/ml) was added to the samples and incubated for 2 min at room temperature. The tubes were mixed for 15 sec, and then 200 µl of loading buffer (Buffer AL) was added and mixed for 15 sec.

The samples were mixed with 200 µl of 100% ethanol and transferred to DNeasy Mini spin columns placed in a 2 ml collection tube and centrifuged at 8000 rpm for 1 min. The flow-through and collection tubes were discarded and the spin column was placed in a new collection tube. The samples were washed with 500 µl each of wash buffers (Buffer AW1 and Buffer AW2) and centrifuged at 8000 rpm for 1 min and 14,000 rpm for 3 min respectively. The flow-through and collection tubes were discarded after each wash. The spin column was placed into a 1.5 ml tube and 200 µl of elution buffer (Buffer AE) was added directly to the membrane, incubated for 1 min and centrifuged at 8000 rpm for 1 min. The spin column was placed into a new 1.5 ml tube and the elution step was repeated. The DNA concentration was determined using the Nanodrop 2000c (Thermo Fisher Scientific, Waltham, USA).

2.5.4.2 Restriction digestion

Genomic DNA extracted from the duodenum was subjected to restriction digestion using the EpiTect Methyl II DNA Restriction kit (Qiagen, Venlo, Netherlands). The reaction mix consisted of 2 µg genomic DNA, 100 µl 1X Restriction Digestion Buffer and RNase-/DNAse-free water in a total volume of 470 µl. The samples were mixed and centrifuged briefly and four digestion reactions were set up according to Table 2.3. The samples were mixed and incubated at 37 °C overnight. After incubation, the enzymes were heat-inactivated at 65 °C for 20 min.

Table 2.3 - Reaction set up for restriction digestion

Component	M_o	M_s	M_d	M_{sd}
Reaction mix	116 µl	116 µl	116 µl	116 µl
Methylation-sensitive enzyme A	–	2 µl	–	2 µl
Methylation-dependent enzyme B	–	–	2 µl	2 µl
RNase-/DNase-free water	4 µl	2 µl	2 µl	–
Final volume	120 µl	120 µl	120 µl	120 µl

2.5.4.3 Methylation PCR arrays

A reaction mix was prepared for the restriction digests according to Table 2.4. The tubes were mixed well and added to the corresponding wells of the EpiTect Methyl II Complete PCR Array (Qiagen, Venlo, Netherlands) 384-well plate (Mouse Colon Cancer DNA Methylation PCR Array, Complete Panel). The plates were run on the LightCycler® (Roche, Basel, Switzerland) 480 with the following conditions: 95 °C for 10 min; 3 cycles of 99 °C for 30 sec and 72 °C for 1 min; and 40 cycles of 97 °C for 15

sec and 72 °C for 1 min. A melt curve analysis was performed after PCR amplification with the following conditions: 97 °C for 1 min, 55 °C for 15 sec and 95 °C on a continuous acquisition mode with the temperature increasing at a rate of 0.11 °C/sec and the runs were analysed using the Second Derivative Maximum.

Table 2.4 - PCR setup for methylation arrays

Component	M_o	M_s	M_d	M_{sd}
RT^2 SYBR® Green qPCR Mastermix	590 µl	590 µl	590 µl	590 µl
M_o digest	120 µl	–	–	–
M_s digest	–	120 µl	–	–
M_d digest	–	–	120 µl	–
M_{sd} digest	–	–	–	120 µl
RNase-/DNase-free water	470 µl	470 µl	470 µl	470 µl
Final volume	1180 µl	1180 µl	1180 µl	1180 µl

2.5.5 Immunohistochemistry

Immunohistochemical staining procedures was performed on paraffin sections of small intestine samples for antibodies such as Ki-67, β-catenin, p16Ink4a, p44/42 Mapk (Erk1/2) and Phospho-p44/42 Mapk (Erk1/2) (Thr202/Tyr204). All the paraffin slides were dewaxed and counterstained (light) with the Leica ST5010 Autostainer XL and coverslipped with the Leica CV 5030 Coverslipper (Leica Biosystems, Nussloch, Germany).

2.5.5.1 Ki-67

Slides were dewaxed, placed in containers filled with 1X Target Retrieval solution (pH 9) (Dako, Glostrup, Denmark) and subjected to heat-induced epitope retrieval (HIER) at 120 °C for 20 min in a Decloaking Chamber™ (Biocare Medical, Concord, USA). After cooling, the slides were washed in 1X tris-buffered saline (TBS) – 5 min/wash. Endogenous peroxidase activity was blocked by incubating the slides in 1% H_2O_2/TBS for 10 min, followed by three 1X TBS washes. Slides were incubated in 10% goat serum/TBS for 30 min to block nonspecific antibody binding. This was followed by incubation with primary monoclonal rat anti-mouse Ki-67 antibody (Dako, Glostrup, Denmark) (TEC-3) with a 1:50 dilution in antibody diluent (Dako, Glostrup, Denmark) for 90 min. Slides were washed with 1X TBS, incubated with Rat Probe (Biocare Medical, Concord, USA) for 20 min, washed in 1X TBS and then incubated in Rat HRP-Polymer (Biocare Medical, Concord, USA) for 20 min. The slides were

washed in 1X TBS and stained with 3,3'-Diaminobenzidine (DAB) for 8 min and counterstained.

2.5.5.2 β-catenin

Slides were dewaxed and subjected to HIER in a decloaking chamber with Tris-EDTA (pH 8.8) at 121 °C for 8 min. After the slides cooled down, they were washed in three changes of 1X PBS (5 min/wash), with the first wash containing 0.025% Tween 20. Slides were incubated in 2% H_2O_2/PBS for 10 min to block endogenous peroxidase activity and washed in 1X PBS three times. Background sniper (Biocare Medical, Concord, USA) was applied to the slides for 30 min, followed by incubation with blocking buffer (10% goat serum and 1% bovine serum albumin (BSA)) in 1X PBS for 30 min. Primary rabbit monoclonal β-catenin antibody (Epitomics, Burlingame, USA) with a 1:500 dilution in blocking buffer was applied to the slides overnight at room temperature. The slides were washed in three changes of 1X PBS, with the first wash containing 0.025% Tween 20. Slides were incubated with MACH3 Rabbit Probe (Biocare Medical, Concord, USA) for 20 min, followed by three washes in 1X PBS wash, incubation with MACH3 Rabbit Polymer (Biocare Medical, Concord, USA) for 20 min and a final set of three 1X PBS washes. The slides were stained with DAB for 5 min and counterstained.

2.5.5.3 p16Ink4a

Slides were dewaxed and transferred to a decloaking chamber for HIER with 1X Target Retrieval solution (pH 9) at 115 °C for 8 min. After the slides cooled down, they were washed in two changes of 1X TBS (2 min/wash), followed by incubation in 1% H_2O_2/tap water for 5 min to block endogenous peroxidase activity. Slides were washed twice in 1X TBS and incubated with Mouse on Mouse™ (M.O.M.) (Vector Laboratories, Inc., Burlingame, USA) Mouse Ig Blocking Reagent (M.O.M.™ Immunodetection kit) for 1 h and washed in two changes of 1X TBS. M.O.M.™ diluent (M.O.M.™ Immunodetection kit) was applied to the slides for 5 min, followed by incubation with primary mouse monoclonal p16 (JC8) antibody (Santa Cruz Biotechnology, Inc., Dallas, USA) with a 1:100 dilution in M.O.M.™ diluent for 90 min. The slides were washed twice in 1X TBS and MACH1 Mouse Probe (Biocare Medical, Concord, USA) was applied for 15 min. This was followed by washes in two

changes of 1X TBS, the application of MACH1 Universal HRP-Polymer (Biocare Medical, Concord, USA) for 30 min and washes in 1X TBS. Slides were stained with DAB for 5 min and lightly counterstained.

2.5.5.4 p44/42 Mapk (Erk1/2) and Phospho-p44/42 Mapk (Erk1/2) (Thr202/Tyr204)

Slides were dewaxed and subjected to HIER in a decloaking chamber with 1X Target Retrieval solution (pH 6) (Dako, Glostrup, Denmark) at 120 °C for 20 min. The slides were cooled down, washed three times in 1X TBS (5 min/wash), incubated in 1% H_2O_2/TBS for 10 min and washed in three changes of 1X TBS. Goat serum (10%) was applied to the slides for 60 min, followed by incubation with primary rabbit polyclonal p44/42 Mapk (Erk1/2) (Cell Signaling Technology, Inc., Danvers, USA) or primary rabbit polyclonal phospho-p44/42 Mapk (Erk1/2) (Thr202/Tyr204) (Cell Signaling Technology, Inc., Danvers, USA) with a dilution of 1:100 overnight. The slides were washed in three changes of 1X TBS and EnVision™+System-HRP Labelled Polymer Anti-Rabbit (Dako, Glostrup, Denmark) was applied to the slides for 30 min, followed by washes in 1X TBS. The slides were stained in DAB for 5 min and lightly counterstained.

2.5.6 Statistical analysis

GraphPad Prism6 V 6.02 software was used to perform the statistical analysis. *P* values for hyperplasia measurements (crypt and villus length) (Section 2.5.2) were calculated using unpaired t test and ordinary one-way Anova for column tables and two-way Anova for grouped tables. *P* values for survival plots were calculated using Log-rank (Mantel-Cox) test.

CHAPTER 3

CIMP AND METHYLATION OF *p16*, *IGFBP7* AND *MLH1*

3. CIMP AND METHYLATION OF *p16, IGFBP7* AND *MLH1*

3.1 INTRODUCTION

Hypermethylation is one of the key features of the serrated pathway and causes inactivation of multiple functionally important genes such as *MLH1*, *p16*, *MGMT*, *TIMP3* and *HLTF* (Kim *et al*, 2006; Toyota *et al*, 1999). Toyota *et al* classified methylation patterns in CRC into two categories - type A or age-specific methylation and type C or cancer-specific methylation. In this study, a group of colorectal tumours exhibited high type C methylation levels in 3 or more loci and this feature was described as CpG island methylator phenotype (CIMP). CIMP is an event in colorectal tumorigenesis and has the potential to silence key tumour suppressor genes (Toyota *et al*, 1999). CIMP was found to be strongly associated with *BRAF* mutation, MSI-H and proximally located colorectal tumours (Barault *et al*, 2008; Hinoue *et al*, 2009).

In 2006, Weisenberger *et al* investigated CIMP in greater detail and developed a new panel of methylation markers to more specifically classify colorectal tumours based on their CIMP status. The MethyLight assay, a real-time based PCR technique was employed to assess the methylation levels in the tumours. This study developed a panel of markers which more accurately defined tumours with high levels of CIMP (CIMP-H) and which were closely associated with *BRAF* mutation (Eads *et al*, 2000; Weisenberger *et al*, 2006). In polyps, CIMP assessment using non-specific markers and non-quantitative methylation-specific PCR (MSP) showed that CIMP was frequent in all serrated polyps, except for GCHPs (O'Brien *et al*, 2006). It is likely that CIMP develops in serrated polyps and plays a role in their progression to malignancy. Although the Weisenberger *et al* panel is more specific and quantitative, it has not been used previously to assess CIMP in all the serrated polyp types (O'Brien *et al*, 2004; O'Brien *et al*, 2006; Weisenberger *et al*, 2006).

The aim of this study was to evaluate CIMP status using the Weisenberger *et al* panel and MethyLight assay in a well-characterised series of serrated polyps, which were used in an earlier study (Spring *et al*, 2006). Methylation levels of *MLH1*, *p16* and *IGFBP7* were also evaluated. Methylation of *p16* and *IGFBP7* were initially assessed in a group of *BRAF* mutant/CIMP-H and *BRAF* wild/CIMP negative tumours. Our hypotheses were that a) CIMP will be rare in HPs and ADs, but will be more prevalent in SSAs which are the immediate precursors to CIMP-H and MSI-H CRC and b) CIMP

will be more prevalent in proximal lesions and c) will be associated with the methylation of genes whose silencing is thought to play a functional role in the serrated neoplastic pathway (*MLH1*, *p16* and *IGFBP7*) and d) methylation of *IGFBP7* and *p16* will be associated with *BRAF* mutant/CIMP-H cancers (Bettington *et al*, 2013).

3.2 RESULTS

3.2.1 Optimization of *IGFBP7* MethyLight assay

The MethyLight assay for *IGFBP7* was optimized with normal mucosa and the colorectal cancer cell line, SW480. The sample group consisted of *Sss*1 treated (methylated), bisulfite modified normal mucosa and SW480; bisulfite modified normal mucosa and SW480 and pooled genomic DNA from normal mucosa obtained from patients. The *IGFBP7* methylation levels of the samples (in terms of PMR) were assessed with reference to *ALU*. Methylation (PMR >10) was observed only in the methylated, bisulfite modified normal mucosa and SW480 samples at the optimized conditions – 500 ng genomic DNA, 0.4 μM each of forward and reverse primers and 0.1 μM probe; cycling conditions – enzyme activation for 15 min at 95 °C; 15 sec at 95 °C and 60 sec at 60 °C.

3.2.2 CIMP and polyp type

Serrated polyps were found to be significantly associated with CIMP-H status (Figure 3.1 & Table 3.1). The SSAs showed the highest percentage of CIMP-H samples (51.43%), while only nine out of 109 HPs (8.26%) were CIMP-H. The number of CIMP-H HPs was similar in GCHPs and MVHPs with 6.78% and 10% respectively. In TVAs, CIMP-H samples were absent and they accounted for only a minor portion in TAs, one out of 52 TAs (1.92%).

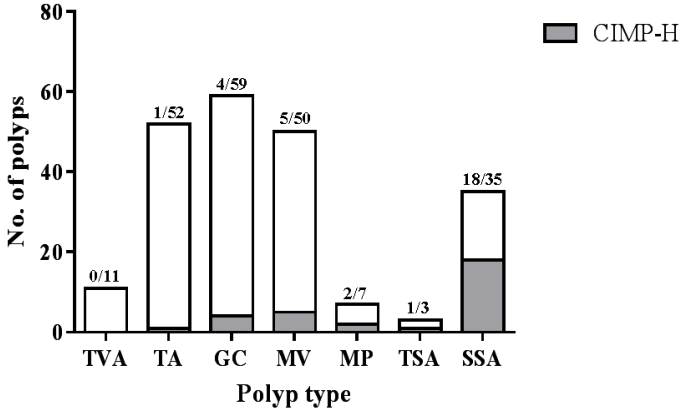

Figure 3.1 - CIMP-H in different polyp types. *TAs and TVAs comprise the adenoma control group, while the serrated polyps consist of GCs, MVs (hyperplastic polyps) and MPs, TSAs and SSAs. CIMP-H status was found to be significantly associated with serrated polyps (P= 0.0002).*

3.2.3 CIMP and anatomic location, polyp size and gender

CIMP-H was significantly associated with proximal colonic location- 30 out of 112 (26.79%) polyps in the proximal colon were CIMP-H as shown in Figure 3.2A ($P < 0.0001$). A majority of the SSAs were proximally located- 27 out of 35 (77.14%); 17 of 27 proximal SSAs were CIMP-H (62.96%). The remaining eight SSAs were located in the distal colon and only one was CIMP-H (12.5%). In the HPs, a similar pattern was observed- all the CIMP-H samples (four GCHPs and five MVHPs) were located in the proximal colon.

Overall, the size of the polyp also had an effect on the CIMP status. CIMP-H increased significantly ($P = 0.0035$) with an increase in polyp size as shown in Figure 3.2B. However, this was not the case for SSAs, which were just as likely to be CIMP-H even if they were small. In the size range of 1-5 mm, six of 12 SSAs (50%) were CIMP-H. In SSAs >5 mm, 12 of 23 (52.17%) were CIMP-H.

There was no significant association between CIMP-H polyps and gender. Females showed a slightly higher incidence of CIMP-H polyps as seen in Figure 3.2C with 19 CIMP-H samples out of 115 (16.52%); while males had 12 CIMP-H polyps out of a total of 102 (11.76%).

Table 3.1 - Correlation between polyp type, location, gender, size, BRAF V600E and KRAS mutations, CIMP and methylation of MLH1, p16 and IGFBP7

Clinical, pathological & molecular features	**All cases**	***BRAF* mutant**	***KRAS* mutant**	**CIMP-H**	***MLH1* methylation**	***p16* methylation**	***IGFBP7* methylation**	***IGFBP7* & *p16* methylation**
All colorectal polyps	217	83 (38.25%)	51 (23.5%)	31 (14.29%)	8 (3.69%)	45 (20.74%)	74 (34.1%)	20 (9.22%)
Patient age (years, SD)	62.36± 13.54	58.8 ± 13.48	61.67 ± 13.87	64 ± 13.51	71 ± 6.05	63.4 ± 14.17	58.45 ± 13.3	58.8 ± 14.98
Gender								
Female	115	50 (43.48%)	26 (22.61%)	19 (16.52%)	4 (3.48%)	28 (24.35%)	49 (42.61%)	16 (13.91%)
Male	102	33 (32.35%)	25 (24.51%)	12 (11.76%)	4 (3.92%)	17 (16.67%)	25 (24.51%)	4 (3.92%)
Location								
Proximal	112	44 (39.29%)	18 (16.07%)	30 (26.79%)	7 (6.25%)	38 (33.93%)	43 (38.39%)	18 (16.07%)
Distal	105	39 (37.14%)	33 (31.43%)	1 (0.95%)	1 (0.95%)	7 (6.67%)	31 (29.52%)	2 (1.9%)
Polyp type								
Serrated polyps	**154**	**82 (53.25%)**	**40 (25.97%)**	**30 (19.48%)**	**8 (5.19%)**	**35 (22.73%)**	**62 (40.26%)**	**19 (12.34%)**
HP	109	48 (44.04%)	35 (32.11%)	9 (8.26%)	1 (0.92%)	16 (14.68%)	35 (32.11%)	4 (3.67%)
GCHP	*59*	*12 (20.34%)*	*30 (50.85%)*	*4 (6.78%)*	*0*	*7 (11.86%)*	*19 (32.2%)*	*2 (3.39%)*
MVHP	*50*	*36 (72%)*	*5 (10%)*	*5 (10%)*	*1 (2%)*	*9 (18%)*	*16 (32%)*	*2 (4%)*
TSA	3	2 (66.67%)	0	1 (33.33%)	0	0	2 (66.67%)	0
MP	7	4 (57.14%)	2 (28.57%)	2 (28.57%)	0	2 (28.57%)	3 (42.86%)	1 (14.29%)
SSA	35	28 (80%)	3 (8.57%)	18 (51.43%)	7 (20%)	17 (48.57%)	22 (62.86%)	14 (40%)
Adenomas	**63**	**1 (1.59%)**	**11 (17.46%)**	**1 (1.59%)**	**0**	**10 (15.87%)**	**12 (19.05%)**	**1 (1.59%)**
TA	52	1 (1.92%)	4 (7.69%)	1 (1.92%)	0	6 (11.54%)	10 (19.23%)	1 (1.92%)
TVA	11	0	7 (63.64%)	0	0	4 (36.36%)	2 (18.18%)	0
Size								
1-5 mm	144	50 (34.72%)	37 (25.69%)	13 (9.03%)	3 (2.08%)	22 (15.28%)	44 (30.56%)	8 (5.56%)
>5 mm	73	33 (45.21%)	14 (19.18%)	18 (24.66%)	5 (6.85%)	23 (31.51%)	30 (41.1%)	12 (16.44%)
***BRAF* status**								
BRAF mutant	83	-	0	28 (33.73%)	7 (8.43%)	27 (32.53%)	44 (53.01%)	17 (20.48%)
BRAF wild	134	-	51 (38.06%)	3 (2.24%)	1 (0.75%)	18 (13.43%)	30 (22.39%)	3 (2.24%)
***KRAS* status**								
KRAS mutant	51	0	-	0	0	7 (13.73%)	8 (15.69%)	1 (1.96%)
KRAS wild	166	83 (50%)	-	31 (18.67%)	8 (4.82%)	38 (22.89%)	66 (39.76%)	19 (11.45%)

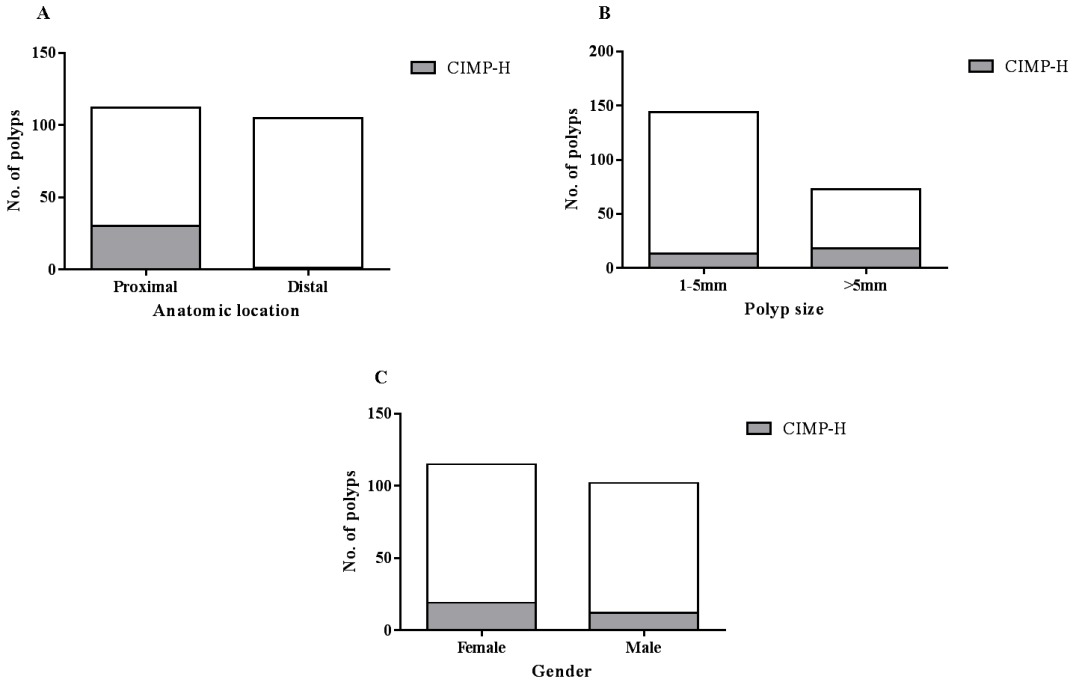

Figure 3.2 - Correlation between CIMP and location, polyp size and gender. *CIMP-H polyps displayed a significant correlation with proximal location (P < 0.0001)* ***(A)*** *and large polyp size (>5mm) (P = 0.0035)* ***(B)****. However, there was no significant correlation between CIMP-H and gender* ***(C)****.*

3.2.4 *BRAF* mutant/CIMP-H status and polyp type with respect to location

As reported in Spring *et al*, *BRAF* mutation was strongly associated with MVHPs and SSAs and *KRAS* mutation was associated with GCHPs and TVAs (Spring *et al*, 2006). The only TA with a *BRAF* mutation was a <5 mm polyp occurring in the setting of multiple SSAs and was the only TA to show CIMP-H. There were no TVAs with *BRAF* mutation or CIMP-H status (Table 3.1).

BRAF mutations were common in MVHPs- 36 *BRAF* mutant polyps out of 50 and three were *BRAF* mutant/CIMP-H. The other two CIMP-H MVHPs were wild-type for both *BRAF* and *KRAS*. Although *KRAS* mutation was predominant in GCHPs and only 20.34% had *BRAF* mutations, three out of the four CIMP-H samples were *BRAF* mutant and the remaining CIMP-H sample was wild-type for both *BRAF* and *KRAS*. TSAs and MPs had the same proportion of *BRAF* mutant/CIMP-H polyps (50%). SSAs had a high percentage of *BRAF* mutant polyps (80%) and had the highest number of *BRAF* mutant/CIMP-H polyps - 18 out of a total of 28 *BRAF* mutant samples (64.29%) (Table 3.2). Overall, there was a very significant association between *BRAF* mutation

and CIMP-H ($P < 0.0001$) and a negative association between *KRAS* mutation and CIMP-H (Table 3.3).

The distribution of *BRAF* mutant/CIMP-H in serrated polyps was assessed with respect to anatomic location (Figure 3.3). In the proximal region, SSAs had a significant ($P = 0.0335$) number of *BRAF* mutated polyps with 24 out of 28 samples (85.71%), out of which 17 SSAs were CIMP-H (70.83%). The SSAs had the least number of distally located *BRAF* mutant samples with only four out of 28 polyps (14.29%) and only one *BRAF* mutant/CIMP-H SSA in the distal colon. In MPs and TSAs, all the *BRAF* mutant and *BRAF* mutant/CIMP-H polyps were proximal, except for one *BRAF* mutant distal MP. Although *BRAF* mutant HPs were more common distally, only proximal HPs showed CIMP-H (Figure 3.3).

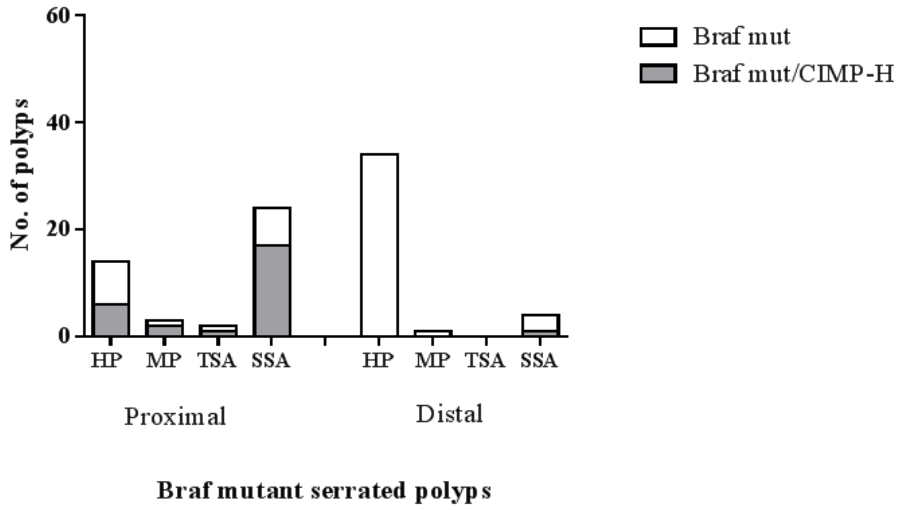

Figure 3.3 - BRAF mutant/CIMP-H in serrated polyps. *A comparative analysis of the distribution of BRAF mutant/CIMP-H samples in serrated polyps with respect to the anatomical location in the human colon. A significant association was observed between BRAF mutant polyps and CIMP-H ($P < 0.0001$).*

Table 3.2 - Serrated polyp subtypes and their association with BRAF V600E and KRAS mutations, CIMP-H status and MLHI, p16 and IGFBP7 methylation

Clinical, pathological & molecular features	**All cases**	***BRAF* mutant**	***KRAS* mutant**	**CIMP-H**	***MLH1* methylation**	***p16* methylation**	***IGFBP7* methylation**	***IGFBP7* & *p16* methylation**
Serrated polyps	154	82 (53.25%)	40 (25.97%)	30 (19.48%)	8 (5.19%)	35 (22.73%)	62 (40.26%)	19 (12.34%)
BRAF mutant								
Serrated polyps	**82**	**-**	**0**	**27 (32.93%)**	**7 (8.54%)**	**26 (31.71%)**	**43 (52.44%)**	**16 (19.51%)**
HP	48	-	0	6 (12.5%)	1 (2.08%)	9 (18.75%)	20 (41.67%)	2 (4.17%)
GCHP	*12*	-	*0*	*3 (25%)*	*0*	*3 (25%)*	*7 (58.33%)*	*1 (8.33%)*
MVHP	*36*	-	*0*	*3 (8.33%)*	*1 (2.78%)*	*6 (16.67%)*	*13 (36.11%)*	*1 (2.78%)*
TSA	2	-	0	1 (50%)	0	0	1 (50%)	0
MP	4	-	0	2 (50%)	0	2 (50%)	2 (50%)	1 (25%)
SSA	28	-	0	18 (64.29%)	6 (21.43%)	15 (53.57%)	20 (71.43%)	13 (46.43%)
KRAS mutant								
Serrated polyps	**40**	**0**	**-**	**0**	**0**	**3 (7.5%)**	**6 (15%)**	**1 (2.5%)**
HP	35	0	-	0	0	3 (8.57%)	5 (14.29%)	1 (2.86%)
GCHP	*30*	*0*	-	*0*	*0*	*2 (6.67%)*	*5 (16.67%)*	*1 (3.33%)*
MVHP	*5*	*0*	-	*0*	*0*	*1 (20%)*	*0*	*0*
TSA	0	0	-	0	0	0	0	0
MP	2	0	-	0	0	0	1 (50%)	0
SSA	3	0	-	0	0	0	0	0
CIMP-H								
Serrated polyps	**30**	**27 (90%)**	**0**	**-**	**6 (20%)**	**21 (70%)**	**21 (70%)**	**16 (53.33%)**
HP	9	6 (66.67%)	0	-	0	6 (66.67%)	4 (44.44%)	3 (33.33%)
GCHP	*4*	*3 (75%)*	*0*	-	*0*	*3 (75%)*	*2 (50%)*	*1 (25%)*
MVHP	*5*	*3 (60%)*	*0*	-	*0*	*3 (60%)*	*2 (40%)*	*2 (40%)*
TSA	1	1 (100%)	0	-	0	0	1 (100%)	0
MP	2	2 (100%)	0	-	0	1 (50%)	2 (100%)	1 (50%)
SSA	18	18 (100%)	0	-	6 (33.33%)	14 (77.78%)	14 (77.78%)	12 (66.67%)

Table 3.3 - Association between CIMP status, BRAF V600E and KRAS mutations in all polyp types

Polyp type	All cases	CIMP-H cases	CIMP-H						CIMP-negative cases	CIMP-negative					
			KRAS		*BRAF*		*KRAS/BRAF*			*KRAS*		*BRAF*		*KRAS/BRAF*	
			Mut	Wild	Mut	Wild	Mut	Wild		Mut	Wild	Mut	Wild	Mut	Wild
SP	**154**	**30 (19.48%)**	**0**	**30 (100%)**	**27 (90%)**	**3 (10%)**	**0**	**3 (10%)**	**124 (80.52%)**	**40 (32.26%)**	**84 (67.74%)**	**55 (44.35%)**	**69 (55.65%)**	**0**	**29 (23.39%)**
HP	109	9 (8.26%)	0	9 (100%)	6 (66.67%)	3 (33.33%)	0	3 (33.33%)	100 (91.74%)	35 (35%)	65 (65%)	42 (42%)	58 (58%)	0	23 (23%)
GCHP	*59*	*4 (6.78%)*	*0*	*4 (100%)*	*3 (75%)*	*1 (25%)*	*0*	*1 (25%)*	*55 (93.22%)*	*30 (54.55%)*	*25 (45.45%)*	*9 (16.36%)*	*46 (83.64%)*	*0*	*16 (29.09%)*
MVHP	*50*	*5 (10%)*	*0*	*5 (100%)*	*3 (60%)*	*2 (40%)*	*0*	*2 (40%)*	*45 (90%)*	*5 (11.11%)*	*40 (88.89%)*	*33 (73.33%)*	*12 (26.67%)*	*0*	*7 (15.56%)*
TSA	3	1 (33.33%)	0	1 (100%)	1 (100%)	0	0	0	2 (66.67%)	0	2 (100%)	1 (50%)	1 (50%)	0	1 (50%)
MP	7	2 (28.57%)	0	2 (100%)	2 (100%)	0	0	0	5 (71.43%)	2 (40%)	3 (60%)	2 (40%)	3 (60%)	0	1 (20%)
SSA	35	18 (51.43%)	0	18 (100%)	18 (100%)	0	0	0	17 (48.57%)	3 (17.65%)	14 (82.35%)	10 (58.82%)	7 (41.18%)	0	4 (23.53%)
AD	**63**	**1 (1.59%)**	**0**	**1 (100%)**	**1 (100%)**	**0**	**0**	**0**	**62 (98.41%)**	**11 (17.74%)**	**51 (82.26%)**	**0**	**62 (100%)**	**0**	**51 (82.26%)**
TA	52	1 (1.92%)	0	1 (100%)	1 (100%)	0	0	0	51 (98.08%)	4 (7.84%)	47 (92.16%)	0	51 (100%)	0	47 (92.16%)
TVA	11	0	0	0	0	0	0	0	11 (100%)	7 (63.64%)	4 (36.36%)	0	11 (100%)	0	4 (36.36%)

3.2.5 *IGFBP7* and *p16* methylation in colorectal tumours

An initial assessment of *IGFBP7* and *p16* methylation was performed in 51 colorectal tumours and correlated with *BRAF* and *KRAS* mutations, CIMP-H, and MSI (Table 3.4). In this group, 30 out of 51 samples were methylated for *IGFBP7* (58.82%). A significant association was observed between *BRAF* mutation and *IGFBP7* methylation in colorectal tumours ($P < 0.0001$) – 24 out of 26 *BRAF* mutant tumours were methylated for *IGFBP7* (92.31%) as shown in Figure 3.4A. In *KRAS* mutant tumours, a majority of the *IGFBP7* methylated samples were wild-type for *KRAS* (Figure 3.4B). Only five out of a total of 14 *KRAS* mutant samples showed *IGFBP7* methylation and was not significant. *IGFBP7* methylation was also significantly associated ($P < 0.0001$) with CIMP-H tumours with 23 out of 25 samples methylated for *IGFBP7* (Figure 3.4C). All the MSI-H tumours (15 in total; $P < 0.0001$); 40% of MSS tumours (12 of 30 samples) and three out of six MSI-L samples were methylated for *IGFBP7* (Figure 3.4D).

p16 methylation was observed in 27 colorectal tumours; out of which 22 had *BRAF* mutations (84.62%) and were significantly associated with *p16* methylation ($P < 0.0001$) (Figure 3.4A). Similar to *IGFBP7* methylation, only five tumours were *KRAS* mutant (35.71%) and this was not a significant correlation (Figure 3.4B). CIMP-H and MSI-H showed a significant association with *p16* methylated colorectal tumours - $P < 0.0001$ and $P = 0.0018$ respectively. Among the CIMP-H tumours, 21 out of 25 samples (84%) were methylated for *p16* as shown in Figure 3.4C. A majority of the MSI-H samples - 13 of 15 tumours; three MSI-L (50%) and 11 MSS (36.67%) samples were also methylated for *p16* (Figure 3.4D).

The combined methylation of *IGFBP7* and *p16* was present in 22 out of 51 colorectal tumours and showed a significant correlation with *BRAF* mutation, CIMP-H and MSI-H ($P < 0.0001$). In the *BRAF* mutant tumours, 21 out of 26 samples (80.77%) showed combined *IGFBP7*/*p16* methylation (Figure 3.4A). Only one *KRAS* mutant (Figure 3.4B), one MSI-L and eight MSS samples were methylated for *IGFBP7* and *p16*. All the MSI-H samples methylated for *p16* (13 in total) were also methylated for *IGFBP7* (86.67%) (Figure 3.4D). In the CIMP-H tumours, 20 out of 25 samples showed combined *p16*/*IGFBP7* methylation (Figure 3.4C).

Table 3.4 - Methylation of IGFBP7 and p16 in colorectal tumours and their association with BRAF and KRAS mutations, CIMP and MSI status

Total No. of cases = 51	***BRAF* status**		***KRAS* status**		***KRAS*/*BRAF* status**		**MSI status**			**CIMP status**		***IGFBP7* methylation**	***p16* methylation**
	Mut	**Wild**	**Mut**	**Wild**	**Mut**	**Wild**	**MSI-H**	**MSI-L**	**MSS**	**CIMP-H**	**CIMP-ve**		
All cases	26 (50.98%)	25 (49.02%)	14 (27.45%)	37 (72.55%)	0	11 (21.57%)	15 (29.41%)	6 (11.76%)	30 (58.82%)	25 (49.02%)	26 (50.98%)	30 (58.82%)	27 (52.94%)
***IGFBP7* meth**	24 (92.31%)	6 (24%)	5 (35.71%)	25 (67.57%)	0	1 (9.09%)	15 (100%)	3 (50%)	12 (40%)	23 (92%)	7 (26.92%)	–	22 (81.48%)
***p16* meth**	22 (84.62%)	5 (20%)	5 (35.71%)	22 (59.46%)	0	0	13 (86.67%)	3 (50%)	11 (36.67%)	21 (84%)	6 (23.08%)	22 (73.33%)	–
***IGFBP7*/*p16* meth**	21(80.77%)	1 (4%)	1 (7.14%)	21 (56.76%)	0	0	13 (86.67%)	1 (16.67%)	8 (26.67%)	20 (80%)	2 (7.69%)	–	–

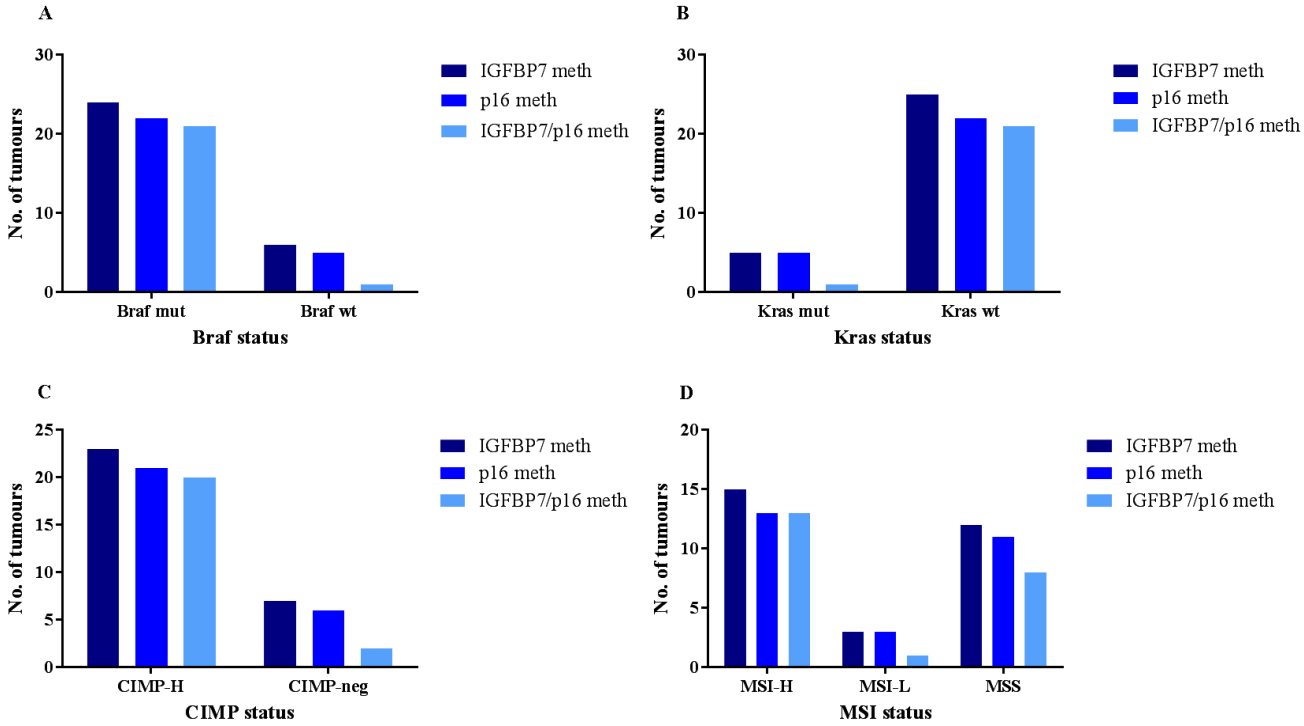

Figure 3.4 - IGFBP7 and p16 methylation in colorectal tumours (n = 51). *IGFBP7, p16 and combined IGFBP7/p16 methylation were more prevalent in BRAF mutant* ***(A)****, KRAS wild type* ***(B)****, CIMP-H* ***(C)*** *and MSI-H* ***(D)*** *colorectal tumours. IGFBP7 methylation and combined IGFBP7 and p16 methylation were significantly associated with BRAF mutation (P < 0.0001), CIMP-H (P < 0.0001) and MSI-H (P < 0.0001). Similarly, a significant association was also observed between p16 methylated tumours and BRAF mutation (P < 0.0001), CIMP-H (P < 0.0001) and MSI-H (P = 0.0018).*

3.2.6 Methylation of *p16* and *IGFBP7* in polyps

The number of *p16* methylated samples was the highest in SSAs with 17 of 35 (48.57%) (Figure 3.5A). In the adenomas only ten samples were methylated for *p16* (15.87%) with the majority being TAs. The levels of *IGFBP7* methylation were similar to the *p16* methylation analysis with the highest number of *IGFBP7* methylated samples in the SSAs with 22 out of 35 samples (62.86%) followed by HPs - 35 *IGFBP7* methylated samples out of 109 (32.11%). In adenomas, only 10 out of 63 samples (19.01%) were methylated for *IGFBP7* (Figure 3.5B).

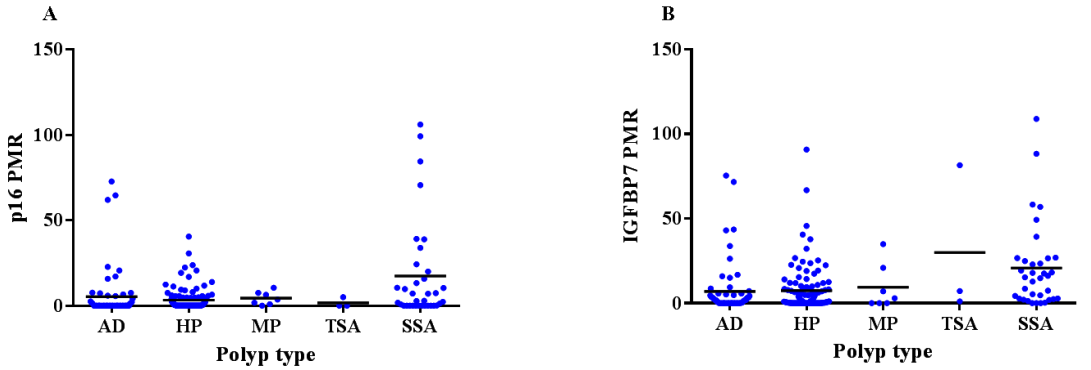

Figure 3.5 - p16 and IGFBP7 methylation in different polyp types. *An assessment of the methylation levels of p16* ***(A)*** *and IGFBP7* ***(B)*** *in polyps by scatter plots. Adenomas consisted of TAs and TVAs; while the HP group included GCHPs and MVHPs.*

3.2.7 *p16* and *IGFBP7* methylation in *BRAF* mutant and CIMP-H polyps

BRAF mutant SSAs had the highest number of *p16* methylated (53.57%), *IGFBP7* methylated (71.43%) and *p16*/*IGFBP7* methylated (46.43%) samples (Figure 3.6A). In the *BRAF* mutant HPs, 20 out of 48 samples (41.67%) were *IGFBP7* methylated, but only nine out of 48 samples were methylated for *p16*. The combined *p16*/*IGFBP7* methylation percentage in the HPs was quite low with only two methylated samples compared to the SSAs with combined *p16*/*IGFBP7* methylation in 13 out of 28 *BRAF* mutant polyps. The analysis of *p16* and *IGFBP7* methylation in CIMP-H polyps was shown in Figure 3.6B. In CIMP-H SSAs, 77.78% were methylated for *p16* and *IGFBP7* and combined *p16*/*IGFBP7* methylation was 66.67%. In the CIMP-H HPs, out of nine samples, six and four samples were methylated for

p16 and *IGFBP7* respectively (Table 3.2). *IGFBP7* methylation was also common in CIMP-negative HPs.

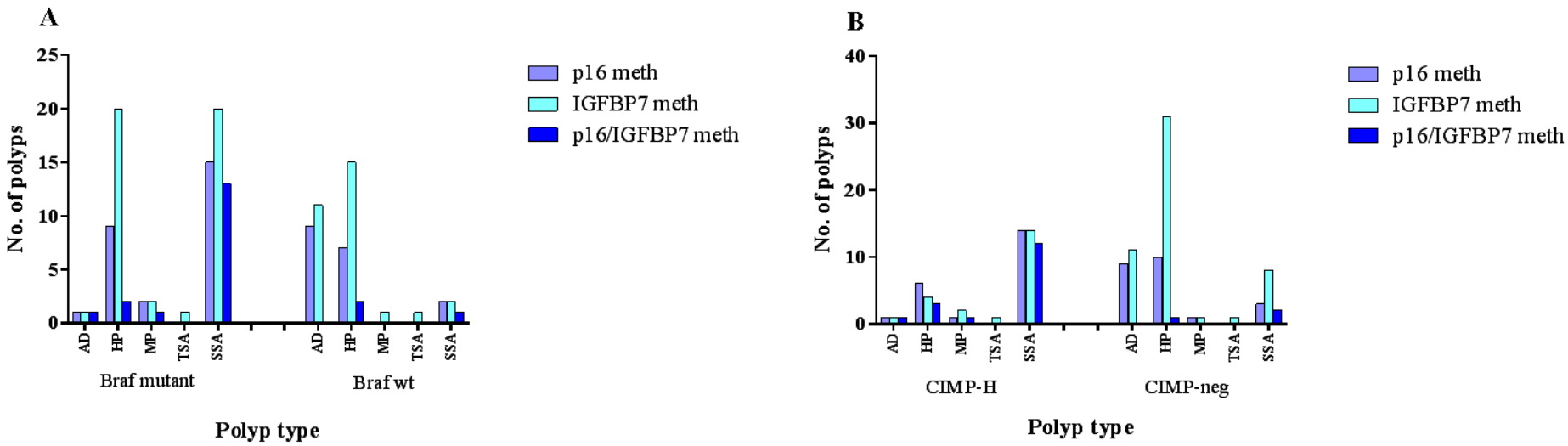

Figure 3.6 - BRAF mutation and CIMP status in p16 and IGFBP7 methylated polyps. *A comparative analysis was performed to assess the percentage of BRAF mutant* ***(A)*** *and CIMP-H* ***(B)*** *samples with p16 and IGFBP7 methylation. The SSAs showed the highest number of p16 and combined p16/IGFBP7 methylated samples in the BRAF mutant and CIMP-H groups and this was closely followed by the HPs.*

3.3 Discussion

Toyota *et al* identified the existence of CIMP in colorectal tumours and preneoplastic adenomatous polyps (Bird, 1986; Toyota *et al*, 1999). There is also a significant association between CIMP-H, MSI and *BRAF* mutations in colorectal cancers (Lee *et al*, 2008a). In colorectal polyps, CIMP was significantly associated with serrated polyps. CIMP-H adenomas constituted a minor proportion and were dependent on the polyp size (>2 cm) and percentage of villous component (>80%) (Kakar *et al*, 2008; Park *et al*, 2003). A variety of methylation markers have been employed to determine CIMP status in polyps including the Toyota *et al* and Weisenberger *et al* panels, *HIC1*, *MGMT* and *RASSF2* using MSP (non-quantitative) and MethyLight (quantitative) assays with a PMR cut-off for methylation ranging from >4 to >10 (Pai *et al*, 2010; Park *et al*, 2003; Vaughn *et al*, 2010).

Several studies have been performed to classify serrated polyps based on their CIMP status; but a majority of them were retrospective, did not include all serrated polyp types and were represented by small sample numbers (Burnett-Hartman *et al*, 2013; Gaiser *et al*, 2013; O'Brien *et al*, 2004; Park *et al*, 2003; Sandmeier *et al*, 2009; Vaughn *et al*, 2010; Yang *et al*, 2004). The choice of methylation markers and the assay does affect the outcome of methylation status in samples. The Weisenberger *et al* panel was more specific than the Toyota *et al* markers for identifying CIMP phenotype associated with *BRAF* mutant and MSI-H colorectal tumours; and quantitative MethyLight assay was more sensitive and specific for methylation analysis compared to non-quantitative MSP (Eads *et al*, 2000; Weisenberger *et al*, 2006).

Our study is one of the first prospective studies to assess the CIMP status of all the colorectal polyp subtypes using the Weisenberger *et al* panel of methylation markers and quantitative MethyLight technology. Our results indicated that CIMP-H status was significantly associated with serrated polyps, proximal location, *BRAF* V600E mutations and increase in polyp size. This study shows a progressive increase in CIMP as the malignant potential of serrated polyps increases (HP vs SSA). CIMP seems more likely to develop when there is a *BRAF* mutation and the polyp is in the proximal colonic environment. SSAs had the highest number of CIMP-H polyps (51.43%), while the HPs and ADs showed a very low frequency of CIMP-H with

8.25% and 1.59% respectively. A majority of other studies showed that SSAs were predominantly CIMP-H; followed by HPs with a higher frequency compared to our study. This could be due to the classification of serrated polyps based on CIMP-H status using MSP and the Toyota *et al* methylation markers (Kim *et al*, 2011; O'Brien *et al*, 2004; O'Brien *et al*, 2006).

In our study, 62.96% of proximal SSAs were CIMP-H and only one CIMP-H SSA was located in the distal colon; while all the CIMP-H HPs were proximal. This was similar to other reports where a majority of CIMP-H SSAs and HPs were proximally located (Maeda *et al*, 2011; O'Brien *et al*, 2004; Vaughn *et al*, 2010). We found that CIMP-H was significantly associated with *BRAF* mutant serrated polyps and a negative association existed between *KRAS* mutation and CIMP-H which was also observed in studies by O'Brien *et al* and Yang *et al* (O'Brien *et al*, 2004; Yang *et al*, 2004). Based on our results and similar studies, *BRAF* mutant, CIMP-H SSAs which are proximally located provide further support for SSAs as potential precursors of *BRAF* mutant, CIMP-H CRCs. A recent retrospective CIMP study by Burnett-Hartman *et al* was carried out on 359 serrated polyps using the Weisenberger *et al* methylation panel and MethyLight assay. Results showed that CIMP-H was more prevalent in SSAs, proximal colon and *BRAF* mutant serrated lesions, which confirms our findings (Burnett-Hartman *et al*, 2013).

MLH1 and *p16* along with *MINT1*, *MINT2* and *MINT31* constitute the Toyota *et al* panel (Toyota *et al*, 1999). *p16* and *MLH1* methylation have been evaluated in numerous studies in colorectal tumours and polyps. In tumours, *MLH1* methylation showed a significant association with CIMP, MSI-H and was mainly located in the proximal colon (Miyakura *et al*, 2001; Toyota *et al*, 1999). In HPs, 3- 21% of the samples were methylated for *MLH1*, while the frequency varied from 16- 23.2% in SSAs (Dong *et al*, 2005; Kim *et al*, 2011; Kim *et al*, 2008; Vaughn *et al*, 2010). Only 7% of the TAs were methylated for *MLH1*, while this was completely absent in the TVAs (Kakar *et al*, 2008; Kim *et al*, 2008). Out of 217 polyps in our study, only 3.69% of the samples were methylated for *MLH1* and all the samples were proximally located except for one MVHP. *MLH1* methylation was detected in 4% of HPs and 17% of SSAs and was completely absent in adenomas and these results were found to

be similar to reports discussed above (Burnett-Hartman *et al*, 2013; Vaughn *et al*, 2010).

p16 methylation is also closely linked to CIMP-H and MSI-H CRCs (Psofaki *et al*, 2010; Toyota *et al*, 1999; Toyota *et al*, 2000). The results from our study indicated that *p16* methylation was correlated with serrated polyp type, proximal location, *BRAF* V600E mutations and CIMP-H status. In a study by Dhir *et al*, *p16* along with *MLH1*, *CDX2* and *TLR2* showed the highest frequency of methylation in SSAs based on an unsupervised clustering analysis (Dhir *et al*, 2011). A similar trend was observed in other studies with the frequency of *p16* methylation being the highest in SSAs with 76.8%; while it was 48% in SAs and 29% in TAs (Kim *et al*, 2011; Park *et al*, 2003). Our results showed a comparatively lower percentage of *p16* methylated samples in SSAs (48.57%) and TAs (11.53%). There was no increase in *p16* methylation from TAs to TVAs as was observed by Psofaki *et al* (Psofaki *et al*, 2010).

IGFBP7 has been implicated as an early event in CRC progression via the serrated pathway. Methylation of *IGFBP7*, a potential tumour suppressor gene was also evaluated in different polyp types. Similar to *p16* methylation, *IGFBP7* methylated polyps were mainly serrated, closely linked to *BRAF* V600E mutations and CIMP-H status. A study by Suzuki *et al* also observed similar correlations between *IGFBP7* methylation and *BRAF* mutation, *p16* methylation and CIMP and an inverse correlation with *KRAS* mutation in colorectal tumours. *IGFBP7* methylation was also detected in 18% of adenomas, which was similar to our results (19%) (Suzuki *et al*, 2010). In a recent study by Kaji *et al*, it was proposed that *IGFBP7* methylation did not affect HPs due to lower PMRs when compared to TSAs or SSAs (Kaji *et al*, 2012). This was also observed in our study with only 32.11% of HPs methylated for *IGFBP7* which was lower than TSAs (66.67%) and SSAs (62.86%) (Kaji *et al*, 2012; Suzuki *et al*, 2010).

To date, the serrated pathway has not yet been fully characterised. In the human colorectal polpy section (Chapter 3), this study showed that CIMP-H was significantly associated with serrated polyps, mainly the SSA sub-group. Only a minority of HPs and ADs were CIMP-H. All the CIMP-H HPs and a significant proportion of CIMP-H SSAs were located in the proximal colon. There was a strong association between *BRAF* V600E mutation and CIMP-H polyps. Methylation of the

functionally important genes *MLH1*, *p16* and *IGFBP7* was the highest in SSAs and was associated with *BRAF* V600E mutation, CIMP-H and proximal location. This study used a stringent definition of CIMP and has highlighted the association of increasing methylation levels in serrated polyps with malignant potential. The application of advanced methodology such as methylation and expression arrays will help to evaluate other genes/markers and potentially contribute towards a more defined understanding of the various changes causing the transformation of a serrated precursor lesion into CRC.

Based on this study, it was observed that *BRAF* V600E mutation and *p16INK4a* are key players in the serrated pathway. The question that needs to be answered is if *BRAF* V600E alone is sufficient to make a significant contribution to colorectal tumorigenesis or is there a requirement for secondary mutation or silencing of other genes such as *p16INK4a* and *p14ARF*? The additional analysis of early lesions and tumours from the BRAF conditional mouse model will further define the role of BRAF and other alterations in the serrated pathway and will be discussed in the subsequent chapters.

CHAPTER 4

CONDITIONAL *BRaf*^{VE} MOUSE MODEL – PHENOTYPIC ANALYSIS

4. CONDITIONAL *BRaf^{VE}* MOUSE MODEL – PHENOTYPIC ANALYSIS

4.1 INTRODUCTION

BRAF, a protein involved in the mitogen activated protein kinase (MAPK) pathway has been implicated in a wide variety of cancers such as melanomas (59%), colorectal cancer (18%), gliomas (11%) and lung cancers (3%), with the highest frequency observed in malignant melanoma. The most common *BRAF* mutation is the V600E mutation present in exon 15 with a basal kinase activity 10.7-fold higher than that of *BRAF* wild type (Davies *et al*, 2002). In CRC, *BRAF* mutations are predominantly associated with the serrated pathway with a high incidence in serrated polyps compared to adenomas (Chan *et al*, 2003; Lee *et al*, 2005). Mutations in the *BRAF* gene are also closely linked with sporadic CRC, which have *MLH1* methylation, CpG island methylator phenotype (CIMP) and high levels of microsatellite instability (Deng *et al*, 2004; O'Brien *et al*, 2006).

The role of *BRAF* mutation in tumour progression has been studied in a variety of cancers with the aid of mouse models. In 2007, a *BRaf^{CA}* mouse model was developed to study the initiation and progression of lung tumours under the influence of *Braf* V600E mutation. This model simulated *BRAF* V600E mutation at a physiologic level in which one copy of *BRaf^{CA}* (wild type) is converted into *BRaf^{VE}* (mutant) by somatic mutation. Mice treated with adenovirus expressing Cre recombinase converted the *BRaf^{CA}* allele into mutant *BRaf^{VE}*, which caused the formation of multiple lung tumours (Dankort *et al*, 2007). This *BRaf^{CA}* mouse was also used to study the effect of *BRaf^{VE}* and its interaction with the *Pten* mouse in the development of melanocytic hyperplasia and metastatic melanoma (Dankort *et al*, 2009). Colorectal cancer based mouse models were also developed to study the effect of mutant *BRAF* on intestinal hyperplasia and tumorigenesis (Carragher *et al*, 2010; Rad *et al*, 2013). The *BRaf^{CA}* mouse was obtained from Professor Martin McMahon (UCSF, USA) in order to understand colorectal cancer that develops via the serrated neoplastic pathway.

The aim of this study was to investigate whether or not *BRAF* V600E mutation alone can induce spontaneous tumorigenesis in the gastrointestinal tract. The study

required developing a conditional intestine specific mouse model to assess the role of mutant *BRAF* in the serrated pathway. This study was designed to determine if *BRAF* mutation alone was sufficient to initiate hyperplasia and serrated lesions in the intestine and also study the progression of the disease. The breeding strategy for generating $BRaf^{CA/+}/A33CreERT2^{+/-}/Lacz^{+/-}$ mice was described in Section 2.2.1. These mice were injected with tamoxifen (Secion 2.3.5) and sacrificed at various time points – 6 weeks, 6 months and 12 months post tamoxifen treatment; while the remaining mice were monitored for tumour formation (Section 2.5).

4.2 RESULTS

4.2.1 Conditional $BRaf^{CA}$ mouse model

The conditional $BRaf^{CA}$ mouse model was developed by Dankort and colleagues to assess the effect of *Braf* mutation in the initiation, development and progress of lung tumours. Homologous recombination in embryonic stem cells was used along with a suitable targeting vector (Figure 4.1) to generate a Cre-dependent $BRaf^{CA}$ mouse. Prior to Cre activation, $BRaf^{CA}$ expressed normal Braf (Figure 4.1B); while activation of Cre resulted in the conversion of one allele of $BRaf^{CA}$ into $BRaf^{VE}$ which was expressed at physiologic levels.

The different *BRaf* mRNAs were distinguished based on silent restriction enzyme polymorphisms incorporated into the targeting vector – BamHI and XbaI for $BRaf^{CA}$ and $BRaf^{VE}$ respectively. A LoxP-flanked cassette contained exons 15-18 which encoded for cDNA of human *BRAF*. A minigene which encoded for *BRAF* V600E was a modified exon 15 and this was located outside the LoxP cassette; which on Cre activation generated the $BRaf^{VE}$ allele (Figure 4.1C) (Dankort *et al*, 2007). The $BRaf^{CA}$ mouse was crossed with $A33CreERT2^{+/-}$ mouse which carried the Cre recombinase gene and this could be activated by tamoxifen treatment (Feil *et al*, 1997). The A33 antigen helped restrict the activity of the Cre recombinase only to the intestinal epithelial cells (Johnstone *et al*, 2002).

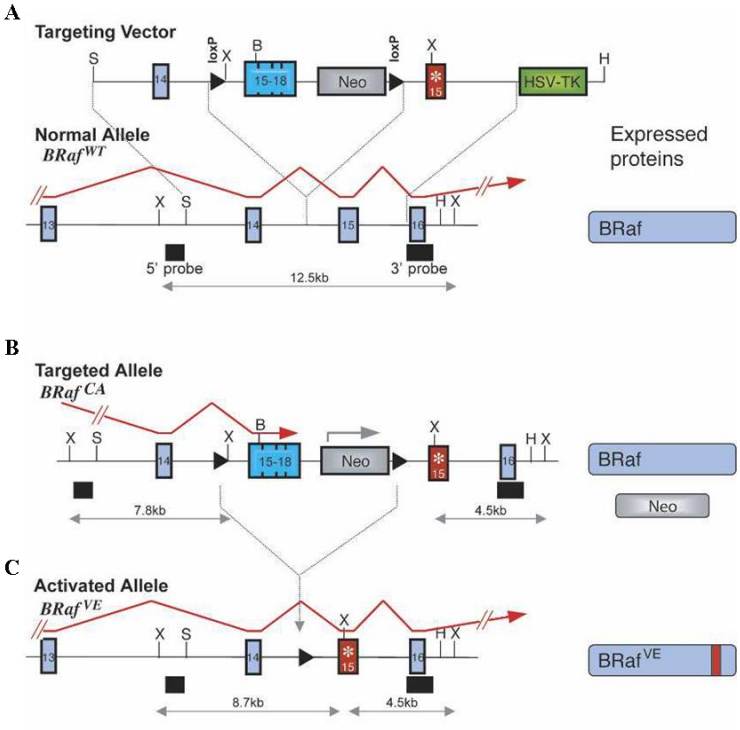

Figure 4.1 – Conditional BRaf^{CA} mouse model. *The targeting vector contained a LoxP-flanked cassette, which consisted of exons 15-18 encoding for human BRAF cDNA. A minigene (*) was situated outside the LoxP-flanked cassette and this encoded for BRAF V600E. The targeting vector expressed normal BRafCA (B) similar to the BRafWT (A) before Cre-activation. The activation of Cre recombinase initiates a recombination event within the LoxP flanked cassette and results in BRafVE expression (C).*

4.2.2 Validation of *BRaf^{VE}* activation in the GI tract

4.2.2.1 Retro-cre activation of *BRaf^{VE}* in immortalized mouse embryonic fibroblasts

Mouse embryonic fibroblasts (MEFs) from *BRaf$^{CA/+}$* were isolated and immortalized (Sections 2.4.3.1 and 2.4.3.2). The MEFs were infected with varying volumes of retro-cre virus to evaluate the viral titer and the conversion of the *BRaf^{CA}* allele into *BRaf^{VE}* (Sections 2.4.3.3, 2.4.3.4 and 2.4.3.5). DNA was extracted from the duodenums of tamoxifen induced male and female mice with the genotype *BRaf$^{CA/+}$*, normal MEFs and MEFs infected with retro-cre virus in varying amounts – 0.5 ml, 1

ml, 1.5 ml, 2 ml and 2.5 ml. The extracted DNA was evaluated for *BRaf*^{CA} to *BRaf*^{VE} conversion using the *BRaf*^{VE} genotyping assay (Section 2.3.4.1).

In Figure 4.2, the *BRaf* wild type and *BRaf*^{CA} amplicons were observed in all the samples at 185 bp and 308 bp respectively with reference to the 100 bp ladder (L). The *BRaf*^{CA} allele showed varying degrees of band intensity depending on the rate of conversion of *BRaf*^{CA} into *BRaf*^{VE}. In the positive controls – PC1 and PC2 and retro-cre infected samples C1 to C5, the *BRaf*^{VE} allele was observed at 335 bp. In the sample group, C1, C2 and C3 showed the highest level of *BRaf*^{CA} to *BRaf*^{VE} conversion (~88%); unlike C4 and C5 where a lower level of *BRaf*^{CA} to *BRaf*^{VE} conversion was observed.

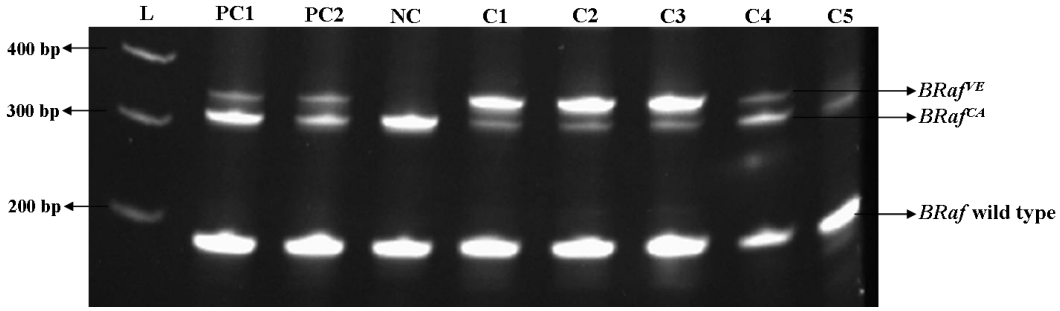

Figure 4.2 - Retro-cre activation of BRaf^{VE} in MEFs. *BRaf^{VE} genotyping assay was used to evaluate the conversion of BRaf^{CA} to BRaf^{VE}. PCR amplicons of 185 bp and 308 bp for wild type and BRaf^{CA} alleles respectively were present in all the samples. BRaf^{VE} amplicon was observed in the positive controls (PC1 and PC2) at 335 bp and this was absent in the negative control (NC). Samples C1 to C5 were positive for the BRaf^{VE} allele and the level of BRaf^{CA} to BRaf^{VE} conversion was the highest in C1 to C3 (~88%) and lowest in C4 and C5 based on the intensity of the BRaf^{VE} amplicon at 335 bp. A 100 bp DNA ladder was used as the reference (L).*

4.2.2.2 Activation of Cre recombinase (*A33CreERT2Lacz*)

Whole mount X-gal staining was performed on mouse colon and small intestine, which was divided into three regions – duodenum, jejunum and ileum (Section 2.4.2). The expression of *A33CreERT2Lacz* gene, which encoded for the enzyme Cre recombinase under the control of tamoxifen was assessed in the proximal and distal ends of the colon and small intestine regions. A patchy, blue stain was observed between the V shaped folds in the proximal colon (control) due to non-

specific X-gal staining, while there was no visible stain in the distal colon (Figure 4.3A). A moderate specific staining pattern was observed in the proximal colon of the tamoxifen treated mouse, which was stronger than the distal end (Figure 4.3B).

Similar to the control colon, there was an absence of X-gal staining in all regions of the control small intestine (Figures 4.3C, 4.3E and 4.3G). However, in the tamoxifen treated mouse, specific X-gal expression was observed in all regions of the small intestine. An increased level of X-gal expression was observed in the duodenum as compared with the other sections of the small intestine (ie. jejunum and ileum). Furthermore, this expression was found to be stronger in the proximal region of the duodenum than the distal region of the tamoxifen treated mouse (Figure 4.3D). This was similar to the X-gal staining pattern in the jejunum, which also decreased from the proximal to the distal end, but was not as strong as the proximal duodenum (Figure 4.3F). However, X-gal expression in the ileum of the tamoxifen treated mouse was lower than the duodenum and jejunum, but was similar to the colon (Figure 4.3H). This suggested that Cre recombinase (*A33CreERT2Lacz*) was highly expressed in the small intestine, which gradually decreased from the duodenum to the ileum.

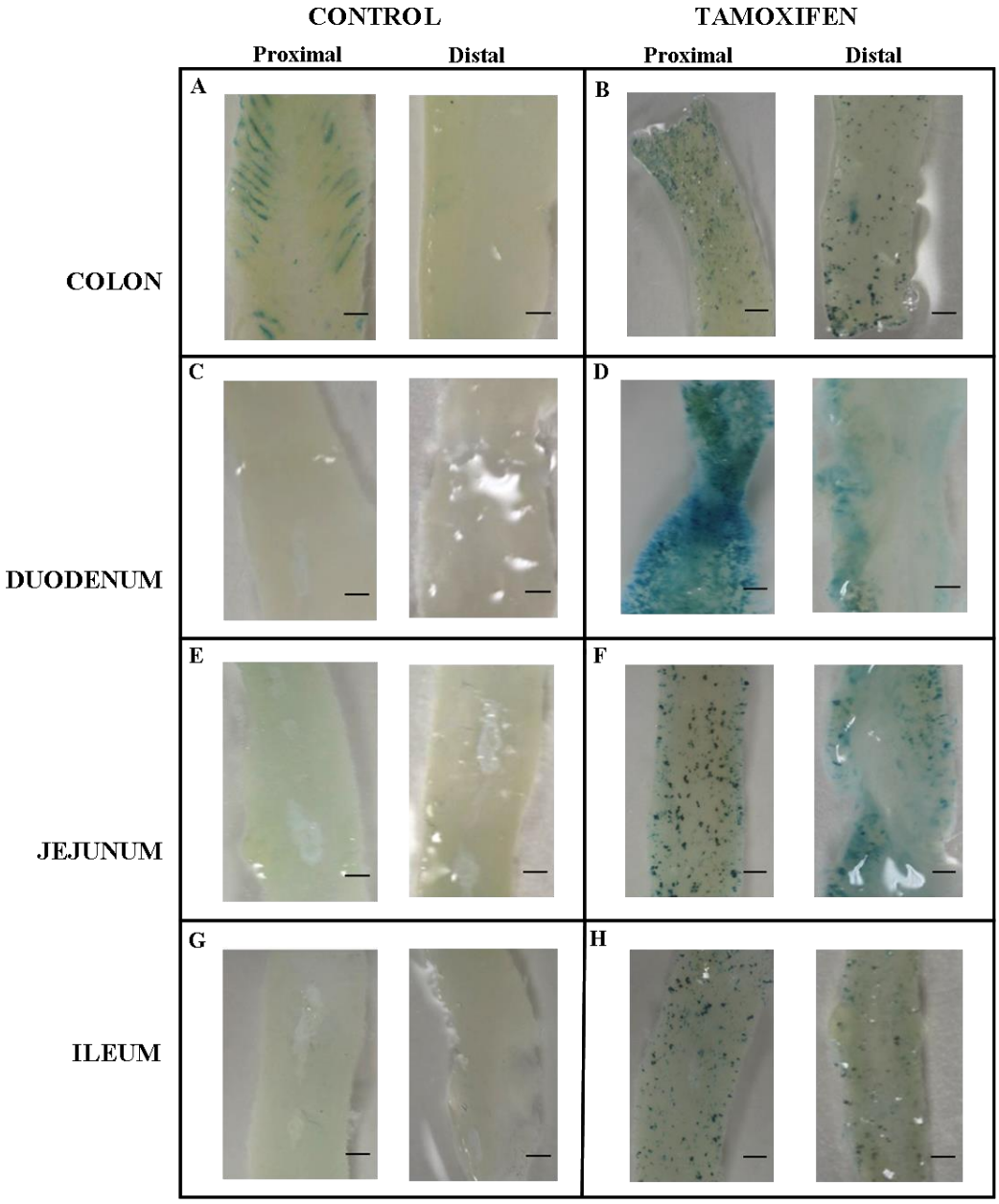

Figure 4.3 - X-gal staining in mouse colon and small intestine. *X-gal staining was absent in the control samples, except for endogenous X-gal staining in the proximal colon* ***(A, C, E and G)****. A moderate expression of X-gal was observed in the tamoxifen treated proximal colon* ***(B)*** *and this was similar to the tamoxifen treated proximal ileum* ***(H).*** *The tamoxifen treated proximal duodenum* ***(D)*** *showed the highest staining pattern compared to all the other samples and this was followed by the proximal end of the jejunum* ***(F)****. Scale bars (A-H) represent 10 mm.*

4.2.2.3 Activation of *BRaf*^{VE} in mouse small intestine and colon

DNA isolated from the colon and small intestine crypts of mice treated with olive oil (control) and tamoxifen were genotyped for the *BRaf*^{VE} allele (Sections 2.4.1 and 2.3.4.1). The colon was divided into two regions - proximal (CT1) and distal (CT2), while the small intestine was divided into three regions – duodenum (ST1), jejunum (ST2) and ileum (ST3). The negative control samples for the small intestine and colon were sourced from the duodenum (SC) and proximal colon (CC) respectively from an olive oil treated mouse, while the DNA isolated from the small intestine crypts of a tamoxifen treated mouse was amplified and used as a positive control (PC).

The *BRaf* wild type and *BRaf*^{CA} amplicons were observed in all the samples at 185 bp and 308 bp respectively (Figure 4.4). In the tamoxifen treated samples of the small intestine, the *BRaf*^{VE} amplicon was observed with varying degrees of intensity at 335 bp. The highest rate of *BRaf*^{CA} to *BRaf*^{VE} conversion was observed in the tamoxifen treated duodenum at ~37% (ST1) followed by the jejunum at ~17% (ST2) and ileum (ST3). The *BRaf*^{VE} amplicon in the tamoxifen-induced proximal colon (CT1) was similar to the jejunum (ST2), but was stronger than the distal colon (CT2), while the positive control showed the highest level of *BRaf*^{CA} to *BRaf*^{VE} conversion.

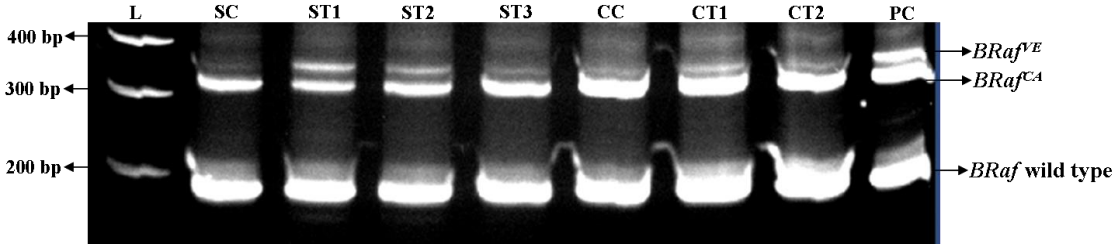

Figure 4.4 - Activation of mutant allele BRaf^{VE} in mice. *BRaf^{VE} genotyping assay was used to evaluate the mutant allele BRaf^{VE} in mice. This was assessed in three regions of the mouse small intestine – duodenum, jejunum and ileum and two regions of the mouse colon – proximal and distal. The BRaf wild type and BRaf^{CA} alleles were observed in all the samples at 185 bp and 308 bp respectively. The negative controls for the small intestine (SC) and colon (CC) were obtained from an olive oil treated mouse. The highest level of BRaf^{CA} to BRaf^{VE} conversion was observed in tamoxifen treated duodenum (ST1), followed by jejunum (ST2) and ileum (ST3).*

4.2.2.4 Assessment of villus and crypt length in conditional $BRaf^{VE}$ mouse model

Hyperplastic changes such as increase in villus or crypt lengths were assessed in mice treated with tamoxifen and olive oil (control mice) 6 weeks post treatment (Section 2.5.2). In the duodenum, the average villus length for the tamoxifen treated mice (650.80 μm) (Table 4.1) was significantly higher (P = 0.0112) than the control duodenum (491.50 μm) (Figures 4.5A, 4.5B and 4.6A). A significant difference (P = 0.0115) was also observed when comparing the average villi length of the jejunum in tamoxifen treated (510.88 μm) and control jejunum samples (357.80 μm) (Figures 4.5C, 4.5D and 4.6B). A similar trend was also observed for ileum where the average villi lengths of the tamoxifen treated and control ileum were 260.65 μm and 205.41 μm respectively with a significant P value of 0.0132 (Figures 4.5E, 4.5F and 4.6C).

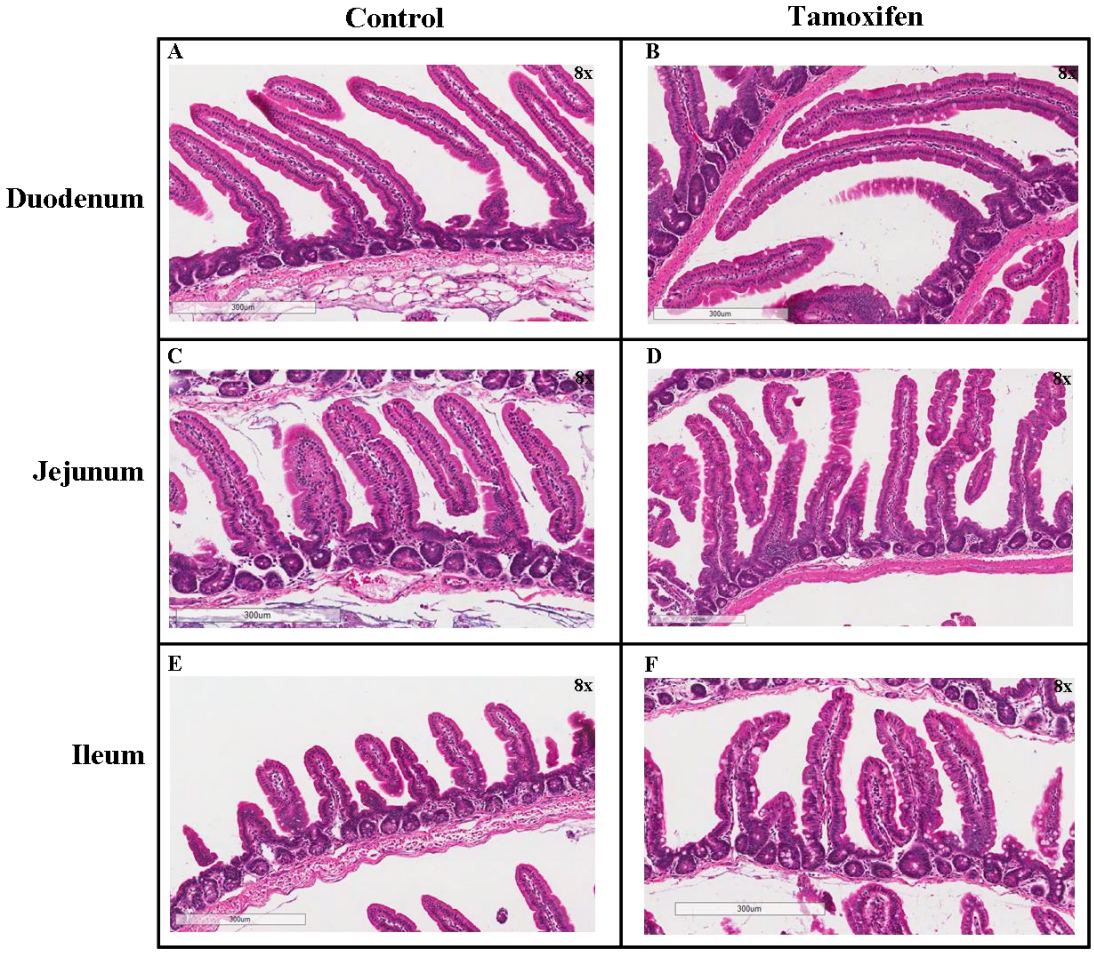

Figure 4.5 - Villi lengths of the small intestine. *Differences in villi lengths could be visually observed in H&E stained small intestine samples of control and tamoxifen induced mice. The duodenum* ***(B)****, jejunum* ***(D)*** *and ileum* ***(F)*** *of tamoxifen treated mice displayed an increase in villi length compared to the corresponding controls* ***(A, C and E)****. Scale bars (A-F) represent 300 μm; magnification (A-F) 8x.*

Table 4.1 - Measurements of crypt and villus lengths of olive oil and tamoxifen treated BRaf$^{CA/+}$/A33CreERT2$^{+/-}$/Lacz$^{-/-}$ mice

Colon/SI regions	Treatment							
	Olive oil (µm)			Average	Tamoxifen (µm)			Average
Colon crypt	171.63	162.25	147.93	**160.60**	168.95	186.08	191.35	**182.13**
Duodenum								
Villus	453.75	519.84	500.92	**491.50**	702.49	650.97	598.94	**650.80**
Crypt	76.74	79.46	80.59	**78.93**	97.13	106.46	97.51	**100.37**
Jejunum								
Villus	346.43	360.64	366.34	**357.80**	571.34	507.90	453.40	**510.88**
Crypt	71.78	79.16	75.73	**75.56**	98.46	98.08	90.63	**95.72**
Ileum								
Villus	202.24	195.81	218.18	**205.41**	244.08	281.97	255.90	**260.65**
Crypt	72.45	78.52	72.25	**74.41**	79.36	80.80	85.74	**81.96**

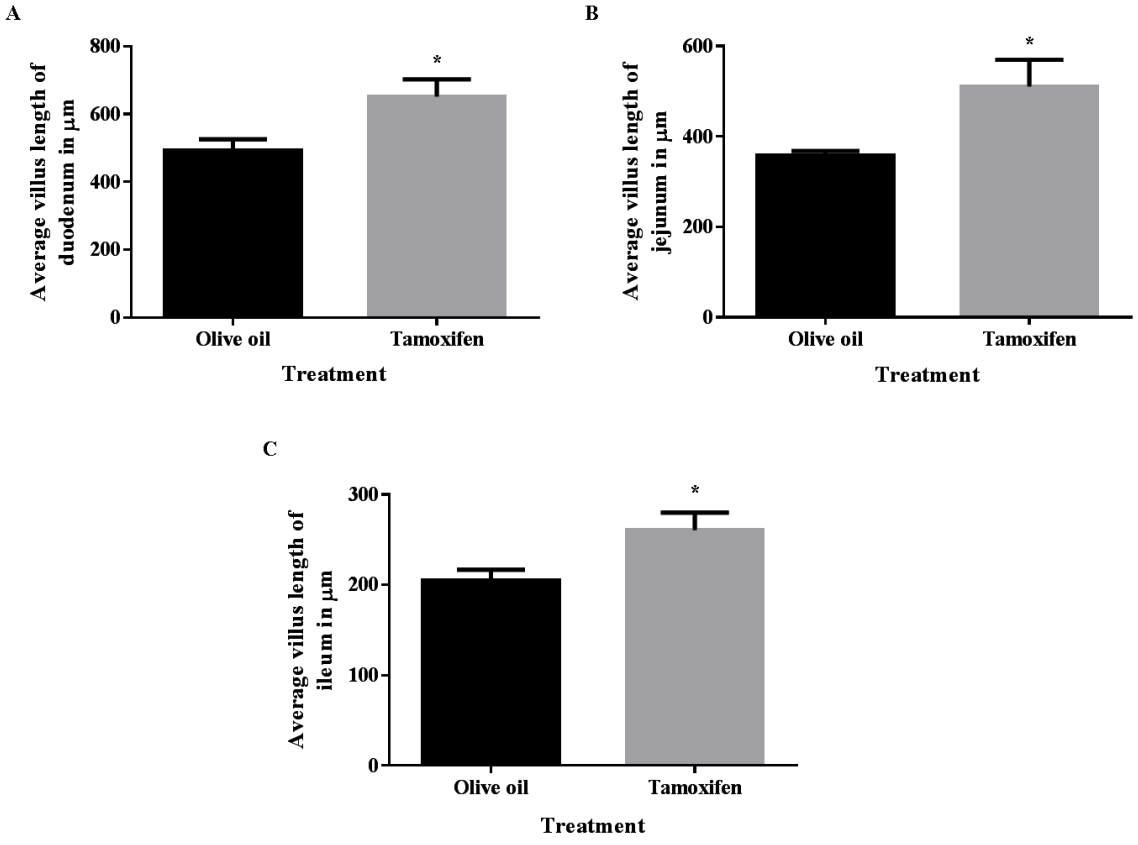

Figure 4.6 – Assessment of villi lengths in mouse small intestine. *The average villi lengths of small intestines of control and tamoxifen treated mice. A significant increase was observed in the duodenum (P = 0.0112) (*)* ***(A)****, jejunum (P = 0.0115) (*)* ***(B)*** *and ileum (P = 0.0132) (*)* ***(C)*** *of all the tamoxifen treated mice. All measurements were in µm; error bars, SEM.*

The lengths of crypts were also assessed in olive oil (control) and tamoxifen treated mice groups as shown in Table 4.1. Crypt lengthening was observed in the colon and all regions of the small intestine 6 weeks post treatment, compared to the corresponding controls. In the duodenum, the average crypt lengths were significantly different (P = 0.0028) between the control (78.93 μm) and tamoxifen treated mice (100.37 μm) respectively (Figure 4.7A) and a similar trend was observed between control (75.56 μm) and tamoxifen treated jejunum (95.72 μm) samples (Figure 4.7B) with a significant P value of 0.0037. However, the ileum exhibited only a marginal, increase in average crypt length in the tamoxifen treated sample (81.96 μm) compared to the control (74.41 μm) (Figure 4.7C). Crypt lengthening was also observed in the colon, which on an average was 160.60 μm in the control and 182.13 μm in the tamoxifen treated samples (Figure 4.7D); but the difference was not significant.

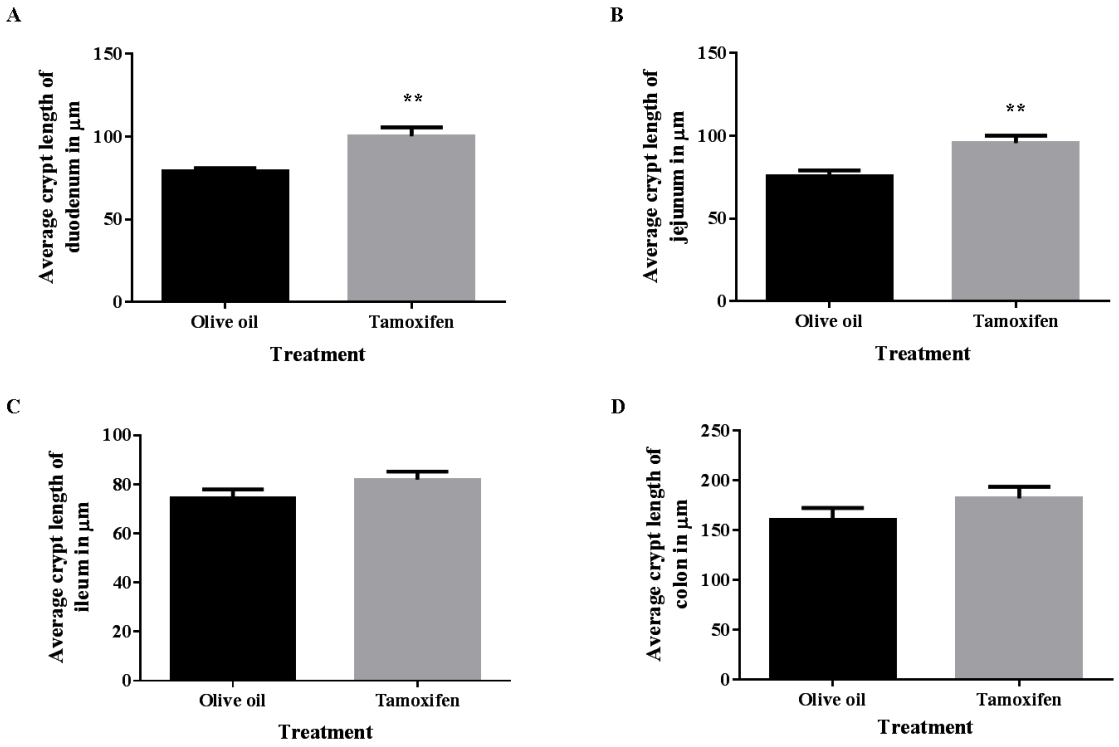

Figure 4.7 – Evaluation of crypt lengths in mouse small intestine and colon. *An increase in average crypt lengths was observed in all regions of the tamoxifen treated small intestine and colon. However, only the duodenum (P = 0.0028) (**)* ***(A)*** *and jejunum (P = 0.0037) (**)* ***(B)*** *exhibited a significant difference in average crypt lengths compared to the corresponding control mice. An increase in average crypt lengths was also observed in the ileum* ***(C)*** *and colon* ***(D)*** *of tamoxifen treated mice, but the difference between the corresponding controls was not significant. All measurements were in µm; error bars, SEM.*

A gradual decrease in the $BRaf^{VE}$ conversion was observed from the duodenum to ileum of the small intestine based on the $BRaf^{VE}$ genotyping results (Section 4.2.1.3). This would cause a difference in villi and crypt length between the SI regions in the tamoxifen treated samples. A comparative analysis to assess crypt lengths was performed between regions of the small intestine in tamoxifen treated mice. A significant difference ($P = 0.0054$) was observed in the average crypt lengths between all regions of the small intestine as shown in Figure 4.8A. The duodenum exhibited the highest increase in average crypt length (100.37 µm), followed by the jejunum (95.72 µm) and ileum (81.96 µm). However, there was no significant difference observed between average crypt lengths of the duodenum and jejunum

(Figure 4.8B). The average crypt length of the ileum was also compared with the duodenum (Figure 4.8C) and jejunum (Figure 4.8D) and the results were significant with *P* values of 0.0070 and 0.0126 respectively. In the case of villus length in control samples, a significant difference was observed between the different regions of the small intestine.

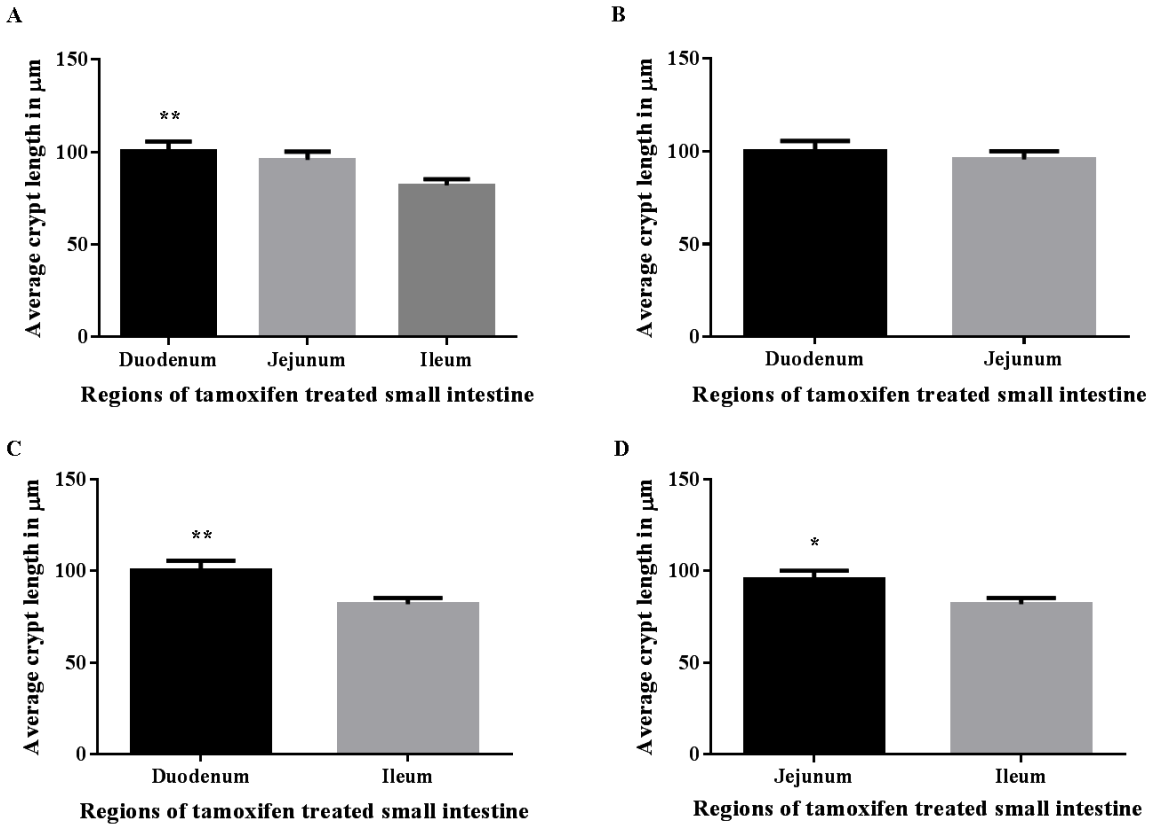

Figure 4.8 – Comparison of crypt lengths between different regions of tamoxifen treated small intestine. *The duodenum exhibited the highest increase in average crypt length compared to the jejunum and ileum (P = 0.0054) (**) **(A)**. Analysis between the average crypt lengths of duodenum and jejunum exhibited no significant difference **(B)**. The difference in average crypt lengths between duodenum and ileum (P = 0.0070) (**) **(C)** and jejunum and ileum (P = 0.0126) (*) **(D)** was significant. All measurements were in µm; error bars, SEM.*

4.2.3 Phenotypic effect of the mutant allele *BRaf^{VE}* in mice – timepoint and longitudinal studies

4.2.3.1 Time point analysis of the *BRaf^{VE}* phenotype

Mice were set up for time point sacrifices at 6 and 12 months post tamoxifen treatment. For the six month time point, five olive oil treated (controls) mice and seven tamoxifen treated mice (referred to as *BRaf^{VE}* mice in the subsequent sections) were sacrificed post treatment. No lesions/polyps were observed in the colons and small intestines of the *BRaf^{VE}* mice and the controls. In the *BRaf^{VE}* mice, only lengthening of the villi was observed in the duodenum of the small intestine. The mice that were sacrificed 12 months post treatment consisted of five olive oil induced (controls) and five *BRaf^{VE}* mice. In the duodenum, lengthening of the villi was observed in two out of five tamoxifen induced mice compared to all the controls. No lesions were also observed in the colons and small intestines of the *BRaf^{VE}* mice. A hepatic adenoma was observed in the liver of only one *BRaf^{VE}* mouse, which was sacrificed 52 weeks (12 months) post tamoxifen treatment.

4.2.3.2 Longitudinal analysis of the phenotypic effect of *BRaf^{VE}* allele

Mice were set up for longitudinal studies for monitoring spontaneous tumour formation and subsequently sacrificed when they exhibited signs of sickness such as weight loss, ruffled coat, rapid breathing and physical abnormalities. The longitudinal study consisted of a set of 22 olive oil induced (controls) mice (*BRaf$^{CA/+}$/A33CreERT2$^{+/-}$/Lacz$^{-/-}$*), 23 tamoxifen induced mice (*BRaf$^{CA/+}$/A33CreERT2$^{+/-}$/Lacz$^{-/-}$*) and 32 mice, which were not treated (controls) (*BRaf$^{CA/+}$/A33CreERT2$^{-/-}$/Lacz$^{-/-}$*). These mice groups will be herein called *BRaf^{VE}* (tamoxifen) and *BRaf^{CA}* (control).

4.2.3.3 Assessment of colorectal polyps in small intestine and colon of tamoxifen treated mice

The mice set up for longitudinal studies were monitored for the development of colorectal polyps or tumours in the small intestine and colon. The small intestines and colons were stained with 0.1% methylene blue to detect lesions or abnormalities

as shown in Figure 4.9A (arrows). In the *BRaf*^{VE} group, 9 out of 23 mice (39.13%) developed abnormalities in the small intestine, while the colons of all the *BRaf*^{VE} mice were found to be normal compared to the controls. All the *BRaf*^{VE} mice which developed lesions were older than 85 weeks at the time of sacrifice, except for one mouse (65.43 weeks old) which developed a tumour in the small intestine (Figure 4.9B – orange). The tumour was located in the proximal end of the duodenum and was identified as a poorly differentiated mixed adenocarcinoma with infiltrating carcinoma, possibly a histiocytic sarcoma.

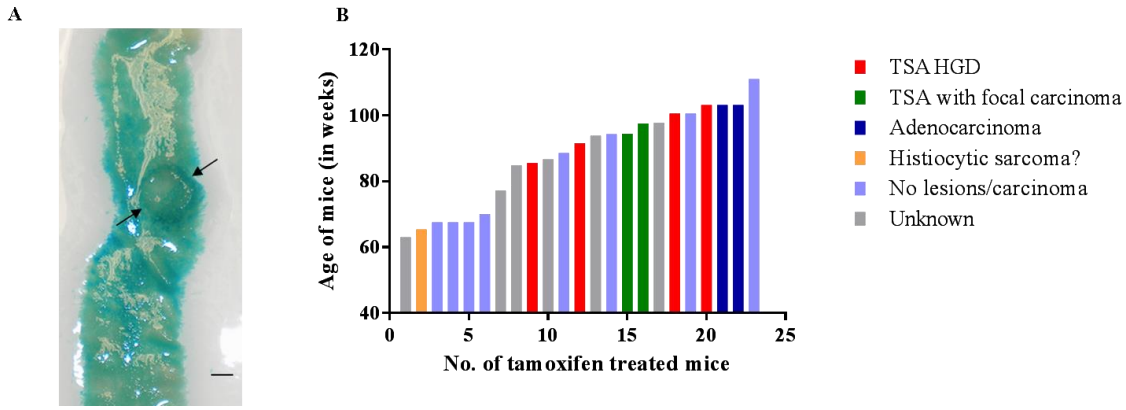

Figure 4.9 – Assessment of colorectal polyps in small intestine of BRaf^{VE} mice. *The small intestines of tamoxifen treated mice were stained with 0.1% methylene blue to detect lesions. A solitary lesion was identified in the proximal end of the duodenum of the small intestine (arrows). Scale bar represents 10 mm* ***(A)****. Abnormalities in the small intestines were observed in 9 out of 23 tamoxifen treated mice. The youngest mouse was 65.43 weeks old (light blue), while the oldest was 103.14 weeks old (dark blue), while the remaining mice were above 85 weeks of age (red and green). The mice exhibited lesions ranging from traditional serrated adenomas with high grade dysplasia to foci of invasive adenocarcinoma and moderately differentiated adenocarcinomas* ***(B)****.*

The common lesion identified in the *BRaf*^{VE} mice was the traditional serrated adenoma (TSA) with high-grade dysplasia (HGD). Multiple TSAs with HGD were observed in the duodenum of four tamoxifen induced mice (Figure 4.9B - red) aged between 85.57 and 103.14 weeks. These were characterised by distorted crypt (Figure 4.10B) and villi (Figure 4.10C) structures compared to the control duodenum (Figure 4.10A). This loss in structural integrity was also observed in the jejunum as shown in

Figures 4.10E and 4.10F compared to the control jejunum (Figure 4.10D). Foci of invasive adenocarcinoma and intramucosal adenocarcinoma (Figure 4.10G) in the duodenum were observed only in two mice (tamoxifen) aged 94.43 weeks and 95.57 weeks and TSAs with HGD were present in both the duodenum and jejunum (Figure 4.9B - green). The older mice aged 103.14 weeks developed moderately differentiated adenocarcinomas (Figure 4.9B – dark blue) in the proximal duodenum, one arising from a TSA with HGD and there were no signs of lesions in the other parts of the duodenum or jejunum. In all the $BRaf^{VE}$ mice, there were no lesions observed in the distal end of the jejunum or the ileum.

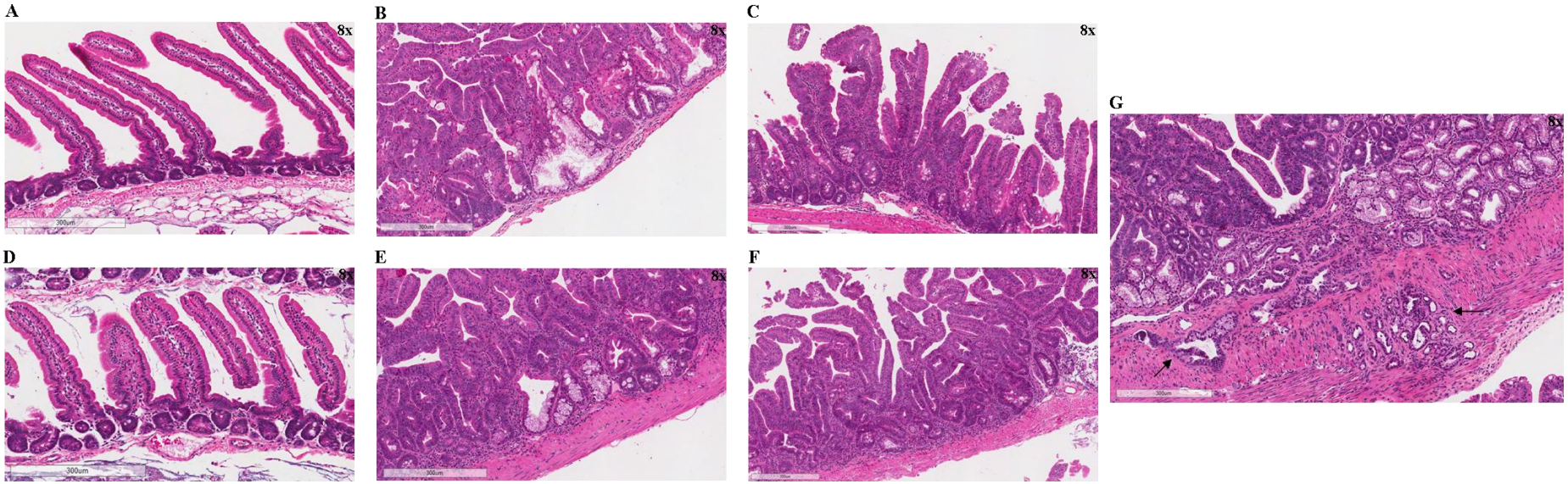

Figure 4.10 – TSAs with HGD in small intestine of BRaf^{VE} mice. *Traditional serrated adenomas with high grade dysplasia were observed mainly in the duodenum* ***(B and C)*** *and jejunum* ***(E and F)*** *of tamoxifen treated mice. A loss of structural configuration was observed in the epithelial crypts* ***(B and E)*** *and villi* ***(C and F)*** *compared to their respective controls - duodenum* ***(A)*** *and jejunum* ***(B)****. A TSA with HGD with intramucosal adenocarcinoma (arrows) was also observed in the duodenum of the small intestine* ***(G)****. Scale bars (A-G) represent 300 μm; magnification 8x (A-G).*

4.2.3.4 Extracolonic abnormalities/tumours in control and tamoxifen treated mice

Mice set up for longitudinal analysis also developed extracolonic abnormalities/tumours in organs such as liver, lungs, kidneys and spleen. A majority of the lesions or tumours were observed in the liver and lungs in all the mice groups including control, non-treated and tamoxifen treated mice. In the controls, abnormalities in the lungs were most commonly observed (Figures 4.11A and 4.11B); with 72.72% and 62.5% in control and non-treated mice respectively and were predominantly lung adenocarcinomas. This was followed by aberrations in the liver, which were prevalent in about 40% of the control and non-treated group (Figures 4.10A and 4.10B). The aberrations ranged from hepatic adenomas to more severe cases of hepatocellular carcinoma and lymphomas. Lesions in the spleen, enlarged kidneys and uterine defects constituted a minor group of abnormalities in the control mice (Figures 4.11A and 4.11B).

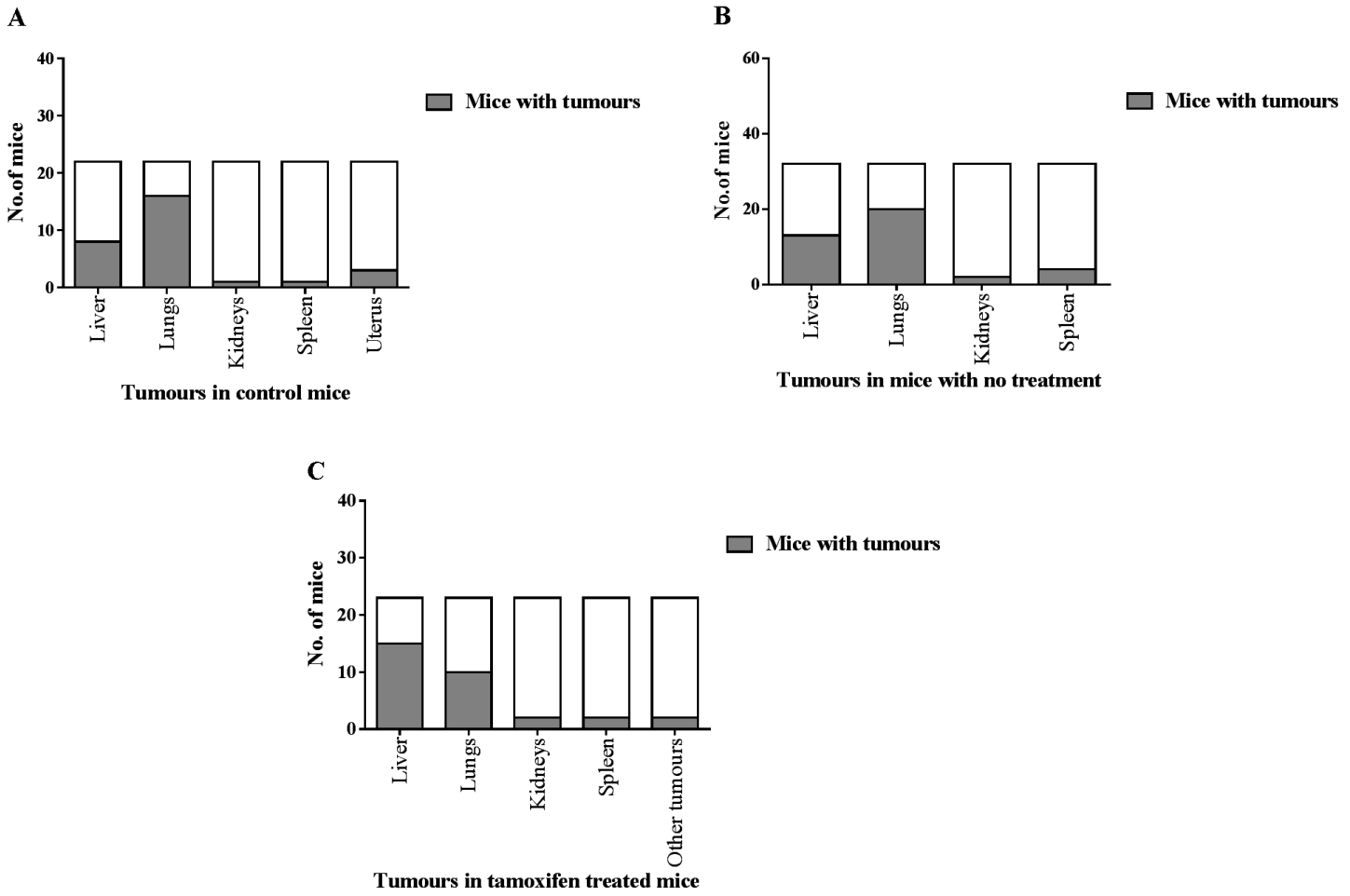

Figure 4.11 – Extracolonic tumours in all mice groups. *Tumours and other abnormalities were observed in organs such as liver, lungs, kidneys and spleen. A majority of the aberrations were present in the lungs and liver in the controls* ***(A and B)*** *and tamoxifen induced mice* ***(C)****.*

In the tamoxifen treated mice, aberrations in the liver were prevalent in 65.22% of the cases (Figure 4.11C) and were predominantly hepatic adenomas or hepatocellular carcinomas, similar to the control groups. This was followed by lesions or tumours in the lungs in 43.48% of the tamoxifen treated mice, which was lower than the control groups. Abnormal pathology in the kidneys were observed in only two mice and an assessment of the H&E stained slides revealed severe renal hydronephrosis (swollen kidney due to failure of drainage of urine from kidney to bladder) in one mouse and focal cortical atrophy (decrease in size of kidney's cortex) in the other mouse. In one $BRaf^{VE}$ mouse, ventricular thrombus (blood clot in the ventricle of the heart) was detected, while the other had a lump on its back, which on further observation was assessed as a possible neurogenic sarcoma. Tumours in all the mice groups were observed in mice older than 65 weeks and could potentially be age-related.

4.2.3.5 Survival rate of $BRaf^{VE}$ mice

The survival rates of all mice groups including mice treated with olive oil (11 mice) and tamoxifen (13 mice) and untreated mice (21 mice) were analysed. Mice that were sacrificed at all time points (6 weeks, 6 months, 12 months and 2 years) were excluded from this analysis. The survival rate of the tamoxifen treated mice (Figure 4.12 – red line) was found to be lower than the controls – olive oil (Figure 4.12 – blue line) and untreated mice (Figure 4.12 – green line); however the difference between the mice groups was not significant. The $BRaf^{VE}$ mice displayed a poor survival rate compared to the controls with the oldest mouse being 97 weeks old at the time of sacrifice. The olive oil treated and the untreated mice survived for 116 weeks and 112 weeks respectively. In the olive oil treated group, two mice were sacrificed as early as 7 weeks and 17 weeks due to visible signs of sickness, but no obvious tumours were detected. However, the tamoxifen treated mice had a 100% survival rate up to 63 weeks; after which, the number of mice declined more rapidly over a short period of time compared to the controls.

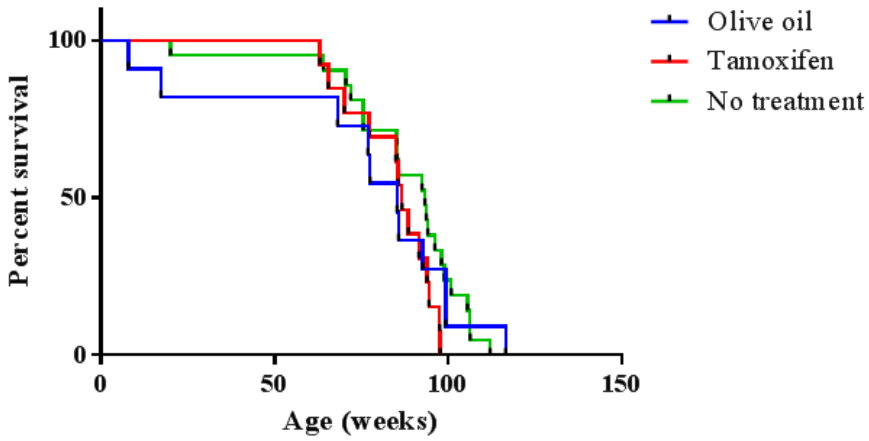

Figure 4.12 – Kaplan-Meier plot of BRaf^{VE} mice. *The BRaf^{VE} mice displayed a poor survival rate compared to the controls – olive oil treated and untreated mice. All the BRaf^{VE} mice were dead by 97 weeks (red line); while the olive oil treated and untreated mice survived up to a maximum of 116 weeks (blue line) and 112 weeks (green line) respectively.*

4.3 DISCUSSION

The development of CRC from a benign serrated lesion to a malignant tumour progresses via the serrated pathway, in which *BRAF* mutation is one of the key factors. This study was aimed at understanding the role of *BRAF* mutation in the formation of intestinal lesions via the serrated pathway using a conditional *BRAF* mouse model. The mouse was developed by Dankort and colleagues and contained an inactive *BRaf^{CA}* allele and was crossed with *A33CreERT2* to facilitate Cre-mediated recombination. This would convert the inactive *BRaf^{CA}* into active, mutant *BRaf^{VE}* (mice with *BRAF* V600E mutation will be referred to as *BRaf^{VE}* in this section) (Dankort *et al*, 2007; Feil *et al*, 1997).

In our study, initial experiments were performed to assess the extent of conversion of the *BRaf^{CA}* allele into mutant *BRaf^{VE}*, six weeks after tamoxifen treatment. The expression of the Cre recombinase was generally restricted to the intestinal tract due to tissue-specific expression directed by the A33 transgene (Johnstone *et al*, 2000; Johnstone *et al*, 2002). Results showed that the expression of *BRaf^{VE}* was elevated in the small intestine; especially the duodenum and jejunum regions compared to the colon. These results were similar to the *Braf$^{+/LSL-}$*

^{V600E};*AhcreER*$^{T+/0}$ mouse model (referred to as *Braf*$^{+/LSL\text{-}V600E}$ in this section) developed by Carragher and colleagues (Carragher *et al*, 2010). In this model, the expression of *AhcreER*^{T} was evident in a range of organs such as small intestine, liver, pancreas and forestomach (nonglandular part of the stomach) and combined by leakiness may contribute to the rapid mortality of these mice as all were dead by 20 weeks (Kemp *et al*, 2004). Another study employed a different strategy using Villin Cre to study the effect of *BRAF* V600E in the intestine – *Vil-Cre*;*Braf*$^{LSL\text{-}V637E/+}$(referred to as *Braf*$^{LSL\text{-}V637E/+}$in this section). Similar to our mouse model, *Villin-Cre* (*Vil-Cre*) expression was directed to the colon and small intestine. The expression levels were higher in the duodenum and jejunum (small intestine) compared to the colon (Rad *et al*, 2013).

Hyperplastic changes such as increase in crypt and villus lengths in the small intestine and colon were assessed six weeks post tamoxifen treatment in our study. A significant increase was observed in the villi lengths of all the regions of the small intestine – duodenum (P = 0.0112), jejunum (P = 0.0115) and ileum (P = 0.0132) compared to the corresponding controls. The crypt lengths in the tamoxifen treated samples were also higher than the controls; however, this increase was significant only in the duodenum (P = 0.0028) and jejunum (P = 0.0037). This could possibly be one of the first reports of a statistically significant increase observed in the lengths of crypts and villus in the *BRaf*^{VE} mice. In the *Braf*$^{+/LSL\text{-}V600E}$ mice, hyperplasia assessment was carried out on mice as early as three days and one week post induction. Lengthening of the crypt and increased cell number in the crypts were observed three days post induction; while increased cell number in the villi and colon crypt and a serrated epihelium were observed one week post induction (Carragher *et al*, 2010).

Rad *et al* observed increased elongation and thickening of the small intestine and colon in the *Braf*$^{LSL\text{-}V637E/+}$ mice compared to the controls, which was also observed in the *BRaf*^{VE} mice used in our study. Hyperplastic polyps such as microvesicular and goblet-cell rich types were detected in the large intestine of *Braf*$^{LSL\text{-}V637E/+}$ mice. However, only the microvesicular type was observed in the small intestine (Rad *et al*, 2013). In contrast, these lesions were not observed in the *BRaf*^{VE} mice used in our study or the *Braf*$^{+/LSL\text{-}V600E}$ mice (Carragher *et al*, 2010). In our study,

the *BRaf*^{VE} mice that were sacrificed at 6 and 12 month time points had no hyperplastic polyps in the colons or small intestines. The only hyperplastic changes visualised were the increases in villi and crypt lengths in the tamoxifen treated mice compared to the controls even at 12 months post tamoxifen treatment. This indicated a sustained hyperplasia and this was found to be similar to the hyperplastic changes observed in the *Braf*$^{LSL\text{-}V637E/+}$ mice (Rad *et al*, 2013). In contrast, hyperplasia was not permanent in the *Braf*$^{+/LSL\text{-}V600E}$ mice and eventually gave rise to suppressed proliferation and the onset of senescence (Carragher *et al*, 2010).

Mice were also set up for longitudinal studies and aged up to 2 years to monitor development of serrated lesions in the intestine and colon. No lesions or abnormalities were detected in the colon of *BRaf*^{VE} mice, while lesions were observed in the small intestine of 7 out of 23 tamoxifen treated *BRaf*^{VE} mice (30.43%), which were older than 85 weeks (1.6 years) at the time of sacrifice. In comparison, the formation of lesions was more rapid in the *Braf*$^{+/LSL\text{-}V600E}$ mice with low-grade adenomatous lesions and advanced dysplastic tumours. These were observed >6 weeks post induction only in the small intestine; while the colons were lesion-free (Carragher *et al*, 2010). On the other hand, the *Braf*$^{LSL\text{-}V637E/+}$ mice were aged up to 18 months, which was similar to our study. However in some mice, dysplasia and macroscopic tumours were observed at 2-3 months, which was not evident until 19 months in our *BRaf*^{VE} mice. The most striking feature between the *Braf*$^{LSL\text{-}V637E/+}$ and *BRaf*^{VE} mice was that all the lesions were identified as TSAs similar to the ones found in humans and no SSAs were observed (Rad *et al*, 2013).

A majority of the TSAs observed in our *BRaf*^{VE} mice had high grade dysplasia, with areas of focal carcinoma and invasive adenocarcinoma. These were observed in a small number of tamoxifen treated mice which were >90 weeks old (20 months). The timeline for the development of invasive carcinoma was reduced by half in the *Braf*$^{LSL\text{-}V637E/+}$ mice with invasive carcinomas being observed in 8.3% of the mice (<10 months old). Low grade and high grade tumours were observed in 13.8% of the mice which were older than 10 months (Rad *et al*, 2013). There was a striking difference between the survival rates of the *BRAF* V600E mouse models. The *Braf*$^{+/LSL\text{-}V600E}$ mice survived only up to 20 weeks post induction and this could be due to the combined effects of lung adenomas and stomach hyperplasia (Carragher *et al*,

2010). In contrast, a 100% survival rate among the *BRaf*^{VE} mice in our study was observed up to 63 weeks, while 4 out of 23 mice survived up to the 2 year time point (104 weeks).

The *BRAF* mouse models discussed above revealed striking differences with regard to (1) the time taken for the onset and maintenance of hyperplasia (2) duration for the development of lesions/tumours (3) frequency of lesions/tumours and (4) survival rates of the mice. These differences can be attributed to the type of tissue-specific Cre transgene used, which in turn influences the activity of mutant *BRAF*. In our mouse model, only ~37% and ~17% recombination efficiencies were observed in the duodenum and jejunum respectively at 6 weeks post treatment. This was lower than the *Braf*$^{+/LSL\text{-}V600E}$ mice which showed ~70% recombination efficiency in the small intestine at 6 weeks post induction.

The findings of our study revealed a more physiologic effect of *BRAF* V600E mutation in the small intestine, in contrast to the *Braf*$^{+/LSL\text{-}V600E}$ mice used by Carragher and colleagues (Carragher *et al*, 2010). However, the low recombination efficiency exhibited in the *BRaf*^{VE} mice was not sufficient for an early onset of serrated lesions as was observed by Rad *et al* (Rad *et al*, 2013). The occurrence of TSAs in the *BRaf*^{VE} mice after 85 weeks of age proved to be a slight disadvantage due to the development of age-related abnormalities in organs such as liver, spleen and lungs. As a result of this, the mice had to be sacrificed and could not be monitored further for the formation of advanced intestinal tumours. The *BRaf*^{VE} mouse used in this study is more suitable to function as model for hyperplasia studies; but is less practical for understanding the entire progression of colorectal cancer. An alternative tissue-specific Cre recombinase mouse such as *Villin-Cre* could be used with the *BRaf*^{CA} mouse to develop a more efficient system for studying colorectal tumorigenesis via the serrated pathway.

CHAPTER 5

MOLECULAR CHARACTERISATION OF *Braf*^{VE} PHENOTYPE

5. MOLECULAR CHARACTERISATION OF *BRaf*^{VE} PHENOTYPE

5.1 INTRODUCTION

In colorectal cancer, *BRAF* V600E mutations are significantly associated with high levels of microsatellite instability (MSI-H), *MLH1* methylation, high levels of CpG island methylator phenotype (CIMP-H), the serrated pathway, proximal location, old age, females and high tumour grade (Chan *et al*, 2003; Deng *et al*, 2004; Kambara *et al*, 2004). Minoo *et al* investigated the role played by *BRAF* V600E mutation in the serrated pathway using a normal colon epithelial cell line, NCM460, which over expressed BRAF V600E. Results showed that BRAF kinase is activated by the MAPK pathway and results in cellular hyperproliferation. It is also responsible for the malignant transformation and invasiveness of cells (Minoo *et al*, 2007).

The contribution of other molecular alterations such as *Pten*, *p16Ink4a* and Dnmt3b to *Braf* V600E driven tumorigenesis has been studied in mice. In the mouse model developed by Carragher and colleagues, after the initial induction of crypt hyperplasia via the Mapk pathway, *Braf* mutation resulted in the development of a serrated epithelium. *Braf* mutation has also associated with Wnt pathway, *p16Ink4a* methylation and an increase in expression of *de novo* methylase Dnmt3b (Carragher *et al*, 2010). The formation of lung tumours in mice due to *Braf* V600E mutation was also attributed to activation of the Mapk pathway using the *BRaf*^{CA} mouse model (Dankort *et al*, 2007). This mouse model was also used to assess the effects of mutant *Braf* in the development of melanocytic lesions. Results showed that *Braf* V600E allele causes the formation of pigmented lesions and its association with *Pten* inactivation resulted in more malignant, invasive and metastatic tumours (Dankort *et al*, 2009).

The Cre mediated induction of the *Braf* V600E mutation in mice using the *BRaf*^{CA} mouse model and the subsequent development of TSAs and adenocarcinomas was described in Chapter 4. The aim of this study was to evaluate the molecular status of factors such as methylation, rate of proliferation and activation of Mapk and Wnt pathways of these *BRaf*^{VE} mice. The hypothesis was that in *BRaf*^{VE} mice, constitutively activated *Braf* due to the presence of *Braf* V600E mutation would result

in continuous proliferative signalling via the Mapk pathway and the induction of cellular hyperproliferation in the small intestine. This would also be followed by an up regulation of Erk and potential activation of the Wnt pathway in the TSAs and adenocarcinomas. Methylation levels were also assessed in hyperplastic samples using Methyl PCR Arrays specific for colon cancer and immunohistochemical analysis was performed to evaluate the activation of Mapk and Wnt pathways and cell proliferation. This study would help to validate the role of *BRAF* V600E mutation in the serrated pathway as was previously observed in human colorectal polyps and tumours.

5.2 RESULTS

5.2.1 Methylation analysis of hyperplasia samples

Methylation analysis was performed on mouse hyperplasia samples using methylation PCR arrays – three olive oil treated (controls) (C1 to C3) and three tamoxifen treated (T1 to T3) duodenum samples (Section 2.5.3). Each array consisted of a panel of 94 genes specific for colon cancer based on literature and two housekeeping genes – Methylation-Sensitive Enzyme Control (SEC) and Methylation-Dependent Enzyme Control (DEC). A heat map was generated based on a hierarchial clustering method with a Pearson correlation and genes with similar methylation levels were grouped or clustered together (Figure 5.1).

Basic helix-loop-helix domain containing, class B9 (*Bhlhb9*), *ubiquitin carboxy-terminal hydrolase L1* (*Uchl1*) and *Wnt inhibitory factor 1* (*Wif1*) were the only genes in which two out of three tamoxifen treated samples were methylated compared to the controls. In *Bhlhb9*, percentage of methylated DNA was 60.22% and 50% in the tamoxifen treated samples compared to 0.04% and 0.02% in the controls. However, one of the control samples also exhibited methylation levels of 51.35%, while the tamoxifen treated sample was 21.93% methylated. In comparison, the methylation levels of control samples ranged from 0.01% to 0.10% for *Uchl1* and *Wif1*. The tamoxifen treated samples were 61.04% and 80.65% methylated in *Uchl1* and 50% and 99.34% methylated in *Wif1*.

Genes such as *cyclin D2* (*Ccnd2*) (50%), *transmembrane protein with EGF-like and two follistatin-like domains 2* (*Tmeff2*) (63.9%), *tissue inhibitor of metalloproteinase 3* (*Timp3*) (62.1%), *vimentin* (*Vim*) (50%), *cyclin A1* (*Ccna1*) (50%), *topoisomerase I binding, arginine/serine-rich* (*Topors*) (50%) and *wingless-related MMTV integration site 5A* (*Wnt5a*) (55.88%) were methylated in only one tamoxifen treated sample compared to the controls. *Exostoses (multiple)-like 3* (*Extl3*) was the only gene which was hypermethylated in the controls and tamoxifen treated samples. A number of genes such as *ras association (RalGDS/AF-6) domain family member 1* (*Rassf1*), *solute carrier family 5 (iodide transporter), member 8* (*Slc5a8*), *mutL homolog 1* (*Mlh1*), *myelin and lymphocyte protein, T-cell differentiation protein* (*Mal*) and *methyl-CpG binding domain protein 2* (*Mbd2*) were methylated only in one control, while the remaining tamoxifen treated and control samples were unmethylated. The other genes analysed were unmethylated in all the tamoxifen treated samples.

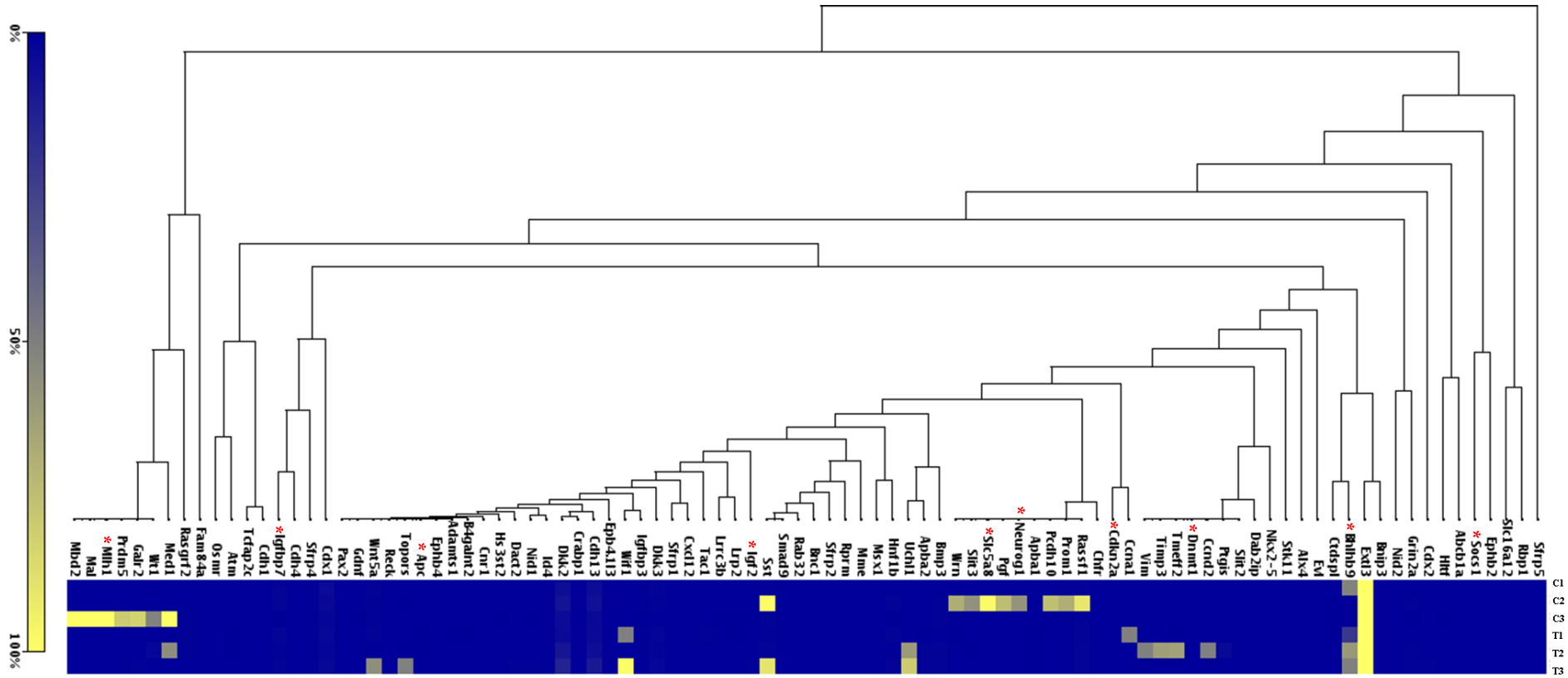

Figure 5.1 – Hierarchial clustering of samples based on similarity between methylation levels. *The control samples were represented by C1, C2 and C3; while T1, T2 and T3 were the tamoxifen treated samples. Genes such as Slc5a8 and Neurog1 and Rassf1 formed one cluster in which a majority of the genes had one methylated control. Important genes implicated in colorectal cancer (*) such as Mlh1, Igfbp7, Apc and Socs1 were unmethylated in the tamoxifen treated samples. The colouring scheme represented the methylation levels with dark blue being 100% unmethylated and yellow being 100% methylated.*

5.2.2 Immunohistochemical analysis of control and tamoxifen treated small intestine in *BRaf*^{CA} mice

5.2.2.1 Ki-67

Ki-67 staining was performed on control and tamoxifen treated small intestine samples to assess proliferation in the cells. In the control duodenum of olive oil treated mice (6 week and 12 month post treatment), the Ki-67 stained cells were restricted to the crypts and were moderately stained (Figures 5.2A and 5.2C). However, in the tamoxifen treated duodenum, the proliferative zone extended to the lower regions of the villi (Figures 5.2B and 5.2C) and the cells were strongly stained compared to the control samples. In the TSAs, the cells in the dysplastic villi stained positive for Ki-67, while the normal villi were negative (Figures 5.3A-C). A difference was also observed in the staining pattern of the crypt region – loss of Ki-67 staining with a few positively stained cells scattered (Figure 5.3C).

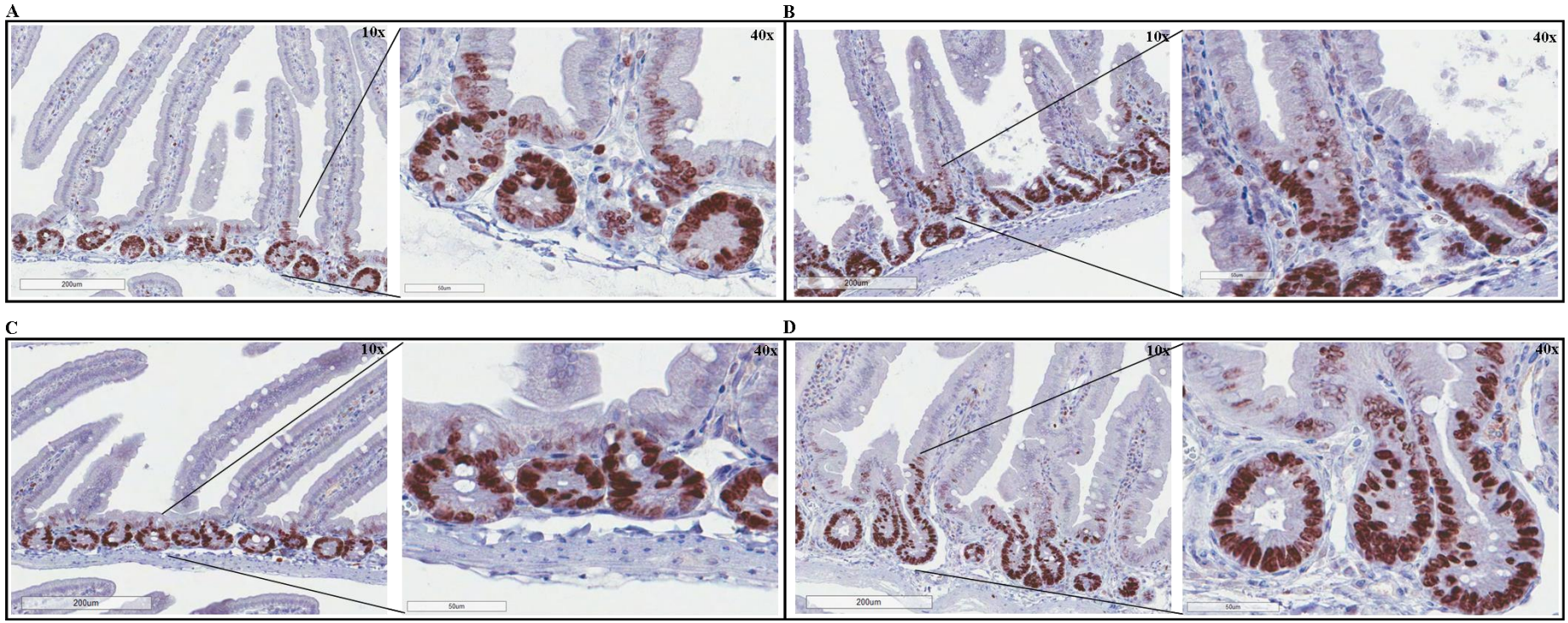

Figure 5.2 – Ki-67 expression in control (n = 2) and tamoxifen treated duodenum (n = 2). *Positive Ki-67 staining was restricted only to the crypts in the control duodenum (6 weeks post olive oil treatment)* ***(A)****; while in the tamoxifen treated sample (6 weeks post tamoxifen treatment; 12 weeks old), the proliferative zone expanded to the base of the villi* ***(B)****. The nuclei were strongly stained the in the tamoxifen treated sample compared to the control. A similar staining pattern was observed in the control and tamoxifen treated duodenum (12 month post treatment; 59 weeks old). In the control sample, only the crypts stained positive for Ki-67* ***(C)****, while the lower regions of the villi were Ki-67 positive in the tamoxifen treated sample* ***(D)****. Lower magnification 10x (A-D); scale bar = 200 μm and higher magnification 40x (A-D); scale bar = 50 μm.*

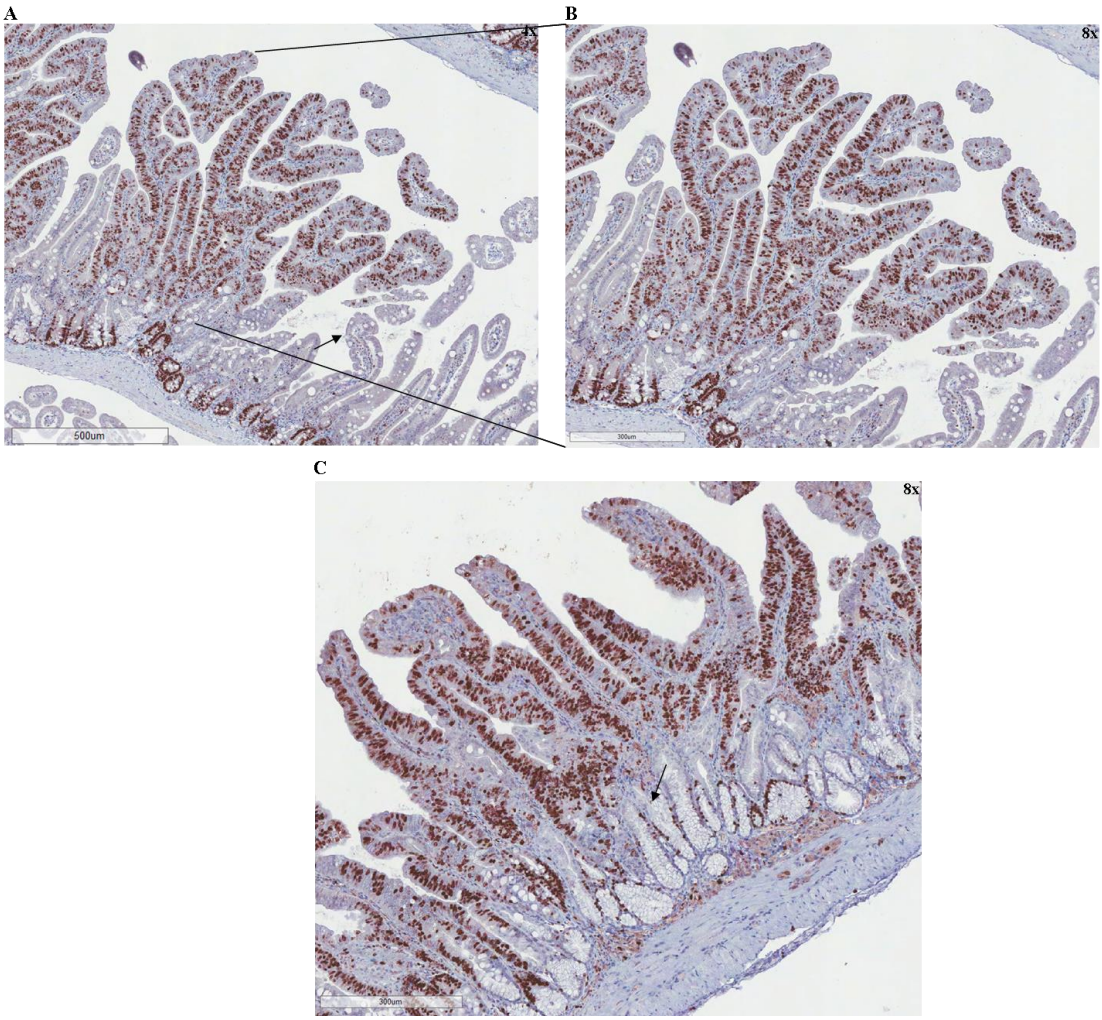

Figure 5.3 – Ki-67 expression in traditional serrated adenomas. *In TSAs, cells stained positively for Ki-67 in the areas of dysplasia, while the cells in the adjacent normal villi (arrow) were negative and only the crypts showed positively stained cells for Ki-67* ***(A and B)****. The proliferative zone also shifted to the middle and upper regions of the villi in a TSA and a loss of Ki-67 expression was observed in the crypts* ***(C)****. No. of mice assessed for Ki-67 expression = 9 (including all mice with abnormal pathology in the intestine) with an age range of 91-103 weeks. Scale bars represent 500 µm (A) and 300 µm (B & C); magnification 4x (A) and 8x (B & C).*

5.2.2.2 β-catenin

Immunohistochemical analysis of β-catenin was performed on six tamoxifen treated small intestine samples. In the olive oil treated small intestine samples, moderate membranous staining and weak cytoplasmic staining was observed (Figure 5.4A). Membranous β-catenin expression was observed in all the samples and was

strong in a majority of the regions in TSAs (Figures 5.4B and 5.4C) and adenocarcinomas (Figures 5.4A and 5.4B). Cytoplasmic staining was observed in five tamoxifen treated samples and was moderately stained in TSAs (Figure 5.4B) and adenocarcinomas (Figure 5.5B). Nuclear β-catenin expression was observed in five samples – weakly stained (TSA in the jejunum), moderately stained (TSA with severe dysplasia) and strongly stained (two adenocarcinomas and multiple TSAs in the duodenum) (Figures 5.4C and 5.5B). Some regions in the adenocarcinomas also showed loss of cytoplasmic β-catenin expression and weak membranous staining (Figure 5.5C).

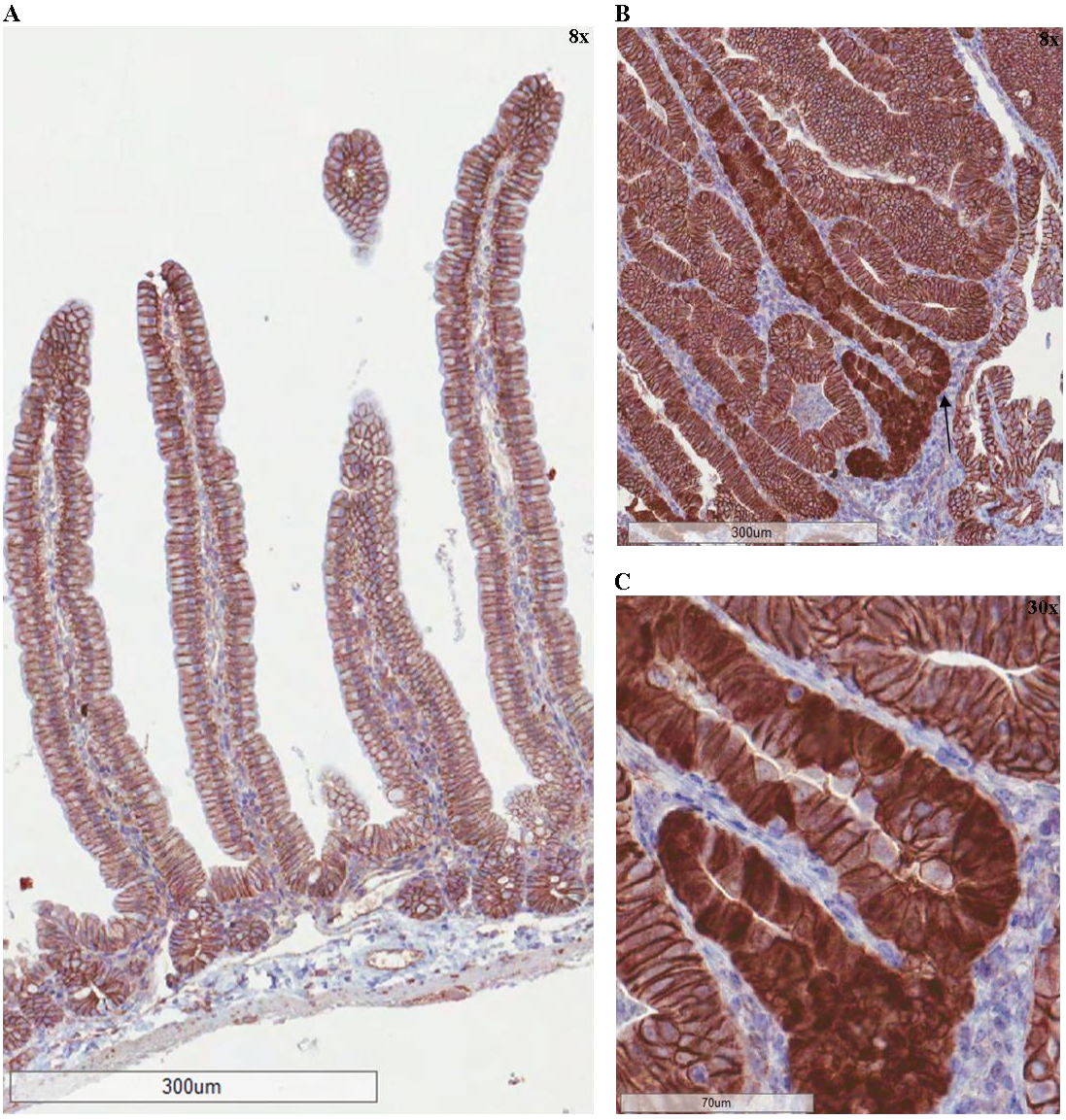

Figure 5.4 – β-catenin expression in olive oil treated (n = 1) and tamoxifen treated (n = 6) small intestine. *Moderate membranous β-catenin expression and weak cytoplasmic staining was observed in olive oil treated duodenum* ***(A)****. In traditional serrated adenoma, strong membranous and moderate cytoplasmic staining was observed in the dysplastic villi with strong nuclear staining (arrow)* ***(B)****, which was not consistent* ***(C)****. Age range of mice: 91-103 weeks; scale bars represent 300 μm (A & B) and 70 μm (C); magnification 8x (A &B) and 30x (C).*

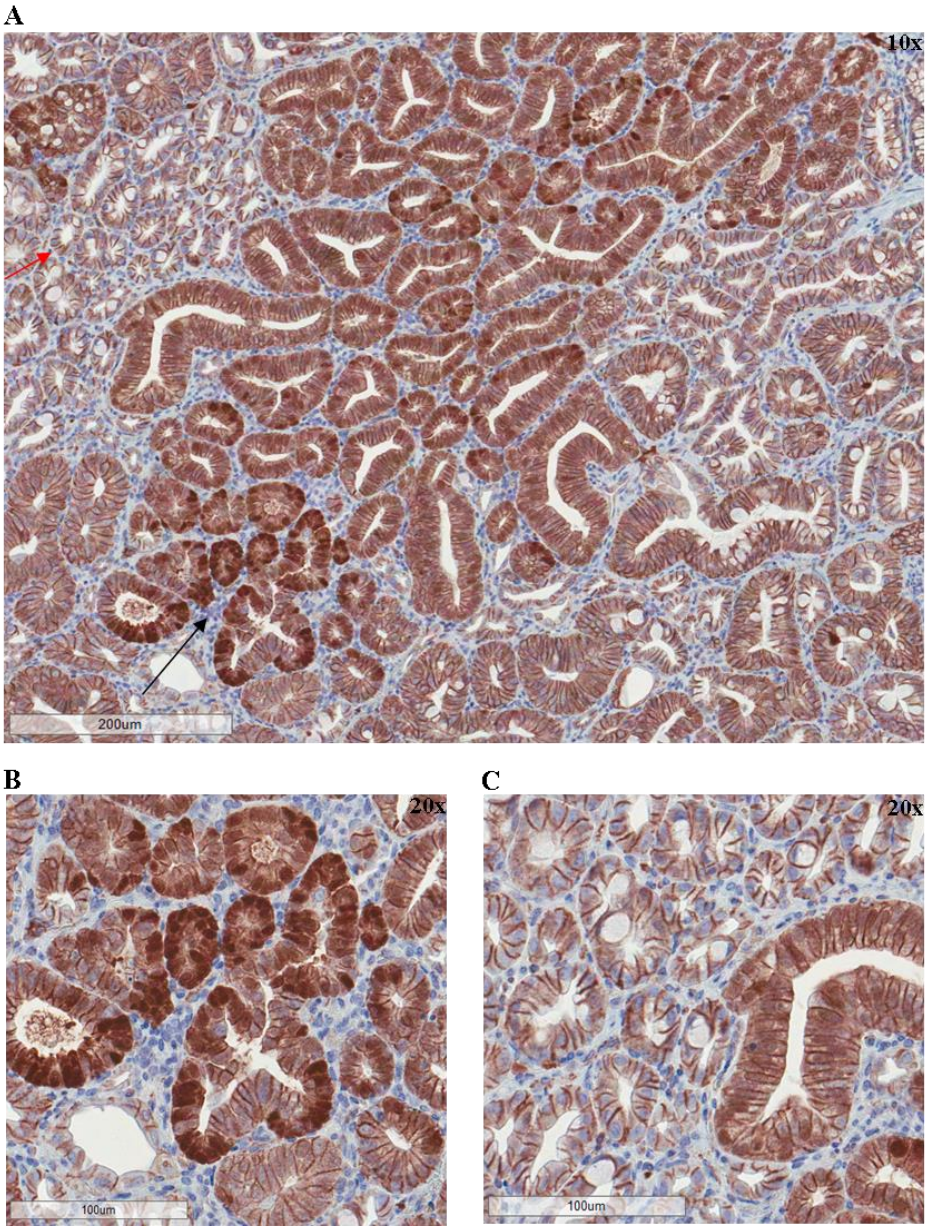

Figure 5.5 – Expression of β-catenin in adenocarcinoma (n = 2). *In adenocarcinoma identified in a tamoxifen treated mouse, a majority of the cells showed weak cytoplasmic staining and moderate membranous staining with some cells staining positive for nuclear β-catenin expression (black arrow)* ***(A)****. The nuclear staining was not consistent as was observed in the TSAs* ***(A and B)****. Loss of cytoplasmic staining and weak membranous staining (red arrow – A) was also observed in some regions of the adenocarcinoma* ***(A and C)****. Age of mice: 103 weeks; scale bars represent 200 µm (A) and 100 µm (B & C); magnification 10x (A) and 20x (B & C).*

5.2.2.3 p44/42 Mapk (Erk1/2) (total Erk)

Total Erk expression was evaluated in six tamoxifen treated small intestine samples. In the villi of olive oil treated duodenum, cytoplasm was weakly stained with no nuclear staining (Figure 5.6A); while moderate nuclear and weak cytoplasmic staining was observed in tamoxifen treated duodenum only in the villi (Figure 5.6B). The TSA with high-grade dysplasia showed strong nuclear and cytoplasmic staining and this increased towards the upper regions of the villi (Figure 5.6C). In tamoxifen treated duodenum with multiple TSAs, loss of expression was observed in certain regions of the TSA (two out of six samples) and regions of undifferentiated malignancy (one out of six samples).

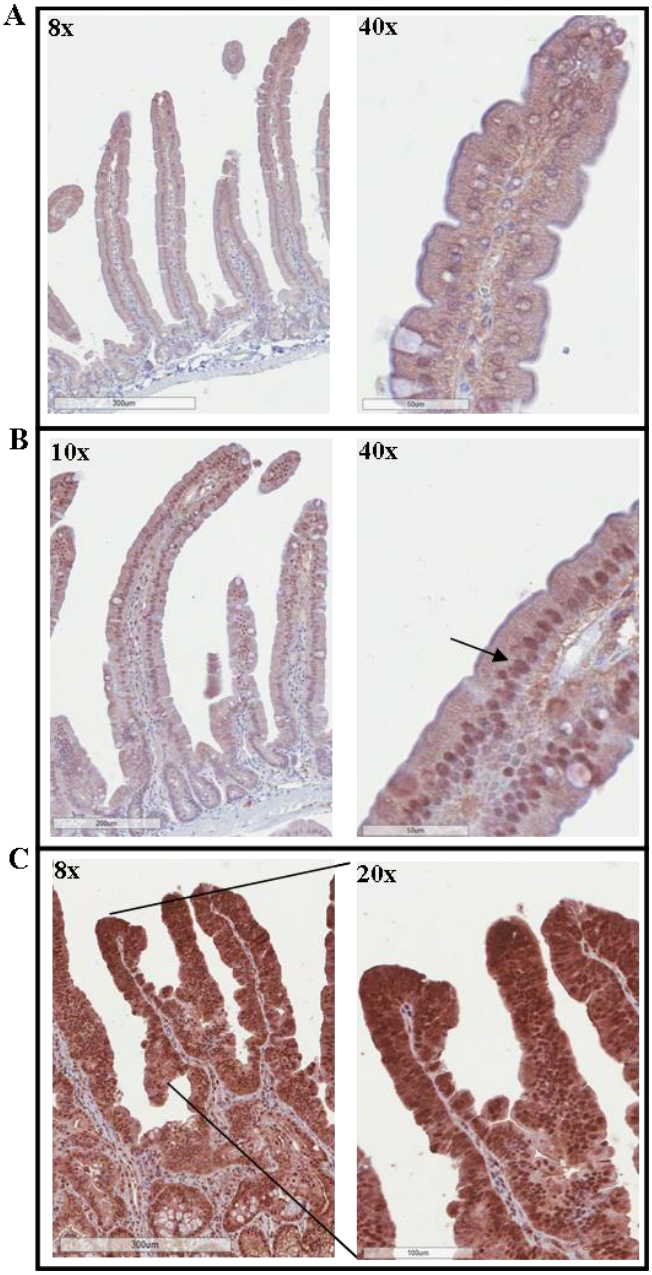

Figure 5.6 – p44/42 Mapk (Erk1/2) (total Erk) expression in small intestine of BRaf^{CA} mice (n = 6). *In the olive oil treated duodenum, cytoplasm was weakly stained in the villi and there was no sign of nuclear staining* ***(A)****. However, in the tamoxifen treated duodenum, moderate nuclear (arrow) and weak cytoplasmic staining was observed in the villi* ***(B)*** *and the total Erk expression increased in the dysplastic villi of traditional serrated adenoma* ***(C)****. Age range of mice: 91-103 weeks; lower magnification 8x, scale bar = 300 μm (A & C), 10x, scale bar = 200 μm (B) and higher magnification 40x (A & B), scale bar = 50 μm, 20x (C), scale bar = 100 μm.*

5.2.2.4 Phospho-p44/42 Mapk (Erk1/2) (Thr202/Tyr204) (phospho Erk)

Phospho Erk expression (activated form of total Erk) was analysed in olive oil and tamoxifen treated small intestine samples. The olive oil treated duodenum (control) showed no phospho Erk expression in the villi and crypts (Figure 5.7A). In contrast, tamoxifen treated duodenum (six weeks post treatment) exhibited positively stained cells in the nucleus and cytoplasm – in the crypts and lower regions of the intestinal villi (Figure 5.7B). Phospho Erk expression increased in older tamoxifen treated mice which developed lesions or adenocarcinomas and nuclear and cytoplasmic expression was stronger in the crypts and villi compared to the six week post tamoxifen treated samples (Figure 5.7C). In traditional serrated adenomas with high-grade dysplasia, inconsistent, strong nuclear staining was observed which was strong in certain regions and moderate cytoplasmic staining was observed throughout the villi (Figure 5.7D).

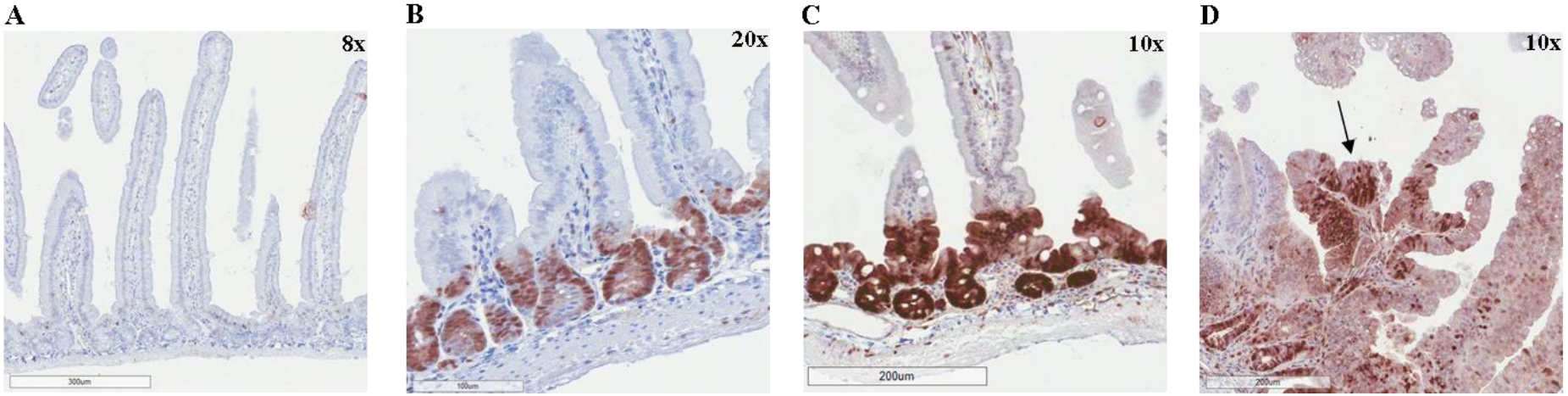

Figure 5.7 – Phospho Erk expression in the small intestine. *The olive oil treated duodenum (n = 1) exhibited no phospho Erk expression* ***(A)****, while the tamoxifen treated duodenum (six weeks post treatment; n =1; age: 12 weeks old) had positive stained cells (nucleus and cytoplasm) in the crypts and lower regions of the villi* ***(B)****. Phospho Erk expression increased in older mice with TSAs (n = 6) with strongly stained nuclei and cytoplasm in the crypts and lower regions of the villi* ***(C)****. TSAs displayed moderate cytoplasmic staining throughout the villi with inconsistent, strong nuclear staining (arrow)* ***(D)****. Age range of mice: 91-103 weeks; scale bars represent 300 μm (A), 100 μm (B) and 200 μm (C & D); magnification 8x (A), 20x (B) and 10x (C & D).*

5.3 DISCUSSION

BRAF V600E mutation plays an important role in colorectal tumorigenesis and is significantly associated with proximal serrated polyps, MSI-H and CIMP-H colorectal tumours (Kambara *et al*, 2004). The previous Chapter (Chapter 4) investigated the role of *Braf* V600E mutation, evaluation of hyperplastic changes and tumour development in the $BRaf^{VE}$ mice. The aim of this Chapter was to assess the molecular status of hyperplasia, traditional serrated adenomas (TSA) and adenocarcinomas observed in the small intestine of $BRaf^{VE}$ mice.

The methylation status of 94 genes was evaluated in the duodenum region of three olive oil (controls) and three tamoxifen treated mice (six weeks post treatment). In the tamoxifen treated samples, *Bhlhb9*, *Uch1* and *Wif1* (two samples methylated); *Ccnd2*, *Tmeff2*, *Timp3*, *Vim*, *Ccna1*, *Topors* and *Wnt5a* (one sample methylated) were ≥ 50% methylated compared to the controls and the remaining 84 genes were unmethylated in the tamoxifen treated samples. Genes such as *a disintegrin-like and metallopeptidase (reprolysin type) with thrombospondin type 1 motif, 1* (*Adamts1*), *cellular retinoic acid binding protein I* (*Crabp1*) and *myelin and lymphocyte protein, T-cell differentiation protein* (*Mal*) were unmethylated in the tamoxifen treated samples. Another study assessed the methylation levels of these genes in normal mucosa, adenomas and carcinomas. Methylation frequencies of *Adamts1* and *Crabp1* increased from adenomas to carcinomas, while the methylation frequency of *Mal* remained the same in all the groups (Ahlquist *et al*, 2008).

Important genes in CRC such as *Cyclin-dependent kinase inhibitor 2A* (*Cdkn2a*), *neurogenin 1* (*Neurog1*), *suppressor of cytokine signaling 1* (*Socs1*), *insulin-like growth factor 2* (*Igf2*), *insulin-like growth factor binding protein 7* (*Igfbp7*) and *adenomatous polyposis coli* (*Apc*) were unmethylated in the tamoxifen treated samples. A majority of the genes in our study were unmethylated in the tamoxifen treated samples and this could be due to the sample type. Samples with initial hyperplastic changes were used and if advanced polyps such as TSAs were evaluated, then there could possibly be more genes methylated in the tamoxifen treated samples.

Immunohistochemical (IHC) analysis was performed on tamoxifen treated samples with TSAs, adenocarcinomas and other aberrations in the small intestine. The

proliferation marker, Ki-67; Mapk pathway proteins, p44/42 Mapk (Erk1/2) (total Erk) and Phospho-p44/42 Mapk (Erk1/2) (Thr202/Tyr204) (phospho Erk); and Wnt pathway protein, β-catenin were employed in this study. In the Ki-67 IHC, a difference was observed between the olive oil treated (control) and tamoxifen treated small intestine samples. Ki-67 expression was restricted to the crypts only in the controls. But, in the tamoxifen treated samples, the cells stained positively for Ki-67 in the crypts and lower regions of the villi. In samples with TSA, the proliferative zone was between the middle and upper regions of the villi, while there was a loss of Ki-67 expression in the crypts.

The Ki-67 expression was similar to the staining pattern observed in a recent study using *Vil-Cre;Braf*$^{LSL\text{-}V637E/+}$ mouse. In the control mice, the positive cells were in the lower regions of the crypts in the colon; while in the *Vil-Cre;Braf*$^{LSL\text{-}V637E/+}$ mice, the mid and upper regions of the crypts were positive for Ki-67 expression. In serrated adenomas, Ki-67 staining was present from the crypt base to the apex of the villi (Rad *et al*, 2013). However, in our study, the TSAs showed a loss of Ki-67 expression in the crypts.

Total Erk and phospho Erk were then assessed to determine Mapk activation. In total Erk IHC, cytoplasmic and nuclear staining increased from tamoxifen treated duodenum samples to TSAs with high-grade dysplasia. Phospho Erk expression was absent in the control samples and was expressed only in the crypt bases and lower regions of the villi in the tamoxifen treated samples. An increase in phospho Erk staining was observed in older tamoxifen treated mice with strong cytoplasmic and nuclear staining in positively stained cells. However, in the TSAs, there is moderate cytoplasmic staining in the villi and scattered strong nuclear staining.

The staining pattern observed was similar to the other reports of phospho Erk staining in mice intestines (Davies *et al*, 2013; Rad *et al*, 2013). Carragher *et al* observed phospho Erk expression in mice as early as 3 days post induction, while in our study the youngest mice assessed were six weeks old post tamoxifen treatment (Carragher *et al*, 2010). Results show that phospho Erk is expressed only in samples with *Braf* V600E mutations and its expression increases with intestinal lesions. This demonstrates that *Braf* V600E mutation results in the activation of the MAPK pathway.

β-catenin expression was also assessed to determine the activation of the Wnt pathway is associated with the presence of *BRAF* V600E mutation. Nuclear accumulation of β-catenin was observed mainly in serrated polyps in humans with either a *BRAF* or *KRAS* mutation and hence could be implicated in the serrated pathway (Yachida *et al*, 2009). Studies have also assessed β-catenin expression in mouse intestine samples. Carragher *et al* observed nuclear β-catenin staining in mice as early as 3 days post induction (Carragher *et al*, 2010). In contrast, the β-catenin staining pattern observed in our samples was similar to a recent study by Rad *et al*. β-catenin nuclear expression was absent in normal mucosa, hyperplastic lesions and TSAs with low-grade dysplasia. An increase in β-catenin nuclear staining was observed only in TSAs with high-grade dysplasia and carcinomas (Rad *et al*, 2013).

In TSAs which develop due to the inactivation of *Pten* and *Kras* mutation, no nuclear β-catenin expression was observed and this suggested that these lesions could develop without the activation of the Wnt pathway (Davies *et al*, 2013). But in another study involving the effect of *Pten* loss in mouse intestine, aberrant nuclear β-catenin expression was observed in adenomas. These studies indicate that the polyp type also influences the activation of the Wnt pathway with the inactivation of the same gene (*Pten*) (Byun *et al*, 2011).

The molecular characterisation of the $BRaf^{VE}$ phenotype in tamoxifen treated mice showed that methylation levels of key genes were low in the initial stages of hyperplasia. Methylation levels could possibly be higher in TSAs or other advanced polyps, which is similar to human colorectal lesions. Positive expression of total Erk and phospho Erk and nuclear β-catenin staining indicated that *Braf* V600E mutation activated both the Mapk and Wnt pathways respectively. The expression of nuclear β-catenin only in TSAs and adenocarcinomas suggest that Wnt pathway activation mainly occurs in advanced serrated polyps such as SSAs and TSAs, which are the precursor lesions thought to develop into colorectal cancer. This study supports the functional role played by *Braf* V600E mutation in the development of colorectal polyps and CRC via the serrated pathway.

CHAPTER 6

INTERACTION BETWEEN ONCOGENIC *BRAF* AND THE CELL CYCLE REGULATORS *p16INK4a* AND *p14ARF*

6. INTERACTION BETWEEN ONCOGENIC *BRAF* AND THE CELL CYCLE REGULATORS *p16INK4a* AND *p14ARF*

6.1 INTRODUCTION

p16INK4a and p14ARF (known as p19Arf in mice) are members of the INK4a locus and are key players in colorectal tumorigenesis. Promoter hypermethylation of *p16INK4a* and *p14ARF* have been observed in about 33% of sporadic colorectal carcinomas and are considered as early events in the development of CRC (Esteller *et al*, 2000). Methylation was found to play an important role in the inactivation of the *p16INK4a* gene as was observed by Herman *et al* and this was similarly observed in the inactivation of *p14ARF* (Esteller *et al*, 2000; Herman *et al*, 1995). The combined methylation of *p16INK4a* and *p14ARF* in colorectal tumours correlated with high tumour grade, proximal location and a high frequency of lymph node metastasis (Burri *et al*, 2001; Lee *et al*, 2006). *p16INK4a* methylation has also been identified as one of the main molecular factors in the development of CRC via the serrated pathway (Fogt *et al*, 2002).

The functional importance of the *Ink4a* locus in colorectal tumorigenesis has been demonstrated using mouse models. Mice with *Braf* V600E mutation were crossed with *Ink4a* locus mutated mice (combined knockout) and this initially induced widespread and sustained hyperplasia (Carragher *et al*, 2010). In a recent study, the absence of p16Ink4a along with *Braf* V600E mutation resulted in an increase in the formation of serrated lesions. This showed that inactivation of p16Ink4a resulted in a more rapid development of the colorectal tumour phenotype via the serrated pathway (Rad *et al*, 2013).

The main aim of this study was to investigate the individual contribution of *p16Ink4a* and *p19Arf* in the development of colorectal cancer along with *Braf* V600E mutation. The hypothesis was that since *p16Ink4a* and *p19Arf* have been implicated in colorectal tumorigenesis via the serrated pathway, the combined effect of each inactive tumour suppressor gene with *Braf* V600E mutation would result in a more aggressive colorectal tumour phenotype compared to the effect of only oncogenic *Braf* mutation. This was achieved using the *p16Ink4a* and *p19Arf* knockout mice, which were individually crossed with $BRaf^{VE}$ mice and monitored for tumour

development. Mice were monitored for initial hyperplastic changes such as crypt and villus lengthening in the colon and small intestines. Longitudinal studies were carried out to assess the time taken for tumour formation, type of lesions observed and the survival of the mice. This study would assist in understanding the functional role played by *p16Ink4a* and *p19Arf* in colorectal cancer and their effects on the serrated pathway.

6.2 RESULTS

6.2.1 Hyperplasia study – assessment of villus and crypts lengths in different mice groups

6.2.1.1 *BRaf$^{CA/+}$/p16Ink4a$^{-/-}$/A33CreERT2$^{+/-}$/Lacz$^{-/-}$*

Hyperplastic changes were observed in *BRaf$^{CA/+}$/p16Ink4a$^{-/-}$/A33CreERT2$^{+/-}$/Lacz$^{-/-}$* mice 6 weeks post tamoxifen treatment (mice treated with tamoxifen or olive oil will be referred to as *BRaf^{VE}/p16* null or *BRaf^{CA}/p16* null mice respectively in the subsequent sections). An average increase in villus and crypt length was observed in the colon and all regions of the small intestine of tamoxifen treated *BRaf^{VE}/p16* null mice (Table 6.1). In the duodenum, the average villus length of tamoxifen treated mice was 721.8 μm which was significantly greater than the controls (P = 0.0149) (Figure 6.1A). A similar trend was also observed in the villus lengths of the jejunum and ileum regions. Significant differences were also observed in the villus of tamoxifen treated mice with average lengths of 579.5 μm and 331.2 μm in the jejunum (P = 0.0094) (Figure 6.1B) (P = 0.0112) and ileum (Figure 6.1C) respectively.

Table 6.1 - Measurements of crypt and villus lengths of olive oil and tamoxifen treated BRaf$^{CA/+}$/p16Ink4a$^{-/-}$/A33CreERT2$^{+/-}$/Lacz$^{-/-}$mice

Colon/SI regions	Treatment							
	Olive oil (µm)			Average	Tamoxifen (µm)			Average
Colon	182.5	178.4	207.6	**189.5**	234.8	199.2	198.2	**210.8**
Duodenum								
Villus	574.9	463.8	498.7	**512.4**	788.6	652.8	724.0	**721.8**
Crypt	94.3	78.2	83.4	**85.3**	134.2	117.2	114.1	**121.8**
Jejunum								
Villus	407.5	294.3	415.1	**372.3**	604.5	538.7	595.3	**579.5**
Crypt	92.7	73.7	78.5	**81.6**	113.7	90.7	101.1	**101.9**
Ileum								
Villus	214.8	176.2	183.0	**191.3**	385.6	286.4	321.6	**331.2**
Crypt	80.6	73.8	72.3	**75.6**	106.9	88.0	89.8	**94.9**

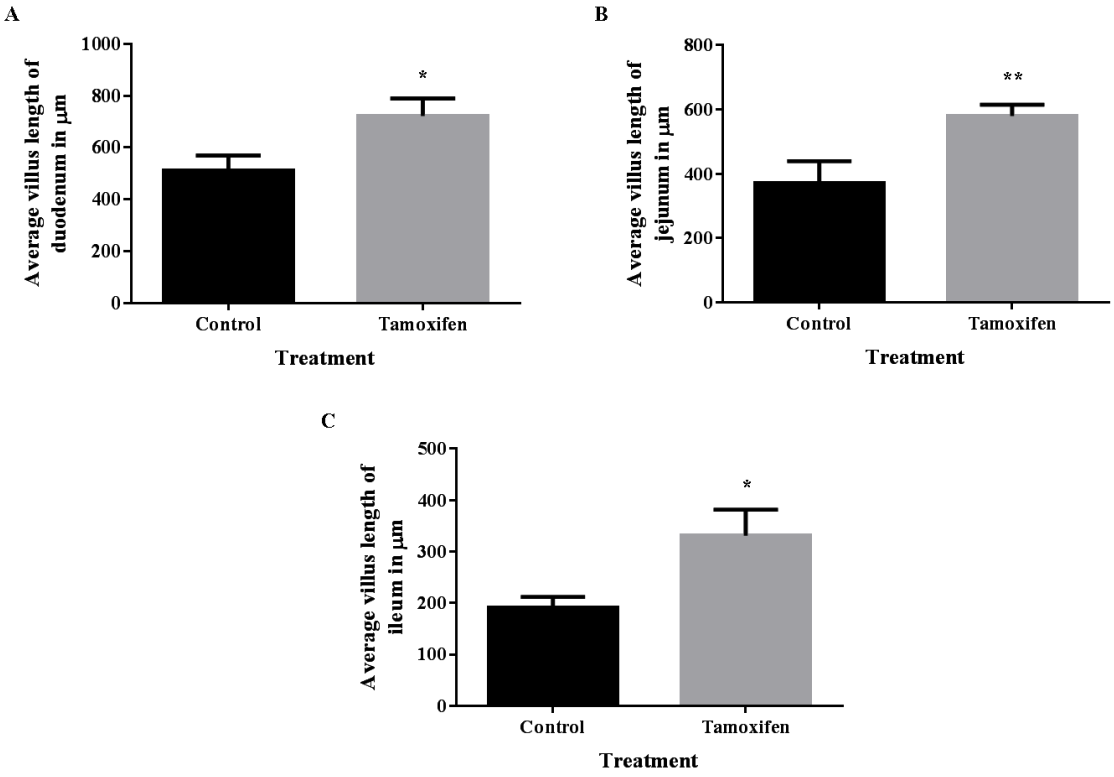

Figure 6.1 - Villus lengths in small intestine of BRaf$^{CA/+}$/p16Ink4a$^{-/-}$/A33CreERT2$^{+/-}$/Lacz$^{-/-}$mice. *Lengthening of the villi was observed in all the small intestine regions of the tamoxifen treated mice compared to the controls. Significant differences were observed in the duodenum **(A)**, jejunum **(B)** and ileum **(C)** with P values of 0.0149 (*), 0.0094 (**) and 0.0112 (*) respectively. All measurements were in µm; error bars, SEM.*

An increase in crypt length was observed in the colon and the small intestine regions – duodenum, jejunum and ileum (Table 6.1). In the duodenum (Figure 6.2A)

(P = 0.0096) and ileum (Figure 6.2C) (P = 0.0415), a significant difference in crypt lengths was observed between the tamoxifen treated samples and controls. The average crypt measurements in the duodenum were 85.3 µm (control) and 121.8 µm (tamoxifen treated) and 75.6 µm (control) and 94.9 µm (tamoxifen treated) in the ileum regions. Crypt lengthening was also observed in the jejunum with average lengths of 101.9 µm and 81.6 µm in the tamoxifen treated and control samples respectively. In the colon, average crypt length was higher in the tamoxifen treated samples compared to the controls with 210.8 µm and 189.5 µm respectively. There was no significant difference observed in the ileum and colon samples between the control and tamoxifen treated mice.

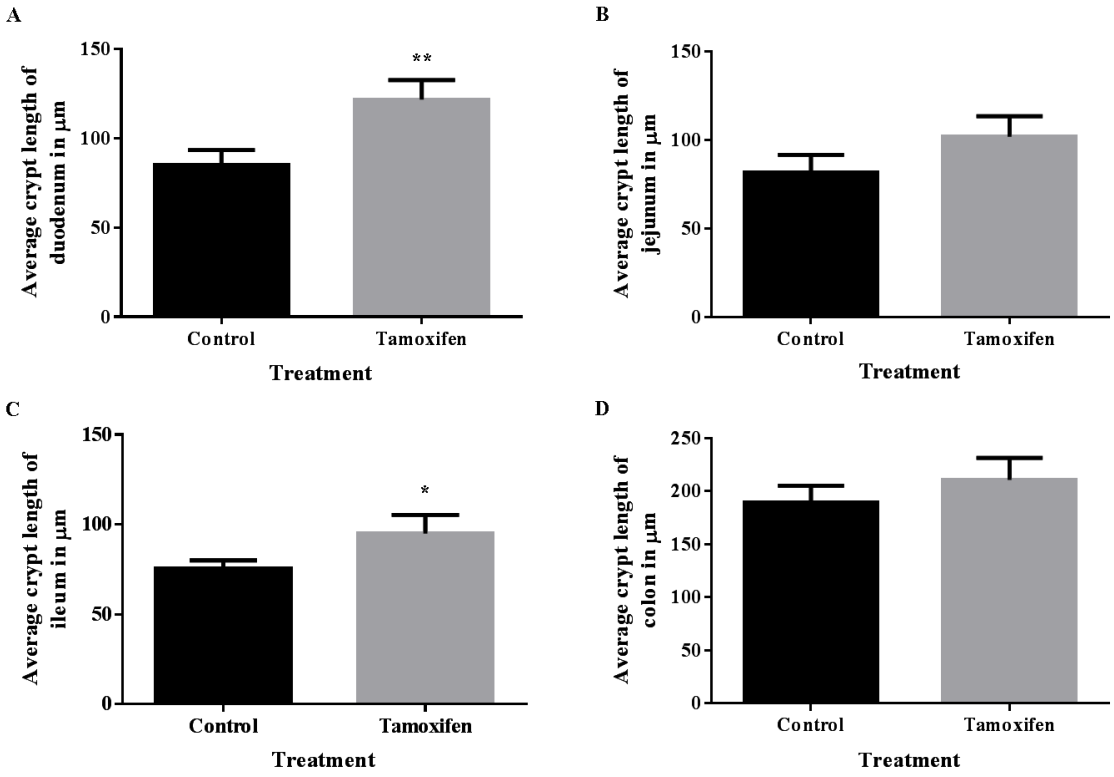

Figure 6.2 – Evaluation of crypt lengths in small intestine and colon of BRaf$^{CA/+}$/p16Ink4a$^{-/-}$/A33CreERT2$^{+/-}$/Lacz$^{-/-}$ mice. *An increase in crypt lengths of tamoxifen treated mice was observed in the duodenum* ***(A)****, jejunum* ***(B)****, ileum* ***(C)*** *and colon* ***(D).*** *Significant differences in crypt lengthening between tamoxifen treated and control mice were observed only in the duodenum (P = 0.0096) (**) and ileum (P = 0.0415) (*). All measurements were in µm; error bars, SEM.*

6.2.1.2 *BRaf$^{CA/+/}$/p16Ink4a$^{+/-}$/A33CreERT2$^{+/-}$/Lacz$^{-/-}$*

Crypt and villus lengthening were observed in tamoxifen treated *BRaf$^{CA/+/}$/p16Ink4a$^{+/-}$/A33CreERT2$^{+/-}$/Lacz$^{-/-}$* mice (mice treated with tamoxifen or olive oil will be referred to as *BRaf^{VE}/p16* het or *BRaf^{CA}/p16* het mice respectively in the subsequent sections) (Table 6.2). Similar to the *BRaf^{VE}/p16* null mice, a significant increase in villus lengths of duodenum (Figure 6.3A) and jejunum (Figure 6.3B) regions was observed in the *BRaf^{VE}/p16* het mice compared to the controls. The average length of villi in the duodenum (P = 0.0004) and jejunum (P = 0.0037) were measured at 675.2 μm and 601.1 μm respectively in the tamoxifen treated samples. Although an increase in average villus length was observed in the tamoxifen treated ileum (242.9 μm) compared to the controls (193.5 μm), this was not significant (Figure 6.3C).

Table 6.2 - Measurements of crypt and villus lengths of olive oil and tamoxifen treated BRaf$^{CA/+/}$/p16Ink4a$^{+/-}$/A33CreERT2$^{+/-}$/Lacz$^{-/-}$ mice

Colon/SI regions	Treatment							
	Olive oil (μm)			Average	Tamoxifen (μm)			Average
Colon	198.8	203.2	174.7	**192.2**	218.6	193.1	180.3	**197.3**
Duodenum								
Villus	532.5	493.6	488.7	**504.9**	670.6	665.5	689.5	**675.2**
Crypt	83.3	83.7	81.7	**82.9**	135.9	114.5	111.7	**120.7**
Jejunum								
Villus	406.8	335.2	305.4	**349.2**	629.7	543.7	629.9	**601.1**
Crypt	85.0	80.4	76.0	**80.5**	114.6	111.2	102.9	**109.6**
Ileum								
Villus	195.1	203.6	181.6	**193.5**	213.7	282.4	232.6	**242.9**
Crypt	83.8	77.7	76.5	**79.3**	96.0	88.9	86.8	**90.6**

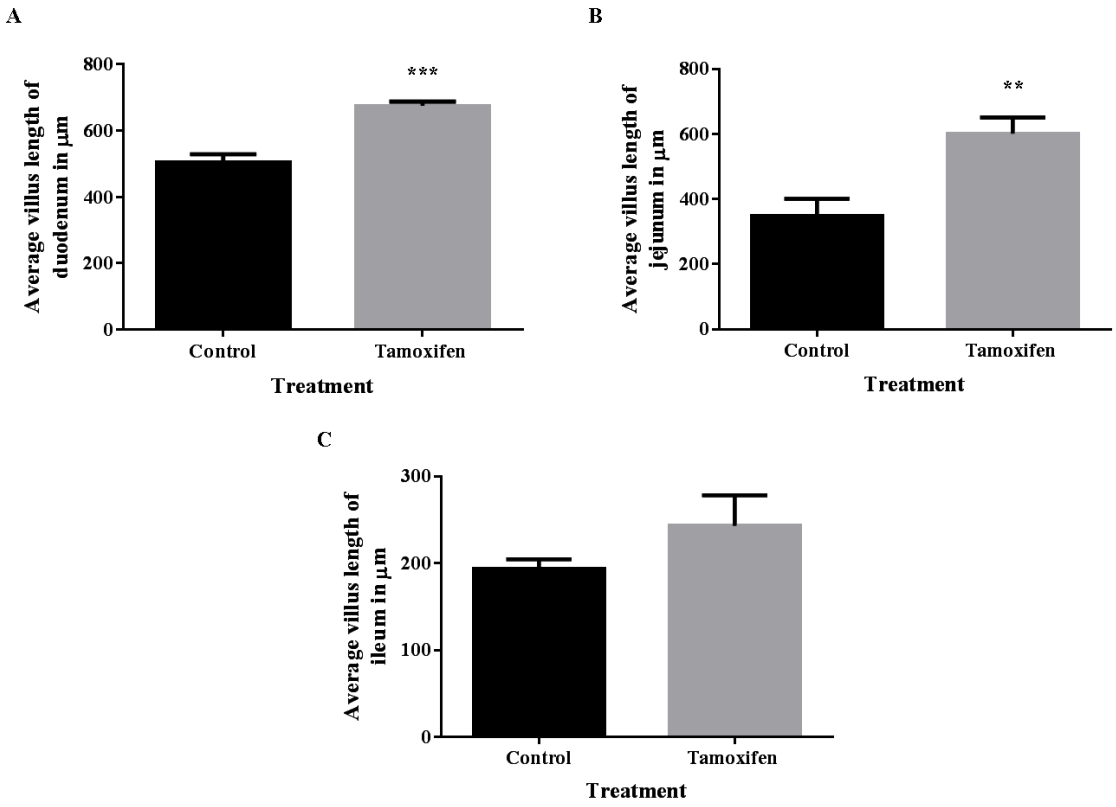

Figure 6.3 - Assessment of villus lengths in small intestine of BRaf$^{CA/+}$/p16Ink4a$^{+/-}$/A33CreERT2$^{+/-}$/Lacz$^{-/-}$mice. *An increase in villus length was observed in all regions of the small intestine in tamoxifen treated mice. Significant increase in average villus length was present only in the duodenum (P = 0.0004) (***) **(A)** and jejunum (P = 0.0037) (**) **(B)** regions of the small intestine. The tamoxifen treated ileum **(C)** exhibited an increase in average villus length compared to the controls; however, this was not significant. All measurements were in µm; error bars, SEM.*

The *BRaf^{VE}/p16* het mice also displayed an increase in average crypt lengths in the tamoxifen treated mice compared to the controls (Table 6.2). In the duodenum region of the small intestine, a significant increase (P = 0.0078) in average crypt length was observed in the tamoxifen treated mice (120.7 µm) compared to the controls (82.9 µm) (Figure 6.4A). A similar trend was also observed in the jejunum (P = 0.0026) and ileum (P = 0.0354) regions with a significant increase in average crypt lengths of tamoxifen treated mice (Figures 6.4B and 6.4C). The average crypt lengths were 109.6 µm and 90.6 µm in tamoxifen treated jejunum and ileum respectively. In the colon of *BRaf^{VE}/p16* het mice, there was an average increase in crypt length which was not significant (Figure 6.4D).

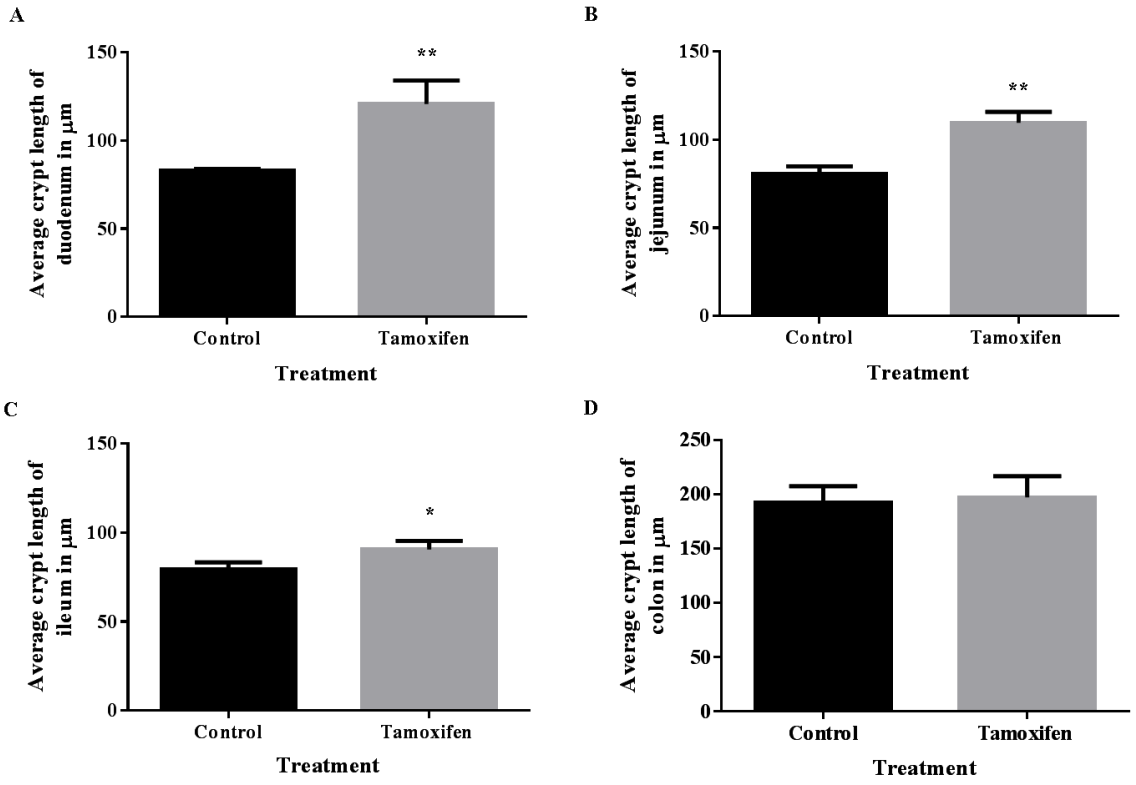

Figure 6.4 - Evaluation of crypt lengths in small intestine and colon of BRaf$^{CA/+}$/p16Ink4a$^{+/-}$/A33CreERT2$^{+/-}$/Lacz$^{-/-}$ mice. *All the tamoxifen treated samples showed an increase in average crypt length compared to their corresponding controls. The duodenum (P = 0.0078) (**) **(A)**, jejunum (P = 0.0026) (**) **(B)** and ileum (P = 0.0354) (*) **(C)** displayed a significant increase in average crypt lengths; however, this increase was not significant in the colon **(D)**. All measurements were in µm; error bars, SEM.*

6.2.1.3 *BRaf$^{CA/+}$/p19Arf$^{-/-}$/A33CreERT2$^{+/-}$/Lacz$^{-/-}$*

Hyperplasia analysis was also carried out to detect changes in crypt and villus lengths in *BRaf$^{CA/+}$/p19Arf$^{-/-}$/A33CreERT2$^{+/-}$/Lacz$^{-/-}$* mice (mice treated with tamoxifen or olive oil will be referred to as *BRaf^{VE}/p19* null or *BRaf^{CA}/p19* null mice respectively in the subsequent sections). An increase in crypt and villus lengths was observed in all the samples of tamoxifen treated mice compared to controls (Table 6.3). In the duodenum, the average villus length of the control mice was 480.9 µm, while it was significantly higher (P = 0.0098) in the tamoxifen treated mice with 652.1 µm (Figure 6.5A). A significant difference (P = 0.0044) was also observed in

the jejunum between the control (332.6 μm) and tamoxifen treated mice (464.6 μm) (Figure 6.5B). However, in the ileum, the increase in villus length was not significant in the tamoxifen treated mice (271.8 μm) compared to the controls (192.7 μm) (Figure 6.5C).

Table 6.3 - Measurements of crypt and villus lengths of olive oil and tamoxifen treated BRaf$^{CA/+}$/p19Arf$^{-/-}$/A33CreERT2$^{+/-}$/Lacz$^{-/-}$ mice

Colon/SI regions	**Treatment**							
	Olive oil (μm)			**Average**	**Tamoxifen (μm)**			**Average**
Colon	178.5	173.2	171.8	**174.5**	185.3	222.8	205.4	**204.5**
Duodenum								
Villus	454.4	547.8	440.4	**480.9**	655.6	676.5	624.3	**652.1**
Crypt	72.4	85.1	66.0	**74.5**	112.8	102.5	101.8	**105.7**
Jejunum								
Villus	335.7	368.8	293.3	**332.6**	452.4	472.7	468.7	**464.6**
Crypt	76.4	82.6	66.0	**75.0**	96.2	103.9	95.7	**98.6**
Ileum								
Villus	185.8	191.0	201.2	**192.7**	328.8	266.2	220.5	**271.8**
Crypt	72.6	73.7	65.2	**70.5**	92.8	95.1	100.4	**96.1**

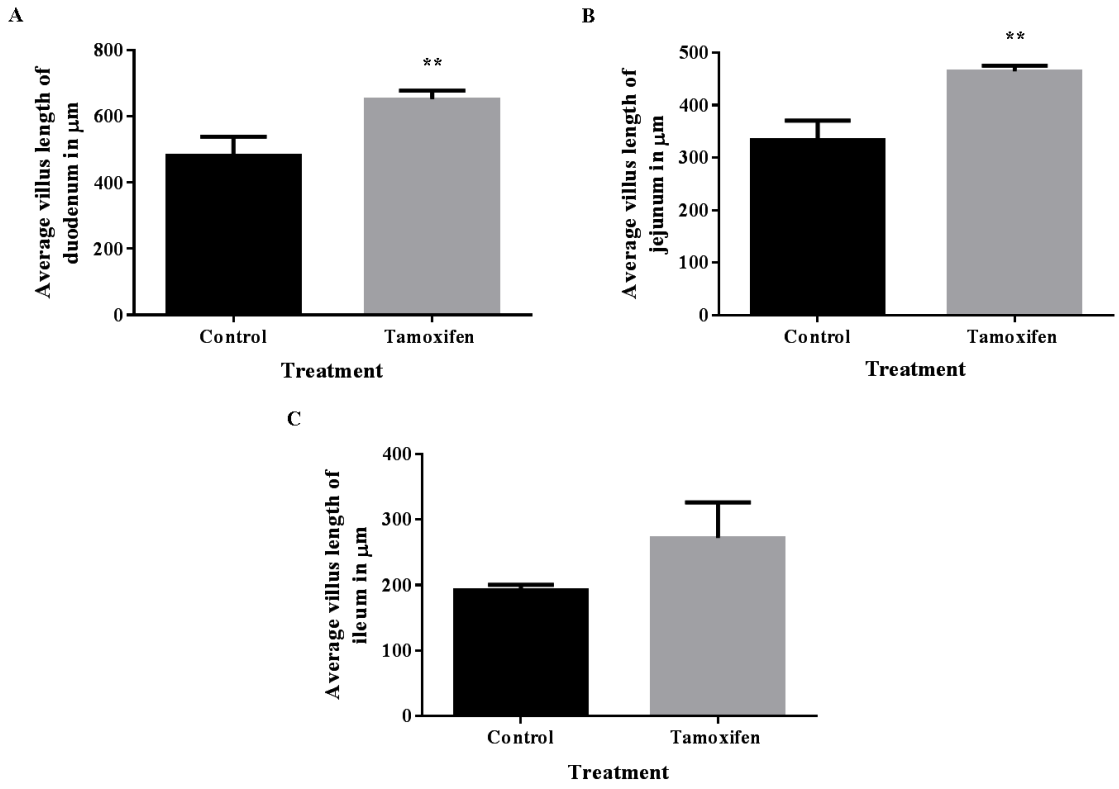

Figure 6.5 – Villus length in small intestine of BRaf$^{CA/+}$/p19Arf$^{-/-}$/A33CreERT2$^{+/-}$/Lacz$^{-/-}$mice. *Villus lengthening was observed in all the regions of the small intestine in BRaf^{VE}/p19 null mice. In the duodenum (P = 0.0098) (**) **(A)** and jejunum (P = 0.0044) (**) **(B)**, there was a significant increase in average villus length in the tamoxifen treated samples compared to the controls. There was also an increase in average villus length in the tamoxifen treated ileum; however, this was not significant. All measurements were in µm; error bars, SEM.*

Crypt lengthening was observed in all regions of the tamoxifen treated small intestine – duodenum, jejunum and ileum (Table 6.3). In the duodenum, the average crypt length was 105.7 µm in the tamoxifen treated mice and this was significantly higher than the controls with 74.5 µm (P = 0.0092) (Figure 6.6A). Similar to the duodenum, the jejunum (P = 0.0131) (Figure 6.6B) and ileum (P = 0.0018) (Figure 6.6C) also exhibited a significant increase in the crypt lengths of tamoxifen treated samples compared to the controls. The average crypt lengths in the jejunum were 75.0 µm (control) and 98.6 µm (tamoxifen treated); and in the ileum were 70.5 µm (control) and 96.1 µm (tamoxifen treated). In the colon, an increase in average crypt

length was observed in the tamoxifen treated mice, but this was not significant (Figure 6.6D).

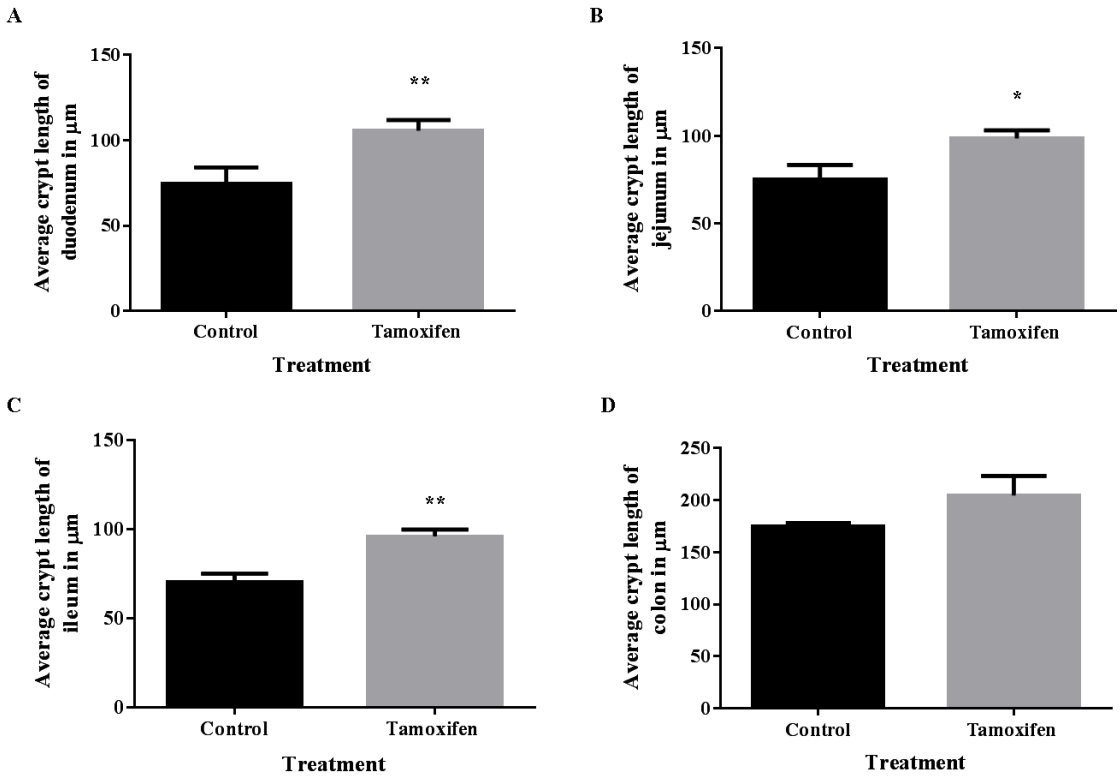

Figure 6.6 - Evaluation of crypt lengths in small intestine and colon of BRaf$^{CA/+}$/p19Arf$^{-/-}$/A33CreERT2$^{+/-}$/Lacz$^{-/-}$ mice. *Crypt lengthening was observed in all the regions of the tamoxifen treated small intestine and colon compared to the controls. The average villus length in the tamoxifen treated small intestine regions - duodenum (P = 0.0092) (**) **(A)**, jejunum (P = 0.0131) (*) **(B)** and ileum (P = 0.0018) (**) **(C)** was significantly higher than the controls. An increase in crypt length was also observed in the colon, but this was not significant in comparison with the control mice **(D)**. All measurements were in µm; error bars, SEM.*

6.2.1.4 *BRaf$^{CA/+}$/p19Arf$^{+/-}$/A33CreERT2$^{+/-}$/Lacz$^{-/-}$*

In the tamoxifen treated *BRaf$^{CA/+}$/p19Arf$^{+/-}$/A33CreERT2$^{+/-}$/Lacz$^{-/-}$* mice (mice treated with tamoxifen or olive oil will be referred to as *BRaf^{VE}/p19 het* or *BRaf^{CA}/p19* het mice respectively in the subsequent sections), villus lengthening was observed in the small intestine regions (Table 6.4). In the duodenum (Figure 6.7A), the average villus lengths were measured at 516.2 µm in the control mice and 672.0 µm in the tamoxifen treated mice, the difference was significant (*P* = 0.0094). The jejunum

region of tamoxifen treated mice also exhibited a significant difference (P = 0.0002) in average villus length between the tamoxifen treated mice (499.0 μm) and controls (311.4 μm) (Figure 6.7B). In the ileum an increase in villus length was observed in the tamoxifen treated samples (302.8 μm) compared to the control samples (221.9 μm); however, this was not significant (Figure 6.7C).

Table 6.4 - Measurements of crypt and villus lengths of olive oil and tamoxifen treated BRaf$^{CA/+/}$/p19Arf$^{+/-}$/A33CreERT2$^{+/-}$/Lacz$^{-/-}$mice

Colon/SI regions	**Treatment**							
	Olive oil (μm)			**Average**	**Tamoxifen (μm)**			**Average**
Colon	182.4	221.8	194.1	**199.4**	219.0	208.2	229.3	**218.8**
Duodenum								
Villus	512.1	575.4	461.0	**516.2**	672.7	676.1	667.1	**672.0**
Crypt	80.7	78.6	92.3	**83.9**	108.5	105.3	110.0	**107.9**
Jejunum								
Villus	326.1	317.9	290.3	**311.4**	505.7	483.3	507.9	**499.0**
Crypt	81.1	86.8	105.3	**91.0**	95.2	96.9	92.1	**94.7**
Ileum								
Villus	198.6	227.4	239.8	**221.9**	362.4	261.7	284.5	**302.8**
Crypt	75.1	77.8	120.7	**91.2**	102.3	106.6	99.5	**102.8**

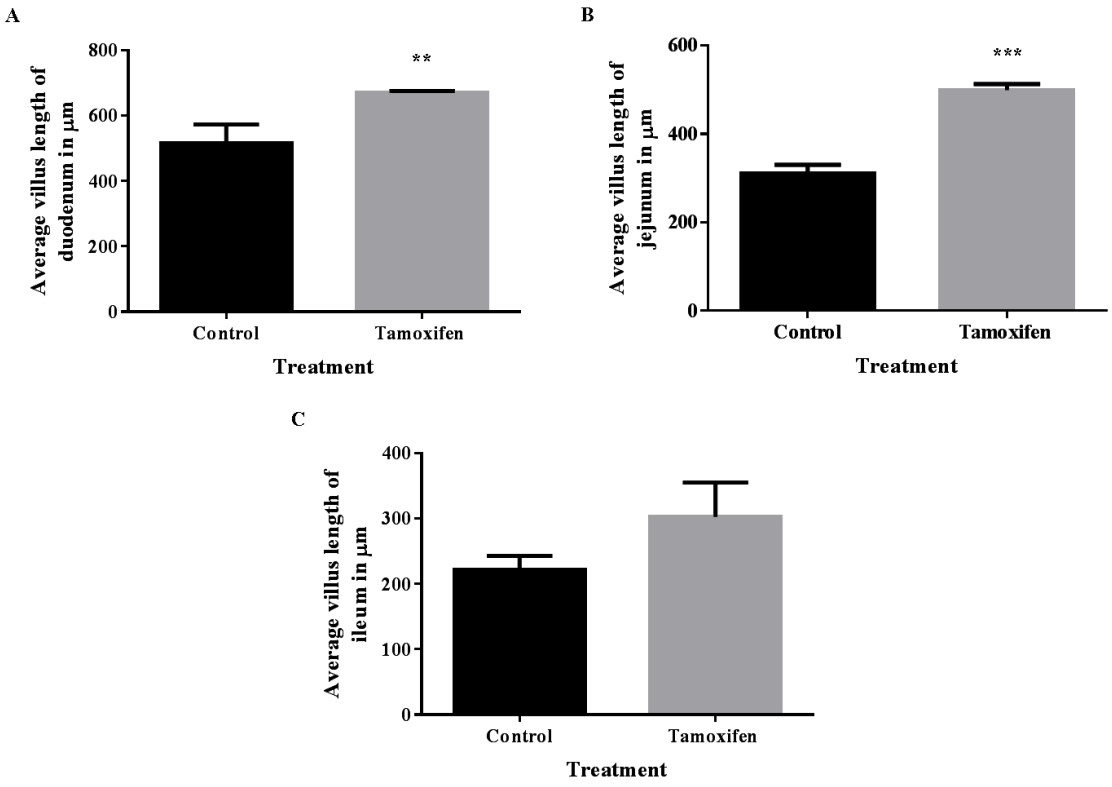

Figure 6.7 - Assessment of villus lengths in small intestine of BRaf$^{CA/+}$/p19Arf$^{+/-}$/A33CreERT2$^{+/-}$/Lacz$^{-/-}$mice. *Villus lengthening was observed in the tamoxifen treated regions of the small intestine – duodenum **(A)**, jejunum **(B)** and ileum **(C)**. This difference in villus length was significant only in the duodenum and jejunum regions of tamoxifen treated mice with P values of 0.0094 (**) and 0.0002 (***) respectively. All measurements were in µm; error bars, SEM.*

A comparative analysis of the crypt lengths was also carried out between the tamoxifen treated mice and controls in *BRaf$^{CA/+}$/p19Arf$^{+/-}$/A33CreERT2$^{+/-}$/Lacz$^{-/-}$*mice (Table 6.4). In the duodenum, average crypt length was measured in the tamoxifen treated (107.9 µm) and control mice (83.9 µm) and this difference was significant (*P* = 0.0059) (Figure 6.8A). However, only a marginal increase was observed in the average crypt length in the tamoxifen treated jejunum (94.7 µm) (Figure 6.8B) compared to the control mice (91.0 µm) and this was not significant. In the ileum (Figure 6.8C) and colon (Figure 6.8D), crypt lengthening was observed in the tamoxifen treated mice in comparison with the controls; however, this was not significant.

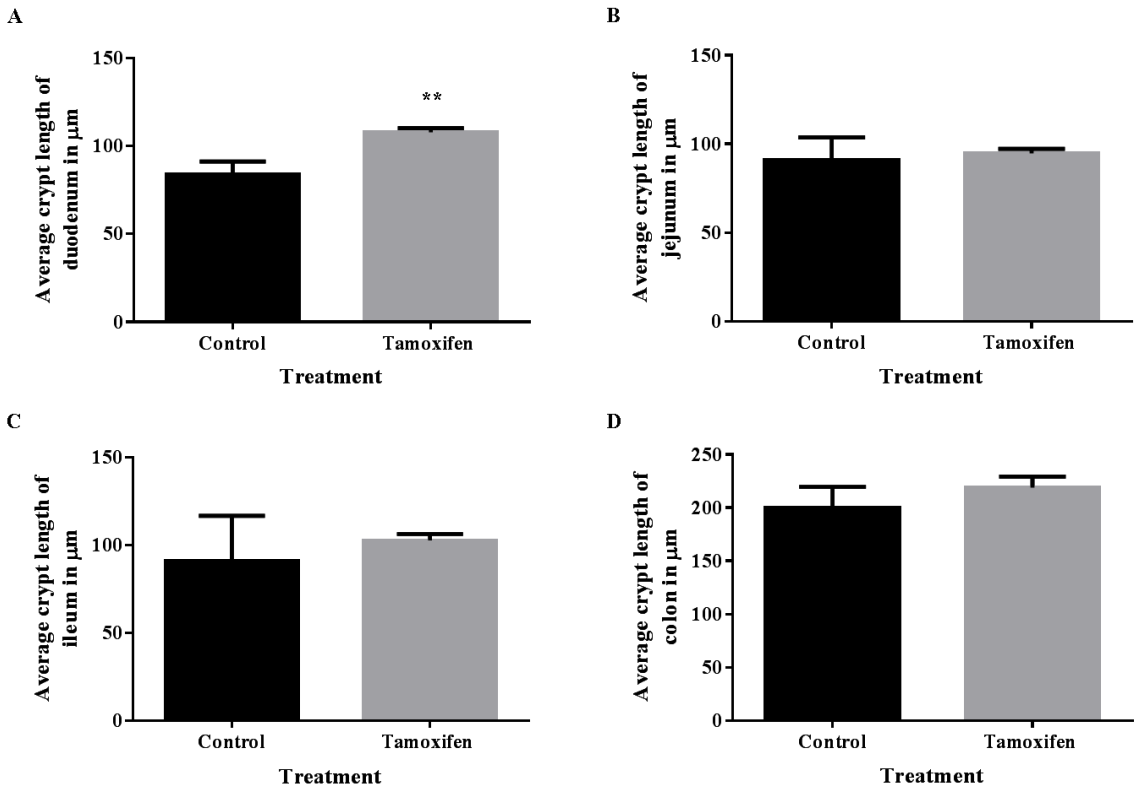

Figure 6.8 - Crypt lengths in small intestine and colon of BRaf$^{CA/+}$/p19Arf$^{+/-}$/A33CreERT2$^{+/-}$/Lacz$^{-/-}$mice. *An increase in crypt lengths was observed in all the small intestine regions and colon of the tamoxifen treated mice. This increase was significant only in the duodenum (P = 0.0059) (**) **(A)**. Only a marginal increase was observed in the jejunum of tamoxifen treated mice and this was not significant **(B)**. Crypt lengthening was also observed in the ileum **(C)** and colon **(D)** of tamoxifen treated mice. All measurements were in µm; error bars, SEM.*

6.2.1.5 Comparative analysis of crypt and villus measurements in all mice groups

The villus lengths of the duodenum in the tamoxifen treated mice were compared in the different mice groups - *BRaf^{VE}*, *BRaf^{VE}/p16* null, *BRaf^{VE}/p16* het, *BRaf^{VE}/p19* null and *BRaf^{VE}/p19* het. Differences were observed in the average villus length in the duodenum between the mice groups and were not significant. The *BRaf^{VE}* and *BRaf^{VE}/p16* null mice exhibited the lowest and highest average villus length with 650.8 µm and 721.8 µm respectively. There was only a marginal difference in average villus length of the duodenum between the *BRaf^{VE}/p16* het (675.2 µm), *BRaf^{VE}/p19* null (652.1 µm) and *BRaf^{VE}/p19* het (672.0 µm) mice groups.

In contrast, a significant difference was observed in the villus length of tamoxifen treated jejunum samples (P = 0.0075). The *BRaf*^{VE}/*p16* het mice (601.1 μm) exhibited the highest average villus length, closely followed by the *BRaf*^{VE}/*p16* null group with 579.5 μm. The *BRaf*^{VE}/*p19* null group had the lowest average villus length with 464.6 μm. In the ileum region, no significant difference was observed in the average villus length between the mice groups. The *BRaf*^{VE}/*p16* null mice (331.2 μm) exhibited the highest average villus length and this was followed by the *BRaf*^{VE}/*p19* het mice (302.8 μm). The lowest villus length (average) was observed in *BRaf*^{VE}/*p16* het mice with 242.9 μm.

A comparative analysis of crypt lengths in the tamoxifen treated mice groups revealed that the *BRaf*^{VE}/*p19* het and *BRaf*^{VE}/*p16* null mice groups were the highest with 218.8 μm and 210.8 μm respectively. This was followed by *BRaf*^{VE}/*p19* null (204.5 μm) and *BRaf*^{VE}/*p16* het mice (197.3 μm), while the *BRaf*^{VE} mice were the lowest with 182.1 μm. The *BRaf*^{VE}/*p16* null and *BRaf*^{VE}/*p16* het mice exhibited the highest average crypt lengths in the duodenum and jejunum; while in the ileum, the *BRaf*^{VE}/*p19* het group was the highest. The difference in crypt lengths of duodenum and ileum between the different tamoxifen treated mice was significant with P values of 0.0417 μm and 0.0158 μm. The crypt and villus lengthening observed in the tamoxifen treated mice compared to the controls indicate hyperplastic changes.

6.2.2 Longitudinal studies – assessment of polyps in the small intestine and colon of tamoxifen treated mice

BRaf^{CA} mice crossed with either *p16Ink4a* or *p19Arf* were set up for longitudinal studies and monitored for development of lesions or tumours or other abnormalities in the colon and small intestine. The different mice groups assessed were *BRaf*^{CA}/*p16* null, *BRaf*^{cA}/*p16* het, *BRaf*^{CA}/*p19* null and *BRaf*^{CA}/*p19* het.

6.2.2.1 *BRaf*^{CA}/*p16 null mice*

In the *BRaf*^{CA}/*p16* null group, 21 mice were treated with tamoxifen (*BRaf*$^{CA/+/}$/*p16Ink4a*$^{-/-}$/*A33CreERT2*$^{+/-}$/*Lacz*$^{-/-}$), 21 mice were used as controls (olive oil injections) (*BRaf*$^{CA/+/}$/*p16Ink4a*$^{-/-}$/*A33CreERT2*$^{+/-}$/*Lacz*$^{-/-}$) and 35 mice were not given any treatment (*BRaf*$^{CA/+/}$/*p16Ink4a*$^{-/-}$/*A33CreERT2*$^{-/-}$/*Lacz*$^{-/-}$) and were also used

as controls. The lesions were found only in the duodenum and jejunum regions of the small intestine of tamoxifen treated mice. No lesions were observed in the colon and small intestine of the control mice - olive oil treated and untreated. The lesions or polyps were evaluated as traditional serrated adenomas (TSA) based on the H&E stained slides.

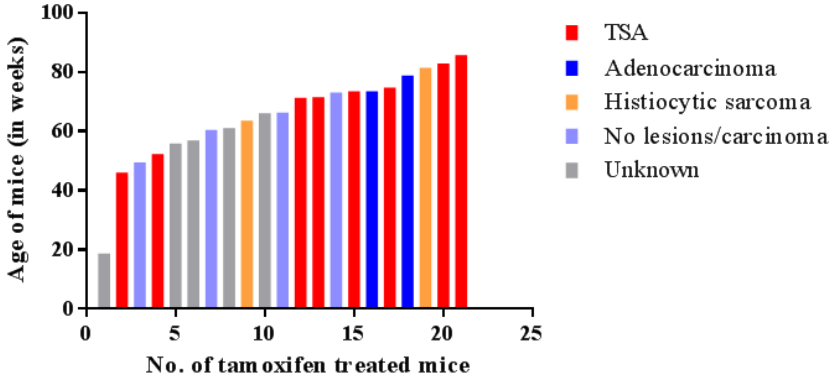

Figure 6.9 – Assessment of abnormalities in the small intestine of tamoxifen treated BRaf^{VE}/p16 null mice. *BRaf^{VE}/p16 null mice treated with tamoxifen (n = 21) were assessed for lesions or tumours in the small intestine. Traditional serrated adenoma (TSA) was observed in eight mice and with either high-grade or low-grade dysplasia (red). Adenocarcinomas were also present with multiple TSAs in two mice (blue), while histiocytic sarcoma was detected in two mice (orange). The small intestines of only four mice were normal (purple), while the GI tract could not be assessed for five mice which were dead for an extended period before dissection (grey).*

TSAs were present in 8 out of 21 tamoxifen treated mice (38.1%) with varying degrees of dysplasia - high-grade (HGD) and low-grade (LGD) (Figure 6.9 - red). A majority of the tamoxifen treated mice which developed TSAs were older than 70 weeks (6 out of 8 mice); while the younger mice were 46 and 52.29 weeks old (Figure 6.10A). Mice younger than 73 weeks (50%) had only a single TSA either in the duodenum or jejunum. However, mice older than 73 weeks developed multiple TSAs in the duodenum and jejunum. In addition to TSAs, adenocarcinomas were detected in two mice aged 73.57 weeks (Figure 6.10B) and 78.86 weeks (Figure 6.9 – blue) with multiple TSAs in the duodenum and jejunum. Histiocytic sarcoma (Figure 6.9 – orange) was also observed in 2 out of 21 mice, while 4 out of 21 mice were lesion-free (Figure 6.9 – purple).

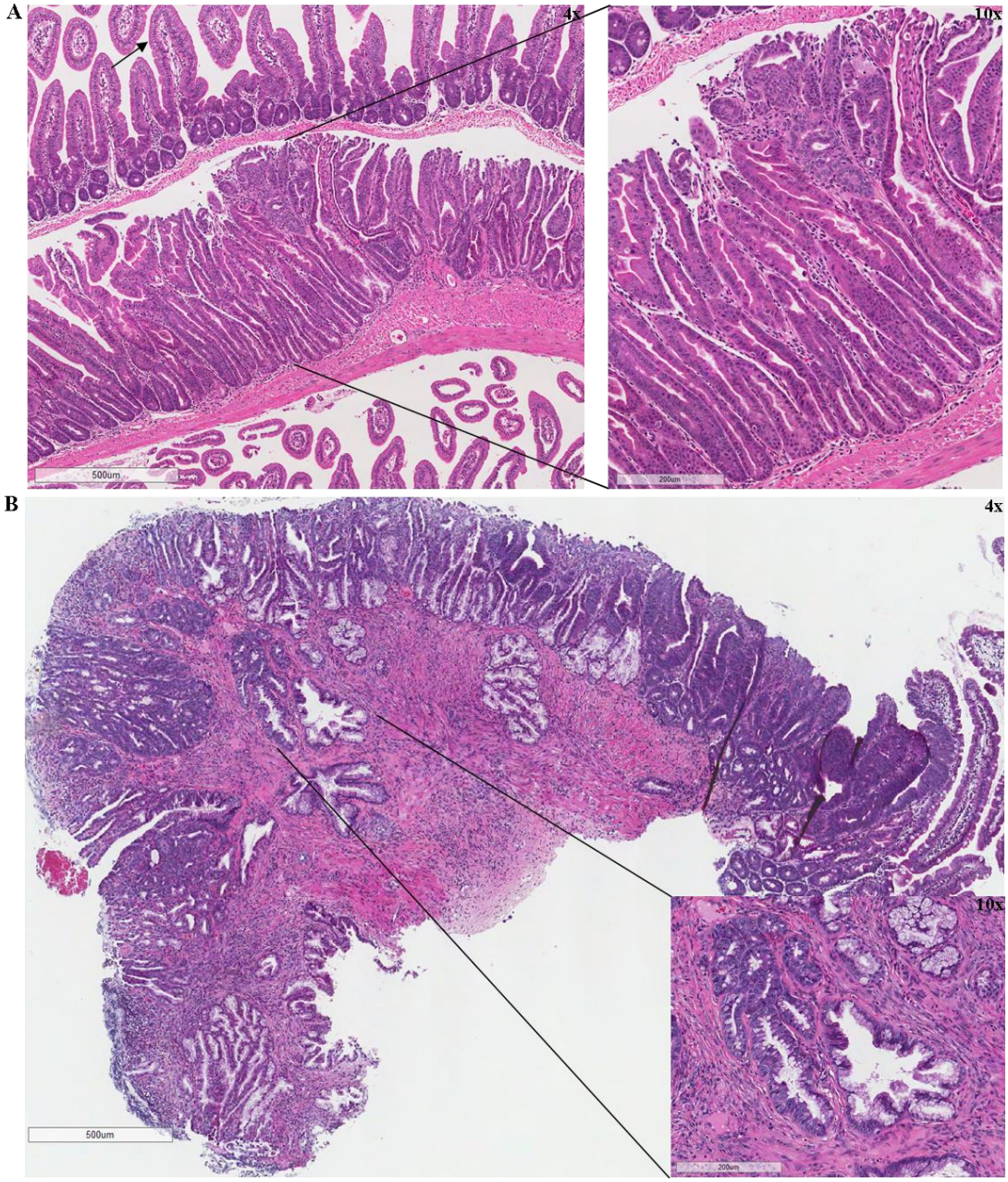

Figure 6.10 – H&E stained sections of TSA and adenocarcinoma in BRaf^{VE}/p16 null mice. *TSA with low-grade dysplasia was observed in the duodenum of a tamoxifen treated BRaf^{VE}/p16 null mouse which was 52.29 weeks old. The loss of villus and crypt integrity was observed (magnification 10x) in comparison with the normal section of the duodenum (arrow)* ***(A)****. An adenocarcinoma was detected in the duodenum* ***(B)*** *infiltrating through the stroma (inset). The mouse was 73.57 weeks old and also presented with an adenocarcinoma in the jejunum and a TSA with high grade dysplasia in the duodenum region. Lower magnification 4x (A & B), scale bar = 500 μm and higher magnification 10x (A & B), scale bar = 200 μm.*

6.2.2.2 *BRaf^{CA}/p16 het mice*

The *BRaf^{CA}/p16* het group consisted of 22 tamoxifen treated mice (*BRaf$^{CA/+}$/p16Ink4a$^{+/-}$/A33CreERT2$^{+/-}$/Lacz$^{-/-}$*), 21 olive oil treated mice (controls) (*BRaf$^{CA/+}$/p16Ink4a$^{+/-}$/A33CreERT2$^{+/-}$/Lacz$^{-/-}$*) and 34 untreated mice (controls). Similar to the *BRaf^{VE}/p16* null mice, lesions were observed only in the duodenum and jejunum regions of the small intestine of tamoxifen treated mice. No lesions were observed in the ileum or colon of tamoxifen treated mice; and the controls (olive oil treated and untreated) were also lesion-free.

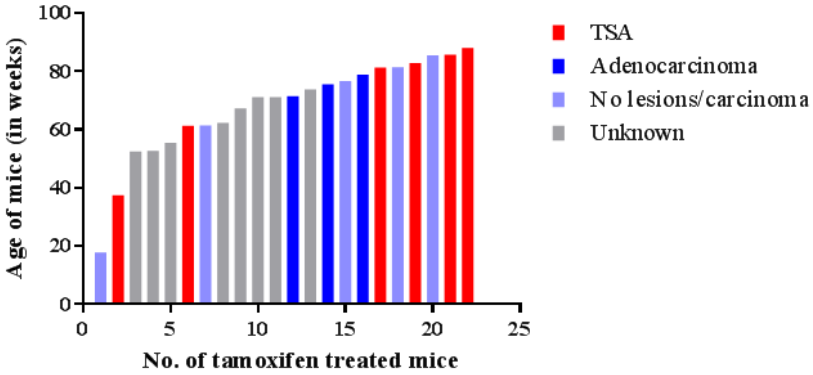

Figure 6.11 – Incidence of TSAs and adenocarcinomas in the small intestine of BRaf^{VE}/p16 het mice (n = 22). *The majority of TSAs (four out of six mice) (red) and all the adenocarcinomas (blue) (three in total) were observed in mice older than 70 weeks. Only five mice had normal small intestines and colon (purple). However, the GI tract could not be assessed properly in a majority of the mice (grey) which were dead for an extended period due to decomposition of the gastrointestinal (GI) tract.*

All the lesions observed in the small intestine were TSAs, similar to the *BRaf^{VE}/p16* null mice. The youngest mouse with a TSA was 37.43 weeks old; while the oldest mouse was 88.14 weeks old. Six mice presented with TSAs mainly in the duodenum region of the small intestine (Figure 6.11 – red). The majority of the mice with TSAs (four out of six) were above 70 weeks of age and multiple TSAs were observed in the older mice. Adenocarcinomas were detected in three mice (Figure 6.11 – blue); all between 71-79 weeks of age and these were found only in the duodenum region (Figures 6.12A and 6.12B). In addition, a number of mice had died before they were identified as sick and sacrificed for autopsy (Figure 6.11 – grey). No

macroscopic tumours were observed; however, since the gastrointestinal (GI) tract was autolysed, the organs could not be assessed properly.

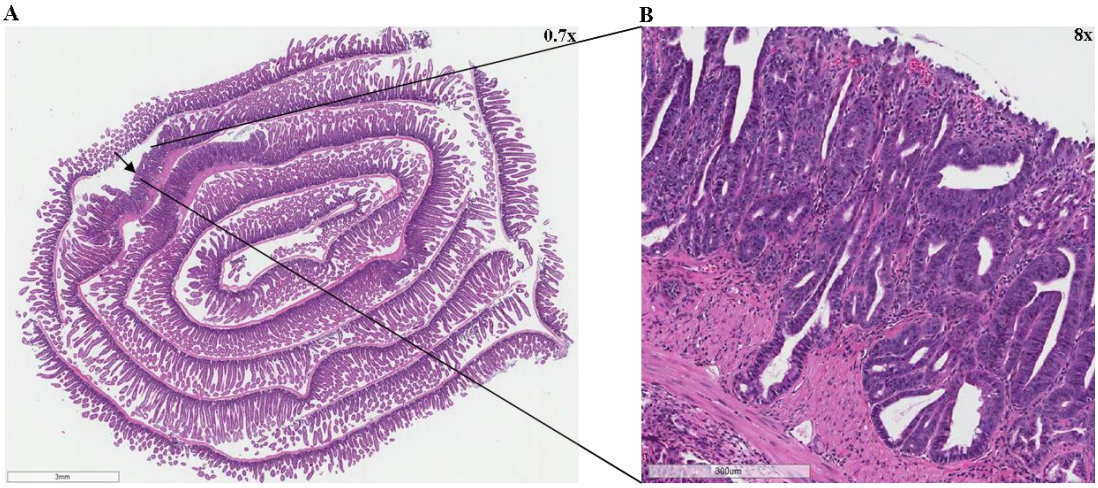

Figure 6.12 – Adenocarcinomas in the small intestine of BRaf^{VE}/p16 het mice. *Adenocarcinomas (black and red arrows) were observed in the duodenum region of the small intestine* ***(A)****. The adenocarcinoma (black arrow) had advanced into the stromal region of the duodenum* ***(B)*** *and a structural loss of villi and crypts was observed. This mouse was 75.57 weeks old and these adenocarcinomas were only observed in the duodenum, while the jejunum and ileum were normal. Scale bars represent 3 mm (A) and 300 µm (B); magnification 0.7x (A) and 8x (B).*

6.2.2.3 *BRaf^{CA}/p19 null mice*

The *BRaf^{CA}/p19* null group were monitored for tumour development and consisted of 21 tamoxifen treated mice (*BRaf$^{CA/+/}$/p19Arf$^{-/-}$/A33CreERT2$^{+/-}$/Lacz$^{-/-}$*), 21 mice treated with olive oil (controls) (*BRaf$^{CA/+/}$/p19Arf$^{-/-}$/A33CreERT2$^{+/-}$/Lacz$^{-/-}$*) and 25 untreated mice (*BRaf$^{CA/+/}$/p19Arf$^{-/-}$/A33CreERT2$^{-/-}$/Lacz$^{-/-}$*). This was the only mouse group with no TSAs observed in the colon and small intestine of tamoxifen treated mice. Adenocarcinomas and undifferentiated malignancies were the only abnormalities detected in the GI tract of tamoxifen treated mice. The GI tracts of all the olive oil treated and untreated mice were normal.

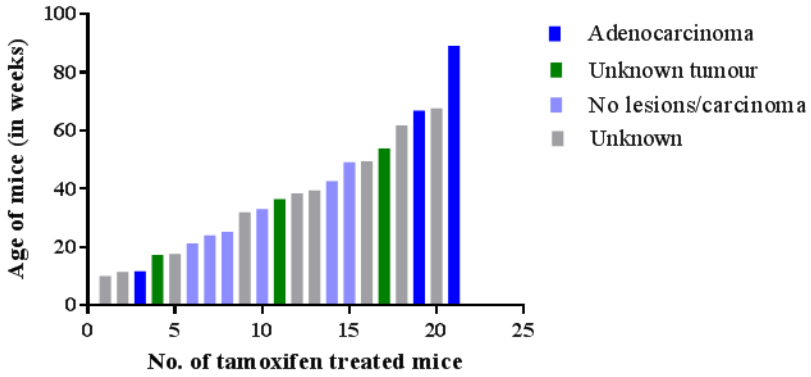

Figure 6.13 – Tumours and other abnormalities in tamoxifen treated BRaf^{VE}/p19 null mice. *In contrast to the other mice groups, no TSAs were observed in the BRaf^{VE}/p19 null group. Adenocarcinomas were observed in three mice out of 21 (blue), while six mice were normal (purple). Tumours with undifferentiated malignancy were observed in three mice younger than 54 weeks (green), with the youngest mouse being 17.29 weeks old. Some of the mice died due to lung tumours and other unknown pathological conditions (grey).*

Tumours were observed in mice as young as 11.71 weeks old, with the oldest being 89.14 weeks old. A colonic tumour assessed as a poorly differentiated adenocarcinoma was detected in the youngest mouse in the midsection of the colon. This mouse showed signs of rectal bleeding, weight loss and enlarged lymph nodes. Adenocarcinomas (Figure 6.13 – blue) were observed in two other mice aged 66.86 weeks and 89.14 weeks (Figures 6.14A and 6.14B). Undifferentiated malignancies were identified in three mice aged between 17 weeks and 54 weeks. They were present in organs such as stomach, caecum, colon and small intestine (Figure 6.13 – green).

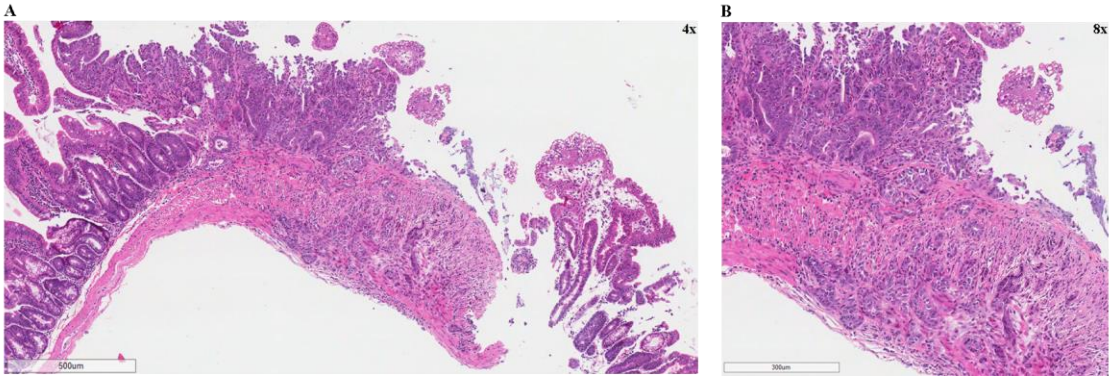

Figure 6.14 – Adenocarcinoma in the duodenum region of a tamoxifen treated BRaf^{VE}/p19 null mouse. *A moderately differentiated adenocarcinoma was observed in the duodenum region* ***(A and B)*** *of the oldest mouse in the BRaf^{VE}/p19 null group (89.14 weeks old). The colon and other regions of the small intestine - jejunum and ileum were normal. This tumour could have possibly risen from an existing TSA with high-grade dysplasia, but no TSA could be identified. Scale bars represent 500 μm (A) and 300 μm (B); magnification 4x (A) and 8x (B).*

6.2.2.4 *BRaf^{CA}/p19 het mice*

The *BRaf^{CA}/p19* het mice monitored for tumour analysis consisted of 21 tamoxifen treated (*BRaf$^{CA/+}$/p19Arf$^{+/-}$/A33CreERT2$^{+/-}$/Lacz$^{-/-}$*), 24 olive oil treated (*BRaf$^{CA/+}$/p19Arf$^{+/-}$/A33CreERT2$^{+/-}$/Lacz$^{-/-}$*) and 26 untreated mice (*BRaf$^{CA/+}$/p19Arf$^{-/-}$/A33CreERT2$^{-/-}$/Lacz$^{-/-}$*). TSAs were the only lesions observed in 4 out of 21 tamoxifen treated mice older than 55 weeks (Figure 6.15 - red). The TSAs mainly had high-grade dysplasia and two mice also had TSAs with signs of early carcinoma (Figure 6.16). These polyps/lesions were present only in the small intestine of tamoxifen treated mice – in the duodenum and jejunum regions (Figures 6.17A and 6.17B); however, the ileum and colon were observed to be normal. The youngest mouse with a TSA was 55.14 weeks old, while the older mice were above 80 weeks and had multiple high-grade dysplastic TSAs.

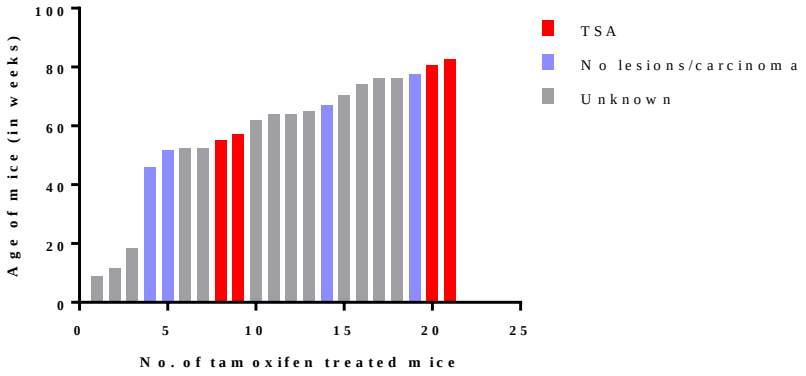

Figure 6.15 – Assessment of lesions or tumours in the small intestine of treated BRaf^{VE}/p19 het mice (n = 21). *TSAs were the only lesions/abnormalities observed in the small intestine of tamoxifen treated mice (red). They were mainly found in the duodenum and jejunum regions and were absent in the ileum and colon. Only 4 out of 21 mice had TSAs (mainly high-grade dysplasia) with multiple TSAs identified in the older mice (80.71 weeks and 82.71 weeks). The GI tracts of only four mice were normal (purple), while a number of mice died prior to sacrifice, they were found to have lung and liver tumours, and the GI tracts could not be assessed due to autolysis (grey).*

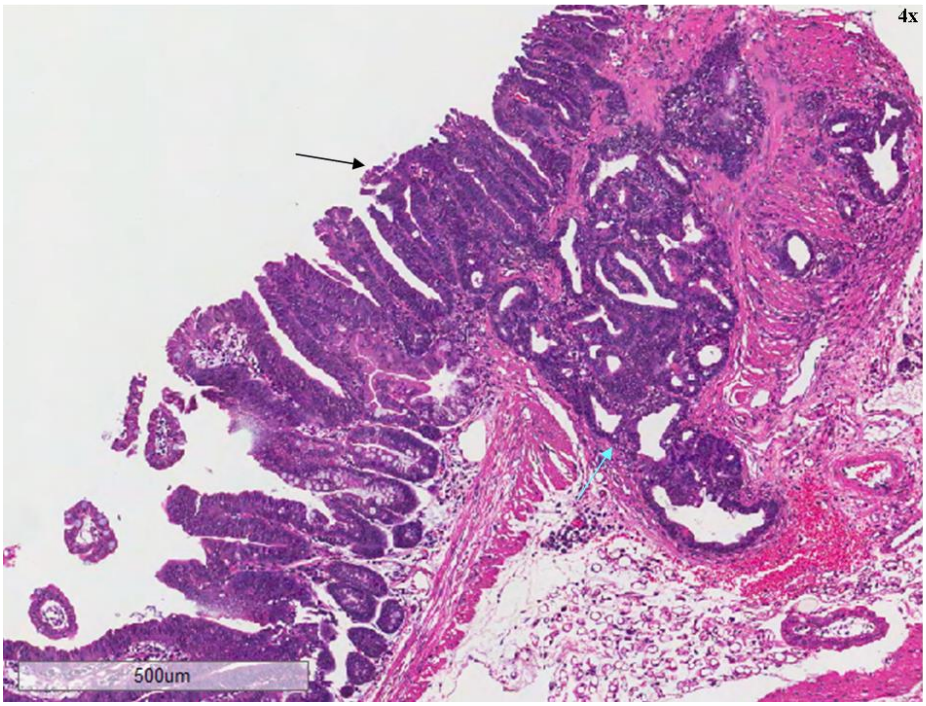

Figure 6.16 – TSA HGD with early carcinoma. *The TSA was identified in the proximal duodenum of a tamoxifen treated mouse, which was 80.71 weeks old. This lesion was assessed as a high-grade dysplastic TSA (black arrow) with carcinoma in the stromal region (blue arrow). Multiple TSAs with high-grade dysplasia were also observed in the duodenum and proximal end of the jejunum. Scale bar represents 500 μm; magnification 4x.*

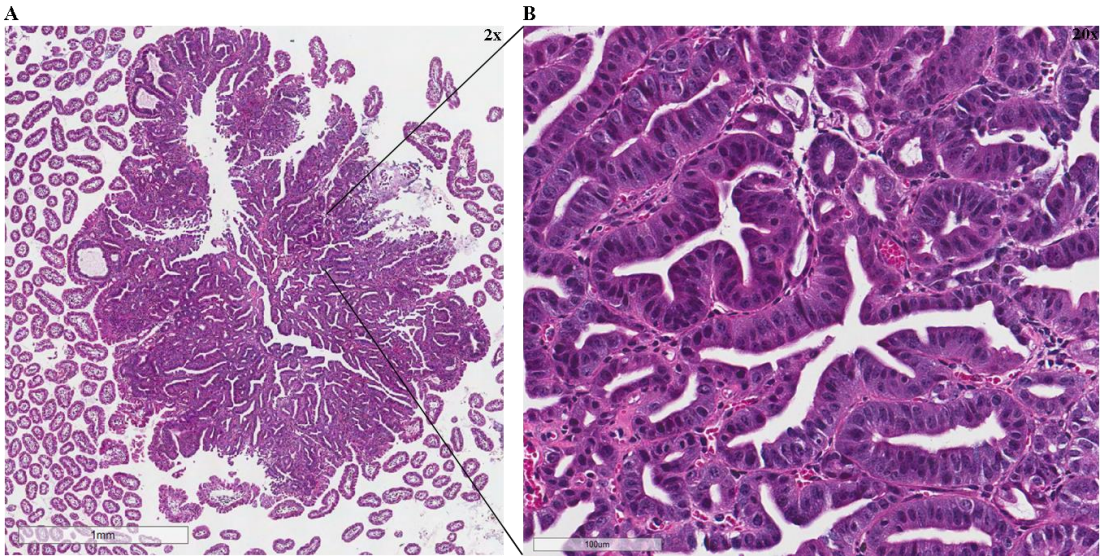

Figure 6.17 – TSA HGD and luminal serration. *The lesion was present in the proximal end of the jejunum and was assessed as a traditional serrated adenoma (TSA) with high-grade dysplasia* ***(A)****. The TSA was found in a 57.29 week old mouse and it was a single lesion observed only in the jejunum. Luminal serration, a characteristic feature of the TSA was observed in many regions* ***(B)****. Scale bars represent 1 mm (A) and 100 µm (B); magnification 2x (A) and 20x (B).*

6.2.2.5 Effect of *p16Ink4a* and *p19Arf* on intestinal lesions

Table 6.5 - TSA and adenocarcinomas in different mice groups

Mice group	Total no. of mice	No. of mice with TSA and TSA with focal carcinoma	No. of mice with adenocarcinoma
Braf^{VE}	23	6	2
Braf^{VE}*/p16 null*	21	8	2
Braf^{VE}*/p16 het*	22	6	3
Braf^{VE}*/p19 null*	21	0	3
Braf^{VE}*/p19 het*	21	4	0

The *Braf*^{VE}*/p16* null mice had the highest number of mice with TSAs with 8 out of 21 (38.1%) mice compared to the *Braf*^{VE} (6 out of 23) and the *Braf*^{VE}*/p16* het (6 out of 22) mice groups. However, no TSA was observed in the *Braf*^{VE}*/p19* null mice; while in the *Braf*^{VE}*/p19* het mice group only 4 mice had TSAs. A significant difference was observed in TSA incidence between the 5 mice groups (P = 0.0393). The loss of *p16Ink4a* or *p19Arf* along with *Braf* V600E mutation did not contribute

significantly to the development of TSAs in the mice. But, there was a significant difference in the number of mice with TSAs between the *Braf^{VE}/p16* and *Braf^{VE}/p19* groups (P = 0.0141). The frequency of adenocarcinomas was low compared to the TSAs across all mice groups and the difference was not significant. The *Braf^{VE}/p16* het and *Braf^{VE}/p19* null mice had the highest number of mice with adenocarcinomas with 3 in each group out of 22 and 21 mice respectively. This was followed by the *Braf^{VE}* (2 out of 23) and *Braf^{VE}/p16* null (2 out of 21) mice, while the *Braf^{VE}/p19* het mice did not develop adenocarcinomas.

6.2.3 Extracolonic abnormalities/tumours in controls and tamoxifen treated mice

The *BRaf^{CA}/p16Ink4a* and *BRaf^{CA}/p19* mouse groups monitored for tumour development in the gastrointestinal tract also developed tumours in other organs such as liver, lungs and spleen. A comparative analysis was done between all the different mice – tamoxifen treated, olive treated (controls) and untreated mice (controls). A broad spectrum of tumours was observed and this could be attributed to old age or absence of the tumour suppressor genes *p16Ink4a* and *p19Arf* in the *BRaf^{CA}/p16Ink4a* null/het and *BRaf^{CA}/p19* null/het mice respectively.

In the tamoxifen treated mice, a majority of the tumours in all the mice groups were lung adenocarcinomas (Figure 6.18A). This was more prevalent in the *BRaf^{VE}* and *BRaf^{VE}/p16Ink4a* mice compared to the *BRaf^{VE}/p19Arf* mice. Liver tumours such as hepatic adenoma, hepatocellular carcinoma and histiocytic sarcoma were mainly observed in *BRaf^{VE}* mice. Abnormalities in the spleen such as histiocytic sarcoma were observed in a small number of tamoxifen treated mice in all the groups. Other tumours such as angiosarcomas and sarcomas were more prevalent in the *BRaf^{VE}/p16Ink4a* and *BRaf^{VE}/p19Arf* mice compared to the *BRaf^{VE}* mice.

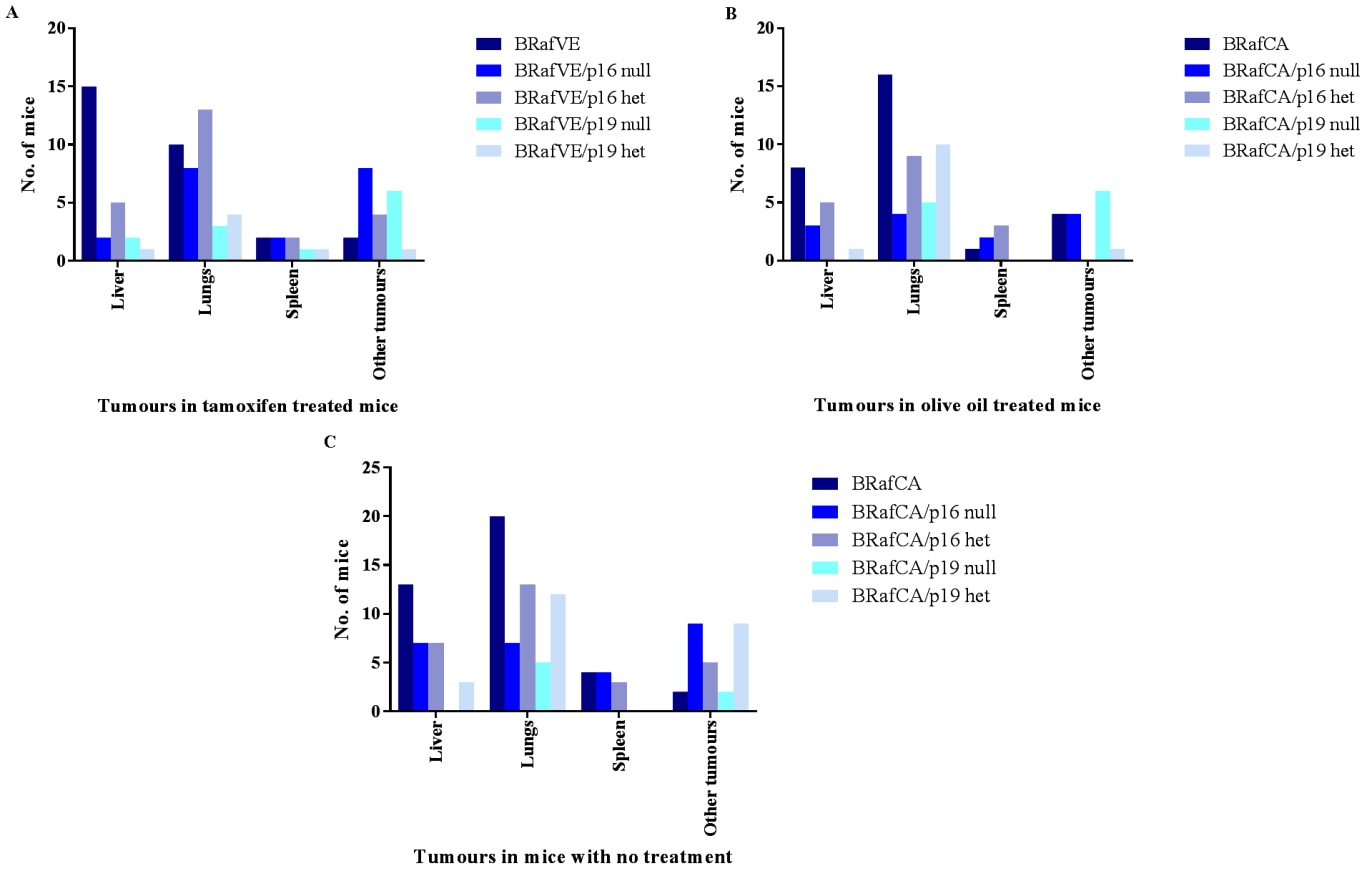

Figure 6.18 – Assessment of tumours in other organs. *Extracolonic tumour formation in other organs was also assessed. In the tamoxifen treated group* ***(A)****, the BRaf^{VE} mice had the highest number of liver abnormalities; while the number of lung adenocarcinomas was highest in the BRaf^{VE}/p16Ink4a het mice. However, in the olive oil treated mice* ***(B)*** *and mice with no treatment* ***(C)****, BRaf^{VE} mice had the highest number of liver and lung tumours.*

In the olive oil treated (Figure 6.18B) and untreated group (Figure 6.18C), a majority of the tumours were prevalent in the liver (hepatocellular carcinomas) and lungs (lung adenocarcinomas) and this was observed in all the mice groups, except for the *BRaf*^{CA}/*p19* null mice. Abnormalities in the lungs and liver were more prevalent in the *BRaf*^{CA} mice compared to the other groups. This was similar to the tamoxifen treated mice. A minority of the mice showed abnormalities in the spleen (histiocytic sarcoma) only in the *BRaf*^{CA} and *BRaf*^{CA}/*p19* control groups. Similar to the tamoxifen treated mice, other tumours such as angiosarcomas and uterine tumours were also observed in the different groups.

6.2.4 Survival analysis

Mice were monitored for tumour development and the survival rates for the different mice groups were assessed. The mice which were sacrificed at different time points (6 weeks and 1.5 years) were not included in this analysis. The 100% survival rate discussed in the subsequent sections represented the number of weeks up to which all the mice survived.

6.2.4.1 *BRaf*^{CA}*/p16Ink4a mice*

The *BRaf*^{CA}/*p16* null group consisted of 17 tamoxifen treated mice, 21 olive oil treated mice (controls) and 35 uninduced mice as controls (mice with no treatment). The tamoxifen treated (red) and the olive oil treated mice (blue) survived up to 81.43 weeks, while the uninduced mice (green) survived only up to 78.71 weeks (Figure 6.19A). All the uninduced mice had a 100% survival rate up to 21 weeks, followed by olive oil treated (19.43 weeks) and tamoxifen treated mice (18.71 weeks). The olive oil treated and the uninduced mice showed a poor survival rate compared to the tamoxifen mice; however the difference in survival rates between the different mouse groups was not significant.

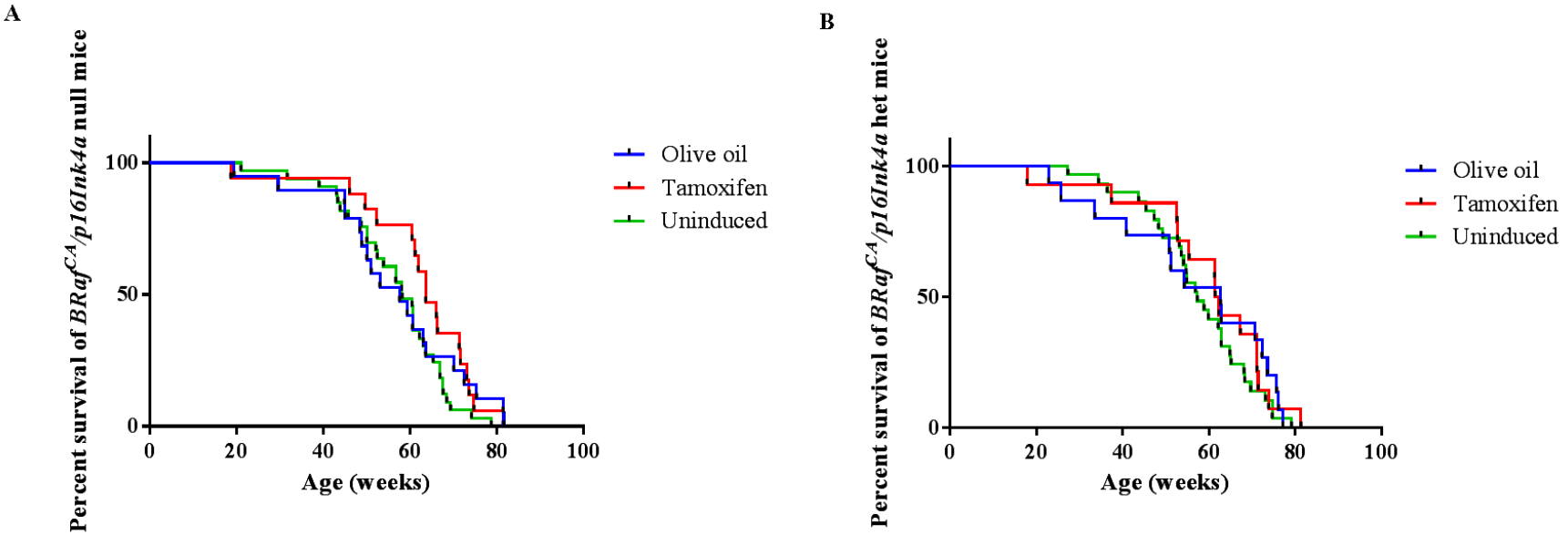

Figure 6.19 – Survival analysis of BRaf^{CA}/p16 mice. *The survival rates of BRaf^{CA}/p16 null* ***(A)*** *and BRaf^{CA}/p16het* ***(B)*** *mice were assessed in the different groups –17 tamoxifen treated (red), 21 olive oil treated (blue) and 35 uninduced (green). In the BRaf^{CA}/p16 null mice, the tamoxifen treated and olive oil treated mice survived up to 81.43 weeks, while the uninduced mice survived only up to 78.71 weeks. This was similar to the BRaf^{CA}/p16 het mice in which the tamoxifen treated mice showed a longer survival rate of 81.29 weeks compared to the olive oil treated (77.14 weeks) and uninduced mice (79.14 weeks).*

In the *BRaf*^{CA}*/p16* het group, survival rates of 14 tamoxifen treated, 15 olive oil treated (controls) and 29 uninduced mice (controls) were assessed (Figure 6.19B). A small, non-significant difference in the survival rates of the different groups was observed. Similar to the *BRaf*^{CA}*/p16* null mice, the tamoxifen treated mice (red) also survived up to 81.29 weeks. The olive oil treated (blue) and uninduced mice (green) survived up to 77.14 weeks and 79.14 weeks respectively. However, the tamoxifen treated mice had a lower 100% survival rate of 17.86 weeks, while this was 22.86 weeks and 27.29 weeks for the olive oil treated and uninduced mice respectively. The *BRaf*^{CA}*/p16* het group showed an improved survival rate compared to the *BRaf*^{CA}*/p16* null group.

6.2.4.2 *BRaf*^{CA}*/p19 mice*

The *BRaf*^{CA}*/p19* null group had 20 tamoxifen treated, 19 olive treated and 26 uninduced mice. A clear, yet non-significant difference was observed between the mice subjected to different treatments (Figure 6.20A). The tamoxifen mice (red) had the lowest survival rate of 67.71 weeks, followed by uninduced mice (green) and olive oil treated mice (blue) with 73 weeks and 78.29 weeks. A 100% survival rate which was only 10.14 weeks was observed in tamoxifen treated mice, while this was lower in the olive treated mice (8.57 weeks). The mice in the uninduced group showed an improved 100% survival rate of 16.29 weeks. There was a rapid decline at an early age (in weeks) in the number of tamoxifen treated mice, compared to the olive treated and uninduced mice.

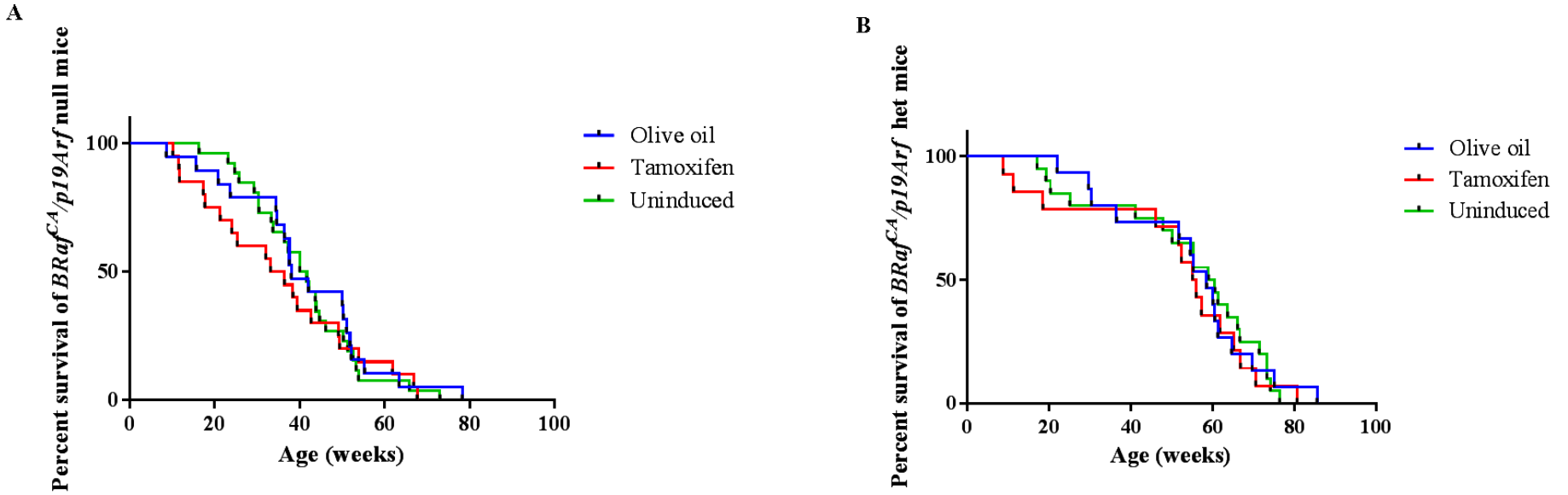

Figure 6.20 – Assessment of survival rates of BRaf^{CA}/p19 mice. *In the BRaf^{CA}/p19 null mice* ***(A)****, the tamoxifen treated mice showed the lowest survival rate with 67.71 weeks (red). The olive oil treated and uninduced mice survived longer than the tamoxifen treated mice with 78.29 weeks (blue) and 73 weeks (green) respectively. The BRaf^{CA}/p19 het mice survived longer than the BRaf^{CA}/p19 null mice* ***(B)****. The survival rate of the olive oil treated mice was the highest mice with 85.57 weeks (blue), followed by the tamoxifen treated (80.71 weeks) (red) and uninduced mice (76.43 weeks) (green).*

In the *BRaf*^{CA}/*p19* het group, there were 14 tamoxifen treated, 15 olive oil treated and 20 uninduced mice (Figure 6.20B). In comparison with the *BRaf*^{CA}/*p19* null group, the tamoxifen treated *BRaf*^{CA}/*p19* het mice had a higher survival rate of 80.71 weeks (red). However, within the *BRaf*^{CA}/*p19* het group, this was lower than the olive oil treated mice (85.57 weeks) (blue); and the uninduced mice (green) showed the lowest survival rate with 76.43 weeks. In contrast, the 100% survival rate was the longest in the control mice – olive oil treated (22 weeks) and uninduced (17.14 weeks) compared to the tamoxifen treated mice with 8.86 weeks. A significant difference was not observed in the survival rates between the different mouse groups.

6.2.4.3 Comparison of survival rates of tamoxifen treated mice in all the groups

The survival rates of tamoxifen treated *BRaf*^{CA}, *BRaf*^{CA}/*p16* null and *BRaf*^{CA}/*p19* null mice were analysed and the difference was significant ($P < 0.0001$) (Figure 6.21A). The *BRaf*^{CA} mice (red) survived up to 97 weeks, while in the *BRaf*^{CA}/*p16* null (blue) and *BRaf*^{CA}/*p19* null (green) groups all the mice were dead at 81.43 weeks and 67.71 weeks respectively. The *BRaf*^{CA} mice had a 100% survival rate up to 63 weeks; however, this was lower in the *BRaf*^{CA}/*p19* null compared to the *BRaf*^{CA}/*p16* null mice with 10.14 weeks and 18.71 weeks respectively. The number of *BRaf*^{CA}/*p19* null mice also declined quite rapidly compared to the *BRaf*^{CA}/*p16* null and *BRaf*^{CA} mice.

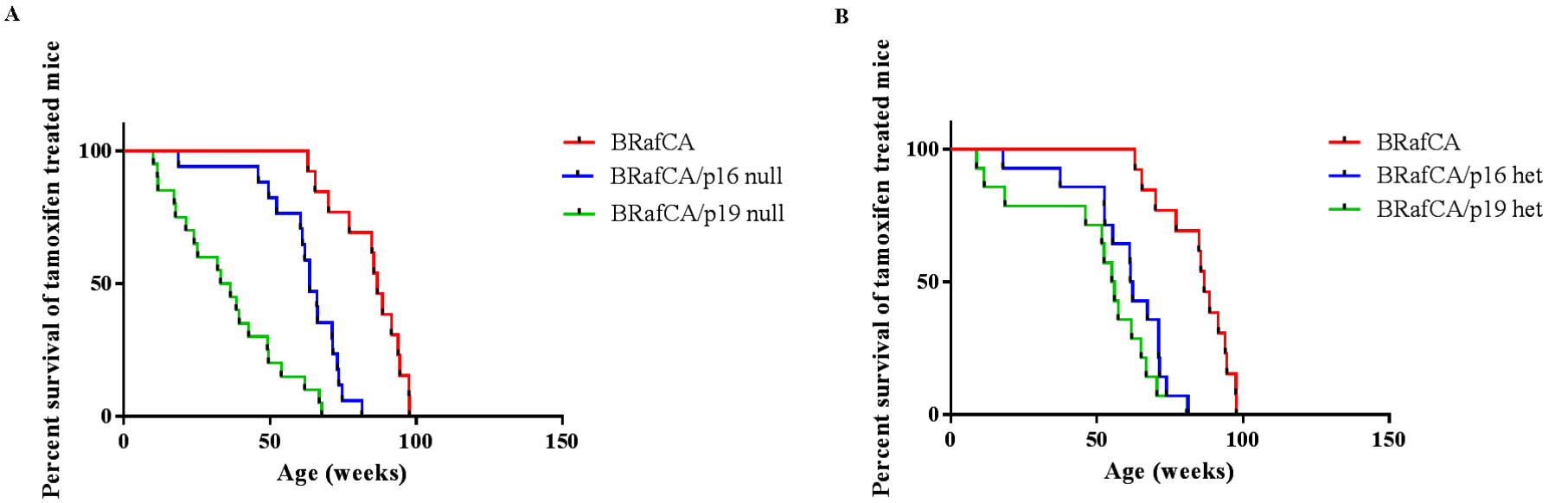

Figure 6.21 – Comparison between survival rates of tamoxifen treated BRaf^{CA}, BRaf^{CA}/p16and BRaf^{CA}/p19 mice. *A significant difference (P < 0.0001) between the BRaf^{CA}, BRaf^{CA}/p16 null and BRaf^{CA}/p19 null mice was observed* ***(A)****. All the BRaf^{CA}/p19 null (green) mice were dead at 67.71 weeks with a 100% survival rate of 10.14 weeks. In contrast, the BRaf^{CA}/p16 null mice (blue) survived up to 81.43 weeks and an improved 100% survival rate with 18.71 weeks. The BRaf^{CA} mice (red) survived the longest up to 97 weeks and also had a higher 100% survival rate of 63 weeks. The BRaf^{CA} (red), BRaf^{CA}/p16 het (blue) and BRaf^{CA}/p19 het mice (green) also revealed a significant difference (P < 0.0001) between the survival rates* ***(B)****. Mice heterozygous for BRaf^{CA}/p16 and BRaf^{CA}/p19 were dead before 82 weeks, while the BRaf^{CA} mice survived up to 97 weeks.*

A significant difference was also observed between survival rates of tamoxifen treated *BRaf*^{CA}, *BRaf*^{CA}/*p16* het and *BRaf*^{CA}/*p19* het mice ($P < 0.0001$) (Figure 6.21B). All the mice in the *BRaf*^{CA}/*p16* het (blue) and *BRaf*^{CA}/*p19* het (green) groups were dead before 82 weeks, while the *BRaf*^{CA} mice (red) survived up to 97 weeks. Similar to the *BRaf*^{CA}/*p19* null mice, the *BRaf*^{CA}/*p19* het mice showed a 100% survival rate up to 8.86 weeks, while for the *BRaf*^{CA}/*p16* het and *BRaf*^{CA} mice it was 17.86 weeks and 63 weeks respectively. The *BRaf*^{CA}/*p16* mice (null and het) revealed a similar survival pattern, while the *BRaf*^{CA}/*p19* null mice showed a more rapid decline in mouse numbers within 82 weeks.

6.2.5 Immunohistochemical analysis

Immunohistochemical (IHC) analysis of β-catenin, p16Ink4a, p44/42 Mapk (Erk1/2) (total Erk) and Phospho-p44/42 Mapk (Erk1/2) (Thr202/Tyr204) (phospho Erk) was performed on a majority of the tamoxifen treated small intestine samples with traditional serrated adenomas and/or adenocarinomas in the *BRaf*^{CA}/*p16* and *BRaf*^{CA}/*p19* groups.

6.2.5.1 β-catenin

In normal cells, the expression of β-catenin was restricted only to the cell membrane and cytoplasm (Figures 6.22A and 6.22B). The tamoxifen treated *BRaf*^{CA}/*p16* group consisted of nine *BRaf*^{CA}/*p16* null mice (seven with TSAs and two with histiocytic sarcomas) and five *BRaf*^{CA}/*p16* het mice (all with TSAs and two with TSA and adenocarcinoma). All the TSAs from *BRaf*^{CA}/*p16* null mice had high-grade dysplasia and showed moderate (two out of seven samples) and strong (five out of seven samples) membranous staining. Cytoplasmic β-catenin expression was weak in four TSAs, moderate in two TSAs and strong in one TSA; and nuclear accumulation of β-catenin was observed in four TSAs (Figure 6.23A). However in the histiocytic sarcomas, nuclear β-catenin staining was observed only in one sample. In contrast, adenocarcinomas identified in the *BRaf*^{CA}/*p16* het mice showed a higher level of β-catenin expression in the nucleus, loss of membranous staining and weak cytoplasmic staining compared to the TSAs (Figures 6.23B-D).

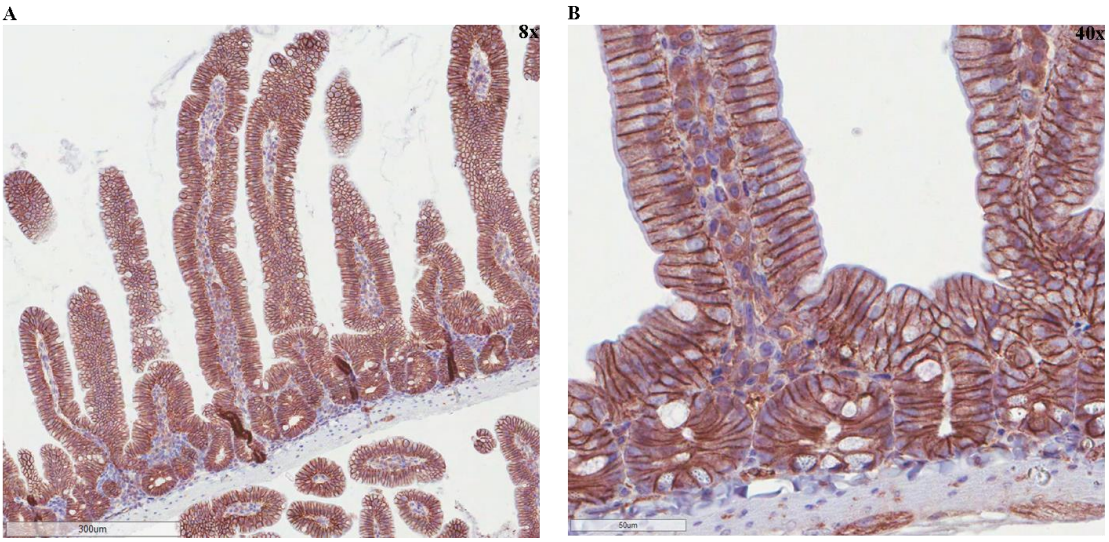

Figure 6.22 – β-catenin staining of normal small intestine villi of BRaf^{CA}/p16 mouse. *The normal expression of β-catenin was restricted to the cell membrane and cytoplasm in the intestinal villi of tamoxifen treated BRaf^{CA}/p16 mouse* ***(A)****. The membranous and cytoplasmic staining was uniform throughout the cells and a lack of nuclear β-catenin expression was observed* ***(B)****. Scale bars represent 300 μm (A) and 50 μm (B); magnification 8x (A) and 40x (B).*

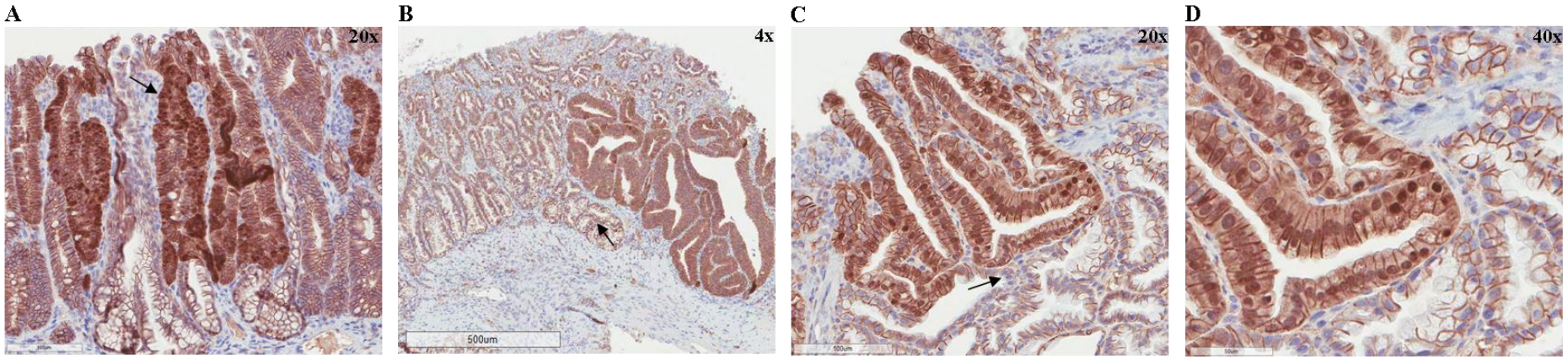

Figure 6.23 - β-catenin expression in a TSA and adenocarcinoma from BRaf^{CA}/p16 mice (n = 14). *The lesions observed in the small intestines of the tamoxifen treated mice were only traditional serrated adenomas (TSA). Moderate membranous and weak cytoplasmic staining was observed along with a strong nuclear expression of β-catenin (arrow)* ***(A)****. The nuclear accumulation of β-catenin was detected only in certain cells of the TSA. In the adenocarcinoma, certain regions showed a loss of membranous staining, weak cytoplasmic staining (arrow)* ***(B and C)*** *and an increase in nuclear β-catenin expression* ***(C to D)****. Age range of mice: 37-88 weeks; scale bars represent 100 μm (A & C), 500 μm (B) and 50 μm (D); magnification 20x (A-D).*

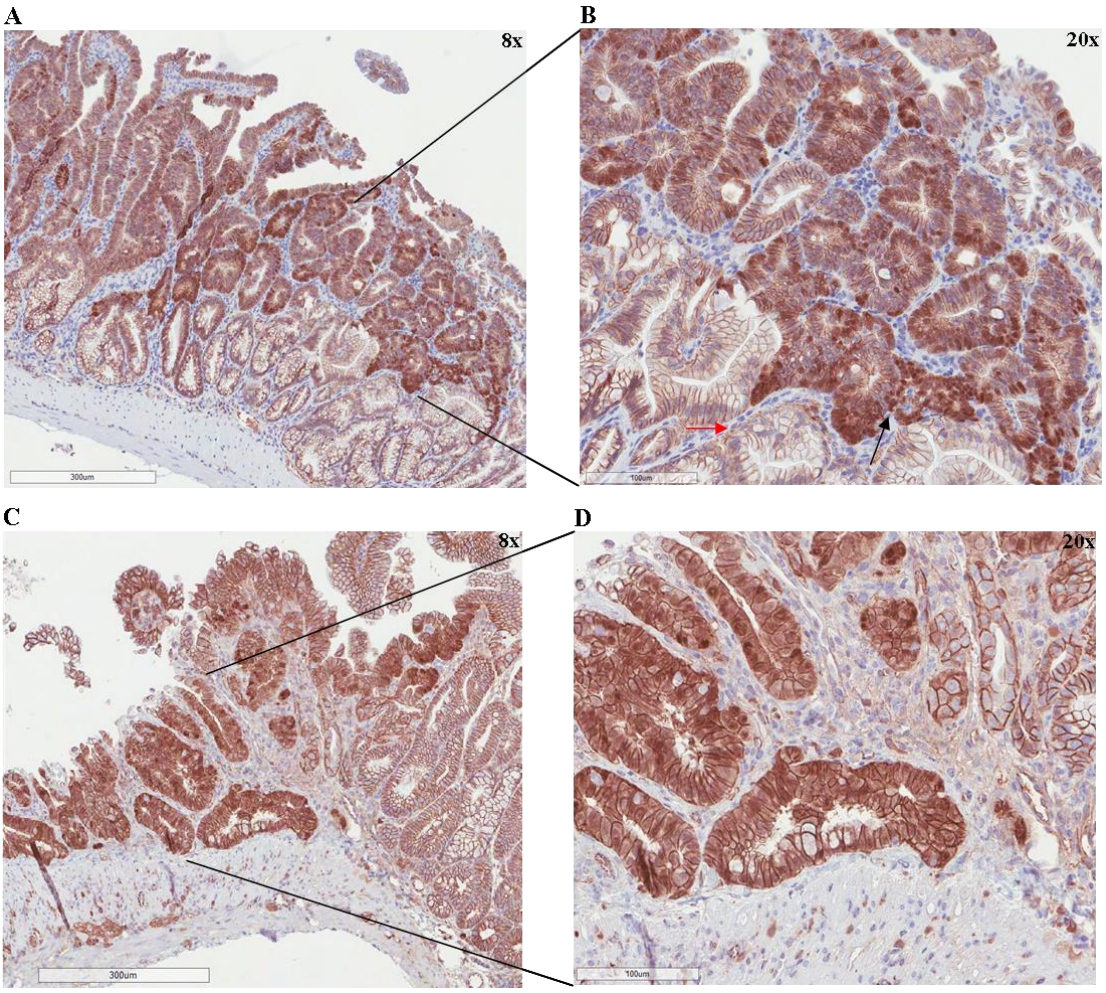

Figure 6.24 – IHC analysis of β-catenin in a TSA and an adenocarcinoma detected in BRaf^{CA}/p19 mice (n = 6). *The staining pattern of β-catenin in the TSA and adenocarcinoma was similar to the BRaf^{CA}/p16 mice. In the TSA* ***(A and B)****, nuclear expression of β-catenin was observed in some regions (black arrow), while a loss of cytoplasmic staining and weak membranous staining was exhibited in adjacent cells (red arrow). In the adenocarcinoma* ***(C and D)****, increased nuclear expression was observed in a majority of the cells with strong cytoplasmic staining. Age range of mice: 53-89 weeks; scale bars represent 300 μm (A & C), 100 μm (B & D); magnification 8x (A & C) and 20x (B & D).*

The *BRaf^{CA}/p19* mice consisted of three *BRaf^{CA}/p19* null mice (adenocarcinomas) and three *BRaf^{CA}/p19* het mice (TSAs with high-grade dysplasia). Membranous staining was observed in all the adenocarcinomas (moderate staining) and TSAs (strong staining) of the *BRaf^{CA}/p19* group; while all the TSAs and adenocarcinomas showed moderate to strong cytoplasmic staining. Nuclear staining

was observed only in one *BRaf*^{CA}/*p19* het sample (Figures 6.24A-B) and in two *BRaf*^{CA}/*p19* null samples (Figures 6.24C-D).

6.2.5.2 p44/42 Mapk (Erk1/2) (total Erk)

The p44/42 Mapk (Erk1/2) (total Erk) expression was assessed in 11 *BRaf*^{CA}/*p16* null mice and six *BRaf*^{CA}/*p16* het mice. In the villi of tamoxifen treated *BRaf*^{CA}/*p16* mice, a moderate expression was observed in the cytoplasm and nucleus of the cells (Figure 6.25A). The expression level (especially the cytoplasmic staining) increased in certain regions of the traditional serrated adenoma (Figure 6.25B) and a similar pattern was also observed in the adenocarcinoma (Figure 6.25C-D). In a majority of the mice in *BRaf*^{CA}/*p16* null and het groups, TSAs showed normal expression levels with an increase in cytoplasmic staining in certain regions of the TSA. However, in mice with multiple TSAs and/or adenocarcinoma, a decrease in the level of total Erk expression was observed (Figure 6.25C). In one histiocytic sarcoma, the total Erk level was normal, while a decrease in expression was observed in the other sample.

In the tamoxifen treated *BRaf*^{CA}/*p19* group, two *BRaf*^{CA}/*p19* null mice and three *BRaf*^{CA}/*p19* het were analysed for p44/42 Mapk (Erk1/2) (total Erk) expression. All the samples with TSAs showed normal expression levels (Figure 6.26A-B); however, a reduced total Erk expression was observed in one mouse with multiple TSAs in the duodenum and jejunum regions of the small intestine with early stage of carcinoma. This was similar to the trend observed in the tamoxifen treated *BRaf*^{CA}/*p16* mice.

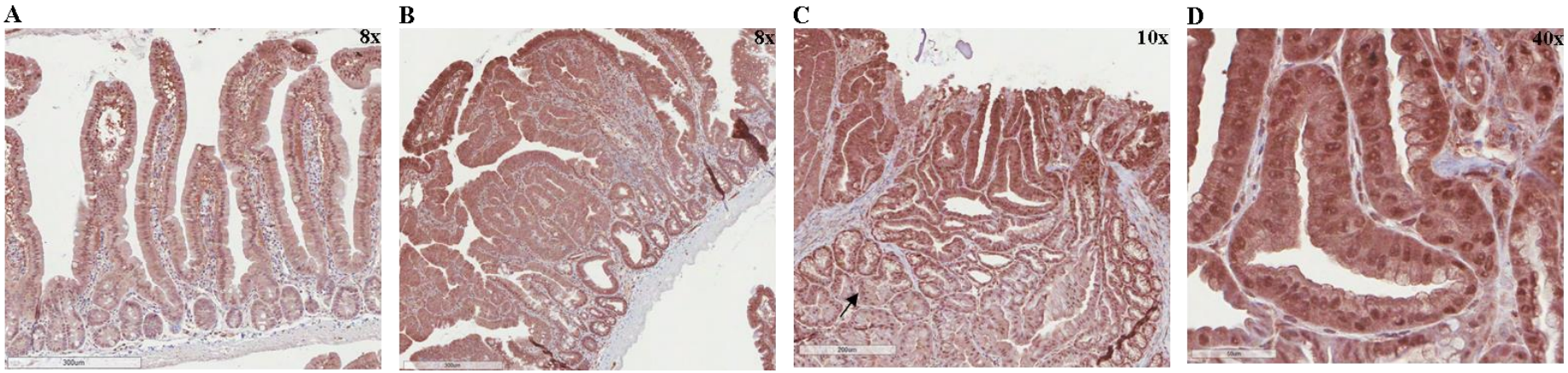

Figure 6.25 – p44/42 Mapk (Erk1/2) (total Erk) expression in BRaf^{CA}/p16 mice (n = 17). *In the normal villi, cytoplasmic and nuclear expression of total Erk was observed* ***(A)*** *and the cytoplasmic expression considerably increased in the traditional serrated adenoma with high-grade dysplasia* ***(B)****. A similar staining pattern was also observed in the adenocarcinoma* ***(D)****, while lower levels of total Erk expression was observed in the adjacent cells (arrow)* ***(C)****. Age range of mice: 37-88 weeks; scale bars represent 300 μm (A &B), 200 μm (C) and 50 μm (D); magnification 8x (A & B), 10x (C) and 40x (D).*

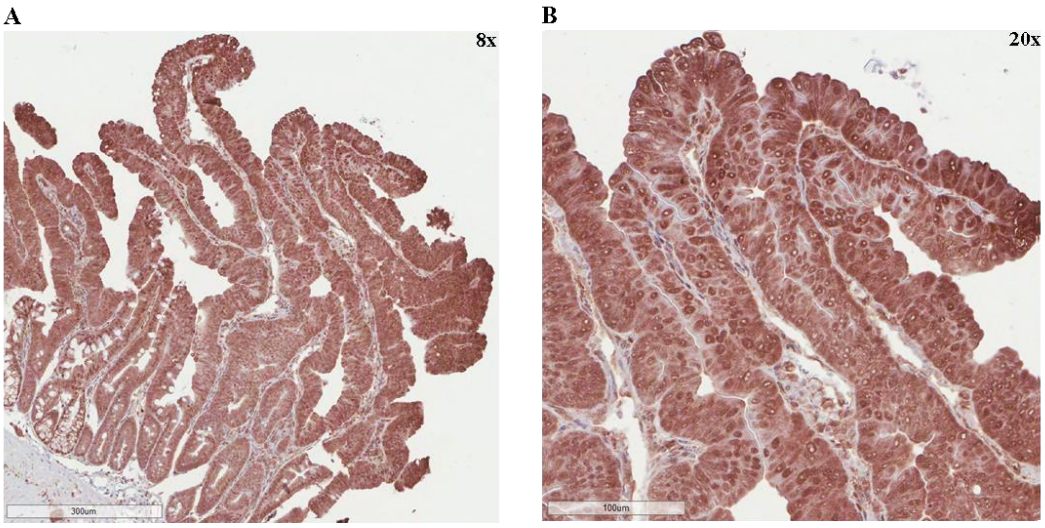

Figure 6.26 – Assessment of p44/42 Mapk (Erk1/2) (total Erk) expression in BRaf^{CA}/p19 mice (n = 5). *The expression levels of total Erk in the BRaf^{CA}/p19 mice was similar to the staining pattern in BRaf^{CA}/p16 mice. Increased cytoplasmic and nuclear staining was observed in traditional serrated adenoma with high-grade dysplasia* ***(A and B)****. Age range of mice: 53-89 weeks; scale bars represent 300 μm (A) and 100 μm (B); magnification 8x (A) and 20x (B).*

6.2.5.3 Phospho-p44/42 Mapk (Erk1/2) (Thr202/Tyr204) (phospho Erk)

The expression of Phospho-p44/42 Mapk (Erk1/2) (Thr202/Tyr204) (phospho Erk) was evaluated in 11 *BRaf^{CA}/p16* null mice and six *BRaf^{CA}/p16* het mice. In normal tamoxifen treated intestinal villi, positively stained cells (cytoplasmic and nuclear) were observed in the lower regions of the crypts (Figure 6.27A). The expression levels of phospho Erk increased in intestinal villi surrounding areas of adenocarcinoma and the positively stained cells were located in the upper regions of the crypts (Figure 6.27B). In the adenocarcinoma, a uniform staining pattern was not observed and only certain cells were positive for phospho Erk expression (Figure 6.27C). This loss of expression was observed in the duodenum and jejunum regions of tamoxifen treated mice which developed multiple TSA or showed signs of adenocarcinoma.

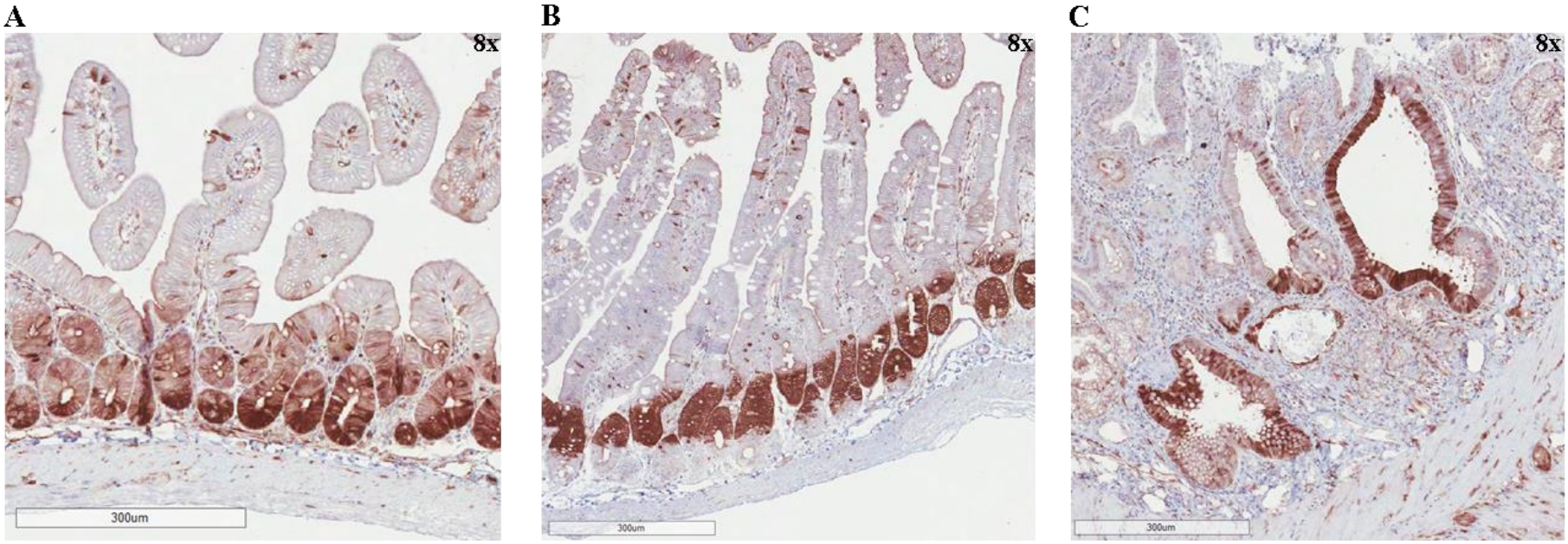

Figure 6.27 – Phospho-p44/42 Mapk (Erk1/2) (Thr202/Tyr204) (phospho Erk) expression in tamoxifen treated BRaf^{CA}/p16 mice (n = 17). *In normal tamoxifen treated villi the cells which stained positive for phospho Erk (cytoplasmic and nuclear staining) were located at the base of the crypts **(A)**. However, in the villi adjacent to an adenocarcinoma, the positive phospho Erk expression was observed in the upper regions of the crypts **(B)**. Small intestine samples with adenocarcinomas and multiple TSAs showed lower, inconsistent expression levels and were observed only in certain cells **(C)**. Age range of mice: 37-88 weeks; scale bars represent 300 μm (A-C); magnification 8x (A-C).*

The *BRaf*^{CA}*/p19* group consisted of two *BRaf*^{CA}*/p19* null mice and three *BRaf*^{CA}*/p19* het mice. Similar to the *BRaf*^{CA}*/p16* mice, all small intestine samples with TSAs showed normal levels of phospho Erk expression with positively stained cells at the base of the crypts. In TSAs, only certain regions of the lesion exhibited an increased level of phospho Erk expression (cytoplasmic and nuclear staining), while the rest of the lesion showed a loss of phospho Erk expression (Figures 6.28A and 6.28B). In a majority of the TSAs, the expression levels were normal, however a loss of expression was observed in mice with multiple TSAs and adenocarcinomas.

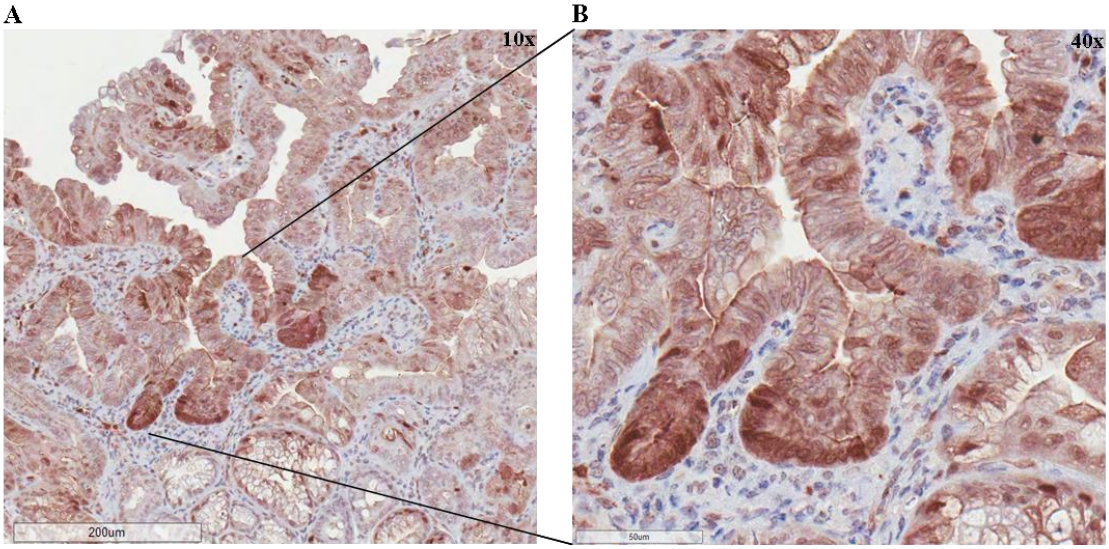

Figure 6.28 – Phospho-p44/42 Mapk (Erk1/2) (Thr202/Tyr204) (phospho Erk) expression in tamoxifen treated BRaf^{CA}/p19 mice (n = 5). *An increase in expression levels of phospho Erk was observed in TSAs with high-grade dysplasia (cytoplasmic and nuclear) and this was not a uniform expression. There were certain regions of the TSA with reduced or loss of phospho Erk expression* ***(A and B)****. Age range of mice: 53-89 weeks; scale bars represent 200 μm (A) and 50 μm (B); magnification 10x (A) and 40x (B).*

6.3 DISCUSSION

The functional role of the *INK4a* genes – *p16INK4a* and *p14ARF* in colorectal cancer has been assessed in a number of other studies (Esteller *et al*, 2000; Lee *et al*, 2006). The present study aimed at understanding the effects of *p16INK4a* and *p14ARF* individually in combination with *BRAF* V600E mutation on the initiation and progression of CRC. *BRaf*^{CA} mice were crossed with mice homozygous and

heterozygous for *p16Ink4a* and *p19Arf* and treated with tamoxifen to induce *BRaf*^{VE} (*BRAF* V600E mutation).

Mice were sacrificed six weeks post tamoxifen treatment and assessed for hyperplastic changes – crypt and villus lengths in the colon and small intestine. In all the mice groups - the *BRaf*^{VE}*/p16* null, *BRaf*^{VE}*/p16* het, *BRaf*^{VE}*/p19* null and *BRaf*^{VE}*/p19* het, crypt and villus lengthening was observed in all the tamoxifen induced colon and small intestine samples compared to the controls. The results indicated that the absence of *p16Ink4a* or *p19Arf* did not have a significant effect on the hyperplastic changes observed in the *BRaf*^{VE} mice. The olive oil treated mice did not display increase in crypt and villus lengths in the *p16Ink4a* and *p19Arf* mice compared to the *BRaf*^{VE} mice.

These data support the finding that *BRaf* V600E mutation is a key player in initiating hyperplastic changes in these mice. *KRAS* mutation has been shown to exert a similar effect in mice in combination with *phosphatase and tensin homolog deleted on chromosome 10* (*PTEN*). Mice with inactivated *PTEN* did not display differences in crypt-villus height or increase in number of cells/hemi crypt. However, loss of *PTEN* and *KRAS* mutation resulted in an increase in number of cells/ hemi crypt (Byun *et al*, 2011; Davies *et al*, 2013).

Mice were monitored for development of lesions and a comparative analysis was done to determine the time taken for the development of lesions, the type and frequency of lesions and survival in the different mice groups. The common lesion observed in all the mice groups was traditional serrated adenoma (TSA) with low-grade or high-grade dysplasia. Some TSAs showed signs of early cancer or gave rise to moderately or poorly differentiated adenocarcinomas. A significant difference was observed in the number of mice with TSAs between the different mice groups (P = 0.0393).

In the *BRaf*^{VE}*/p16* mice, a majority of the tamoxifen treated mice developed TSAs after 70 weeks of age. TSA incidence was the highest in the *BRaf*^{VE}*/p16* group with 14 of 43 mice (32.6%) compared to the other mice groups. In the *BRaf*^{VE}*/p16* null group, mice older than 73 weeks developed multiple TSAs, while adenocarcinomas were observed in *BRaf*^{VE}*/p16* het mice older than 72 weeks. In contrast, no TSAs were observed in the *BRaf*^{VE}*/p19* null group and adenocarcinomas

were observed in mice as early as 11.71 weeks. However, the *BRaf*^{VE}/*p19* het group had mice with multiple TSAs and they were older than 80 weeks; while the youngest was 55.14 weeks. The time taken for the development of TSAs in the *BRaf*^{VE} mice was longer than the other mouse groups - >85.57 weeks and mice older than 103 weeks developed adenocarcinomas.

In the Carragher *et al* study, *Braf*$^{+/LSLV600E}$*;AhcreER*$^{T+/0}$ mice crossed with a *Cdkn2a*$^{\Delta Ex2,3/\Delta Ex2,3}$ *(p16INK4a* locus knockout i.e. combined *p16Ink4a* and *p19Arf)* did not survive beyond 6 weeks post induction due to the rapid development of aggressive tumours in a range of other organs (Carragher *et al*, 2010). A recent study showed that mice with loss of *p16Ink4a* and *BRAF* V600E mutation developed intestinal hyperplastic polyps as early as 14 weeks. In the same group of mice, the number of TSAs also rapidly increased after 43 weeks, while a significant increase in the number of macroscopic tumours was observed after 43 weeks in the *BRAF* mutant mice with absence of *p16Ink4a* compared to mice with only *BRAF* mutation (Rad *et al*, 2013). The *BRAF* mutant mice displayed a more aggressive tumour phenotype than the mice used in our study. This could be due to the effect of Cre recombinase, which in turn affects the *BRAF* mutant activity and increases the time taken for the development of TSAs and their frequency.

Loss of *PTEN* and *KRAS* mutation in mice gave rise to a range of lesions from hyperplastic polyps to metastatic colorectal cancers within 71 weeks (Davies *et al*, 2013). In another study, *PTEN* inactivation alone causes mice to develop invasive cancers in the small intestine at 52 weeks (Byun *et al*, 2011). In our study, many of the *p16Ink4a* and *p19Arf* mice developed tumours in other organs and the mice had to be sacrificed at an earlier age. This was similar to the Carragher *et al* study in which the combined knockout of *p16Ink4a* and *p19Arf* reduced the survival of the mice to six weeks (Carragher *et al*, 2010). However, the mouse model employed to study the effect of *PTEN* loss in CRC was deleted only in the intestine and this allowed for a better understanding of the progression of CRC up to 71 weeks (Byun *et al*, 2011).

The ubiquitous loss of *p16Ink4a* and *p19Arf* also affected survival of the mice in our study due to the development of spontaneous tumours. Some of the frequently observed tumours were hepatic adenomas, hepatocellular carcinomas, lung adenocarcinomas, angiosarcomas and histiocytic sarcomas. These tumours were

similar to those observed in the study by Sharpless and colleagues; lung carcinomas, angiosarcomas and histiocytic lymphomas were identified in the *p19Arf* null mice and *p16Ink4a* null mice (Sharpless *et al*, 2004). The $BRaf^{VE}$ mice survived up to 97 weeks, while the $BRaf^{VE}$/*p16* null, $BRaf^{VE}$/*p16* het and $BRaf^{VE}$/*p19* het survived up to 82 weeks. The $BRaf^{VE}$/*p19* null mice exhibited the worst survival rate with 67 weeks due to a more aggressive tumour phenotype in other organs such as lungs and liver. The control mice – *p16Ink4a* null and *p19Arf* null mice survived only up to 78 weeks and 73 weeks respectively. The survival rates were lower than the *p16Ink4a* null and *p19Arf* null mice monitored in a study by Sharpless *et al*. The tumour-free survival rates were up to 90 weeks and 100 weeks for *p19Arf* null mice and *p16Ink4a* null mice respectively (Sharpless *et al*, 2004).

The traditional serrated adenomas obtained were assessed for activation of the Wnt pathway (β-catenin expression), and the Mapk pathway (total Erk and phospho Erk expression). The Wnt pathway was activated in a majority of the TSAs with high-grade dysplasia, TSAs with invasive carcinomas and adenocarcinomas based on the nuclear accumulation of β-catenin. This was consistent with the different mice groups and the inactivation of *p16Ink4a* and *p19Arf* did not increase the nuclear expression of β-catenin significantly. These results support similar observations by Carragher *et al* and Rad *et al* in their *BRAF* mutant mice (Carragher *et al*, 2010; Rad *et al*, 2013).

The expression of total Erk and phospho Erk expression in $BRaf^{VE}$ mice demonstrated the activation of the Mapk pathway in the TSAs and adenocarcinomas observed in our study. In the case of total Erk expression, increased nuclear expression was observed in TSAs with high-grade dysplasia, areas of invasive carcinoma and adenocarcinomas. However, there was a deviation from this expression pattern in mice with multiple TSAs in which a loss of total Erk expression was observed in certain regions of the TSAs and adenocarcinomas. Phospho Erk expression pattern was different in the normal mucosa (positive stained cells at the base of the crypts) compared to regions with high-grade dysplastic TSAs and adenocarcinomas (positive nuclear staining) and this was similar to other studies (Carragher *et al*, 2010; Rad *et al*, 2013).

The *Braf* V600E mutation and its interaction with the cell cycle regulators – *p16Ink4a* and *p19Arf* helped to understand the contribution of each gene in colorectal

tumorigenesis. The development of TSAs due to *Braf* V600E mutation and/or the inactivation of either *p16Ink4a* or *p19Arf* emphasize their role in the serrated pathway. The tumorigenic effect of *p16Ink4a* or *p19Arf* loss increased the development of lesions via the serrated pathway and also affected the overall survival rates of the different groups of mice and these results confirmed the role of *p16Ink4a* with *BRAF* V600E mutation in CRC based on human studies.

CHAPTER 7

FINAL DISCUSSION AND FUTURE DIRECTIONS

7. FINAL DISCUSSION AND FUTURE DIRECTIONS

Colorectal tumours are classified as conventional or serrated adenocarcinomas depending on the type of polyp, their molecular features and the pathway by which they develop. Serrated adenocarcinomas arise from serrated polyps via the serrated neoplastic pathway; are proximally located; and significantly associated with *BRAF* V600E mutations and MSI-H (Garcia-Solano *et al*, 2012; Garcia-Solano *et al*, 2010). The serrated pathway was more recently described and a number of studies have been conducted to investigate the molecular alterations associated with this pathway. This has involved assessment of *BRAF*, *KRAS* mutations and methylation status in the precursor lesions of the serrated pathway – serrated polyps (Chan *et al*, 2003; Kambara *et al*, 2004; Lee *et al*, 2005; Yang *et al*, 2004)

DNA promoter hypermethylation plays an important role in the serrated pathway and involves the epigenetic silencing of important genes such as *p16*, *MGMT* and *MLH1* (Dong *et al*, 2005; Herman *et al*, 1995; Kane *et al*, 1997). Toyota *et al* (1999) identified two types of methylation in CRC – aging-specific methylation or type A and cancer-specific methylation or type C. High levels of type C methylation in three or more loci were observed in colorectal tumours and this was linked to the transcriptional silencing of specific genes associated with colorectal cancer. This phenomenon was defined as the CpG island methylator phenotype or CIMP (Toyota *et al*, 1999). In sporadic CRC, CIMP is significantly associated with *BRAF* and MSI-H and inversely associated with chromosomal instability (Goel *et al*, 2007; Kambara *et al*, 2004; Toyota *et al*, 2000; Weisenberger *et al*, 2006). CIMP has been evaluated in serrated polyps using the Issa *et al* and Weisenberger *et al* panels of methylation markers (Toyota *et al*, 1999; Weisenberger *et al*, 2006). However, a majority of these studies did not include all the different serrated polyp types; were retrospective and had small sample numbers (Burnett-Hartman *et al*, 2013; Dhir *et al*, 2011; Gaiser *et al*, 2013; Maeda *et al*, 2011; O'Brien *et al*, 2004; Vaughn *et al*, 2010).

The first part of my research study involved evaluating the CIMP status in serrated polyps and its association with factors such as *BRAF* and *KRAS* mutations, methylation of *MLH1*, *p16* and *IGFBP7*, polyp location, size and gender. CIMP was found to be associated with serrated polyp type (especially SSAs), *BRAF* mutation, proximal location and methylation of *MLH1*, *p16* and *IGFBP7*. This is one of the first

prospective studies, which involved methylation analysis on all the serrated polyp subtypes.

Our study divided the polyps into CIMP-H (3 or more methylated markers out of five) and CIMP-0 (0 to 2 methylated markers out of five). A third group was proposed by Ogino and colleagues called CIMP-low in which colorectal tumours were methylated in one to three markers (out of five markers). However, there was an overlap between CIMP-0 (no methylation in any of the five markers) and CIMP-low colorectal tumours (methylation in 1 to two markers out of five) (Ogino *et al*, 2006). Further analysis revealed 18q loss of heterozygosity as a molecular factor which potentially distinguished the CIMP-0 group from the CIMP-low samples (Ogino *et al*, 2007). A recent study using MassARRAY identified three methylation clusters in colorectal tumours– high-, intermediate- and low-methylation epigenotypes. Each epigenotype could also be differentiated based on its association with other factors. A majority of the tumours with high methylation epigenotype (HME) were proximally located, *BRAF* mutant, MSI-H and *KRAS* wild. The intermediate- (IME) and low-methylation epigenotypes (LME), which differed based on their *KRAS* status – 63% and 26% respectively were mainly distal, *BRAF* wild and MSS (Yagi *et al*, 2010). Based on further analysis, these methylation clusters were grouped into CIMP-H (HME cluster), CIMP-low (LME cluster) and CIMP-0 (IME cluster) (Karpinski *et al*, 2013).

The concept of CIMP-low was not defined or analysed in our study and based on previous reports, the polyps could be reclassified as CIMP-H, CIMP-low and CIMP-0. The investigation of CIMP-low with the various molecular alterations such as *BRAF* V600E and *KRAS* mutations; and methylation of *MLH1*, *p16* and *IGFBP7* might be worthwhile as part of future studies. This would possibly provide additional understanding of polyps with low levels of promoter methylation and their role in the serrated pathway.

In order to study the role of *BRAF* V600E mutation in the initiation and development of CRC via the serrated neoplastic pathway, I utilized a $BRaf^{CA}$ mouse model to gain insights into this process. The original $BRaf^{CA}$ mouse was developed by Dankort *et al* to study the effect of oncogenic *BRAF* V600E mutations in the development of lung tumours (Dankort *et al*, 2007). In my study, this $BRaf^{CA}$ mouse

was crossed with the *A33CreERT2* mouse to enable the tissue-specific induction of $BRaf^{VE}$ allele by tamoxifen. Oncogenic *Braf* V600E mutation resulted in hyperplastic changes in the normal mucosa and the development of traditional serrated adenomas (TSA) like polyps and adenocarcinomas. The TSA like polyps and tumours were observed only in the duodenum and jejunum regions of the small intestine of the tamoxifen-treated mice.

During the course of my studies a number of other publications have now described the effect of *BRAF* V600E mutation in the gastrointestinal tract of the mouse. The study by Carragher and colleagues (2010) using $Braf^{+/LSL\text{-}V600E}/AhcreER^{T+/0}$ mice demonstrated a very aggressive effect of *Braf* V600E mutation which resulted in the mice surviving only up to 20 weeks post treatment. This was due to the extracolonic tumours, which developed in the lungs and stomach as a result of expression of oncogenic *Braf* V600E outside of the gastrointestinal tract. Due to the short survival of these mice, it was difficult to assess the initiation, development and progression of *Braf* V600E induced tumours in the gastrointestinal tract (Carragher *et al*, 2010). The $BRaf^{VE}$ /$A33CreERT2^{+/-}$ mouse model used in my study expressed oncogenic *Braf* V600E at low levels in the GI tract, without the additional expression in other organs, and therefore more amenable to studying tumorigenesis over a longer timeframe, which is more similar to CRC development in humans. However, the time taken to develop a tumour phenotype in these mice was longer than initially expected.

Recently another *BRAF* mouse model (*Vil-Cre*/$Braf^{LSL\text{-}V637E/+}$) has been described (Rad *et al*, 2013). The *Vil-Cre*/$Braf^{LSL\text{-}V637E/+}$ mice used in the Rad *et al* study developed lesions earlier (>21 weeks) than the $BRaf^{VE}$/*A33CreERT2* mice used in my study (>85 weeks) (Rad *et al*, 2013). A disadvantage of the long latency before the development of gastrointestinal tumours was that age-related tumours and other pathologies also begin to develop. In future studies, the $BRaf^{CA}$ mice could be crossed with another gastrointestinal tissue-specific Cre mouse such as *Villin-Cre* to evaluate the onset of lesions and their progression to adenocarcinomas (Rad *et al*, 2013).

Methylation analysis was performed on duodenum samples from tamoxifen and olive oil treated mice (six weeks post treatment). Methyl PCR arrays were used to assess methylation using a 94-gene panel specific for colon cancer. Only ten genes were methylated in one or more of the tamoxifen treated samples relative to olive oil

treated control samples. This low number of methylated genes indicated that early hyperplasia (6 weeks) has little or no effect on developing a more methylating epithelial phenotype. However, hyperplasia sustained over a longer period may lead to increased methylation. Experiments would need to be performed to determine if this was the case. In addition, methylation profiling of the TSA like polyps and adenocarcinomas would be worthwhile to perform in the future, as it is likely that more extensive methylation changes will occur. Another alternative for understanding the effect of methylation would be to assess the tumour formation in compound *BRaf*$^{VE/+}$*/A33CreERT2*$^{+/-}$/*Rosa*M2-rtTA$^{+/-}$/*Dnmt3b-tg* mice. These mice over-express inducible *de novo* Dnmt3b and could be used for longitudinal studies to monitor tumour phenotype.

The cell cycle regulator genes, *p16INK4a* and *p14ARF* (*p19Arf* in mouse) have been implicated in colorectal tumorigenesis and their individual interaction with *BRAF* V600E mutation was also assessed (Lee *et al*, 2006). The close association of *p16INK4a* methylation with human serrated polyps observed in my study also revealed its importance in the serrated pathway. Hyperplasia studies were performed on tamoxifen treated and olive oil treated (controls) mice (six weeks post treatment). Similar to the *BRaf*^{VE} mice, lengthening of crypt and villus was observed in the colon and small intestine of tamoxifen treated mice - *BRaf*^{VE}*/p16Ink4a* and *BRaf*^{VE}*/p19Arf*.

TSA like polyps and adenocarcinomas were observed in both mouse groups, except for the *BRaf*^{VE}*/p19Arf* null group. In the *BRaf*^{VE}*/p16Ink4a* group and *BRaf*^{VE}*/p19Arf* het group, multiple TSA like polyps with high-grade dysplasia were observed in mice older than 70 weeks and 80 weeks respectively. There was a significant difference in TSA incidence between the mice groups, with the highest frequency of TSAs observed in the *BRaf*^{VE}*/p16Ink4a* mice. This showed that the interaction of *p16Ink4a* with *Braf* mutation contributed to an increase in the development of TSAs. Mice in all the groups developed more extracolonic tumours than the *BRaf*^{VE} mice due to the ubiquitous loss of *p16Ink4a* or *p19Arf*. This reduced the survival of *BRaf*^{VE}*/p16Ink4a* and *BRaf*^{VE}*/p19Arf* mice considerably compared to the *BRaf*^{VE} mice.

The combined knockout of *p16Ink4a* and *p19Arf* reduced the survival rate of mice drastically to only six weeks post induction. This would not be effective in

studying the gradual progression of colorectal cancer from precursor lesions (Carragher *et al*, 2010). The mouse model used in our study assessed the individual contribution of *p16Ink4a* and *p19Arf* in the development of serrated polyps. However, the rapid development of extracolonic tumours in a majority of the mice (especially the *BRaf*^{VE}/*p19Arf* null group) in organs such as liver, lung and spleen did not allow the mice to be monitored for an extended period. A more suitable alternative would be to utilize tissue-specific, inducible *p16Ink4a* and *p19Arf* mouse models such as TetOp16 (developed by Dr. Greg Enders, Fox Chase Cancer Center) and TRE-shARF_157 respectively. These mice could be crossed with mice carrying the reverse tetracycline-controlled transactivator (rtTA) transgenes in the tissue of interest. Methylation analysis using Methyl PCR arrays could also be performed to assess the level of methylation in the TSA like polyps and adenocarcinomas as compared with the methylation status of *BRaf*^{VE} mice.

The methylation status of *IGFBP7* was evaluated in colorectal polyps and tumours. It was identified as a potential senescence marker involved in *BRAF* V600E-mediated senescence pathway (Wajapeyee *et al*, 2008). Carragher *et al* observed the induction of senescence markers such as senescence-associated-β-galactosidase and p16Ink4a expression in *BRAF* mutated crypts of mice (Carragher *et al*, 2010). Another aspect of our mouse study which was planned (but not completed due to lack of time) and will need to be followed up as part of future work is the assessment of senescence markers such as senescence-associated-β-galactosidase (SA-β-gal), senescence-associated heterochromatin foci (SAHF) and Dec-1 expression in the *BRaf*^{VE}, *BRaf*^{VE}/*p16Ink4a* and *BRaf*^{VE}/*p19Arf* mice (Di Micco *et al*, 2011; Dimri *et al*, 1995; Qian *et al*, 2008).

Serrated polyps with *BRAF* mutations along with inactivation of genes such as *p16INK4a* due to hypermethylation could result in oncogene-induced senescence (OIS). Figure 7.1 is a proposed senescence pathway for serrated polyps with *BRAF* mutations. The loss of tumour suppressor genes decides the fate of colorectal polyps – will they enter the pathway to senescence or overcome the senescence barrier and progress to serrated carcinoma? Investigating these molecular pathways will provide an insight into the evasion of OIS by some colorectal polyps (serrated) and their further development into *BRAF* mutant, CIMP-H CRC.

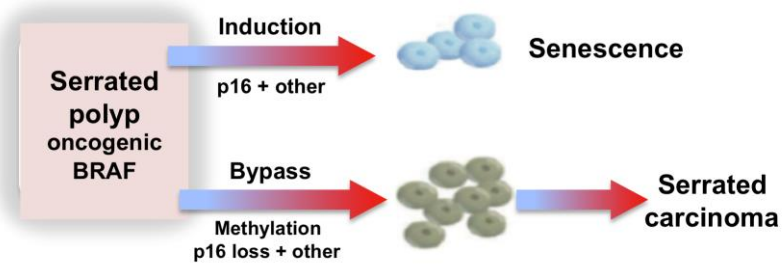

Figure 7.1 - Induction and bypass of senescence pathways implicated in serrated neoplasia. *This is a proposed senescence pathway for serrated polyps with oncogenic BRAF. Activation of genes such as p16INK4a, p14ARF and p53 via their respective pathways could result in cellular senescence. On the other hand, loss of key tumour suppressor genes such as p16INK4a due to promoter hypermethylation results in gene silencing. This would cause the serrated polyps with activating BRAF mutations to evade this senescence pathway and progress to serrated carcinoma.*

The present study aimed at gaining a better insight into the molecular characterization of the serrated pathway using human colorectal polyps and tumours and mouse models. The first part of the study evaluated the CIMP status and methylation of specific genes in different serrated polyp types and correlated this with other molecular and clinical variables. CIMP was associated with serrated polyp type (especially SSAs), *BRAF* V600E mutations, proximal location, methylation of *MLH1*, *p16* and *IGFBP7*.

In order to analyse the role of *Braf* V600E mutation, a tissue-specific, inducible *BRaf*^{CA} mouse model was employed to monitor initiation of hyperplasia, development of serrated polyps and its progression to CRC. The interaction of *BRAF* V600E mutation with cell cycle regulator genes was also assessed using mice with loss of *p16Ink4a* or *p19Arf* genes. The results observed were hyperplastic changes, development of serrated lesions (TSA like polyps) and adenocarcinomas in the small intestine. This shows that *BRAF* V600E mutation along with *p16Ink4a* and *p19Arf* contribute to colorectal tumorigenesis via the serrated pathway.

The hypothesis being tested was to determine if oncogenic *BRAF* V600E mutation, combined with CIMP associated epigenetic silencing of *p16INK4a* and *IGFBP7* resulted in the initiation and progression of large proximally located serrated

polyps. Based on the human polyp study, a significant association was observed between *BRAF* V600E mutation, CIMP, methylation of *p16INK4a* and *IGFBP7*, proximal location and large serrated polyps and therefore supports the hypothesis. Further, with the *Braf* mouse model the only intestinal lesions found in the mice were TSAs and were associated with loss of *p16Ink4a* and *p19Arf*. Additional analysis of these TSAs will need to be performed to determine the association of CIMP and loss of *IGFBP7* in the development of serrated lesions in the *Braf* mutant mice.

The role played by *BRAF* V600E mutation and its interaction with *p16INK4a* and *p19ARF* in colorectal tumorigenesis is of great importance in studying the serrated pathway. This study highlights the capacity of *BRAF* alone in driving the initiating of dysplastic lesions and the possibly progression to adenocarcinoma. Screening patients for *BRAF* V600E mutations could provide a platform for determining patients' responses to different molecular therapies. The development of a Braf mouse model has important translational implications as potentially this model could be used to test tumour responses to novel drug combinations in the pre-clinical setting that could then inform human clinical trials for colorectal cancers that develop along the serrated pathway. Currently, a study is in progress at the Memorial Sloan-Kettering Cancer Center, USA to test a combination of the drugs panitumumab and vemurafenib on patients with metatstatic *BRAF* mutant colorectal tumours. An extensive understanding of the association between *BRAF* mutation and methylation of key genes could help explore the unknown aspects of the serrated pathway and possibly reduce the incidence and mortality of CRC.

8. REFERENCES

Aaltonen LA, Peltomaki P, Leach FS, Sistonen P, Pylkkanen L, Mecklin JP, Jarvinen H, Powell SM, Jen J, Hamilton SR et al (1993) Clues to the pathogenesis of familial colorectal cancer. Science 260**:** 812-816

Aaltonen LA, Peltomaki P, Mecklin JP, Jarvinen H, Jass JR, Green JS, Lynch HT, Watson P, Tallqvist G, Juhola M et al (1994) Replication errors in benign and malignant tumors from hereditary nonpolyposis colorectal cancer patients. Cancer Res 54**:** 1645-1648

Agger K, Cloos PA, Rudkjaer L, Williams K, Andersen G, Christensen J, Helin K (2009) The H3K27me3 demethylase JMJD3 contributes to the activation of the INK4A-ARF locus in response to oncogene- and stress-induced senescence. Genes Dev 23**:** 1171-1176

Ahlquist T, Lind GE, Costa VL, Meling GI, Vatn M, Hoff GS, Rognum TO, Skotheim RI, Thiis-Evensen E, Lothe RA (2008) Gene methylation profiles of normal mucosa, and benign and malignant colorectal tumors identify early onset markers. Mol Cancer 7**:** 94

AIHW, AACR (2012) Cancer in Australia: an overview, 2012
Cancer series No. 74

Al-Tassan N, Chmiel NH, Maynard J, Fleming N, Livingston AL, Williams GT, Hodges AK, Davies DR, David SS, Sampson JR et al (2002) Inherited variants of MYH associated with somatic G:C-->T:A mutations in colorectal tumors. Nat Genet 30**:** 227-232

Aust DE, Baretton GB (2010) Serrated polyps of the colon and rectum (hyperplastic polyps, sessile serrated adenomas, traditional serrated adenomas, and mixed polyps)-proposal for diagnostic criteria. Virchows Arch 457**:** 291-297

Baker K, Zhang Y, Jin C, Jass JR (2004) Proximal versus distal hyperplastic polyps of the colorectum: different lesions or a biological spectrum? J Clin Pathol 57**:** 1089-1093

Barault L, Charon-Barra C, Jooste V, de la Vega MF, Martin L, Roignot P, Rat P, Bouvier AM, Laurent-Puig P, Faivre J et al (2008) Hypermethylator phenotype in sporadic colon cancer: study on a population-based series of 582 cases. Cancer Res 68**:** 8541-8546

Bardeesy N, Aguirre AJ, Chu GC, Cheng KH, Lopez LV, Hezel AF, Feng B, Brennan C, Weissleder R, Mahmood U et al (2006) Both p16(Ink4a) and the p19(Arf)-p53 pathway constrain progression of pancreatic adenocarcinoma in the mouse. Proc Natl Acad Sci U S A 103**:** 5947-5952

Bariol C, Hawkins NJ, Turner JJ, Meagher AP, Williams DB, Ward RL (2003) Histopathological and clinical evaluation of serrated adenomas of the colon and rectum. Mod Pathol 16**:** 417-423

Barradas M, Anderton E, Acosta JC, Li S, Banito A, Rodriguez-Niedenfuhr M, Maertens G, Banck M, Zhou MM, Walsh MJ et al (2009) Histone demethylase JMJD3 contributes to epigenetic control of INK4a/ARF by oncogenic RAS. Genes Dev 23**:** 1177-1182

Barry EL, Baron JA, Grau MV, Wallace K, Haile RW (2006) K-ras mutations in incident sporadic colorectal adenomas. Cancer 106**:** 1036-1040

Beach R, Chan AO, Wu TT, White JA, Morris JS, Lunagomez S, Broaddus RR, Issa JP, Hamilton SR, Rashid A (2005) BRAF mutations in aberrant crypt foci and hyperplastic polyposis. Am J Pathol 166**:** 1069-1075

Behrens J (2005) The role of the Wnt signalling pathway in colorectal tumorigenesis. Biochem Soc Trans 33**:** 672-675

Bennecke M, Kriegl L, Bajbouj M, Retzlaff K, Robine S, Jung A, Arkan MC, Kirchner T, Greten FR (2010) Ink4a/Arf and oncogene-induced senescence prevent tumor progression during alternative colorectal tumorigenesis. Cancer Cell 18**:** 135-146

Bettington M, Walker N, Clouston A, Brown I, Leggett B, Whitehall V (2013) The serrated pathway to colorectal carcinoma: current concepts and challenges. Histopathology 62**:** 367-386

Bird AP (1986) CpG-rich islands and the function of DNA methylation. Nature 321**:** 209-213

Bird RP (1987) Observation and quantification of aberrant crypts in the murine colon treated with a colon carcinogen: preliminary findings. Cancer Lett 37**:** 147-151

Bocker T, Diermann J, Friedl W, Gebert J, Holinski-Feder E, Karner-Hanusch J, von Knebel-Doeberitz M, Koelble K, Moeslein G, Schackert HK et al (1997) Microsatellite instability analysis: a multicenter study for reliability and quality control. Cancer Res 57**:** 4739-4743

Bodmer WF, Bailey CJ, Bodmer J, Bussey HJ, Ellis A, Gorman P, Lucibello FC, Murday VA, Rider SH, Scambler P et al (1987) Localization of the gene for familial adenomatous polyposis on chromosome 5. Nature 328**:** 614-616

Boland CR, Thibodeau SN, Hamilton SR, Sidransky D, Eshleman JR, Burt RW, Meltzer SJ, Rodriguez-Bigas MA, Fodde R, Ranzani GN et al (1998) A National Cancer Institute Workshop on Microsatellite Instability for cancer detection and familial predisposition: development of international criteria for the determination of microsatellite instability in colorectal cancer. Cancer Res 58**:** 5248-5257

Bond CE, Umapathy A, Ramsnes I, Greco SA, Zhen Zhao Z, Mallitt KA, Buttenshaw RL, Montgomery GW, Leggett BA, Whitehall VL (2012) p53 mutation is common in microsatellite stable, BRAF mutant colorectal cancers. Int J Cancer 130**:** 1567-1576

Bosman FT (2010) WHO classification of tumours of the digestive system. Lyon: International Agency for Research on Cancer

Burcin MM, O'Malley BW, Tsai SY (1998) A regulatory system for target gene expression. Front Biosci 3**:** c1-7

Burnett-Hartman AN, Newcomb PA, Potter JD, Passarelli MN, Phipps AI, Wurscher MA, Grady WM, Zhu LC, Upton MP, Makar KW (2013) Genomic aberrations occurring in subsets of serrated colorectal lesions but not conventional adenomas. Cancer Res 73**:** 2863-2872

Burri N, Shaw P, Bouzourene H, Sordat I, Sordat B, Gillet M, Schorderet D, Bosman FT, Chaubert P (2001) Methylation silencing and mutations of the p14ARF and p16INK4a genes in colon cancer. Lab Invest 81**:** 217-229

Byun DS, Ahmed N, Nasser S, Shin J, Al-Obaidi S, Goel S, Corner GA, Wilson AJ, Flanagan DJ, Williams DS et al (2011) Intestinal epithelial-specific PTEN inactivation results in tumor formation. Am J Physiol Gastrointest Liver Physiol 301**:** G856-864

Carragher LA, Snell KR, Giblett SM, Aldridge VS, Patel B, Cook SJ, Winton DJ, Marais R, Pritchard CA (2010) V600EBraf induces gastrointestinal crypt senescence and promotes tumour progression through enhanced CpG methylation of p16INK4a. EMBO Mol Med 2**:** 458-471

Chan AO, Broaddus RR, Houlihan PS, Issa JP, Hamilton SR, Rashid A (2002) CpG island methylation in aberrant crypt foci of the colorectum. Am J Pathol 160**:** 1823-1830

Chan TL, Zhao W, Leung SY, Yuen ST (2003) BRAF and KRAS mutations in colorectal hyperplastic polyps and serrated adenomas. Cancer Res 63**:** 4878-4881

Chung SM, Chen YT, Panczykowski A, Schamberg N, Klimstra DS, Yantiss RK (2008) Serrated polyps with "intermediate features" of sessile serrated polyp and microvesicular hyperplastic polyp: a practical approach to the classification of nondysplastic serrated polyps. Am J Surg Pathol 32**:** 407-412

Cooper HS, Patchefsky AS, Marks G (1979) Adenomatous and carcinomatous changes within hyperplastic colonic epithelium. Dis Colon Rectum 22**:** 152-156

Crespo P, Xu N, Simonds WF, Gutkind JS (1994) Ras-dependent activation of MAP kinase pathway mediated by G-protein beta gamma subunits. Nature 369**:** 418-420

Cunningham KS, Riddell RH (2006) Serrated mucosal lesions of the colorectum. Curr Opin Gastroenterol 22**:** 48-53

Dankort D, Curley DP, Cartlidge RA, Nelson B, Karnezis AN, Damsky WE, Jr., You MJ, DePinho RA, McMahon M, Bosenberg M (2009) Braf(V600E) cooperates with Pten loss to induce metastatic melanoma. Nat Genet 41**:** 544-552

Dankort D, Filenova E, Collado M, Serrano M, Jones K, McMahon M (2007) A new mouse model to explore the initiation, progression, and therapy of BRAFV600E-induced lung tumors. Genes Dev 21**:** 379-384

Das P, Jain D, Vaiphei K, Wig JD (2008) Abberant crypt foci -- importance in colorectal carcinogenesis and expression of p53 and mdm2: a changing concept. Dig Dis Sci 53**:** 2183-2188

Daum G, Eisenmann-Tappe I, Fries HW, Troppmair J, Rapp UR (1994) The ins and outs of Raf kinases. Trends Biochem Sci 19**:** 474-480

Davies EJ, Marsh Durban V, Meniel V, Williams GT, Clarke AR (2013) PTEN loss and KRAS activation leads to the formation of serrated adenomas and metastatic carcinoma in the mouse intestine. J Pathol

Davies H, Bignell GR, Cox C, Stephens P, Edkins S, Clegg S, Teague J, Woffendin H, Garnett MJ, Bottomley W et al (2002) Mutations of the BRAF gene in human cancer. Nature 417**:** 949-954

de la Chapelle A (2004) Genetic predisposition to colorectal cancer. Nat Rev Cancer 4**:** 769-780

Deng G, Bell I, Crawley S, Gum J, Terdiman JP, Allen BA, Truta B, Sleisenger MH, Kim YS (2004) BRAF mutation is frequently present in sporadic colorectal cancer with methylated hMLH1, but not in hereditary nonpolyposis colorectal cancer. Clin Cancer Res 10**:** 191-195

Dhir M, Yachida S, Van Neste L, Glockner SC, Jeschke J, Pappou EP, Montgomery EA, Herman JG, Baylin SB, Iacobuzio-Donahue C et al (2011) Sessile serrated adenomas and classical adenomas: an epigenetic perspective on premalignant neoplastic lesions of the gastrointestinal tract. Int J Cancer 129**:** 1889-1898

Dhomen N, Da Rocha Dias S, Hayward R, Ogilvie L, Hedley D, Delmas V, McCarthy A, Henderson D, Springer CJ, Pritchard C et al (2010) Inducible expression of (V600E) Braf using tyrosinase-driven Cre recombinase results in embryonic lethality. Pigment Cell Melanoma Res 23**:** 112-120

Di Micco R, Sulli G, Dobreva M, Liontos M, Botrugno OA, Gargiulo G, Dal Zuffo R, Matti V, d'Ario G, Montani E et al (2011) Interplay between oncogene-induced DNA damage response and heterochromatin in senescence and cancer. Nat Cell Biol 13**:** 292-302

Dietmaier W, Wallinger S, Bocker T, Kullmann F, Fishel R, Ruschoff J (1997) Diagnostic microsatellite instability: definition and correlation with mismatch repair protein expression. Cancer Res 57**:** 4749-4756

Dimri GP, Lee X, Basile G, Acosta M, Scott G, Roskelley C, Medrano EE, Linskens M, Rubelj I, Pereira-Smith O et al (1995) A biomarker that identifies senescent human cells in culture and in aging skin in vivo. Proc Natl Acad Sci U S A 92**:** 9363-9367

Dong SM, Lee EJ, Jeon ES, Park CK, Kim KM (2005) Progressive methylation during the serrated neoplasia pathway of the colorectum. Mod Pathol 18**:** 170-178

Drahovsky D, Boehm TL (1980) Enzymatic DNA methylation in higher eukaryotes. Int J Biochem 12**:** 523-528

Eads CA, Danenberg KD, Kawakami K, Saltz LB, Blake C, Shibata D, Danenberg PV, Laird PW (2000) MethyLight: a high-throughput assay to measure DNA methylation. Nucleic Acids Res 28**:** E32

Esteller M, Tortola S, Toyota M, Capella G, Peinado MA, Baylin SB, Herman JG (2000) Hypermethylation-associated inactivation of p14(ARF) is independent of p16(INK4a) methylation and p53 mutational status. Cancer Res 60**:** 129-133

Estrada RG, Spjut HJ (1980) Hyperplastic polyps of the large bowel. Am J Surg Pathol 4**:** 127-133

Fang JY, Richardson BC (2005) The MAPK signalling pathways and colorectal cancer. Lancet Oncol 6**:** 322-327

Farris AB, Misdraji J, Srivastava A, Muzikansky A, Deshpande V, Lauwers GY, Mino-Kenudson M (2008) Sessile serrated adenoma: challenging discrimination from other serrated colonic polyps. Am J Surg Pathol 32**:** 30-35

Fatemi M, Hermann A, Gowher H, Jeltsch A (2002) Dnmt3a and Dnmt1 functionally cooperate during de novo methylation of DNA. Eur J Biochem 269**:** 4981-4984

Fearon ER, Vogelstein B (1990) A genetic model for colorectal tumorigenesis. Cell 61**:** 759-767

Feil R, Wagner J, Metzger D, Chambon P (1997) Regulation of Cre recombinase activity by mutated estrogen receptor ligand-binding domains. Biochem Biophys Res Commun 237**:** 752-757

Fenoglio-Preiser CM, Hutter RV (1985) Colorectal polyps: pathologic diagnosis and clinical significance. CA Cancer J Clin 35**:** 322-344

Fenoglio CM, Lane N (1974) The anatomical precursor of colorectal carcinoma. Cancer 34**:** suppl:819-823

Fishel R, Lescoe MK, Rao MR, Copeland NG, Jenkins NA, Garber J, Kane M, Kolodner R (1993) The human mutator gene homolog MSH2 and its association with hereditary nonpolyposis colon cancer. Cell 75**:** 1027-1038

Fogt F, Brien T, Brown CA, Hartmann CJ, Zimmerman RL, Odze RD (2002) Genetic alterations in serrated adenomas: comparison to conventional adenomas and hyperplastic polyps. Hum Pathol 33**:** 87-91

Fransen K, Klintenas M, Osterstrom A, Dimberg J, Monstein HJ, Soderkvist P (2004) Mutation analysis of the BRAF, ARAF and RAF-1 genes in human colorectal adenocarcinomas. Carcinogenesis 25**:** 527-533

Frazin G, Zamboni G, Scarpa A, Dina R, Iannucci A, Novelli P (1984) Hyperplastic (metaplastic) polyps of the colon. A histologic and histochemical study. Am J Surg Pathol 8**:** 687-698

Frommer M, McDonald LE, Millar DS, Collis CM, Watt F, Grigg GW, Molloy PL, Paul CL (1992) A genomic sequencing protocol that yields a positive display of 5-methylcytosine residues in individual DNA strands. Proc Natl Acad Sci U S A 89**:** 1827-1831

Fu B, Yachida S, Morgan R, Zhong Y, Montgomery EA, Iacobuzio-Donahue CA (2012) Clinicopathologic and genetic characterization of traditional serrated adenomas of the colon. Am J Clin Pathol 138**:** 356-366

Fujita K, Yamamoto H, Matsumoto T, Hirahashi M, Gushima M, Kishimoto J, Nishiyama K, Taguchi T, Yao T, Oda Y (2011) Sessile serrated adenoma with early neoplastic progression: a clinicopathologic and molecular study. Am J Surg Pathol 35**:** 295-304

Gaiser T, Meinhardt S, Hirsch D, Killian JK, Gaedcke J, Jo P, Ponsa I, Miro R, Ruschoff J, Seitz G et al (2013) Molecular patterns in the evolution of serrated lesion of the colorectum. Int J Cancer 132**:** 1800-1810

Garcia-Solano J, Conesa-Zamora P, Carbonell P, Trujillo-Santos J, Torres-Moreno DD, Pagan-Gomez I, Rodriguez-Braun E, Perez-Guillermo M (2012) Colorectal serrated adenocarcinoma shows a different profile of oncogene mutations, MSI status and DNA repair protein expression compared to conventional and sporadic MSI-H carcinomas. Int J Cancer 131**:** 1790-1799

Garcia-Solano J, Perez-Guillermo M, Conesa-Zamora P, Acosta-Ortega J, Trujillo-Santos J, Cerezuela-Fuentes P, Makinen MJ (2010) Clinicopathologic study of 85 colorectal serrated adenocarcinomas: further insights into the full recognition of a new subset of colorectal carcinoma. Hum Pathol 41**:** 1359-1368

Goel A, Arnold CN, Niedzwiecki D, Chang DK, Ricciardiello L, Carethers JM, Dowell JM, Wasserman L, Compton C, Mayer RJ et al (2003) Characterization of sporadic colon cancer by patterns of genomic instability. Cancer Res 63**:** 1608-1614

Goel A, Nagasaka T, Arnold CN, Inoue T, Hamilton C, Niedzwiecki D, Compton C, Mayer RJ, Goldberg R, Bertagnolli MM et al (2007) The CpG island methylator phenotype and chromosomal instability are inversely correlated in sporadic colorectal cancer. Gastroenterology 132**:** 127-138

Goldstein NS, Bhanot P, Odish E, Hunter S (2003) Hyperplastic-like colon polyps that preceded microsatellite-unstable adenocarcinomas. Am J Clin Pathol 119**:** 778-796

Griffioen G, Bosman FT, Verspaget HW, de Bruin PA, Biemond I, Lamers CB (1989) Mucin profiles and potential for malignancy of human colorectal adenomatous polyps. Cancer 63**:** 1587-1591

Groden J, Thliveris A, Samowitz W, Carlson M, Gelbert L, Albertsen H, Joslyn G, Stevens J, Spirio L, Robertson M et al (1991) Identification and characterization of the familial adenomatous polyposis coli gene. Cell 66**:** 589-600

Ha L, Ichikawa T, Anver M, Dickins R, Lowe S, Sharpless NE, Krimpenfort P, Depinho RA, Bennett DC, Sviderskaya EV et al (2007) ARF functions as a melanoma tumor suppressor by inducing p53-independent senescence. Proc Natl Acad Sci U S A 104**:** 10968-10973

Half E, Bercovich D, Rozen P (2009) Familial adenomatous polyposis. Orphanet J Rare Dis 4**:** 22

Han Y, Zhou ZY (2011) Clinical features and molecular alterations of traditional serrated adenoma in sporadic colorectal carcinogenesis. J Dig Dis 12**:** 193-198

Herman JG, Graff JR, Myohanen S, Nelkin BD, Baylin SB (1996) Methylation-specific PCR: a novel PCR assay for methylation status of CpG islands. Proc Natl Acad Sci U S A 93**:** 9821-9826

Herman JG, Merlo A, Mao L, Lapidus RG, Issa JP, Davidson NE, Sidransky D, Baylin SB (1995) Inactivation of the CDKN2/p16/MTS1 gene is frequently associated with aberrant DNA methylation in all common human cancers. Cancer Res 55**:** 4525-4530

Hermann A, Goyal R, Jeltsch A (2004) The Dnmt1 DNA-(cytosine-C5)-methyltransferase methylates DNA processively with high preference for hemimethylated target sites. J Biol Chem 279**:** 48350-48359

Higuchi T, Sugihara K, Jass JR (2005) Demographic and pathological characteristics of serrated polyps of colorectum. Histopathology 47**:** 32-40

Hill MJ, Morson BC, Bussey HJ (1978) Aetiology of adenoma--carcinoma sequence in large bowel. Lancet 1**:** 245-247

Hinoue T, Weisenberger DJ, Pan F, Campan M, Kim M, Young J, Whitehall VL, Leggett BA, Laird PW (2009) Analysis of the association between CIMP and BRAF in colorectal cancer by DNA methylation profiling. PLoS One 4**:** e8357

Hirai H, Roussel MF, Kato JY, Ashmun RA, Sherr CJ (1995) Novel INK4 proteins, p19 and p18, are specific inhibitors of the cyclin D-dependent kinases CDK4 and CDK6. Mol Cell Biol 15**:** 2672-2681

Hsu DW, Lin MJ, Lee TL, Wen SC, Chen X, Shen CK (1999) Two major forms of DNA (cytosine-5) methyltransferase in human somatic tissues. Proc Natl Acad Sci U S A 96**:** 9751-9756

Humphries A, Wright NA (2008) Colonic crypt organization and tumorigenesis. Nat Rev Cancer 8**:** 415-424

Hyman NH, Anderson P, Blasyk H (2004) Hyperplastic polyposis and the risk of colorectal cancer. Dis Colon Rectum 47**:** 2101-2104

Iino H, Jass JR, Simms LA, Young J, Leggett B, Ajioka Y, Watanabe H (1999) DNA microsatellite instability in hyperplastic polyps, serrated adenomas, and mixed polyps: a mild mutator pathway for colorectal cancer? J Clin Pathol 52**:** 5-9

Ikawa S, Fukui M, Ueyama Y, Tamaoki N, Yamamoto T, Toyoshima K (1988) B-raf, a new member of the raf family, is activated by DNA rearrangement. Mol Cell Biol 8**:** 2651-2654

Ishii T, Notohara K, Umapathy A, Mallitt KA, Chikuba H, Moritani Y, Tanaka N, Rosty C, Matsubara N, Jass J et al (2011) Tubular adenomas with minor villous changes show molecular features characteristic of tubulovillous adenomas. Am J Surg Pathol 35**:** 212-220

Iwamoto M, Ahnen DJ, Franklin WA, Maltzman TH (2000) Expression of beta-catenin and full-length APC protein in normal and neoplastic colonic tissues. Carcinogenesis 21**:** 1935-1940

Jasperson KW, Tuohy TM, Neklason DW, Burt RW (2010) Hereditary and familial colon cancer. Gastroenterology 138**:** 2044-2058

Jass JR (2007) Classification of colorectal cancer based on correlation of clinical, morphological and molecular features. Histopathology 50**:** 113-130

Jass JR, Baker K, Zlobec I, Higuchi T, Barker M, Buchanan D, Young J (2006) Advanced colorectal polyps with the molecular and morphological features of serrated polyps and adenomas: concept of a 'fusion' pathway to colorectal cancer. Histopathology 49**:** 121-131

Jass JR, Biden KG, Cummings MC, Simms LA, Walsh M, Schoch E, Meltzer SJ, Wright C, Searle J, Young J et al (1999) Characterisation of a subtype of colorectal

cancer combining features of the suppressor and mild mutator pathways. J Clin Pathol 52**:** 455-460

Jass JR, Iino H, Ruszkiewicz A, Painter D, Solomon MJ, Koorey DJ, Cohn D, Furlong KL, Walsh MD, Palazzo J et al (2000) Neoplastic progression occurs through mutator pathways in hyperplastic polyposis of the colorectum. Gut 47**:** 43-49

Ji H, Ramsey MR, Hayes DN, Fan C, McNamara K, Kozlowski P, Torrice C, Wu MC, Shimamura T, Perera SA et al (2007) LKB1 modulates lung cancer differentiation and metastasis. Nature 448**:** 807-810

Johnstone CN, Tebbutt NC, Abud HE, White SJ, Stenvers KL, Hall NE, Cody SH, Whitehead RH, Catimel B, Nice EC et al (2000) Characterization of mouse A33 antigen, a definitive marker for basolateral surfaces of intestinal epithelial cells. Am J Physiol Gastrointest Liver Physiol 279**:** G500-510

Johnstone CN, White SJ, Tebbutt NC, Clay FJ, Ernst M, Biggs WH, Viars CS, Czekay S, Arden KC, Heath JK (2002) Analysis of the regulation of the A33 antigen gene reveals intestine-specific mechanisms of gene expression. J Biol Chem 277**:** 34531-34539

Kaji E, Uraoka T, Kato J, Hiraoka S, Suzuki H, Akita M, Saito S, Tanaka T, Ohara N, Yamamoto K (2012) Externalization of saw-tooth architecture in small serrated polyps implies the presence of methylation of IGFBP7. Dig Dis Sci 57**:** 1261-1270

Kakar S, Deng G, Cun L, Sahai V, Kim YS (2008) CpG island methylation is frequently present in tubulovillous and villous adenomas and correlates with size, site, and villous component. Hum Pathol 39**:** 30-36

Kambara T, Simms LA, Whitehall VL, Spring KJ, Wynter CV, Walsh MD, Barker MA, Arnold S, McGivern A, Matsubara N et al (2004) BRAF mutation is associated with DNA methylation in serrated polyps and cancers of the colorectum. Gut 53**:** 1137-1144

Kanai Y, Ushijima S, Kondo Y, Nakanishi Y, Hirohashi S (2001) DNA methyltransferase expression and DNA methylation of CPG islands and peri-centromeric satellite regions in human colorectal and stomach cancers. Int J Cancer 91**:** 205-212

Kane MF, Loda M, Gaida GM, Lipman J, Mishra R, Goldman H, Jessup JM, Kolodner R (1997) Methylation of the hMLH1 promoter correlates with lack of expression of hMLH1 in sporadic colon tumors and mismatch repair-defective human tumor cell lines. Cancer Res 57**:** 808-811

Kannan K, Sharpless NE, Xu J, O'Hagan RC, Bosenberg M, Chin L (2003) Components of the Rb pathway are critical targets of UV mutagenesis in a murine melanoma model. Proc Natl Acad Sci U S A 100**:** 1221-1225

Karpinski P, Walter M, Szmida E, Ramsey D, Misiak B, Kozlowska J, Bebenek M, Grzebieniak Z, Blin N, Laczmanski L et al (2013) Intermediate- and low-methylation epigenotypes do not correspond to CpG island methylator phenotype (low and -zero) in colorectal cancer. Cancer Epidemiol Biomarkers Prev 22**:** 201-208

Kellokumpu I, Husa A (1987) Colorectal adenomas: morphologic features and the risk of developing metachronous adenomas and carcinomas in the colorectum. Scand J Gastroenterol 22**:** 833-841

Kemp R, Ireland H, Clayton E, Houghton C, Howard L, Winton DJ (2004) Elimination of background recombination: somatic induction of Cre by combined transcriptional regulation and hormone binding affinity. Nucleic Acids Res 32**:** e92

Kim KM, Lee EJ, Ha S, Kang SY, Jang KT, Park CK, Kim JY, Kim YH, Chang DK, Odze RD (2011) Molecular features of colorectal hyperplastic polyps and sessile serrated adenoma/polyps from Korea. Am J Surg Pathol 35**:** 1274-1286

Kim YH, Kakar S, Cun L, Deng G, Kim YS (2008) Distinct CpG island methylation profiles and BRAF mutation status in serrated and adenomatous colorectal polyps. Int J Cancer 123**:** 2587-2593

Kim YH, Petko Z, Dzieciatkowski S, Lin L, Ghiassi M, Stain S, Chapman WC, Washington MK, Willis J, Markowitz SD et al (2006) CpG island methylation of genes accumulates during the adenoma progression step of the multistep pathogenesis of colorectal cancer. Genes Chromosomes Cancer 45**:** 781-789

King-Yin Lam A, Ong K, Ho YH (2006) Colorectal mucinous adenocarcinoma: the clinicopathologic features and significance of p16 and p53 expression. Dis Colon Rectum 49**:** 1275-1283

Kleihues P, Sobin LH (2000) World Health Organization classification of tumors. Cancer 88**:** 2887

Kominami K, Nagasaka T, Cullings HM, Hoshizima N, Sasamoto H, Young J, Leggett BA, Tanaka N, Matsubara N (2009) Methylation in p14(ARF) is frequently observed in colorectal cancer with low-level microsatellite instability. J Int Med Res 37**:** 1038-1045

Konishi F, Morson BC (1982) Pathology of colorectal adenomas: a colonoscopic survey. J Clin Pathol 35**:** 830-841

Konishi K, Yamochi T, Makino R, Kaneko K, Yamamoto T, Nozawa H, Katagiri A, Ito H, Nakayama K, Ota H et al (2004) Molecular differences between sporadic serrated and conventional colorectal adenomas. Clin Cancer Res 10**:** 3082-3090

Lash RH, Genta RM, Schuler CM (2010) Sessile serrated adenomas: prevalence of dysplasia and carcinoma in 2139 patients. J Clin Pathol 63**:** 681-686

Lee EJ, Choi C, Park CK, Maeng L, Lee J, Lee A, Kim KM (2005) Tracing origin of serrated adenomas with BRAF and KRAS mutations. Virchows Arch 447**:** 597-602

Lee M, Sup Han W, Kyoung Kim O, Hee Sung S, Sun Cho M, Lee SN, Koo H (2006) Prognostic value of p16INK4a and p14ARF gene hypermethylation in human colon cancer. Pathol Res Pract 202**:** 415-424

Lee S, Cho NY, Choi M, Yoo EJ, Kim JH, Kang GH (2008a) Clinicopathological features of CpG island methylator phenotype-positive colorectal cancer and its adverse prognosis in relation to KRAS/BRAF mutation. Pathol Int 58**:** 104-113

Lee SK, Chang HJ, Kim TI, Kim WH, Park CK, Chang DK, Park DI, Sohn JH, Byeon JS, Yang SK et al (2008b) Clinicopathologic findings of colorectal traditional and sessile serrated adenomas in Korea: a multicenter study. Digestion 77**:** 178-183

Leevers SJ, Marshall CJ (1992) MAP kinase regulation--the oncogene connection. Trends Cell Biol 2**:** 283-286

Leggett BA, Devereaux B, Biden K, Searle J, Young J, Jass J (2001) Hyperplastic polyposis: association with colorectal cancer. Am J Surg Pathol 25**:** 177-184

Levine DS, Haggitt RC (1989) Normal histology of the colon. Am J Surg Pathol 13**:** 966-984

Li L, Fu X, Zhang W, Xiao L, Qiu Y, Peng Y, Shi L, Chen X, Zhou X, Deng M (2013) Wnt signaling pathway is activated in right colon serrated polyps correlating to specific molecular form of beta-catenin. Hum Pathol 44**:** 1079-1088

Lin J, Lai M, Huang Q, Ma Y, Cui J, Ruan W (2007) Methylation patterns of IGFBP7 in colon cancer cell lines are associated with levels of gene expression. J Pathol 212**:** 83-90

Longacre TA, Fenoglio-Preiser CM (1990) Mixed hyperplastic adenomatous polyps/serrated adenomas. A distinct form of colorectal neoplasia. Am J Surg Pathol 14**:** 524-537

Lynch HT, de la Chapelle A (2003) Hereditary colorectal cancer. N Engl J Med 348**:** 919-932

Lynch HT, Lanspa S, Smyrk T, Boman B, Watson P, Lynch J (1991) Hereditary nonpolyposis colorectal cancer (Lynch syndromes I & II). Genetics, pathology, natural history, and cancer control, Part I. Cancer Genet Cytogenet 53**:** 143-160

Lynch HT, Smyrk T, McGinn T, Lanspa S, Cavalieri J, Lynch J, Slominski-Castor S, Cayouette MC, Priluck I, Luce MC (1995) Attenuated familial adenomatous polyposis (AFAP). A phenotypically and genotypically distinctive variant of FAP. Cancer 76**:** 2427-2433

Maeda T, Suzuki K, Togashi K, Nokubi M, Saito M, Tsujinaka S, Kamiyama H, Konishi F (2011) Sessile serrated adenoma shares similar genetic and epigenetic features with microsatellite unstable colon cancer in a location-dependent manner. Exp Ther Med 2**:** 695-700

Makinen MJ, George SM, Jernvall P, Makela J, Vihko P, Karttunen TJ (2001) Colorectal carcinoma associated with serrated adenoma--prevalence, histological features, and prognosis. J Pathol 193**:** 286-294

Marisa L, de Reynies A, Duval A, Selves J, Gaub MP, Vescovo L, Etienne-Grimaldi MC, Schiappa R, Guenot D, Ayadi M et al (2013) Gene expression classification of colon cancer into molecular subtypes: characterization, validation, and prognostic value. PLoS Med 10**:** e1001453

McLellan EA, Bird RP (1988) Aberrant crypts: potential preneoplastic lesions in the murine colon. Cancer Res 48**:** 6187-6192

Michaloglou C, Vredeveld LC, Mooi WJ, Peeper DS (2008) BRAF(E600) in benign and malignant human tumours. Oncogene 27**:** 877-895

Minoo P, Moyer MP, Jass JR (2007) Role of BRAF-V600E in the serrated pathway of colorectal tumourigenesis. J Pathol 212**:** 124-133

Miyaki M, Seki M, Okamoto M, Yamanaka A, Maeda Y, Tanaka K, Kikuchi R, Iwama T, Ikeuchi T, Tonomura A et al (1990) Genetic changes and histopathological types in colorectal tumors from patients with familial adenomatous polyposis. Cancer Res 50**:** 7166-7173

Miyakura Y, Sugano K, Konishi F, Ichikawa A, Maekawa M, Shitoh K, Igarashi S, Kotake K, Koyama Y, Nagai H (2001) Extensive methylation of hMLH1 promoter region predominates in proximal colon cancer with microsatellite instability. Gastroenterology 121**:** 1300-1309

Moran BJ, Jackson AA (1992) Function of the human colon. Br J Surg 79**:** 1132-1137

Morikawa T, Kuchiba A, Liao X, Imamura Y, Yamauchi M, Qian ZR, Nishihara R, Sato K, Meyerhardt JA, Fuchs CS et al (2012) Tumor TP53 expression status, body mass index and prognosis in colorectal cancer. Int J Cancer 131**:** 1169-1178

Morson B (1974) President's address. The polyp-cancer sequence in the large bowel. Proc R Soc Med 67**:** 451-457

Moskal A, Norat T, Ferrari P, Riboli E (2007) Alcohol intake and colorectal cancer risk: a dose-response meta-analysis of published cohort studies. Int J Cancer 120**:** 664-671

Ngo NT, Tan E, Tekkis P, Peston D, Cohen P (2010) Differential expression of p53 and p504s in hyperplastic polyp, sessile serrated adenoma and traditional serrated adenoma. Int J Colorectal Dis 25**:** 1193-1200

Nielsen M, de Miranda NF, van Puijenbroek M, Jordanova ES, Middeldorp A, van Wezel T, van Eijk R, Tops CM, Vasen HF, Hes FJ et al (2009a) Colorectal carcinomas in MUTYH-associated polyposis display histopathological similarities to microsatellite unstable carcinomas. BMC Cancer 9**:** 184

Nielsen M, Joerink-van de Beld MC, Jones N, Vogt S, Tops CM, Vasen HF, Sampson JR, Aretz S, Hes FJ (2009b) Analysis of MUTYH genotypes and colorectal phenotypes in patients With MUTYH-associated polyposis. Gastroenterology 136**:** 471-476

Nieuwenhuis MH, Vogt S, Jones N, Nielsen M, Hes FJ, Sampson JR, Aretz S, Vasen HF (2012) Evidence for accelerated colorectal adenoma--carcinoma progression in MUTYH-associated polyposis? Gut 61**:** 734-738

Nilsson TK, Lof-Ohlin ZM, Sun XF (2013) DNA methylation of the p14ARF, RASSF1A and APC1A genes as an independent prognostic factor in colorectal cancer patients. Int J Oncol 42**:** 127-133

Nucci MR, Robinson CR, Longo P, Campbell P, Hamilton SR (1997) Phenotypic and genotypic characteristics of aberrant crypt foci in human colorectal mucosa. Hum Pathol 28**:** 1396-1407

O'Brien MJ, Yang S, Clebanoff JL, Mulcahy E, Farraye FA, Amorosino M, Swan N (2004) Hyperplastic (serrated) polyps of the colorectum: relationship of CpG island methylator phenotype and K-ras mutation to location and histologic subtype. Am J Surg Pathol 28**:** 423-434

O'Brien MJ, Yang S, Mack C, Xu H, Huang CS, Mulcahy E, Amorosino M, Farraye FA (2006) Comparison of microsatellite instability, CpG island methylation phenotype, BRAF and KRAS status in serrated polyps and traditional adenomas indicates separate pathways to distinct colorectal carcinoma end points. Am J Surg Pathol 30**:** 1491-1501

Ogino S, Kawasaki T, Kirkner GJ, Loda M, Fuchs CS (2006) CpG island methylator phenotype-low (CIMP-low) in colorectal cancer: possible associations with male sex and KRAS mutations. J Mol Diagn 8**:** 582-588

Ogino S, Kawasaki T, Kirkner GJ, Ohnishi M, Fuchs CS (2007) 18q loss of heterozygosity in microsatellite stable colorectal cancer is correlated with CpG island methylator phenotype-negative (CIMP-0) and inversely with CIMP-low and CIMP-high. BMC Cancer 7**:** 72

Okano M, Xie S, Li E (1998) Dnmt2 is not required for de novo and maintenance methylation of viral DNA in embryonic stem cells. Nucleic Acids Res 26**:** 2536-2540

Oono Y, Fu K, Nakamura H, Iriguchi Y, Yamamura A, Tomino Y, Oda J, Mizutani M, Takayanagi S, Kishi D et al (2009) Progression of a sessile serrated adenoma to an early invasive cancer within 8 months. Dig Dis Sci 54**:** 906-909

Ostwald C, Linnebacher M, Weirich V, Prall F (2009) Chromosomally and microsatellite stable colorectal carcinomas without the CpG island methylator phenotype in a molecular classification. Int J Oncol 35**:** 321-327

Otori K, Oda Y, Sugiyama K, Hasebe T, Mukai K, Fujii T, Tajiri H, Yoshida S, Fukushima S, Esumi H (1997) High frequency of K-ras mutations in human colorectal hyperplastic polyps. Gut 40**:** 660-663

Pai RK, Mackinnon AC, Joseph L, Noffsinger A, Hart J (2010) Identification of histologically distinct conventional adenomas that arise predominately in patients with sessile serrated adenomas. Am J Surg Pathol 34**:** 355-363

Park SJ, Rashid A, Lee JH, Kim SG, Hamilton SR, Wu TT (2003) Frequent CpG island methylation in serrated adenomas of the colorectum. Am J Pathol 162**:** 815-822

Parks TG, Bussey HF, Lockhart-Mummery HE (1970) Familial polyposis coli associated with extracolonic abnormalities. Gut 11**:** 323-329

Pretlow TP, Barrow BJ, Ashton WS, O'Riordan MA, Pretlow TG, Jurcisek JA, Stellato TA (1991) Aberrant crypts: putative preneoplastic foci in human colonic mucosa. Cancer Res 51**:** 1564-1567

Psofaki V, Kalogera C, Tzambouras N, Stephanou D, Tsianos E, Seferiadis K, Kolios G (2010) Promoter methylation status of hMLH1, MGMT, and CDKN2A/p16 in colorectal adenomas. World J Gastroenterol 16**:** 3553-3560

Qian Y, Zhang J, Yan B, Chen X (2008) DEC1, a basic helix-loop-helix transcription factor and a novel target gene of the p53 family, mediates p53-dependent premature senescence. J Biol Chem 283**:** 2896-2905

Quelle DE, Cheng M, Ashmun RA, Sherr CJ (1997) Cancer-associated mutations at the INK4a locus cancel cell cycle arrest by p16INK4a but not by the alternative reading frame protein p19ARF. Proc Natl Acad Sci U S A 94**:** 669-673

Rad R, Cadinanos J, Rad L, Varela I, Strong A, Kriegl L, Constantino-Casas F, Eser S, Hieber M, Seidler B et al (2013) A genetic progression model of Braf(V600E)-induced intestinal tumorigenesis reveals targets for therapeutic intervention. Cancer Cell 24**:** 15-29

Rashid A, Shen L, Morris JS, Issa JP, Hamilton SR (2001) CpG island methylation in colorectal adenomas. Am J Pathol 159**:** 1129-1135

Razin A, Riggs AD (1980) DNA methylation and gene function. Science 210**:** 604-610

Robert MF, Morin S, Beaulieu N, Gauthier F, Chute IC, Barsalou A, MacLeod AR (2003) DNMT1 is required to maintain CpG methylation and aberrant gene silencing in human cancer cells. Nat Genet 33**:** 61-65

Roncucci L, Stamp D, Medline A, Cullen JB, Bruce WR (1991) Identification and quantification of aberrant crypt foci and microadenomas in the human colon. Hum Pathol 22**:** 287-294

Rosenberg DW, Yang S, Pleau DC, Greenspan EJ, Stevens RG, Rajan TV, Heinen CD, Levine J, Zhou Y, O'Brien MJ (2007) Mutations in BRAF and KRAS differentially distinguish serrated versus non-serrated hyperplastic aberrant crypt foci in humans. Cancer Res 67**:** 3551-3554

Roussel MF (1999) The INK4 family of cell cycle inhibitors in cancer. Oncogene 18**:** 5311-5317

Ruan WJ, Lin J, Xu EP, Xu FY, Ma Y, Deng H, Huang Q, Lv BJ, Hu H, Cui J et al (2006) IGFBP7 plays a potential tumor suppressor role against colorectal carcinogenesis with its expression associated with DNA hypomethylation of exon 1. J Zhejiang Univ Sci B 7**:** 929-932

Rubio CA (2002) Colorectal adenomas: time for reappraisal. Pathol Res Pract 198**:** 615-620

Rubio CA, Rodensjo M (1995) p53 overexpression in flat serrated adenomas and flat tubular adenomas of the colorectal mucosa. J Cancer Res Clin Oncol 121**:** 571-576

Rustgi AK (2007) The genetics of hereditary colon cancer. Genes Dev 21**:** 2525-2538

Samowitz WS, Curtin K, Ma KN, Schaffer D, Coleman LW, Leppert M, Slattery ML (2001) Microsatellite instability in sporadic colon cancer is associated with an improved prognosis at the population level. Cancer Epidemiol Biomarkers Prev 10**:** 917-923

Sandmeier D, Benhattar J, Martin P, Bouzourene H (2009) Serrated polyps of the large intestine: a molecular study comparing sessile serrated adenomas and hyperplastic polyps. Histopathology 55**:** 206-213

Sandmeier D, Seelentag W, Bouzourene H (2007) Serrated polyps of the colorectum: is sessile serrated adenoma distinguishable from hyperplastic polyp in a daily practice? Virchows Arch 450**:** 613-618

Sauer B (1998) Inducible gene targeting in mice using the Cre/lox system. Methods 14**:** 381-392

Schulz WA (2005) Molecular Biology of Human Cancers. pp 174-176. Springer

Scurr LL, Pupo GM, Becker TM, Lai K, Schrama D, Haferkamp S, Irvine M, Scolyer RA, Mann GJ, Becker JC et al (2010) IGFBP7 is not required for B-RAF-induced melanocyte senescence. Cell 141**:** 717-727

Serrano M, Hannon GJ, Beach D (1993) A new regulatory motif in cell-cycle control causing specific inhibition of cyclin D/CDK4. Nature 366**:** 704-707

Sharpless NE, Bardeesy N, Lee KH, Carrasco D, Castrillon DH, Aguirre AJ, Wu EA, Horner JW, DePinho RA (2001) Loss of p16Ink4a with retention of p19Arf predisposes mice to tumorigenesis. Nature 413**:** 86-91

Sharpless NE, Ramsey MR, Balasubramanian P, Castrillon DH, DePinho RA (2004) The differential impact of p16(INK4a) or p19(ARF) deficiency on cell growth and tumorigenesis. Oncogene 23**:** 379-385

Shen L, Kondo Y, Hamilton SR, Rashid A, Issa JP (2003) P14 methylation in human colon cancer is associated with microsatellite instability and wild-type p53. Gastroenterology 124**:** 626-633

Shimizu K, Goldfarb M, Suard Y, Perucho M, Li Y, Kamata T, Feramisco J, Stavnezer E, Fogh J, Wigler MH (1983) Three human transforming genes are related to the viral ras oncogenes. Proc Natl Acad Sci U S A 80**:** 2112-2116

Shimomura T, Hiyama T, Oka S, Tanaka S, Yoshihara M, Shimamoto F, Chayama K (2011) Frequent somatic mutations of mitochondrial DNA in traditional serrated adenomas but not in sessile serrated adenomas of the colorectum. J Gastroenterol Hepatol 26**:** 1565-1569

Shinya H, Wolff WI (1979) Morphology, anatomic distribution and cancer potential of colonic polyps. Ann Surg 190**:** 679-683

Smalley MJ, Dale TC (1999) Wnt signalling in mammalian development and cancer. Cancer Metastasis Rev 18**:** 215-230

Smith G, Carey FA, Beattie J, Wilkie MJ, Lightfoot TJ, Coxhead J, Garner RC, Steele RJ, Wolf CR (2002) Mutations in APC, Kirsten-ras, and p53--alternative genetic pathways to colorectal cancer. Proc Natl Acad Sci U S A 99**:** 9433-9438

Snover DC (2011) Update on the serrated pathway to colorectal carcinoma. Hum Pathol 42**:** 1-10

Spjut HJ, Appel MF (1979) Epithelial polyps of the large bowel: a pathological and colonoscopic study. Curr Probl Cancer 4**:** 23-42

Spring KJ, Zhao ZZ, Karamatic R, Walsh MD, Whitehall VL, Pike T, Simms LA, Young J, James M, Montgomery GW et al (2006) High prevalence of sessile serrated adenomas with BRAF mutations: a prospective study of patients undergoing colonoscopy. Gastroenterology 131**:** 1400-1407

Stanczak A, Stec R, Bodnar L, Olszewski W, Cichowicz M, Kozlowski W, Szczylik C, Pietrucha T, Wieczorek M, Lamparska-Przybysz M (2011) Prognostic significance of Wnt-1, beta-catenin and E-cadherin expression in advanced colorectal carcinoma. Pathol Oncol Res 17**:** 955-963

Sternberg N, Hamilton D (1981) Bacteriophage P1 site-specific recombination. I. Recombination between loxP sites. J Mol Biol 150**:** 467-486

Suehiro Y, Hinoda Y (2008) Genetic and epigenetic changes in aberrant crypt foci and serrated polyps. Cancer Sci 99**:** 1071-1076

Suzuki H, Igarashi S, Nojima M, Maruyama R, Yamamoto E, Kai M, Akashi H, Watanabe Y, Yamamoto H, Sasaki Y et al (2010) IGFBP7 is a p53-responsive gene specifically silenced in colorectal cancer with CpG island methylator phenotype. Carcinogenesis 31**:** 342-349

Takayama T, Katsuki S, Takahashi Y, Ohi M, Nojiri S, Sakamaki S, Kato J, Kogawa K, Miyake H, Niitsu Y (1998) Aberrant crypt foci of the colon as precursors of adenoma and cancer. N Engl J Med 339**:** 1277-1284

Takayama T, Ohi M, Hayashi T, Miyanishi K, Nobuoka A, Nakajima T, Satoh T, Takimoto R, Kato J, Sakamaki S et al (2001) Analysis of K-ras, APC, and beta-catenin in aberrant crypt foci in sporadic adenoma, cancer, and familial adenomatous polyposis. Gastroenterology 121**:** 599-611

Teoh HH, Delahunt B, Isbister WH (1989) Dysplastic and malignant areas in hyperplastic polyps of the large intestine. Pathology 21**:** 138-142

Thibodeau SN, Bren G, Schaid D (1993) Microsatellite instability in cancer of the proximal colon. Science 260**:** 816-819

Thibodeau SN, French AJ, Roche PC, Cunningham JM, Tester DJ, Lindor NM, Moslein G, Baker SM, Liskay RM, Burgart LJ et al (1996) Altered expression of hMSH2 and hMLH1 in tumors with microsatellite instability and genetic alterations in mismatch repair genes. Cancer Res 56**:** 4836-4840

Thompson JJ, Enterline HT (1981) The macroscopic appearance of colorectal polyps. Cancer 48**:** 151-160

Thullberg M, Bartkova J, Khan S, Hansen K, Ronnstrand L, Lukas J, Strauss M, Bartek J (2000) Distinct versus redundant properties among members of the INK4 family of cyclin-dependent kinase inhibitors. FEBS Lett 470**:** 161-166

Torlakovic E, Skovlund E, Snover DC, Torlakovic G, Nesland JM (2003) Morphologic reappraisal of serrated colorectal polyps. Am J Surg Pathol 27**:** 65-81

Torlakovic E, Snover DC (1996) Serrated adenomatous polyposis in humans. Gastroenterology 110**:** 748-755

Torlakovic EE, Gomez JD, Driman DK, Parfitt JR, Wang C, Benerjee T, Snover DC (2008) Sessile serrated adenoma (SSA) vs. traditional serrated adenoma (TSA). Am J Surg Pathol 32**:** 21-29

Toyota M, Ahuja N, Ohe-Toyota M, Herman JG, Baylin SB, Issa JP (1999) CpG island methylator phenotype in colorectal cancer. Proc Natl Acad Sci U S A 96**:** 8681-8686

Toyota M, Ohe-Toyota M, Ahuja N, Issa JP (2000) Distinct genetic profiles in colorectal tumors with or without the CpG island methylator phenotype. Proc Natl Acad Sci U S A 97**:** 710-715

Uchida H, Ando H, Maruyama K, Kobayashi H, Toda H, Ogawa H, Ozawa T, Matsuda Y, Sugimura H, Kanno T et al (1998) Genetic alterations of mixed hyperplastic adenomatous polyps in the colon and rectum. Jpn J Cancer Res 89**:** 299-306

Urbanski SJ, Kossakowska AE, Marcon N, Bruce WR (1984) Mixed hyperplastic adenomatous polyps--an underdiagnosed entity. Report of a case of adenocarcinoma arising within a mixed hyperplastic adenomatous polyp. Am J Surg Pathol 8**:** 551-556

Van Aelst L, Barr M, Marcus S, Polverino A, Wigler M (1993) Complex formation between RAS and RAF and other protein kinases. Proc Natl Acad Sci U S A 90**:** 6213-6217

Vaughn CP, Wilson AR, Samowitz WS (2010) Quantitative evaluation of CpG island methylation in hyperplastic polyps. Mod Pathol 23**:** 151-156

Vogelstein B, Kinzler KW (2002) Genetic Basis of Human Cancers. pp 311-313. McGraw Hill

Vu HT, Lopez R, Bennett A, Burke CA (2011) Individuals with sessile serrated polyps express an aggressive colorectal phenotype. Dis Colon Rectum 54**:** 1216-1223

Wajapeyee N, Kapoor V, Mahalingam M, Green MR (2009) Efficacy of IGFBP7 for treatment of metastatic melanoma and other cancers in mouse models and human cell lines. Mol Cancer Ther 8**:** 3009-3014

Wajapeyee N, Serra RW, Zhu X, Mahalingam M, Green MR (2008) Oncogenic BRAF induces senescence and apoptosis through pathways mediated by the secreted protein IGFBP7. Cell 132**:** 363-374

Wajapeyee N, Serra RW, Zhu X, Mahalingam M, Green MR (2010) Role for IGFBP7 in senescence induction by BRAF. Cell 141**:** 746-747

Wakai K, Hirose K, Matsuo K, Ito H, Kuriki K, Suzuki T, Kato T, Hirai T, Kanemitsu Y, Tajima K (2006) Dietary risk factors for colon and rectal cancers: a comparative case-control study. J Epidemiol 16**:** 125-135

Wan PT, Garnett MJ, Roe SM, Lee S, Niculescu-Duvaz D, Good VM, Jones CM, Marshall CJ, Springer CJ, Barford D et al (2004) Mechanism of activation of the RAF-ERK signaling pathway by oncogenic mutations of B-RAF. Cell 116**:** 855-867

Weber CK, Slupsky JR, Kalmes HA, Rapp UR (2001) Active Ras induces heterodimerization of cRaf and BRaf. Cancer Res 61**:** 3595-3598

Weisenberger DJ, Siegmund KD, Campan M, Young J, Long TI, Faasse MA, Kang GH, Widschwendter M, Weener D, Buchanan D et al (2006) CpG island methylator phenotype underlies sporadic microsatellite instability and is tightly associated with BRAF mutation in colorectal cancer. Nat Genet 38**:** 787-793

Wish TA, Hyde AJ, Parfrey PS, Green JS, Younghusband HB, Simms MI, Fontaine DG, Dicks EL, Stuckless SN, Gallinger S et al (2010) Increased cancer predisposition in family members of colorectal cancer patients harboring the p.V600E BRAF mutation: a population-based study. Cancer Epidemiol Biomarkers Prev 19**:** 1831-1839

Wogan GN, Hecht SS, Felton JS, Conney AH, Loeb LA (2004) Environmental and chemical carcinogenesis. Semin Cancer Biol 14**:** 473-486

Woods MO, Younghusband HB, Parfrey PS, Gallinger S, McLaughlin J, Dicks E, Stuckless S, Pollett A, Bapat B, Mrkonjic M et al (2010) The genetic basis of colorectal cancer in a population-based incident cohort with a high rate of familial disease. Gut 59**:** 1369-1377

Wynter CV, Walsh MD, Higuchi T, Leggett BA, Young J, Jass JR (2004) Methylation patterns define two types of hyperplastic polyp associated with colorectal cancer. Gut 53**:** 573-580

Yachida S, Mudali S, Martin SA, Montgomery EA, Iacobuzio-Donahue CA (2009) Beta-catenin nuclear labeling is a common feature of sessile serrated adenomas and correlates with early neoplastic progression after BRAF activation. Am J Surg Pathol 33**:** 1823-1832

Yagi K, Akagi K, Hayashi H, Nagae G, Tsuji S, Isagawa T, Midorikawa Y, Nishimura Y, Sakamoto H, Seto Y et al (2010) Three DNA methylation epigenotypes in human colorectal cancer. Clin Cancer Res 16**:** 21-33

Yang S, Farraye FA, Mack C, Posnik O, O'Brien MJ (2004) BRAF and KRAS Mutations in hyperplastic polyps and serrated adenomas of the colorectum: relationship to histology and CpG island methylation status. Am J Surg Pathol 28**:** 1452-1459

Yen RW, Vertino PM, Nelkin BD, Yu JJ, el-Deiry W, Cumaraswamy A, Lennon GG, Trask BJ, Celano P, Baylin SB (1992) Isolation and characterization of the cDNA encoding human DNA methyltransferase. Nucleic Acids Res 20**:** 2287-2291

Yuen ST, Davies H, Chan TL, Ho JW, Bignell GR, Cox C, Stephens P, Edkins S, Tsui WW, Chan AS et al (2002) Similarity of the phenotypic patterns associated with BRAF and KRAS mutations in colorectal neoplasia. Cancer Res 62**:** 6451-6455

Zhang BH, Guan KL (2000) Activation of B-Raf kinase requires phosphorylation of the conserved residues Thr598 and Ser601. EMBO J 19**:** 5429-5439

Zhang Y, Xiong Y, Yarbrough WG (1998) ARF promotes MDM2 degradation and stabilizes p53: ARF-INK4a locus deletion impairs both the Rb and p53 tumor suppression pathways. Cell 92**:** 725-734

APPENDIX